Universidade de São Paulo
Faculdade de Filosofia, Ciências e Letras de Ribeirão Preto
Departamento de Química
Programa de Pós-Graduação em Química

Avaliação do efeito sinérgico da LPMO *Af*AA9_B de *Aspergillus fumigatus* nos processos de hidrólise de material lignocelulósico.

Luis Eduardo Gerolamo

Tese apresentada à Faculdade de Filosofia, Ciências e Letras de Ribeirão Preto da Universidade de São Paulo, como parte das exigências para a obtenção do título de Doutor em Ciências, Área: **Química**

RIBEIRÃO PRETO - SP

2022

Universidade de São Paulo
Faculdade de Filosofia, Ciências e Letras de Ribeirão Preto
Departamento de Química
Programa de Pós-Graduação em Química

Avaliação do efeito sinérgico da LPMO *Af*AA9_B de *Aspergillus fumigatus* nos processos de hidrólise de material lignocelulósico.

Luis Eduardo Gerolamo

Tese apresentada à Faculdade de Filosofia, Ciências e Letras de Ribeirão Preto da Universidade de São Paulo, como parte das exigências para a obtenção do título de Doutor em Ciências, Área: **Química**

Orientadora: Profa. Dra. Taisa Magnani Dinamarco

RIBEIRÃO PRETO - SP

2022

Gerolamo, Luis Eduardo

Avaliação do efeito sinérgico da LPMO *Af*AA9_B de *Aspergillus fumigatus* nos processos de hidrólise de material lignocelulósico. Ribeirão Preto, 2022.

156 p. : il. ; 30 cm

Tese de Doutorado, apresentada à Faculdade de Filosofia, Ciências e Letras de Ribeirão Preto/USP. Área de concentração: Química.

Orientador: Dinamarco, Taisa Magnani.

1. *Aspergillus fumigatus*. 2. Materiais lignocelulósicos. 3. LPMO. 4. Clonagem e caracterização bioquímica. 5. Ensaios de hidrólise com coquetel de celulases.

FOLHA DE APROVAÇÃO

Nome: GEROLAMO, Luis Eduardo

Título: Avaliação do efeito sinérgico da LPMO *Af*AA9_B de *Aspergillus fumigatus* nos processos de hidrólise de material lignocelulósico

Tese apresentada à Faculdade de Filosofia, Ciências e Letras de Ribeirão Preto da Universidade de São Paulo, como parte das exigências para a obtenção do título de Doutor em Ciências, Área: **Química**

Aprovado em: ___/___/___

Banca Examinadora

Prof. Dr.: _____ Instituição:_____

Julgamento: _____ Assinatura: _____

Prof. Dr.: _____ Instituição: _____

Julgamento: _____ Assinatura: _____

Prof. Dr.: _____ Instituição: _____

Julgamento: _____ Assinatura: _____

Prof. Dr.: _____ Instituição: _____

Julgamento: _____ Assinatura: _____

Dedicatória

Dedico essa dissertação aos meus pais e familiares que sempre me apoiaram ao longo da minha vida,

Aos meus colegas de laboratório, os quais nunca negaram ajuda nas ocasiões em que mais precisei,

Aos professores que já me deram aula na escola, na graduação e que me auxiliaram durante a pós-graduação e realização de experimentos,

Aos membros da banca, aos quais tenho muito respeito e sou grato por terem aceitado participar,

E em especial à minha orientadora Profa. Dra. Taisa Magnani Dinamarco, a qual depositou sua confiança em mim e tornou tudo isso possível.

Agradecimentos

Os meus agradecimentos, em especial, vão para:

O Prof. Sérgio Akira Uyemura por compartilhar as dependências de seu laboratório conosco durante às etapas iniciais do projeto.

O Prof. Arthur Henrique Cavalcante de Oliveira por me auxiliar em diversas ocasiões e me ensinar sobre a técnica de dicroísmo circular em conjunto com o técnico André Justino.

A Profa. Taisa Magnani Dinamarco por aceitar ser minha orientadora e me instruir durante todo o desenvolvimento do projeto, acompanhando-o sempre de perto.

Os meus colegas do laboratório Labiomol (Aline, Paula, Lucas e Deborah) pelas várias vezes em que foram prestativos e me ajudaram nas tarefas rotineiras.

Ao Programa de Pós-Graduação em Química (PPGQ-RP) por me receber como estudante e oferecer plenas condições de desenvolver o meu projeto.

E as agências de fomento Capes, FAPESP e CNPq pelo financiamento das pesquisas realizadas.

Pensamos raras vezes no

que temos, mas sempre no

que nos falta.

Arthur Schopenhauer

Resumo

GEROLAMO, L. E. **Avaliação do efeito sinérgico da LPMO *Af*AA9_B de *Aspergillus fumigatus* nos processos de hidrólise de material lignocelulósico.** 2022. 156f. Tese (doutorado). Faculdade de Filosofia, Ciências e Letras de Ribeirão Preto, Universidade de São Paulo, Ribeirão Preto, 2022.

Desde o advento da revolução industrial o consumo de energia global aumentou exponencialmente, tendo como principal matriz os combustíveis fósseis. Como consequência, atualmente o mundo enfrenta não somente escassez de energia como também problemas com a poluição gerada com a queima desses materiais. Nesse cenário, materiais como a biomassa lignocelulósica, até então vistos como resíduos, ganham destaque. Esses materiais formados por 3 componentes principais (32-55% celulose; 19-32% hemicelulose; e 19-32% lignina), devido aos seus polissacarídeos constituintes são ricos em energia e se apresentam como uma possível alternativa sustentável para a geração de energia e produção de combustíveis, como por exemplo, o etanol de segunda geração (2G) obtido a partir do bagaço de cana-de-açúcar. Contudo, tais materiais são altamente recalcitrantes e necessitam de tratamentos prévios para que os polissacarídeos se tornem disponíveis e sejam quebrados em unidades de açúcares simples para posterior fermentação. Nesse sentido, as Glicosil Hidrolases (GHs) juntamente com as Monooxigenases Líticas de Polissacarídeos (LPMOs) destacam-se como uma das principais enzimas atuantes na quebra dos mesmos. As LPMOs são enzimas da classe AA (Atividade Auxiliar) com mecanismos de ação oxidorredutivos que atuam nos carbonos C1 e/ou C4 das ligações glicosídicas de açúcares complexos como a celulose e quitina e que podem intensificar a ação de outras celulases canônicas. A fim de contribuir com o estudo de novas enzimas, nesse trabalho caracterizamos o novo gene AFUA_4G07850 codificante da *Af*AA9_B, uma LPMO de *Aspergillus fumigatus* secretada quando crescido na presença de bagaço de cana explodido (SEB). O alinhamento da sequência com as demais LPMOs descritas na literatura, permitiu a identificação dos resíduos His1, His86 e Tyr175 conservados como constituintes da braçadeira de histidina, estrutura catalítica característica desse tipo de enzima. Análises das estruturas secundárias e terciárias realizadas via dicroísmo circular (CD) e emissão de fluorescência intrínseca de triptofano (ITFE), respectivamente, demonstraram a presença de 8,3% de alfa hélices, 31,4% de folhas beta, 11,9% de alças e 48,4% de estruturas desordenadas e que seus resíduos de Trp tornam-se mais expostos ao meio aquoso com o aumento da temperatura. Além disso, o valor da temperatura de transição da enzima (T_m) do estado nativo para o desnaturado foi de 55,22 °C via CD e 53,60 °C via ITFE. A caracterização da atividade da enzima demonstrou que a enzima atua melhor em pH=9, sendo capaz de manter 100% de sua atividade mesmo após incubações de 24 a 72 horas na faixa de pH de 3 a 10. A enzima também é capaz de manter aproximadamente 70% de sua atividade após 72 horas a 50°C e mais de 50% após 48 horas a 60°C. As constantes cinéticas (usando 2,6-DMP como substrato) apresentaram valores de K_M = 0,79 µM e V_{max} = 1481 U/g quando em pH=9. A *Af*AA9_B é tolerante a Tween 20, SDS, SLS e Triton X-100, e a produtos de hidrólise como glicose e celobiose, apresentando mais de 80% da atividade residual. Por fim, em ensaios de atividade sob CMC na presença de outras GHs de *A. fumigatus* (também induzidas pela presença de SEB no meio de cultivo), foi constatado que a *Af*AA9_B não atua em sinergia com a celobiohidrolase *Af*Cel6A, porém na presença de coquetel Celluclast® 1,5L e da endoglucanase *Af*-EGL7, a adição de LPMO foi responsável por aumentos de 3,5 e 8X na liberação de açúcares, respectivamente. Em ensaios de hidrólise com SEB e sabugo de milho, a suplementação da *Af*AA9_B resultou em aumento na degradação de 2X na presença de coquetel, e de 1,5X na presença da *Af*-EGL7, respectivamente. Tais resultados reforçam o potencial da *Af*AA9_B como enzima passível de ser adicionada em coquetéis comerciais e empregada em biorrefinarias com foco na produção de etanol 2G.

Abstract

GEROLAMO, L. E. **Evaluation of the synergistic effect of LPMO *Af*AA9_B from Aspergillus fumigatus in the hydrolysis of lignocellulosic material.** 2022. 156f. Doctoral thesis. Faculdade de Filosofia, Ciências e Letras de Ribeirão Preto, Universidade de São Paulo, Ribeirão Preto, 2022.

Since the advent of the industrial revolution, global energy consumption has increased exponentially, with fossil fuels as the main source. As a result, the world currently faces not only energy shortage but also problems with the pollution generated by the burning of these materials. In this scenario, materials such as lignocellulosic biomass hitherto seen as waste gain prominence. These materials formed by 3 main components (32-55% cellulose; 19-32% hemicellulose; and 19-32% lignin), due to their constituent polysaccharides, are rich in energy and present themselves as a possible sustainable alternative for energy generation and production of fuels such as second generation ethanol (2G) obtained from sugarcane bagasse. However, such materials are highly recalcitrant and require previous treatments for the polysaccharides to become available and to be broken down into simple sugar units for further fermentation. In this sense, the Glycosyl Hydrolases (GHs) together with the Lytic Polysaccharide Monooxygenases (LPMOs) stand out as the main enzymes acting in their breakdown. LPMOs are class AA enzymes (Auxiliary Activity) with oxidoreductive mechanisms of action that act on the C1 and/or C4 carbons of the glycosidic bonds of complex sugars such as cellulose and chitin and that can intensify the action of other canonical cellulases. In order to contribute to the study of new enzymes, in this work we characterized the new gene AFUA_4G07850 encoding *Af*AA9_B, an LPMO of *Aspergillus fumigatus* secreted when in presence of sugarcane exploded bagasse (SEB). Alignment of the sequence with other LPMOs described in the literature allowed the identification of conserved His1, His86 and Tyr175 residues as constituents of the histidine bracer, a catalytic structure characteristic of this type of enzyme. Analyzes of secondary and tertiary structures performed via circular dichroism (CD) and intrinsic tryptophan fluorescence emission (ITFE), respectively, showed the presence of 8.3% of alpha helices, 31.4% of beta sheets, 11.9% of loops and 48.4% of disordered structures and that their Trp residues become more exposed to the aqueous medium as the temperature increases. Furthermore, the value of the enzyme transition temperature (T_m) from the native to the denatured state was 55.22 °C via CD and 53.60 °C via ITFE. The characterization of the enzyme activity showed the LPMO works better at pH=9, being able to maintain 100% of its activity even after incubations of 24 to 72 hours in the pH range from 3 to 10. The enzyme is also able to maintain approximately 70% of its activity after 72 hours at 50°C and more than 50% after 48 hours at 60°C. The kinetic constants (using 2,6-DMP as substrate) showed values of K_M = 0.79 µM and V_{max} = 1481 U/g under pH=9. Another aspect observed was the high tolerance of the enzyme (>80% residual activity) in the presence of detergents such as Tween 20, SDS, SLS and Triton X-100, as well as hydrolysis products such as glucose and cellobiose. Finally, on CMC activity assays in the presence of other *A. fumigatus* GHs (also induced by SEB presence in the medium), it was found that *Af*AA9_B does not act synergistically with cellobiohydrolase *Af*Cel6A, while in the presence of Celluclast® 1.5L cocktail and *Af*-EGL7 endoglucanase, the addition of LPMO was responsible for increases of 3.5 and 8X in the sugar releasing, respectively. In hydrolysis assays with SEB and corn cob, *Af*AA9_B supplementation resulted in a degradation increase of 2X in the presence of cocktail, and 1.5X in the presence of *Af*-EGL7, respectively. These results reinforce the potential of *Af*AA9_B as an enzyme that can be added to commercial cocktails and employed in biorefineries focused on the production of 2G ethanol.

Lista de Figuras

Lista de Figuras Suplementares

Lista de Tabelas

Lista de Tabelas Suplementares

Lista de abreviaturas, siglas, unidades e símbolos

°C	Graus Celsius
g	Força centrífuga relativa
Ω	Ohm
®	Marca Registrada
™	Trademark
λ	Comprimento de onda
ε	Coeficiente de absortividade molar
Δε	Unidade delta epsilon (dicroísmo circular molar)
θ	Unidade teta (elipticidade)
µF	Microfarad
µg	Micrograma
µL	Microlitro
µmol	Micromol
2G	Segunda Geração
3D	Tridimensional
AA	Atividades Auxiliares
AOX	Álcool Oxidase
BMGY	Buffered Glycerol-complex Medium
BMMY	Buffered Methanol-complex Medium
CAZy	Carbohydrate-Active Enzymes
CBH	Celobiohidrolase
CBM	Módulo de ligação a carboidrato
CD	Dicroísmo Circular
cDNA	DNA complementar
cm	Centímetro
CMC	Carboximetilcelulose
CPEC	Circular Polymerase Extension Cloning
D.I.T.	Digital Integration Time
D.O.	Densidade Óptica
DMSO	Dimetilsulfóxido
DNS	Dinitrosalicílico

dNTP	Desoxirribonucleotídeo trifosfato (dATP, dCTP, dGTP, dTTP)
DTT	Ditiotreitol
EC	Enzyme Comission
EDTA	Ácido etilenodiaminotetracético
Endo H	Endoglicosidase H
Fw	Forward (senso)
FPU	Filter Paper Unit (unidade de papel de filtro)
g	Grama
GH	Glicosil Hidrolases
h	Hora
HiFi	High Fidelity
His	Histidina
ITFE	Emissão Fluorescente Intrínseca de Triptofano
k_{cat}	Número de renovação
k_{cat}/K_M	Eficiência catalítica
kDa	Quilodalton
kg	Quilograma
K_M	Constante de Michaelis-Menten
kV	Quilovolt
L	Litro
LB	Luria-Bertani
LPMO	Monooxigenase Lítica de Polissacarídeos
M	Molar
mdeg	Miligraus
Meio TB	Terrific-Broth
mg	Miligrama
min	Minuto
Miniprep	Minipreparação Plasmidial
mL	Mililitro
mM	Milimolar
mmol	Milimol
MOPS	Ácido 3-morfolinopropano 1-sulfônico

MRW	Mean Residue Weight
ng	Nanograma
nm	Nanômetro
ORF	Open Reading Frame
Organosolv	Pré-tratamento por organosolvatação da lignina e hemicelulose
p/v	Peso/volume
pb	Pares de bases
PCR	Reação em Cadeia de Polimerase
PDB	Protein Data Bank
pH	Potencial Hidrogeniônico
Phe	Fenilalanina
Rv	Reverse (antisenso)
rpm	Revolução Por Minuto
s	Segundo
SDS	Dodecil sulfato de sódio
SDS-PAGE	Eletroforese em gel de poliacrilamida-SDS
SEB	Sugarcane Exploded Bagasse
SLS	Lauril sulfato de sódio
SOB	Super Optimal Broth
SOC	Super Optimal broth with Catabolites repression
Solução TB	Transformation Buffer
$t_{1/2}$	Tempo de meia vida
TAE	Tris-Acetato-EDTA
TEMED	N,N,N',N'-Tetrametiletilenodiamina
T_m	Melting temperature (Temperatura de fusão)
T_{mapp}	Apparent melting temperature (Temperatura de fusão aparente)
Tris	Tris-(hidroximetil)aminoetano
Trp	Triptofano
TWh	Terawatt-hora
Tyr	Tirosina
U	Unidade de atividade enzimática
V	Volt

v/v	Volume/volume
V_{max}	Velocidade máxima
YAG	Yeast extract-Agar-Glucose
YPD	Yeast extract-Peptone-Dextrose
YPDS	Yeast extract-Peptone-Dextrose-Sorbitol

Siglas de aminoácidos

A	Alanina
C	Cisteína
D	Aspartato
E	Glutamato
F	Fenilalanina
G	Glicina
H	Histidina
I	Isoleucina
K	Lisina
L	Leucina
M	Metionina
N	Asparagina
P	Prolina
Q	Glutamina
R	Arginina
S	Serina
T	Treonina
V	Valina
W	Triptofano
Y	Tirosina

Sumário

1. Introdução

1.1) Cenário energético atual, cana-de-açúcar e produção de etanol no Brasil

Em meio à crescente demanda energética mundial provocada pelo advento da revolução industrial ainda no início do século XIX, fatores como a crise do petróleo de 1970, crescimento populacional, aumento da urbanização, riscos de esgotamento das reservas de combustíveis fósseis e aumento na emissão de gases causadores do efeito estufa alavancaram a busca em várias nações por fontes de energia alternativas renováveis e também mais limpas (AYDIN, 2019; BISSARO et al., 2020; REBELLO et al., 2020; ZHOU et al., 2018).

Por definição, combustíveis fósseis tais como petróleo (e seus derivados), carvão e gás natural - os quais representam mais de 80% das fontes de energia utilizada no mundo (MILLER, 2015) - são aqueles oriundos de processos de decomposição de matéria orgânica animal e vegetal formados ao longo de milhões de anos em regiões profundas sob ação de microrganismos e elevadas temperaturas e pressões, dessa forma sendo então considerados recursos limitados (SATO, 1991). Já as fontes renováveis, são aquelas consideradas regeneráveis e inesgotáveis (ou praticamente) compreendendo a eólica, hidrelétrica, solar, geotérmica, e aquelas mais modernas provenientes de resíduos urbanos, industriais e agrícolas como a própria biomassa (BULL, 2001; FOGAÇA, 2020; PAO; FU, 2013).

Atualmente, conforme pode ser observado na Figura 1A, observa-se que até 2018, os combustíveis fósseis foram responsáveis pelo fornecimento de aproximadamente 81% de toda a energia utilizada no mundo (IEA, 2020). Ao longo dos últimos anos, a utilização de tais fontes tem apresentado acentuado crescimento, enquanto as ditas renováveis praticamente mantiveram-se estagnadas. Por outro lado, no Brasil (Figura 1B), recursos não renováveis representam 52% do consumo energético total, ao passo que matrizes renováveis como biocombustíveis e a água (hidrelétricas) forneceram 32% e 12% do total consumido no ano de 2019. O maior crescimento em relação ao resto do mundo no uso de fontes sustentáveis observado para o Brasil é uma tendência refletida nos países integrantes do BRICS (Brasil, Rússia, Índia, China e África do Sul), os quais com exceção da Rússia, são grandes produtores de variedades agrícolas (AYDIN, 2019; CHANDEL et al., 2019; LIU et al., 2020).

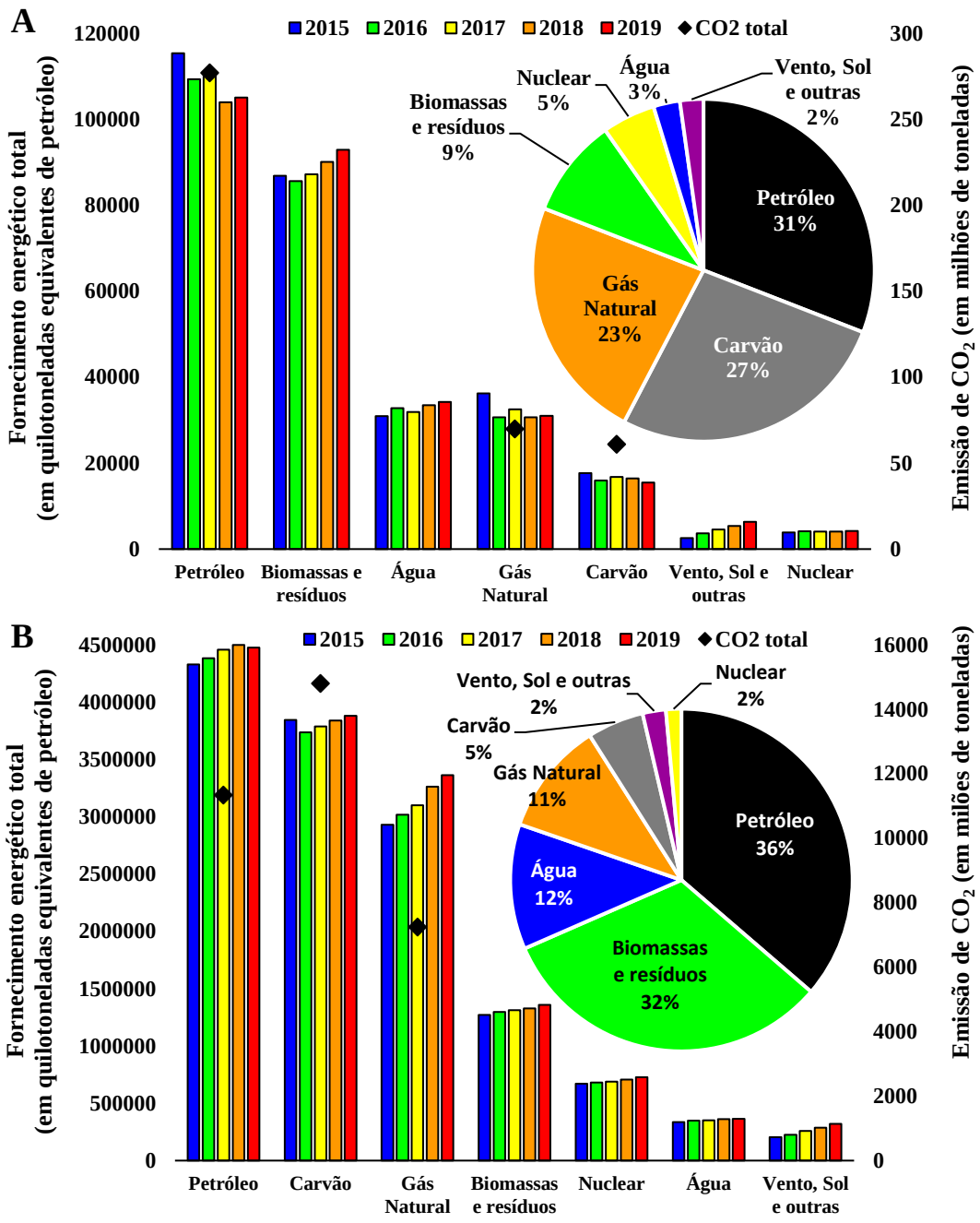

Figura 1. Comparativo entre as distribuições de diferentes matrizes energéticas ao longo dos últimos anos e quantidade de CO_2 emitido por combustíveis fósseis no mundo (A) e no Brasil (B) em 2019. Nos respectivos gráficos de pizza são exibidas as contribuições relativas de cada matriz para o fornecimento total de energia no mundo (A) e no Brasil (B) em 2019 (Fonte: https://www.iea.org/data-and-statistics).

Dentre as principais potências produtoras de biocombustíveis, os EUA aparecem liderando a lista, seguido pelo Brasil, Indonésia, Alemanha e China, os quais apresentaram produção (em 2020) de aproximadamente 374; 245; 79; 41; e 39 TWh, respectivamente (OUR WORLD IN DATA, 2021). Estima-se que o cultivo de cana-de-açúcar utilizada para a produção de etanol, isoladamente, represente algo em torno de 13

a 19% de toda a matriz energética brasileira (BERGMANN et al., 2018; KHATIWADA et al., 2016). De acordo com previsões para 2050, considerando-se apenas o cultivo de cana-de-açúcar no Brasil, cuja safra poderá ser de 5200 milhões de toneladas, espera-se produzir 214 bilhões de litros de etanol, quantidade essa que pode evitar a emissão de 380 megatoneladas de CO_2 provenientes da combustão de gasolina (KUMARA et al., 2016).

Diante desse cenário, de acordo com o ranking da FAO, países como Brasil, Índia, China, Tailândia e Paquistão tem ganhado notoriedade, devido suas elevadas produções de cana-de-açúcar para a produção de etanol e açúcar, como pode ser conferido na Figura 2.

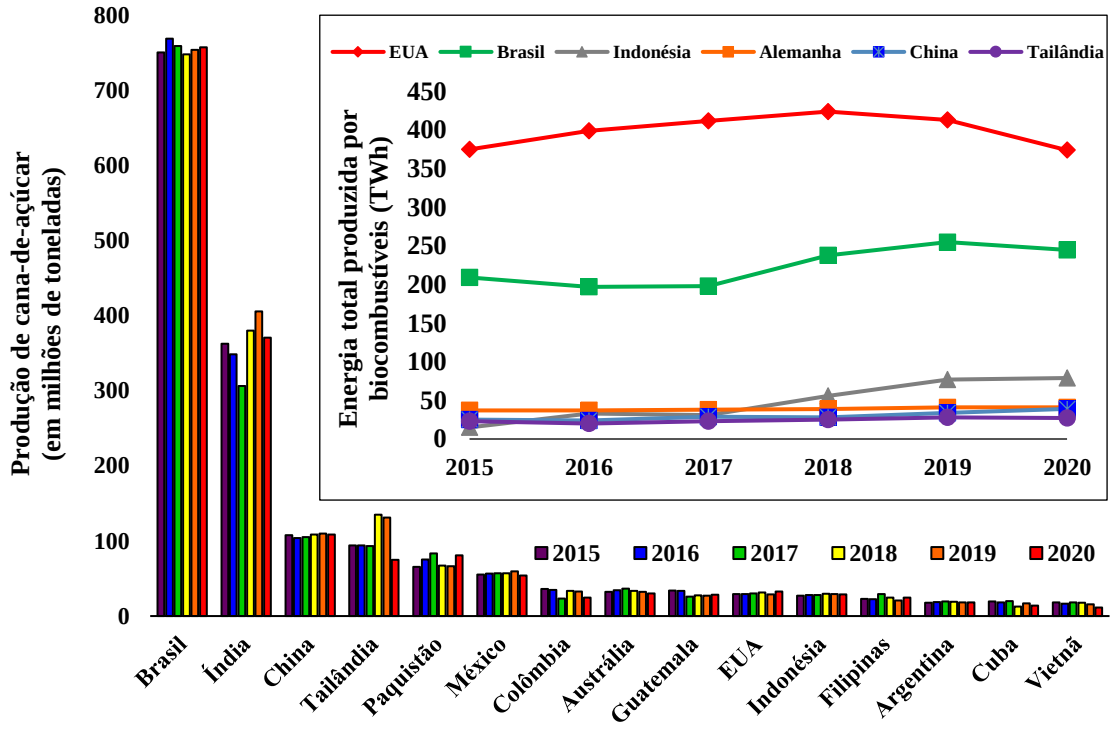

Figura 2. Colheita registrada nos 15 maiores países produtores de cana-de-açúcar durante o período de 2015 a 2020 (Fonte: http://www.fao.org/faostat/en/#data/QC/visualize); e os 5 países com maior produção energética oriunda de biocombustíveis (https://ourworldindata.org/grapher/biofuel-production).

Segundo estimativa fornecida pela CONAB (https://www.conab.gov.br/info-agro/safras/cana) para a safra 2021/2022 (3° levantamento), o país que hoje conta com a maior produção de cana-de-açúcar do mundo, tem previsão para registrar uma colheita de 568,4 milhões de toneladas, das quais somente o estado de São Paulo é responsável pela produção de 287,4 milhões de toneladas, o que corresponde a 50,5% do montante. Dos mais de 8,2 milhões de hectares de área de cultivo da cultura, é esperado a produção de 24,8 bilhões de litros de etanol total (anidro e hidratado), valor esse aproximadamente

16,6% menor que a safra anterior, em decorrência dos impactos causados pela pandemia de COVID-19. Sabendo-se que para cada 1 tonelada de cana-de-açúcar é gerada aproximadamente 250 Kg (50% de umidade) de bagaço (BERGMANN et al., 2018; CHANDEL et al., 2012), e com isso é prevista a geração de 142,1 milhões de toneladas desse importante subproduto para a safra em questão.

1.2) Biomassa, composição da cana-de-açúcar e enzimas envolvidas em sua degradação

O termo biomassa lignocelulósica é designado para todo material orgânico de origem vegetal como matérias primas e resíduos agrícolas (lenha, grama e folhagens) cuja constituição básica é formada por 3 componentes principais: celulose, hemicelulose e lignina (LIU et al., 2019a).

A principal biomassa residual gerada no Brasil é o bagaço de cana-de-açúcar (gimnosperma gramínea com variedades pertencentes ao gênero Saccharum). Esse resíduo apresenta composição média de 32-55% celulose; 19-32% hemicelulose; e 19-32% lignina. Possui um elevado potencial biotecnológico, pois a cada tonelada pode render aproximadamente 287 litros de etanol 2G (LIU et al., 2019a; SANTOS et al., 2020; SILVEIRA; VANELLI; CHANDEL, 2018).

No entanto, devido à forte interação entre os 3 componentes principais e da alta recalcitrância (resistência a tratamentos físicos, químicos e biológicos) a ação enzimática em conjunto com algum tipo de pré-tratamento é imprescindível para o processo (SHARMA GHIMIRE et al., 2016). É nesse contexto que o emprego das chamadas CAZymes (enzimas ativas em carboidratos), catalogadas no banco de dados CAZy (CANTAREL et al., 2009), tem desempenhado papel fundamental para a desconstrução dos componentes da biomassa lignocelulósica durante a etapa de sacarificação, como pode ser conferido na Figura 3.

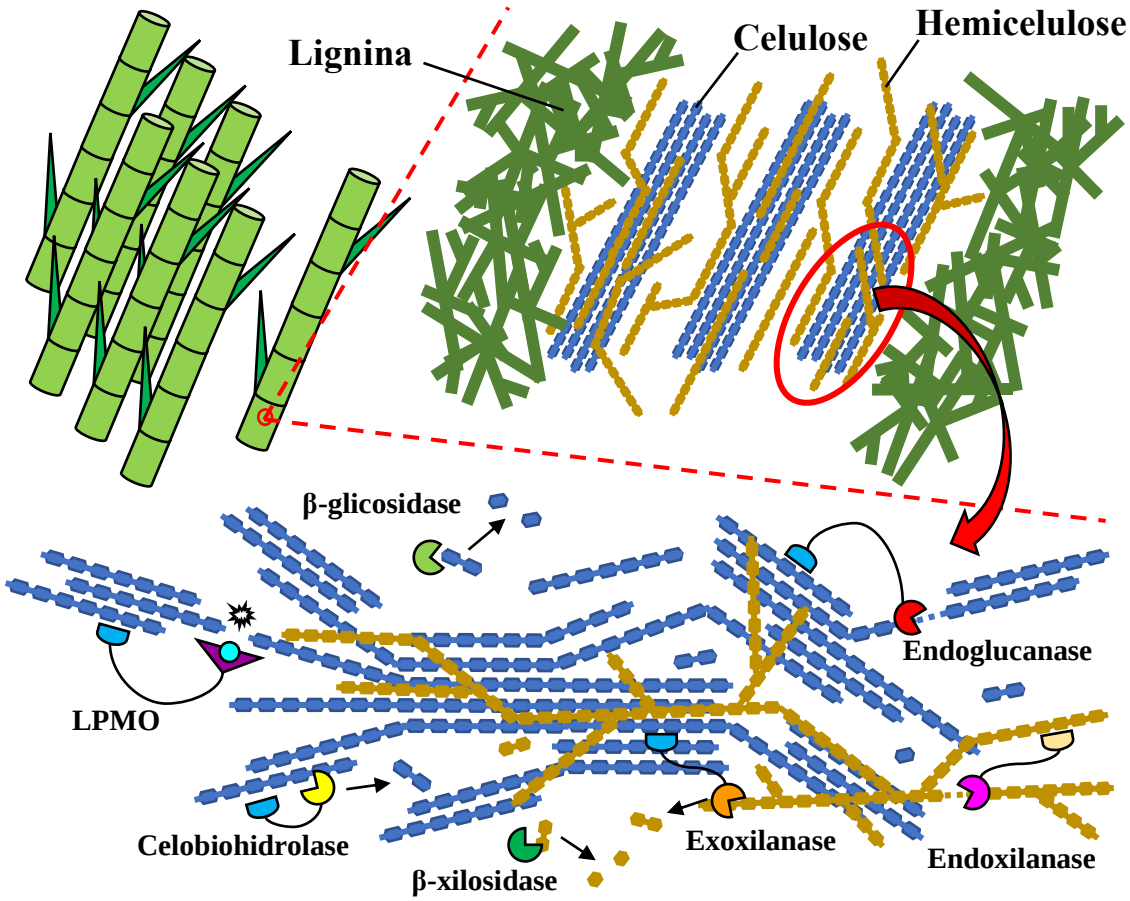

Figura 3. Ilustração ampliada dos principais constituintes da cana-de-açúcar (parte superior), bem como de importantes enzimas envolvidas na degradação de seus polissacarídeos estruturais (parte inferior). Nessa figura, para simplificar, apenas polímeros de D-xilose foram utilizados para representar a xilana e consequentemente a própria hemicelulose. As enzimas em destaque não necessariamente apresentam CBMs (módulos de ligação aos carboidratos). Fonte: autoria própria.

A celulose é o componente da biomassa lignocelulósica de maior predominância, e de fato o polímero natural mais abundantemente encontrado na Terra. Constituído unicamente por monômeros de D-glicose (mais de 10.000 subunidades) ligados através de ligações glicosídicas do tipo β(1→4), apresenta fórmula geral $(C_6H_{12}O_5)_n$ e trata-se de um homopolímero capaz de realizar diversas ligações de hidrogênio tanto intramoleculares entre seus grupamentos hidroxila, como intermoleculares entre os mesmos grupamentos de moléculas adjacentes. Por causa dessa forte interação (cerca de 6-8 moléculas de celulose), as chamadas microfibrilas unem-se resultando em macrofibrilas altamente lineares e coesas que conferem à celulose resistência mecânica, impermeabilidade e insolubilidade a diversos solventes além da água (ABRAHAM et al., 2020; LIU et al., 2019a; LORENCI WOICIECHOWSKI et al., 2020; SANTOS et al., 2020).

Apesar de ser relativamente cristalina, a celulose possui regiões de menor cristalinidade sobre as quais enzimas hidrolíticas como as celulases clássicas (endoglucanases, celobiohidrolases e β-glicosidases) são mais ativas (LIU et al., 2020; LORENCI WOICIECHOWSKI et al., 2020; YOO et al., 2020; ZOGHLAMI; PAËS, 2019). Por outro lado, em regiões de maior cristalinidade, enzimas como as LPMOs, as quais serão apresentadas no capítulo seguinte, mostram-se mais efetivas (HEMSWORTH et al., 2014; YOO et al., 2020).

De modo geral, a hidrólise da celulose ocorre pela ação sinérgica de 3 principais classes de enzimas: as endoglucanases (EGs) (E.C. 3.2.1.4) que clivam ligações glicosídicas β(1→4) em regiões internas do polímero e geram novas extremidades redutoras; as exoglucanases ou celobiohidrolases (CBHs) que atuam clivando as mesmas ligações em suas extremidades redutoras (tipo I) (E.C. 3.2.1-) e não redutoras da cadeia (tipo II) (E.C. 3.2.1.91) liberando moléculas de celobiose; e β-glucosidades (BGs) (E.C. 3.2.1.21) que clivam as ligações β(1→4) da celobiose e de outros glico-oligômeros solúveis promovendo a liberação de D-glicose (COTA et al., 2015; TETER; SUTTON; EMME, 2014; WANG et al., 2020).

A hemicelulose trata-se da camada polissacarídica heteropolimérica adjacente às fibras de celulose. De natureza amorfa e estrutura altamente variável rica em ramificações, é constituída por monômeros de D-xilose, D-glicose, L-arabinose, D-galactose, D-manose, ácido D-glucurônico e ácido D-4-O-metil-glucurônico (500-3000 subunidades). Dentre as principais estruturas encontradas, que incluem xilanas, xiloglucanas, arabinoxilanas e galactoglicomananas a maioria delas apresentam em comum esqueletos principais majoritariamente formados por ligações β(1→4) entre as moléculas de D-xilose, monômero mais abundantemente encontrado na hemicelulose (GIBSON, 2012; LIU et al., 2019b; MALGAS et al., 2019; PACKAGING, 2020; PHAKEENUYA et al., 2020; ULAGANATHAN et al., 2015).

Devido ao menor nível organizacional quando comparada à estrutura da celulose, a fração hemicelulósica oferece baixa resistência a ação da maioria dos pré-tratamentos aplicáveis, sendo consideravelmente removida durante essa etapa nas biorrefinarias (MAGA et al., 2019; SANTOS et al., 2020). Apesar de não possuir estrutura uniforme, sua hidrólise também ocorre de maneira sinérgica envolvendo enzimas como endoxilanases (E.C. 3.2.1.8), exoxilanases (E.C. 3.2.1.8 e E.C. 3.2.1.156) e β-xilosidases

(E.C. 3.2.1.37), as quais de maneira análoga às celulases atuam nas estruturas em seu interior, extremidades (ambas) e dímeros ou oligômeros de D-xilose liberados, respectivamente (CARVALHO et al., 2009; MALGAS et al., 2019; MAMO, 2019; ULAGANATHAN et al., 2015).

Além dessas enzimas que promovem a degradação das cadeias principais, há também a participação daquelas que atuam nas ramificações e removendo grupos químicos adicionados, as quais no caso das xilanas e xiloglucanas são a α-glucuronidase (E.C. 3.2.1.131) que atuam na hidrólise das ligações α(1→2) com ácido D-4-O-metil-glucurônico; a acetilxilana esterase (E.C. 3.1.1.72) na clivagem de ligações éster com grupos acetil nas as posições 2 e 3; a α-arabinofuranosidase (E.C. 3.2.1.55) na quebra das ligações α(1→2) ou α(1→3) com unidades ou cadeia de L-arabinoses pelas extremidades não redutoras, ou a α-arabinase (E.C. 3.2.1.99) que atua clivando ligações α(1→5) internas entre as L-arabinoses; e a ferruloil esterase (E.C. 3.1.1.73) na remoção de resíduos de ácido ferrúlico unidos por ligação éster à posição 5 de L-arabinoses (MALGAS et al., 2019; MAMO, 2019; MELLO et al., 2017; PACKAGING, 2020; PHAKEENUYA et al., 2020; ULAGANATHAN et al., 2015).

As galactoglicomananas são encontradas em gimnospermas (12-15% da composição), cujo esqueleto principal é composto majoritariamente por unidades de D-manose com presença intercalante menos frequente de unidades D-glicose, ambas unidas por ligações β(1→4). As principais ramificações são compostas por unidades de D-galactose unidas por ligações α(1→6). As principais enzimas que degradam essas estruturas são a α-galactosidase (E.C. 3.2.1.22), que atuam sob as extremidades não redutoras promovendo a liberação de D-galactose ou galacto-oligossacarídeos; a endomananase (E.C. 3.2.1.78) agem sob ligações β(1→4) randômicas e internas do esqueleto de D-manose fragmentando sua estrutura em polímeros menores, e β-manosidases (E.C. 3.2.1.25) atuam nessas mesmas ligações porém sob extremidades não redutoras de pequenos mano-oligossacarídeos levando a produção de unidades de D-manose livres (CARVALHO et al., 2009; DE VRIES; VISSER, 2001; MALGAS et al., 2019; MELLO et al., 2017; ULAGANATHAN et al., 2015).

A lignina é o segundo biopolímero mais abundantemente encontrado na Terra, ficando atrás apenas da celulose. Conforme pode ser observado na Figura 4, a lignina consiste em um heteropolímero amorfo e complexo composto por estruturas repetitivas

tanto aromáticas como alifáticas designadas fenilpropanoides (C3C6) metoxilados que são os álcoois coniferílicos, sinapílicos e p-cumarílico. Quando tais unidades encontram-se incorporados à estrutura, passam a ser identificadas como guaiacil (G); siringil (S); e p-hidroxifenil (H), respectivamente. A variação da proporção desses três compostos acarreta em diferenças nas propriedades da lignina (GIL-CHÁVEZ et al., 2019; NGUYEN et al., 2020).

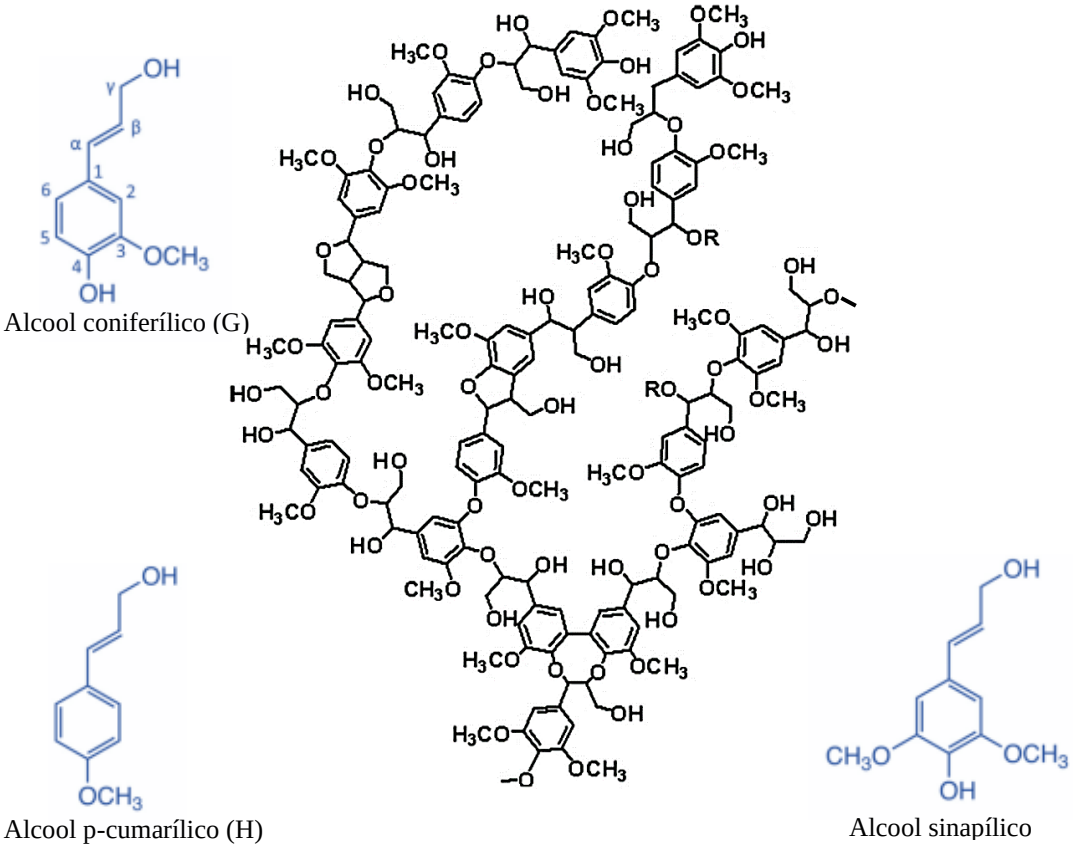

Figura 4. Modelo representativo da estrutura da lignina e suas principais subunidades. Fonte: figura adaptada de Gil-Chávez et al., 2019 e http://www.icfar.ca/lignoworks/content/what-lignin.html.

Apesar do petróleo ser a maior fonte de compostos aromáticos para a produção de produtos derivados, a lignina trata-se da maior fonte renovável existente, e por isso é de interesse tanto econômico como industrial. Pode ser utilizada, dentre outros, para produção de produtos químicos, aditivos alimentares, fármacos, estabilizantes de emulsão, carreadores de pesticidas, bioplásticos e biocompósitos (GIL-CHÁVEZ et al., 2019; HARRIS et al., 2018; YOO et al., 2020; ZHANG et al., 2020).

De maneira geral, dentre as enzimas mais importantes que atuam em sua degradação, destacam-se as chamadas enzimas modificadoras da lignina (LME), incluindo as lignina peroxidases (LiPs) (EC 1.11.1.14), peroxidase versáteis (VPs) (EC

1.11.1.16) e manganês peroxidases (MnPs) (1.11.1.13), sendo essas dependentes de H_2O_2; e também as lacases (E.C. 1.3.10.2), consideradas as mais importantes. Tais enzimas apresentam centros metálicos, que uma vez oxidados, realizam ataques às unidades fenólicas abundantemente encontradas na estrutura da lignina oxidando-as e gerando assim na maioria dos casos espécies radicalares. Esses culminam com a fragmentação da mesma em unidades menores devido às reações de propagação que ocorrem até que a etapa de terminação (extinção das espécies com elétrons desemparelhados) seja atingida. Atualmente, as chamadas enzimas auxiliares de degradação da lignina (LDA) tem ganhado maior destaque nas biorrefinarias. Essas enzimas, apesar de não serem capazes de degradar a lignina isoladamente, são necessárias para auxiliar na atuação das demais, dentre as quais destacam-se as glioxal oxidases (E.C. 1.2.3.5); álcool aril oxidases (E.C. 1.1.3.7); piranose 2-oxidases (E.C. 1.1.3.10), que auxiliam na produção de H_2O_2; e celobiose desidrogenases (E.C. 1.1.99.18) e glicose desidrogenases (E.C. 1.1.99.10) que atuam na mediação das reações de oxidorredução (CARVALHO et al., 2009; JANUSZ et al., 2017; SHARMA; AGGARWAL, 2020; ZHANG et al., 2020).

1.3) LPMOs: características principais, famílias conhecidas e mecanismos de ação propostos

As LPMOs, denominadas mono-oxigenases líticas de polissacarídeos são metaloenzimas cuja ação se soma ao arsenal de enzimas já pré-existentes capazes de atuar sobre resíduos lignocelulósicos. As LPMOs foram em um primeiro momento classificadas como módulos de ligação à quitina e endoglucanses fracas pertencentes às antigas famílias CBM33 e GH61, as quais passaram a ser designadas AA10 e AA9, respectivamente (BISSARO et al., 2020; VAAJE-KOLSTAD et al., 2017; ZHANG, 2020; ZHOU; ZHU, 2020).

Atualmente, são classificadas em 8 famílias diferentes, e englobam as AA9, AA11, AA13, AA14, AA16 e AA17 de origem principalmente eucariótica; as AA10 de origem bacteriana e viral e até mesmo vegetal, e as AA15 oriundas de eucariotos incluindo artrópodes. Diferindo das demais enzimas hidrolíticas clássicas, ilustradas anteriormente na Figura 3, as LPMOs são dotadas de um mecanismo oxidorredutivo com atuação principalmente sob regiões cristalinas de substratos polissacarídicos, o qual por sua vez não somente facilita a ação em conjunto de outras enzimas, como também pode

intensificar a atividade das mesmas (COURTADE et al., 2017; FILIATRAULT-CHASTEL et al., 2019; SABBADIN et al., 2021; VAAJE-KOLSTAD et al., 2017; ZHOU; ZHU, 2020).

De acordo com a literatura, as LPMOs são ativas em uma ampla gama de substratos incluindo celulose, xiloglucanas, glucomanas, β-glucanas, quitina, amido e inclusive xilana. Na maioria dos substratos, são capazes de realizar clivagem da ligação glicosídica apenas a partir da oxidação do carbono C1, contudo no caso dos polímeros ricos em D-glicose unida por ligações β(1→4) como a celulose, as enzimas da família AA9 podem atuar tanto na posição C1 resultando em lactonas que se convertem em ácidos aldônicos (extremidade redutora), como também em C4 originando cetoaldoses (extremidade não redutora). Para cada ligação clivada é gerada uma metade oxidada e outra não oxidada, como pode ser visto na Figura 5 (BISSARO et al., 2020; FRANDSEN; LO LEGGIO, 2016; MUSADDIQUE et al., 2020; VAAJE-KOLSTAD et al., 2017; ZHOU et al., 2019).

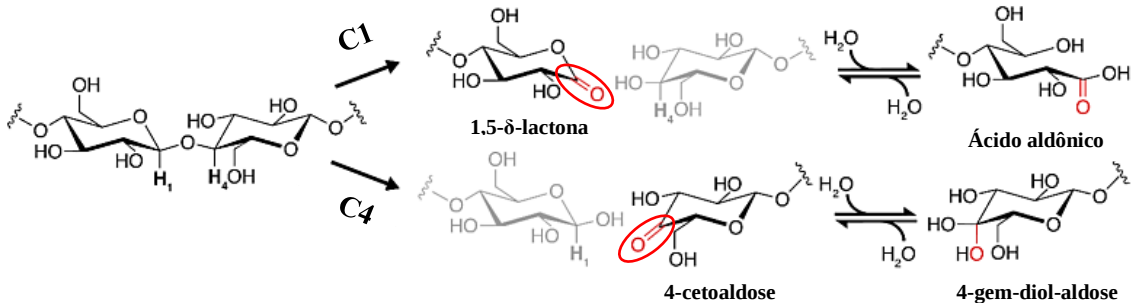

Figura 5. Produtos resultantes da oxidação de uma AA9 em C1 ou C4, com ênfase nas oxidações introduzidas, indicadas em vermelho. Nessa ilustração são apresentadas as duas extremidades geradas em ambos os casos com a quebra da ligação glicosídica, com destaque para as metades oxidadas suas respectivas formas hidratadas com as quais encontram-se em equilíbrio químico. Fonte: figura adaptada de Chylenski *et al*., 2019.

As principais características estruturais comuns a quaisquer LPMOs são: (1) a braçadeira de histidina, uma estrutura catalítica na qual um átomo de Cu^{2+} (centro metálico) encontra-se ligado em T a 3 átomos de nitrogênios, sendo 2 deles provenientes do anel e cadeia lateral da histidina N-terminal, e o outro oriundo da cadeia lateral de uma segunda histidina; (2) a necessidade de um redutor como o ácido ascórbico ou enzimas como a celobiose desidrogenase para doar elétrons e ativar o centro metálico; (3) a presença de co-substrato, que podem ser moléculas de O_2 ou H_2O_2; (4) sítio ativo de topologia achatada formados por núcleos contendo de 7 a 9 folhas-β antiparelelas em

conformação de sanduíche e interligando por loops; e (5) a presença não obrigatória de um ou mais módulos de ligação aos substratos como as CBMs em suas estruturas (BERTINI et al., 2018; BISSARO et al., 2020; CIANO et al., 2018; COURTADE et al., 2017; FILIATRAULT-CHASTEL et al., 2019; VAAJE-KOLSTAD et al., 2017).

Com relação a estrutura geral das mesmas, apresentam diversos loops, como pode ser verificado na Figura 6, a qual permite conferir algumas das principais diferenças estruturais entre as famílias AA9 e AA10, as duas mais ostensivamente estudadas.

O loop L2 conservam sequências importantes para a manutenção da atividade, os quais em famílias já bem estudadas como a AA9 está localizado entre as folhas β1 e β2, e entre β1 e β3 no caso da AA10 (VAAJE-KOLSTAD et al., 2017; ZHOU; ZHU, 2020). De acordo com dados da literatura, enzimas das famílias AA9, AA13, AA14 e AA16 apresentam os loops adicionais LC (próximo à extremidade C-terminal) e LS (curto), os quais também estão associados à especificidade das mesmas (FILIATRAULT-CHASTEL et al., 2019). Em algumas LPMOs como as AA9s por exemplo, existem ainda um loop L3 entre as folhas β3 e β4, no qual encontra-se inserida a histidina não terminal coordenada ao Cu^{2+}; e um loop L8 localizado entre as folhas β5 e β6 no qual localizam-se dois importantes resíduos catalíticos conservados, uma histidina e uma glutamina que participam da esfera de coordenação secundária. Acredita-se que todos os loops influam na especificidade e regiosseletividade das LPMOs por meio do estabelecimento de interações fracas, principalmente entre os resíduos aromáticos neles presentes com os anéis dos substratos polisssacarídicos (BERTINI et al., 2018; HEMSWORTH et al., 2014; SPAN et al., 2017; VAAJE-KOLSTAD et al., 2017; ZHOU et al., 2019; ZHOU; ZHU, 2020).

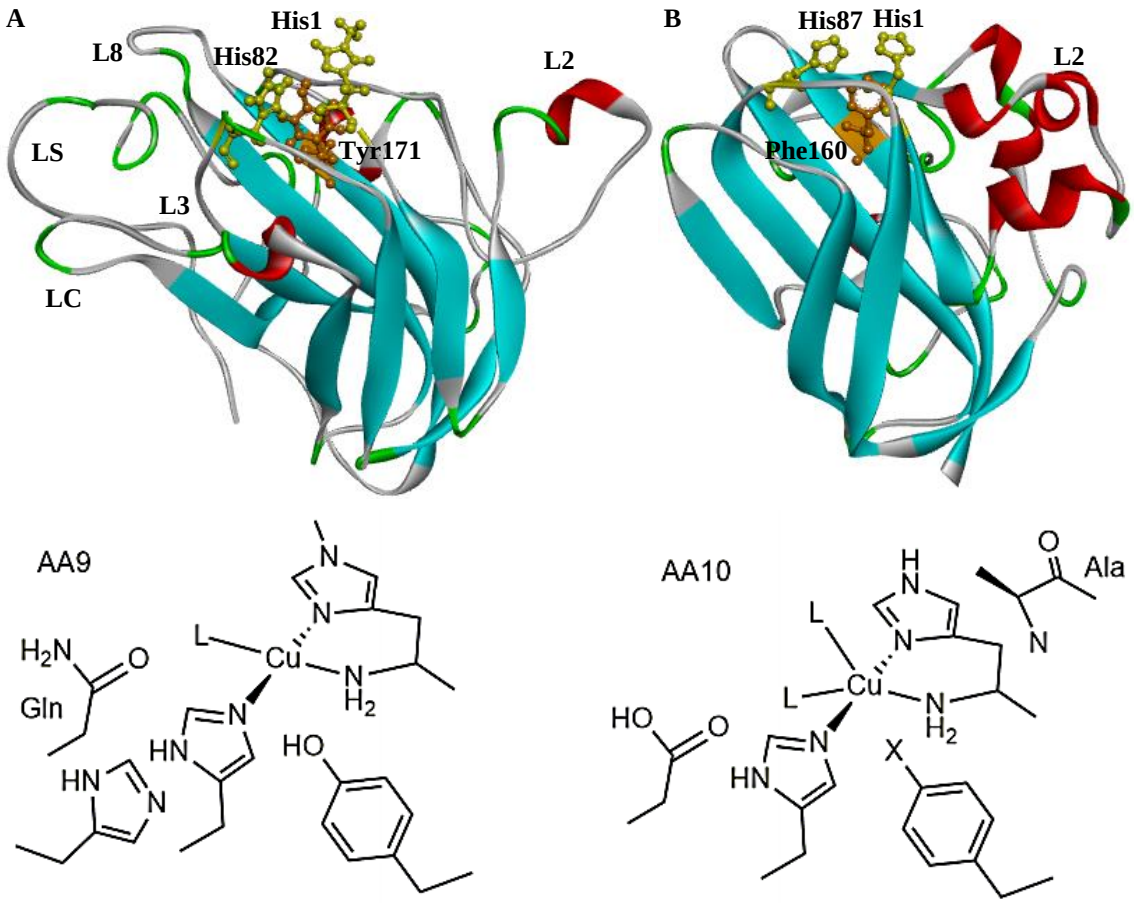

Figura 6. Estrutura tridimensional da AA9 *Nc*LPMO9M (PDB: 4EIS) (A) e da AA10 CBP21 (PDB: 2BEM) (B). As histidinas e resíduos aromáticos das braçadeiras estão indicados em amarelo e laranja, respectivamente. Abaixo estão representadas as estruturas químicas dos principais resíduos coordenados às braçadeiras de histidina das famílias AA9 e AA10, tal que X pode ser H ou OH. Figura adaptada de Vaaje-Kolstad *et al*., 2017 e Ciano *et al*., 2018.

As enzimas AA9 (899 catalogadas), como já discutido anteriormente, são secretadas principalmente por fungos e ativas em celulose e substratos ricos em ligações β(1→4) entre unidades de D-glicose, sendo categorizadas como PMO1, PMO2 e PMO3 quando são ativas em C1, C4 e C1/C4, respectivamente (FILIATRAULT-CHASTEL et al., 2019; HEMSWORTH et al., 2014; VAAJE-KOLSTAD et al., 2017). Há ainda as PMO3* ativas em C1. As AA9s tipicamente apresentam coordenado ao Cu^{2+} uma tirosina, e nelas a presença do loop L2 está associado diretamente com a regiosseletividade das LPMOs sob as posições C1 ou C4, de modo que a remoção de um resíduo conservado de tirosina já é responsável por ocasionar a perda de atuação sobre C4 (VU et al., 2014a; ZHANG, 2020). Recentemente foi demonstrado que a AA9 *Ct*PMO1 é capaz de oxidar a ligação glicosídica tanto nas posições C1 e C4 levando à quebra do polímero como também na posição C6. Apesar de ainda não ser muito claro, é

possível que ocorra a conversão a ácido glucurônico por outra enzima, facilitando assim uma posterior remoção pela ação de uma polissacarídeo liase pertencente à família 20 (PL20) (CHEN et al., 2018; ZHANG, 2020). Nas enzimas AA9, existem dois motivos conservados que são a sequência Hx_nGP para a histidina não terminal e QxYxxC para a tirosina da braçadeira de histidina, no qual o átomo de Cu^{2+} tipicamente se encontra numa geometria de coordenação octaédrica (VAAJE-KOLSTAD et al., 2017; VU et al., 2014a).

As AA10 (8099 catalogadas) produzidas por bactérias, vírus e até mesmo espécies vegetais, são ativas em substratos como celulose e quitina. Diferentemente das AA9, apresentam na maioria dos casos uma fenilalanina coordenada à braçadeira ao invés de uma tirosina e atividade catalítica apenas na posição C1 das ligações glicosídicas. Além disso o cobre encontra-se coordenado aos ligantes em geometria do tipo bipiramidal trigonal (HEMSWORTH et al., 2014; VAAJE-KOLSTAD et al., 2017). Localizado em seu loop L2, responsável pela especificidade das mesmas, encontram-se os motivos conservados Y(W)EPQSVE ou Y(W)NWFGVL quando ativas em quitina ou celulose, respectivamente (ZHOU et al., 2019).

Com relação as demais famílias, as AA11, AA13, AA14, AA16 e AA17 são majoritariamente de origem fúngica e ativas sobre as ligações β(1→4) da quitina; α(1→4) e α(1→6) do amido; β(1→4) da xilana envolvendo fibras celulósicas; β(1→4) da celulose; e α(1→4) da pectina, respectivamente (COUTURIER et al., 2018; FILIATRAULT-CHASTEL et al., 2019; HEMSWORTH et al., 2014; SABBADIN et al., 2021; VU et al., 2014b). As AA16s diferem das AA9s em termos de sequência e estrutura, de modo que a *Af*AA16 não apresenta hélices, apenas um núcleo rico em folhas-β e loops formados por alças (MUSADDIQUE et al., 2020). As AA15 foram as primeiras LPMOs encontradas em artrópodes e podem ser ativas tanto em celulose quanto em quitina, como é o caso da enzima *Td*AA15A (SABBADIN et al., 2018). As AA17, por outro lado, são LPMOs exclusivamente encontradas em fungos fitopatogênicos e atuam como fatores de virulência auxiliando no processo invasivo através da quebra do esqueleto de pectina da parede celular das plantas (SABBADIN et al., 2021).

Atualmente, aceita-se que o co-substrato utilizado pelas LPMOs possam ser tanto moléculas de O_2, atuando propriamente como uma monooxigenase, ou então H_2O_2, atuando como uma peroxigenase (FORSBERG et al., 2019). Dessa forma, na Figura 7 a seguir, são exibidas todas as reações associadas com as LPMOs ao longo do ciclo ativo das mesmas sob uma cadeia celulósica genérica.

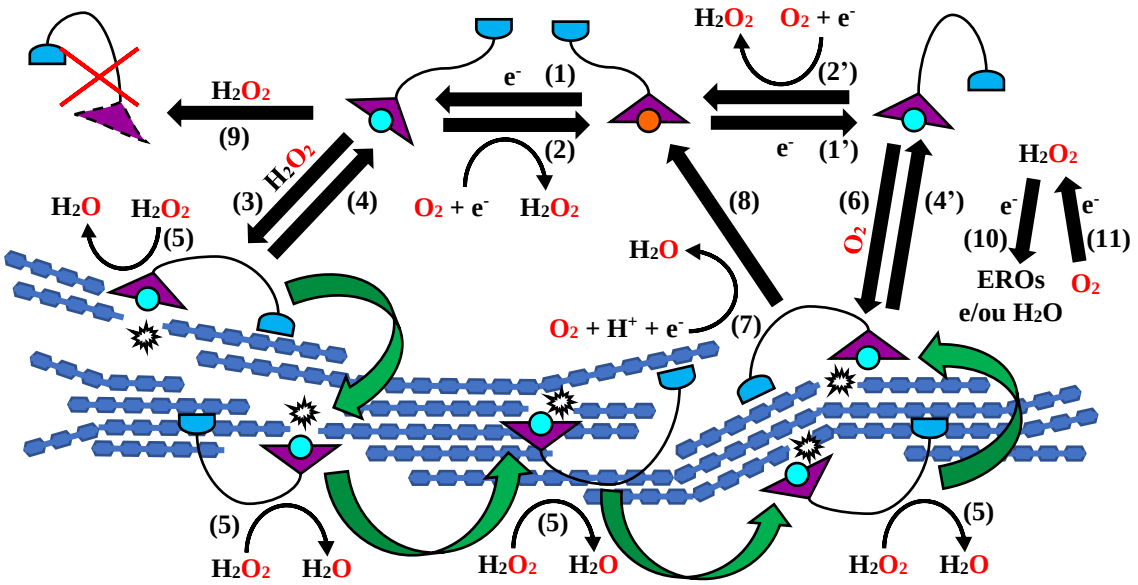

Figura 7. Esquema simplificado de atuação das LPMOs na degradação da celulose e principais reações paralelas envolvidas. As setas verdes representam um percurso hipotético da enzima ao longo de seu ciclo ativo. Legenda: 1 – Reação iniciadora da LPMO, marcada pela redução do Cu^{2+} (círculo laranja) para Cu^{+} (círculo azul claro) mediada por um doador externo; 2 – Redução do O_2 presente a H_2O_2 pela LPMO na ausência de substrato; 3 – Ligação da LPMO à celulose usando H_2O_2 como co-sustrato; 4 – Desacoplamento da enzima com o substrato; 5 – Oxidação da ligação glicosídica utilizando-se H_2O_2; 6 – Ligação da LPMO à celulose usando O_2 como co-sustrato; 7 – Oxidação da ligação glicosídica utilizando-se O_2; 8 – Desacoplamento da LPMO reoxidada após o término da reação; 9 – Inativação da enzima desligada do substrato devido a oxidação de resíduos importantes mediada por H_2O_2; 10 – Redução do O_2 a H_2O_2; 11 – Redução do H_2O_2 a água ou espécies reativas de oxigênio. A LPMO aqui representada em roxo apresenta um CBM em sua estrutura (não obrigatório). Fonte: autoria própria.

Como já mencionado, a oxidação promovida pelas LPMOs é dependente de H_2O_2 ou O_2, porém as enzimas assim como os co-substratos podem participar de uma série de outras reações paralelas. Considerando-se a utilização do H_2O_2 (3) (modo peroxigenase), observa-se que após a ocorrência da reação iniciadora (1), na qual há a redução do centro metálico para Cu^{+}, a LPMO torna-se ativa e uma vez nesse estado é capaz de oxidar diversas ligações glicosídicas (5) até eventualmente desacoplar do substrato (4) e reagir com o O_2 dissolvido no meio (modo oxidase), gerando mais H_2O_2 e reoxidando o metal para Cu^{+} (2); ou então até ser inativada devido à ação oxidativa do H_2O_2 em resíduos catalíticos (9) (CHYLENSKI et al., 2019; FORSBERG et al., 2019).

No caso da utilização do O_2 (modo oxigenasse) (6), após a redução do metal ocorrida na reação iniciadora (1'), a LPMO liga-se ao substrato e é capaz de oxidar a

ligação glicosídica (7), contudo requer a doação de um elétron adicional proveniente de um redutor externo. Ao final da reação com O_2, a enzima retorna ao estado oxidado inicial (8) e pode recomeçar o ciclo, contudo necessita de quantidades estequiométricas de redutor para manter-se ativa, diferentemente de quando se utiliza o outro substrato. Vale destacar que a enzima nesse caso também pode desacoplar (4'), reoxidar sem catalisar a clivagem (2') e até sofrer inativação posteriormente, como indicado em (9). Ocorrem ainda reações paralelas envolvendo a oxidação do doador de elétron como a redução do O_2 a H_2O_2 (10); e ainda a redução do H_2O_2 a água e/ou espécies reativas de oxigênio (EROs) (11), as quais também podem causar a inativação da enzima. Apesar dos mecanismos não estarem 100% elucidados, as LPMOs podem atuar utilizando ambos os co-substratos de maneira alternada no meio reacional (BERTINI et al., 2018; CHYLENSKI et al., 2019; FORSBERG et al., 2019).

1.4) *Aspergillus fumigatus*, enzimas e análise da LPMO *Af*AA9_B

O *Aspergillus fumigatus* é uma espécie de fungo mesofílica e saprofítica capaz de degradar matéria orgânica e crescer em temperaturas acima de 55°C, suportando temperaturas de até 70 °C. De comportamento reprodutivo predominantemente assexuado, produz esporos (ou conídeos) verde escuros com cerca de 2–3 µm de diâmetro em seus conidióforos, os quais conferem igual coloração à suas colônias (LATGE, 2001), como pode ser conferido na Figura 8 abaixo.

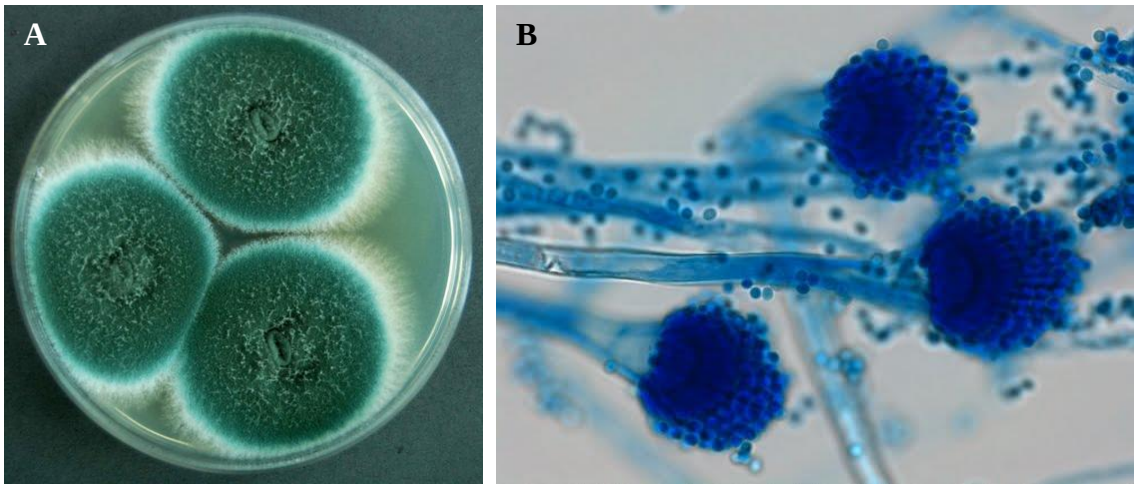

Figura 8. Imagens de cultivo de *Aspergillus fumigatus* em placa (A) (fonte: http://fungi.myspecies.info/file-colorboxed/941) e de microscopia (B) (fonte: https://www.aspergillus.org.uk/wp-content/uploads/2018/04/A.-fumigatus-conidia.jpg) com ênfase na estrutura dos conidióforos.

Por outro lado, o fungo em questão é reconhecido também por ser um dos principais seres patogênicos responsáveis pela ocorrência de infecções hospitalares. Devido à presença ubíqua de seus esporos pelo ar, é capaz de provocar desde alergias de menor periculosidade até quadros mais graves como a aspergilose invasiva (AI) principalmente em pacientes imunocomprometidos (CHO et al., 2017; MALACCO et al., 2019; NAKANO et al., 2020). Por conta de ocasionar sérios danos aos tecido pulmonar e da crescente resistência ao antibiótico mais utilizado para o tratamento (drogas azólicas), a taxa de letalidade em pacientes acometidos de IA oscila na faixa de 50-100%, baseado em dados registrados (LESTRADE et al., 2019; NAKANO et al., 2020).

A utilização do extrato enzimático produzido por microrganismos encontrados no solo é uma prática comumente adotada em bioprocessos das mais diferentes áreas, tais como na agricultura; obtenção de ácidos orgânicos, solventes, aminoácidos, lipídeos, bioplásticos e coquetéis enzimáticos; geração de energia e biocombustíveis; e nas indústrias de papel, detergentes, alimentícia (animais e humanos) e têxtil (SAHOO et al., 2020). No caso específico das biorrefinarias que produzem etanol a partir da biomassa lignocelulósica, são necessários fungos, bactérias ou actinobactérias que secretem quantidades significativas de enzimas principalmente celulolíticas, capazes de atuarem na desconstrução de seus componentes em açúcares simples passíveis de serem convertidos pela levedura *Saccharomyces cerevisiae* (MAGA et al., 2019; MUSADDIQUE et al., 2020; SAHOO et al., 2020; SAWANT; SALUNKE; KIM, 2015). Em específico, fungos do gênero *Aspergillus* em geral são considerados importantes degradadores de biomassa lignocelulósica e em decorrência disso, são exemplos de espécies amplamente empregadas pelas indústrias para a produção de enzimas e outros bioprodutos (ADAV; RAVINDRAN; SZE, 2015).

Nesse contexto, o fungo *Aspergillus fumigatus* torna-se atrativo pois apesar de patogênico, é capaz de secretar um extrato rico em celulases equiparável ao do *Trichoderma reesei*, fungo amplamente utilizado para a produção de coquetéis enzimáticos comerciais. Comparativamente, enquanto o fungo *T. reesei* é capaz de secretar 200 GHs diferentes e possui apenas 16 genes codificantes de hemicelulases em seu genoma, o *A. fumigatus* apresenta 263 GHs e 36 genes de hemicelulases (ADAV; RAVINDRAN; SZE, 2015). O extrato bruto da cepa de *A. fumigatus* NITDGPKA3 apresenta atividade celulolítica total de aproximadamente 2,4 U/mL quando obtido na presença de palha de arroz em meio alcalino (MUSADDIQUE et al., 2020). A cepa de

Aspergilus fumigatus LF9 por sua vez demonstra ser capaz de secretar diferentes conjuntos de enzimas diante da presença de variadas fontes de carbono. Na presença de xilana, a atividade xilanolítica mostrou-se elevada atingindo quase 10 U/mL ao passo que na presença de celulose e amido houve prevalência das atividades de endoglucanase, registrando-se valores de aproximadamente 4 U/mL e 8 U/mL, respectivamente (ADAV; RAVINDRAN; SZE, 2015).

Baseado em resultados prévios obtidos por nosso grupo de pesquisa, quando incubado na presença de bagaço de cana-de-açúcar explodido (SEB) por 24 horas, a cepa de *Aspergillus fumigatus* Af293 secretou um total de 132 enzimas, das quais 58% foram identificadas como CAZymes incluindo a 3 LPMOs distintas pertencentes à família AA9 (DE GOUVÊA et al., 2018). Dentre as LPMOs mencionadas, aquela codificada pelo gene AFUA_4G07850, aqui referida como *Af*AA9_B, mostrou-se também altamente expressa ainda nas primeiras horas de indução. Portanto, tal enzima foi escolhida como objeto central deste estudo, e expressa no organismo *Pichia pastoris* X33 visando-se obter uma maior compreensão acerca de sua ação em conjunto com outras celulases (sob diferentes tipos de biomassas lignocelulósicas), bem como investigar seu potencial para a aplicação em eventuais processos biotecnológicos.

2. Objetivos

O objetivo central desse trabalho foi determinar as propriedades bioquímicas e constantes cinéticas da *Af*AA9_B, bem como avaliar sua atividade quando suplementada com outras celulases sob CMC e diferentes biomassas lignocelulósicas.

3. Material e métodos

3.1) Meios de cultura para o cultivo de *Aspergillus fumigatus*

A cepa de *Aspergillus fumigatus* Af293 (gentilmente fornecida pelo Prof. Dr. Sérgio Akira Uyemura – Faculdade de Ciências Farmacêuticas de Ribeirão Preto) foi inicialmente cultivada em placas contendo meio YAG sólido [2% (m/v) glicose; 1,8% (m/v) ágar; 1% (m/v) suplemento de vitaminas; 0.5% (m/v) extrato de levedura; 0,1% (m/v) solução de elementos traços] até esporular, sendo incubada a 37ºC durante 48 horas. Após raspagem da superfície com solução tampão PBS + 1% Tween 20, realizou-se o inóculo de 2 X 10^6 conídios frescos/mL em meio YNB líquido [5% solução de sais; 0,1% elementos traços; 0,05% extrato de levedura] adicionado de 1% (m/v) frutose seguido de incubação por 16 horas a 37ºC e 200 rpm (pré-inóculo). Em seguida, os micélios foram lavados com H_2O estéril e transferidos para meio YNB líquido contendo 1% (m/v) de bagaço de cana-de-açúcar explodido (SEB) mantido a 37ºC sob agitação de 200 rpm.

3.2) Tratamento do bagaço de cana-de-açúcar (SEB)

O bagaço de cana-de-açúcar explodido, generosamente cedido pelo Prof. Dr. João Atílio Jorge (Faculdade de Filosofia, Ciências e Letras de Ribeirão Preto), foi lavado até a completa remoção de impurezas e açúcares redutores (verificado através do método DNS), seco em estufa a 40 °C e moído em moinho de facas. O bagaço foi autoclavado no momento do preparo dos meios de cultura YNB.

3.3) Procedimentos para a extração e tratamento do RNA total

O micélio formado após a incubação dos meios líquidos contendo SEB foi separado através de centrifugação de 2.050 *g* por 20 minutos, descartando-se o sobrenadante. Após filtração a vácuo, o micélio foi mergulhado em nitrogênio líquido, macerado e recebeu adição de Trizol® (Life Technologies) (1ml/100 mg). Depois de homogeneizar, foi incubado durante 5 minutos a temperatura ambiente, e recebeu adição de clorofórmio (200 µL/mL de Trizol®) e agitou-se vigorosamente. Após centrifugar a 12.000 *g* por 10 minutos a 4ºC, a fase aquosa superior foi coletada e recebeu adição de isopropanol (500 µL/mL de Trizol®). Na sequência, após 10 minutos de incubação em temperatura ambiente, centrifugou-se a 12.000 *g* por 10 minutos a 4ºC e o precipitado

obtido foi lavado com etanol 75% (m/v), seco a temperatura ambiente e solubilizado em água-DEPC. O RNA total extraído foi quantificado no espectrofotômetro NanoDrop 2000 (Thermo Fisher Scientific Inc., Waltham, MA, EUA) e tratado com a enzima RQ1 RNase-Free DNase (Promega) para eliminar traços de DNA residuais.

3.4) Síntese de cDNA

A síntese de cDNA foi realizada a partir do RNAm contido no RNA total tratado, o qual foi submetido a reação de RT-PCR com emprego da enzima transcriptase reversa, utilizando o kit comercial SuperScript® II (Invitrogen), seguindo-se as recomendações do fabricante.

3.5) Reações em cadeia da polimerase (PCR)

As amplificações do gene AFUA_4G07850 foram realizadas de acordo com Saiki *et al*., (1985) e Mezei & Storts, (1994), utilizando-se um Termociclador (Mastercycler Eppendorf®). Para as reações foi empregado 300 ng dos cDNAs sintetizados a uma mistura contendo 0,5 µM de ambos os *primers* descritos na Tabela 1; 0,2 mM dNTPs, 3% DMSO e 20% tampão HF 5X contendo 7,5 mM $MgCl_2$ (volume final de 50 µL). A amplificação ocorreu com a adição de 1,0 U da enzima Phusion® High-Fidelity DNA Polymerase (Thermo Scientific) e foi realizada seguindo-se a ciclagem: 1x 98 ºC por 30 segundos / 30x [98 °C por 10 segundos / 55 °C por 30 segundos / 72 ºC por 1 minuto] / 1x 72 °C por 10 minutos / 4 °C - ∞.

Tabela 1: Sequência dos *primers*

Primer	**Sequência**
Primer Forward **CPEC AFUA_4G07850 A**	5´–<u>CAAAAAACAACTAATTATTCGAAACGAGGAATTCC</u>ATGACTTTGTCCAAGATCAC – 3´
Primer Reverse **CPEC AFUA_4G07850 B**	5´– <u>CAGATCCTCTTCTGAGATGAGTTTTTGTTCTAG</u>AGCGTTGAACAGTGCAGGAC – 3´

OBS: As bases sublinhadas (35 e 33 para os *primers Forward* e *Reverse*, respectivamente) constituem as regiões de sobreposição ao vetor pPICZB após sua digestão.

3.6) Digestão do vetor pPICZB

O vetor de expressão pPICZB, foi digerido [5 µg] usando-se separadamente as enzimas de restrição *Xba*I e *Eco*RI (Invitrogen), conforme recomendado pelo fornecedor (2 horas / 37°C / volume final de 20 µL em 5 tubos).

Para purificar os vetores semidigeridos (com *XbaI*) do meio reacional e evitar interferências na digestão seguinte (com *EcoRI*), os tubos receberam adição de clorofórmio (1:1), foram agitados por 1 min e centrifugados a 1.500 *g* por 10 minutos. A fase aquosa coletada em cada tubos recebeu adição de 200 µL de isopropanol a -20 °C e foi incubada nessa mesma temperatura por 2 horas. Depois de centrifugar novamente a 1.500 *g* por 10 minutos a 4 °C, o sobrenadante foi descartado. O precipitado contido nos tubos foi lavado com 200 µL de etanol 70% e centrifugado nas mesmas condições por 1 minuto. Após descarte do sobrenadante e secagem em temperatura ambiente, os precipitados foram ressuspendidos em água deionizada para volume final de 20 µL.

3.7) Eletroforese, extração de gel e purificação das bandas recortadas

Os produtos de PCR receberam adição de DNA loading buffer 6X (Thermo Fisher Scientific) e Gel Red (Biotium) 1:500 (diluições finais de 1X e 10%, respectivamente), sendo aplicados em gel de agarose 1% para realização de eletroforese com voltagem de 110 V por cerca de 90 min. As bandas foram recortadas e purificadas usando-se QIAquick Gel Extraction Kit (Qiagen). Ao fim, o inserto amplificado e vetor digerido foram eluídos em volumes de 50 µL e quantificados em espectrofotômetro NanoDrop 2000 (Thermo Fisher Scientific Inc., Waltham, MA, EUA).

3.8) Clonagem por polimerase de extensão circular (CPEC)

A ligação do gene AFUA_4G07850 (750 pb) no vetor pPICZB (3328 pb) digerido pelas enzimas *Xba*I *e Eco*RI (ver Figura Suplementar 2), foi realizada pela técnica de CPEC (*Circular Polymerase Extension Cloning*) (QUAN; TIAN, 2011). A reação mediada pela enzima Phusion® High-Fidelity DNA Polymerase (1U em 25 µL de meio reacional) ocorreu na presença de 150 ng do vetor; 67,6 ng de inserto (fração molar de 2:1); 3% DMSO; 0,4 mM dNTPs e 20% tampão HF contendo 7,5 mM $MgCl_2$. A ciclagem utilizada foi: 1x 98ºC por 30 segundos / 35x [98 °C por 10 segundos / 50 °C por 30 segundos / 72 ºC por 2 minutos e 30 segundos] / 1x 72 °C por 10 minutos / 4 °C - ∞.

3.9) Preparo de *E. coli* DH10-β quimiocompetentes

Células de *E. coli* DH10-β foram inoculadas em 10 mL de meio LB líquido [1% (m/v) triptona; 0,5% (m/v) extrato de levedura; 0,05% NaCl], a 37ºC, por 200 rpm, durante 16 horas. Após esse período, inoculou-se em 50 mL de meio SOB [2% (m/v) triptona; 0,5% (m/v) extrato de levedura; 0,05% (m/v) NaCl] e incubou-se nas mesmas condições até atingir uma DO_{600nm} entre 0,4 e 0,6. Posteriormente transferiu-se todo o volume para tubos cônicos, sendo mantidos em gelo por 10 min e em seguida centrifugados a 2.500 *g*, por 10 minutos, a 4ºC. O sobrenadante foi descartado e o precipitado ressuspendido com 16 mL de solução TB resfriada [10 mM solução PIPES (pH 7,0); 55 mM $MnCl_2$; 15 mM $CaCl_2$; 250 mM KCl], sendo mantido em gelo por 10 minutos. Após centrifugação, o sobrenadante foi descartado e o precipitado ressuspendido em 4 mL de solução TB resfriada + 300 µL de DMSO. Após manter em gelo por 10 minutos, alíquotas de 200 µL da suspensão de bactérias foram congeladas em nitrogênio líquido para armazenamento em -80ºC.

3.10) Transformação em *E. coli* DH10-β quimiocompetentes

Para transformação das bactérias DH10-β com o vetor de clonagem, alíquotas de bactérias foram descongeladas e mantidas em gelo. Volumes de 100 µL dessas alíquotas foram transferidas para novos microtubos juntamente com 5 µL do vetor montado com o gene AFUA_4G07850 via CPEC. As misturas foram mantidas em gelo por 30 minutos, seguida de choque térmico em temperatura de 42 °C por 45 segundos. Em seguida foram mantidas novamente em gelo por 3 minutos e adicionadas de 600 µL de meio SOC [2% (m/v) triptona; 0,5% (m/v) extrato de levedura; 0,05% (m/v) NaCl; 2 mM KCl; 10 mM $MgCl_2$; 20 mM glicose], com posterior incubação de 1 hora sob temperatura de 37 °C e agitação de 200 rpm.

Ao final da incubação, com auxílio de alça de Drigalski, as bactérias transformadas foram plaqueadas em meio LB sólido low salt [1% triptona; 0,5% extrato de levedura; 0,5% NaCl; 1,5% ágar] contendo 50 µg/mL zeocina e as placas foram incubadas a 37 °C overnight.

3.11) Checagem das transformações, preparo de estoques e miniprep do vetor recombinante pPICZB::AFUA_4G07850.

Após checagem das placas, as colônias obtidas foram inoculadas em 1 mL de meio LB líquido low salt suplementado com zeocina (50 µg/mL), mantido em incubação overnight a 37ºC. Após confirmação por PCR de colônia (dados não apresentados), as colônias positivas foram preparadas para estocagem a -80 °C (714 µL meio de cultura + 286 µL glicerol 70%) e os vetores recombinantes pPICZB::AFUA_4G07850 foram extraídos utilizando-se o QIAprep Spin Miniprep Kit (Qiagen).

3.12) Análise por sequenciamento

Os vetores extraídos foram preparados para a reação de sequenciamento segundo Sanger *et al*., (1977), utilizando-se as instruções do kit Big Dye® Terminator Cycle Sequencing (Applied Biosystems). As amostras foram sequenciadas no Laboratório de Sequenciamento de Ácidos Nucleicos da FCFRP-USP. Com o auxílio do site Clustal Omega (https://www.ebi.ac.uk/Tools/msa/clustalo/) (SIEVERS; HIGGINS, 2014), mediante alinhamento das sequências obtidas com a ORF do gene AFUA_4G07850 disponível no banco de dados genômico de *Aspergillus fumigatus* CADRE (www.cadre-genomes.org.uk) (Mabey Gilsenan *et al*., 2012), foi possível observar alinhamento de 100% e constatar a ausência de mutações.

3.13) Linearização do vetor pPICZB::AFUA_4G07850 com *Pme*I

Para possibilitar a integração do vetor ao genoma da *P. pastoris* após a etapa de eletroporação, foi realizada a linearização do mesmo [1µg] através da reação de digestão com a *Pme*I (New England BioLabs) seguindo o protocolo do fabricante (37 °C / 1 hora). Após eletroforese, as bandas foram recortadas e purificadas como descrito no ítem 3.7).

3.14) Preparo de *Pichia pastoris* X33 eletrocompetente

A partir de uma cultura prévia de *Pichia pastoris* X33, uma colônia foi selecionada e crescida em 5 mL de meio líquido YPD [1% m/v extrato de levedura; 2% m/v peptona; 2% m/v glicose] mantido a 30 °C, 200 rpm, overnight. Um inóculo de 100 µL desse cultivo foi realizado em 100 mL de novo meio YPD e a incubação foi mantida até a densidade ótica (DO) atingir valores entre 1,3-1,5. As células foram centrifugadas (1.500

g, 4 °C por 5 minutos) e o sobrenadante descartado. Após ressuspender o precipitado em 100 mL de água gelada, as células foram centrifugadas novamente sob mesmas condições, o sobrenadante descartado, e dessa vez ressuspendidas em 50 mL de água gelada. Novamente, centrifugando-se sob mesmas condições, após o descarte do sobrenadante, foi feita a ressuspensão em 4 mL de sorbitol 1M gelado. Desse volume, duas alíquotas de 1,5 mL foram centrifugadas da mesma forma e as células precipitadas foram finalmente ressuspendidas em 200 µL de sorbitol 1M, tornando-se assim competentes e sendo necessário mantê-las em gelo até usá-las para transformação no mesmo dia.

3.15) Transformação em *Pichia pastoris* X33 eletrocompetentes

Para a transformação, 80 µL das células de *P. pastoris* eletrocompetentes foram misturados com 10 µL do vetor pPICZB::AFUA_4G07850 linearizado com a enzima *Pme*I. A mistura foi transferida para uma cubeta de eletroporação de 0,2 cm gelada e a mesma incubada em gelo por 5 minutos. Em seguida, usando-se um eletroporador Gene Pulser Xcell™ (Bio-Rad), aplicou-se um pulso configurado para tensão de 2 kV, capacitância de 25 µF e resistência de 200 Ω. Imediatamente, adicionou-se à cubeta 300 µL de sorbitol 1M gelado e o conteúdo foi cuidadosamente transferido para um tubo, o qual foi incubado a 30 °C por 1 hora e sem agitação. Após essa etapa, foi realizada a semeadura de 200 µL em placas contendo meio YPDS sólido [1% m/v extrato de levedura; 2% m/v peptona; 1,5% m/v ágar; 2% m/v glicose; 1M sorbitol] com zeocina (100 µg/mL), as quais foram incubadas a 30 °C por 3 dias.

3.16) Checagem das transformações e repique das colônias positivas

As colônias identificadas nas placas foram repicadas, crescidas em novas placas contendo YPDS (posteriormente armazenadas a 4 °C) e submetidas a PCR de colônia para confirmação da integração do vetor por recombinação nas mesmas. Diferentemente da PCR realizada no item 3.5, foi preciso solubilizar previamente as colônias em 20 µL de 0,2% SDS, fervê-las a 90 °C por 5 minutos e centrifugá-las (1.800 *g* por 1 minuto) para coletar apenas o sobrenadante contendo o material genético.

3.17) Expressão da enzima *Af*AA9_B em *P. pastoris*

A partir do estoque de colônias de *P. pastoris* transformadas e confirmadas para a presença do gene AFUA_4G07850 integrado em seu genoma (item 3.16), uma única colônia foi selecionada e inoculada em 25 mL de meio BMGY [1% (m/v) extrato de levedura; 2% (m/v) peptona; 10% (v/v) tampão fosfato de sódio 1M - KH_2PO_4 (0,868 M) / K_2HPO_4 (0,132 M); 1% m/v YNB; 0,0004% (m/v) biotina; 1% (v/v) glicerol] incubado overnight à 30 °C e 220 rpm. Na sequência, 2 mL do inóculo foram transferidos para 50 mL de novo meio BMGY sob as mesmas condições até a DO atingir faixa entre 2 e 6.

Para induzir a expressão da enzima *Af*AA9_B, foi feito o inóculo a partir do pellet coletado (via centrifugação de 3000 *g* por 5 min) em 100 mL de meio BMMY [1% (m/v) extrato de levedura; 2% (m/v) peptona; 10% (v/v) tampão fosfato de sódio 1 M; 1% (m/v) YNB; 0,0004% (m/v) biotina; 1% (v/v) metanol], de modo que o valor $D.O._{600nm}$ = 1. A indução foi mantida durante 6 dias à 30 °C e 220 rpm com adições diárias de metanol para manter a concentração final de 1%.

Ao término, o meio de indução foi centrifugado (3000 *g* por 5 min à 4 °C) e o sobrenadante coletado foi concentrado para cerca de 1 mL usando-se tubos filtro de centrífuga Amicon® Ultra-15 (Millipore) com limite de corte para proteínas de 10 kDa (de acordo com instruções do fabricante).

3.18) Purificação da proteína *Af*AA9_B e incubação com Cu^{2+}

O sobrenadante concentrado recebeu adição de tampão fosfato de sódio (pH=7,4) 20 mM + 0,5 M NaCl até completar 20 mL e foi novamente concentrado para cerca de 1 mL para eliminar traços do meio de indução. Após ajustar o volume para 10 mL usando-se o mesmo tampão, foi realizada a sua incubação com 2 mL de resina de níquel equilibrada Ni Sepharose® 6 Fast Flow (GE Heathcare) para purificação da *Af*AA9_B fusionada com uma cauda de histidina (de acordo com recomendações do fabricante). A eluição da LPMO recombinante foi realizada aplicando-se gradiente linear de 0 a 500 mM de imidazol em solução aquosa. Todas as frações da purificação foram coletadas.

Após nova troca de tampão para remoção do excesso de imidazol, a concentração da enzima *Af*AA9_B purificada foi quantificada pelo método de Greenberg (GREENBERG; CRADDOCK, 1982). Posteriormente, foi incubada com solução de

$CuSO_4$ em excesso na proporção molar 1:3, à 4 ºC, durante 30 minutos. Em seguida, a enzima foi submetida a diálise em tampão 20 mM fosfato de sódio (pH=7,4) + 0,5 M NaCl durante 48 horas, à 4 ºC, sob agitação para remoção do excesso de cobre. O tampão da diálise foi substituído a cada 12 horas.

3.19) Eletroforese em gel SDS-PAGE

As amostras proteicas foram submetidas a eletroforese de acordo com Laemmli, (1970). Foram tratadas com tampão de amostra 5X, aquecidas a 98 °C por 5 minutos e aplicadas em gel SDS-PAGE 10% (110V, 90 min) (ver Material suplementar) para visualização das bandas proteicas . Para a revelação, os géis foram corados com solução *Coomassie Brillant Blue G* por 1 hora e descorados em água sob aquecimento moderado.

3.20) Alinhamento da sequência de aminoácidos da *Af*AA9_B com outras AA9s e construção de árvore filogenética

O alinhamento múltiplo da sequência de aminoácidos da *Af*AA9_B com outras AA9s do tipo 3 (C1-C4) previamente descritas na literatura, foi realizado utilizando-se o servidor MAFFT (https://mafft.cbrc.jp/alignment/server/) (KATOH; ROZEWICKI; YAMADA, 2018). Valores de identidade foram determinados através do alinhamento múltiplo pela ferramenta BLAST® (JOHNSON et al., 2008) da base de dados NCBI (https://blast.ncbi.nlm.nih.gov/Blast.cgi) disponibilizados em Tabela Suplementar 1.

Para uma visão mais abrangente, a enzima *Af*AA9_B foi alinhada com outras 25 LPMOs dos 3 principais tipos usando-se configurações padrão do Clustal Omega (https://www.ebi.ac.uk/Tools/msa/clustalo/) (ver Figura Suplementar 3) e a partir do mesmo, uma árvore filogenética radial foi construída utilizando-se o programa online FigTree v.1.4.4 (http://tree.bio.ed.ac.uk/software/figtree/).

3.21) Análise da estrutura e suas modificações: modelagem 3D computacional, CD, ITFE

A modelagem 3D da enzima *Af*AA9_B foi realizada com base em sua sequência de aminoácidos (estrutura primária) com o auxílio do servidor online Phyre2

(http://www.sbg.bio.ic.ac.uk/~phyre2) (KELLEY et al., 2015). Para uma melhor visualização da enzima e comparação com a estrutura cristalizada PDB:5X6A (LO LEGGIO et al., 2018), foi utilizado o programa Discovery Studio 2016 (Dassault Systemes BIOVIA) assim como o algoritmo para predição de estruturas secundárias Kabsch & Sander (KABSCH; SANDER, 1983).

Para realizar as análises de estrutura secundária via dicroísmo circular (CD) foi utilizado o espectropolarímetro JASCO-810. A enzima *Af*AA9_B purificada (com ou sem Cu^{2+}), diluída em tampão fosfato de sódio 20 mM (pH=7,4) + 0,5 M NaCl (ver item 3.18) foi aplicada em tubos filtro de centrífuga Amicon® Ultra-15 (Millipore) com limite de corte para proteínas de 10 kDa. Seguindo-se as recomendações do fabricante, após a completa remoção do NaCl, as amostras foram aplicadas em cubetas de quartzo com 1 mm de espessura na concentração de 0,021 mg/mL em 0,2 mL e aquelas contendo Cu^{2+}, incubadas em termociclador (Mastercycler Eppendorf®) a 25 °C por 24 horas; 50 °C e 60 °C por 24, 48 e 72 horas; e 70 °C por 24 horas. As leituras foram realizadas em quadruplicatas usando-se velocidade de varredura = 50 nm / min, largura de banda = 3 nm e D.I.T. = 1 s. Os espectros médios subtraídos do branco foram convertidos de θ em mdeg (unidade fornecida pelo equipamento) para Δε em $M^{-1}.cm^{-1}$ de acordo com a seguinte equação:

$$\Delta\varepsilon = \frac{\theta . MRW}{d . c . 32980}$$

-OBS: “MRW” é o peso médio residual, definido como o peso molecular da enzima em Da dividido pelo número de resíduos – 1 (para *Af*AA9_B = 114,66); “d” é a distância do caminho ótico em cm; e “c” a concentração em mg/mL. Os percentuais de estruturas secundárias foram determinados com auxílio do servidor gratuito BeStSel (MICSONAI et al., 2018) (Ver Tabela Suplementar 2).

Para as análises de emissão de fluorescência intrínseca de triptofano (ITFE), as amostras submetidas às mesmas condições usadas para o CD foram aplicadas em cubetas de quartzo de 1 cm. Com o auxílio do espectrofluorômetro HITACHI-F4500, foram selecionados comprimentos de onda de 295 nm para excitação e de 300 a 450 nm para detecção da emissão fluorescente. A correção dos espectros médios (quadruplicata) também foi realizada subtraindo-se o espectro do branco.

O valor da Tm aparente (temperatura de fusão) foi determinado através da derivada primeira do gráfico de elipticidade registrada a 205 nm (CD) X temperatura; e através do gráfico de comprimento de onda máximo (ITFE) X temperatura. Os gráficos e cálculos foram realizados usando o software OriginPro 9.0 (OriginLab). Ambos os gráficos foram ajustados usando-se função de Boltzmann e suavizados com filtro Savitzky-Golay (SAVITZKY; GOLAY, 1964).

3.22) Análises de glicosilação

A predição de possíveis sítios de N-glicosilações foi realizada através do servidor NetNGlyc 1.0 (http://www.cbs.dtu.dk/services/NetNGlyc/) e de O-glicosilações através do servidor NetO-Glyc 4.0 (http://www.cbs.dtu.dk/services/NetOGlyc/). No caso da *Af*AA9_B, 1 µg da LPMO foi previamente aquecida a 100 °C por 10 minutos (desnaturação) e submetida a deglicosilação usando-se a enzima Endo H (New England BioLabs), conforme descrito no manual do fabricante (37 °C / overnight).

3.23) Determinação da atividade *Af*AA9_B com substrato cromogênico

A atividade de peroxidase da *Af*AA9_B purificada foi analisada conforme descrito por Breslmayr et al., (2018) com algumas modificações. Para o preparo da mistura reacional, adicionou-se em microplaca de 96 poços 1 mM do reagente cromogênico 2,6-dimetoxifenol (2,6-DMP) (Sigma – Aldrich, St. Louis, MO, EUA), 100 µM de H_2O_2 e quantidades variáveis da enzima *Af*AA9_B em diferentes tampões e valores de pH. Para o branco da reação, a LPMO adicionada foi previamente desnaturada a 99 °C por 30 minutos. A leitura das absorbâncias em 469 nm foi realizada após incubar as reações a 30 °C por 5 minutos. Ver Figura Suplementar 4 para visualizar a reação química.

3.24) Propriedades bioquímicas e determinação de constantes enzimáticas da *Af*AA9_B

A determinação do pH ótimo da *Af*AA9_B (0,25 µM) foi realizado variando-se o pH na faixa de 3,0 – 8,0 em tampão McIlvaine (ácido cítrico-Na_2HPO_4) e de 9,0 – 10,0 com uso de tampão glicina-NaOH 100 mM, em temperatura fixa de 30 °C. A atividade

relativa foi calculada em triplicata considerando-se como 100% o valor máximo obtido (pH=9,0).

A estabilidade da enzima ao pH foi determinada através das medidas em triplicata da atividade residual, após a *Af*AA9_B (0,25 µM) ser pré-incubada (ausência de substrato) sob a mesma faixa de pH de 3,0 – 10,0 à 4 °C (10 µL LPMO + 10 µL tampão). A estabilidade térmica foi determinada de maneira análoga em pH = 9,0 após incubação prévia da enzima na ausência de substrato, sob temperaturas de 50 e 60 °C. Em ambos os experimentos, as reações que ocorreram durante períodos de 24, 48 e 72 horas tiveram seu volume ajustado para 200 µL com adição de tampão (pH = 9,0), substrato e co-substrato. A atividade enzimática obtida sem a pré incubação foi considerada como 100%.

As constantes cinéticas da *Af*AA9_B, como a constante de Michaelis-Menten (K_m), velocidade máxima (V_{max}) e a constante catalítica (k_{cat}) foram determinadas empregando-se concentrações variando entre 0,1 – 10 mM para o substrato 2,6-DMP e entre 1 – 500 mM para o co-substrato H_2O_2. As reações (200 µL) foram realizadas em triplicata e as análises foram realizadas tanto na presença de tampão de fosfato de sódio 50 mM (pH 6,0 com 0,5 µM da LPMO) quanto na de tampão glicina-NaOH 100 mM (pH 9,0 com 0,1 µM da LPMO), ambas na temperatura de 50 °C. Através de análises gráficas, os valores foram determinados por regressão não linear de Michaelis-Menten no software OriginPro 9.0 (OriginLab).

3.25) Efeito de aditivos e inibição por produtos sob a atividade da *Af*AA9_B

Para avaliar o efeito dos íons Mn^{2+}, Co^{2+}, Ca^{2+}, Fe^{2+}, Zn^{2+}, Mg^{2+}, Cu^{2+}, $NH4^{+}$, K^{+} e Ag^{+} e de aditivos como EDTA, SDS, Tween 20, Triton X-100, SLS, β-mercaptoetanol, DTT e DMSO, todos foram adicionados ao meio reacional (200 µL) em concentração final de 5 mM (pH = 9,0). As atividades residuais registradas foram calculadas considerando-se como 100% a atividade observada na ausência dos mesmos.

A análise dos efeitos inibitórios por produtos foi realizada com a adição de glicose (10 – 250 mM) e de celobiose (10 – 100 mM) ao meio reacional (200 µL) contendo a *Af*AA9_B (0,25 µM). Assim como anteriormente, as atividades residuais foram definidas com base na atividade registrada sem a presença dos açúcares, definida como 100%.

3.26) Determinação das atividades da *Af*AA9_B e/ou *Af*Cel6A na presença de CMC em associação com a enzima *Af*-EGL7

Buscando verificar a o efeitos de associações enzimáticas, ensaios com a LPMO *Af*AA9_B foram realizados juntamente com as enzimas *Af*Cel6A (celobiohidrolase) e *Af*-EGL7 (endoglucanase), ambas enzimas recombinantes originárias de *Aspergillus fumigatus* Af293 e caracterizadas por nosso grupo de pesquisa (BERNARDI et al., 2018, 2019, 2021; DE GOUVÊA et al., 2019).

Ensaios combinando a enzima *Af*AA9_B com a *Af*Cel6A foram realizados nas proporções de 10:1, 1:1, 10:10 e 1:10, nas concentrações de 5 e 50 µg/g CMC para cada uma.

As reações na presença de *Af*-EGL7 foram preparadas associando-se 1 µg da endoglucanase com 50 µg de *Af*AA9_B (proporção 1:50); ou – para comparar o grau de sinergia com uma celobiohidrolase – com 10 µg de *Af*Cel6A (proporção 1:10) por cada grama de CMC.

A associação em conjunto das três enzimas foi executada empregando-se concentrações de 1 µg/g CMC para *Af*-EGL7 e 10 µg/g CMC para *Af*AA9_B e *Af*Cel6A (proporção 1:10:10).

Os meios reacionais foram preparados com CMC 1% (m/v) em tampão fosfato de sódio 50 mM (pH 6,0) + ácido ascórbico 1 mM. As reações foram realizadas em volume final de 1 mL (em microtubos de 2 mL) e incubadas em termomixer (Eppendorf) a 50 °C sob agitação de 1000 rpm durante períodos de 4, 8 e 24 horas. A degradação do CMC foi calculada através dos açúcares redutores liberados empregando-se o método DNS (MILLER, 1959) descrito em mais detalhes em Apêndice. Todos os experimentos foram realizados em triplicata.

3.27) Determinação das atividades da *Af*AA9_B e/ou *Af*Cel6A na presença de CMC em associação com o coquetel comercial Celluclast® 1.5L

Para investigar a sinergia da *Af*AA9_B com o coquetel enzimático comercial Celluclast® 1.5L (Novozymes), foram preparados meios reacionais contendo 0,05 FPU/g CMC do coquetel em associação com 50 µg de *Af*AA9_B (proporção 1 FPU:1000 µg)

ou– para comparar grau de sinergia – com 5 µg de *Af*Cel6A (proporção 1 FPU:100 µg). Os meios reacionais foram preparados como descrito no item 3.26.

Para avaliar o efeito em conjunto das enzimas *Af*AA9_B e *Af*Cel6A na degradação do substrato, utilizou-se novamente carga fixa de 0,05 FPU g/CMC para o coquetel e as concentrações de 0,5 µg/g CMC para a *Af*AA9_B e 5 µg/g CMC para a *Af*Cel6A (proporção 1 FPU:10 µg:100 µg). Todas as reações foram realizadas (em triplicata) sob as mesmas condições descritas anteriormente e as degradações analisadas pelo método DNS.

3.28) Determinação da atividade da *Af*AA9_B e/ou *Af*Cel6A sob diferentes resíduos agrícolas em associação com a enzima *Af*-EGL7 ou coquetel Celluclast® 1.5L

A sacarificação dos resíduos agrícolas analisados foi realizada de acordo com Bernardi et al., (2018) com algumas alterações. As reações foram realizadas em tampão fosfato de sódio 50 mM (pH 6,0) contendo 1% (m/v) de uma das 3 biomassas raladas, sendo essas SEB (bagaço de cana-de-açúcar explodido), palha de arroz e sabugo de milho.

Os ensaios de sacarificação com a *Af*-EGL7 foram realizados utilizando-se concentrações de 18 µg/g biomassa para a endoglucanase em associação com 900 µg/g biomassa para a *Af*AA9_B (proporção 1:50); ou com 180 µg/g biomassa para a *Af*Cel6A (proporção 1:10) (para comparar grau de sinergia).

De modo similar, os ensaios com Celluclast 1.5L foram conduzidos utilizando-se concentração de 0,9 FPU/g biomassa para o coquetel em associação com 900 µg/g biomassa para a *Af*AA9_B (proporção 1 FPU:1000 µg); ou com 90 µg/g biomassa para a *Af*Cel6A (proporção 1 FPU:100 µg) (para comparar grau de sinergia).

As reações (em triplicata) foram incubadas sob as condições descritas em 3.26 por períodos de 24 e 48 horas. O resultado de todas as sacarificações foi determinado através do método DNS.

4. Resultados e discussão

4.1) Clonagem do gene AFUA_4G07850 em vetor pPICZB, expressão em *Pichia pastoris* X33 e purificação da proteína recombinante *Af*AA9_B

O gene AFUA_4G07850 (codificante da proteína LPMO *Af*AA9_B) foi amplificado por reações de PCR, (com sequência nativa do peptídeo sinal) utilizando-se o cDNA de *Aspergillus fumigatus* Af293 como molde e os *primers* A e B descritos em 3.5. A Figura 9 ilustra as bandas do produto da PCR e correspondem ao tamanho de fragmento esperado, de aproximadamente 750 pb. Posteriormente as bandas foram recortadas para a extração do produto amplificado do gel.

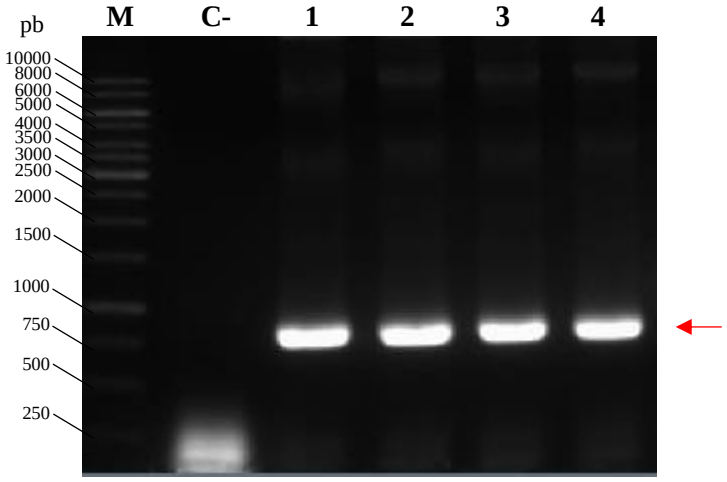

Figura 9. Fotografia do gel de agarose 1% do produto da PCR para amplificação do gene AFUA_4G07850 (1-4). Legenda: M-marcador; C- controle negativo.

Posteriormente, o gene foi clonado no vetor de expressão pPICZB (3328 pb), Nesse vetor, o gene foi fusionado à uma cauda de 6 histidinas à região C-terminal da LPMO, após a digestão do vetor e do gene com as enzimas de restrição *Eco*RI e *Xba*I. A reação de ligação dos mesmos foi realizada através da reação de CPEC e o produto da ligação foi transformado em *E. coli* DH10β competente.

Após transformação, foram selecionadas algumas colônias positivas, e a confirmação da transformação foi realizada por PCR de colônia. O vetor recombinante pPICZB::AFUA_4G07850 foi purificado e linearizado com a enzima de restrição *Pme*I (Figura 10).

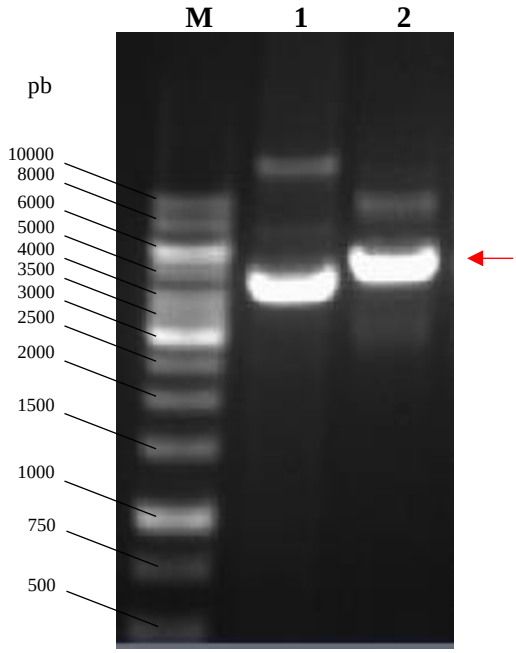

Figura 10. Fotografia da eletroforese em gel de agarose 1% do produto da digestão do vetor pPICZB::AFUA_4G07850 com a enzima PmeI. Legenda: M-Marcador; 1-Linearização do vetor pPICZB; 2-Linearização do vetor pPICZB::AFUA_4G07850.

Posteriormente, o vetor linearizado pPICZB::AFUA_4G07850 foi transformado em *Pichia pastoris* X33. Após seleção dos clones positivos, realizou-se PCR de colônia, com os *primers* 5'AOX1 e 3'AOX1 (específicos para região do vetor pPICZB), o que permitiu confirmar a integração do gene no DNA genômico da levedura (Figura 11).

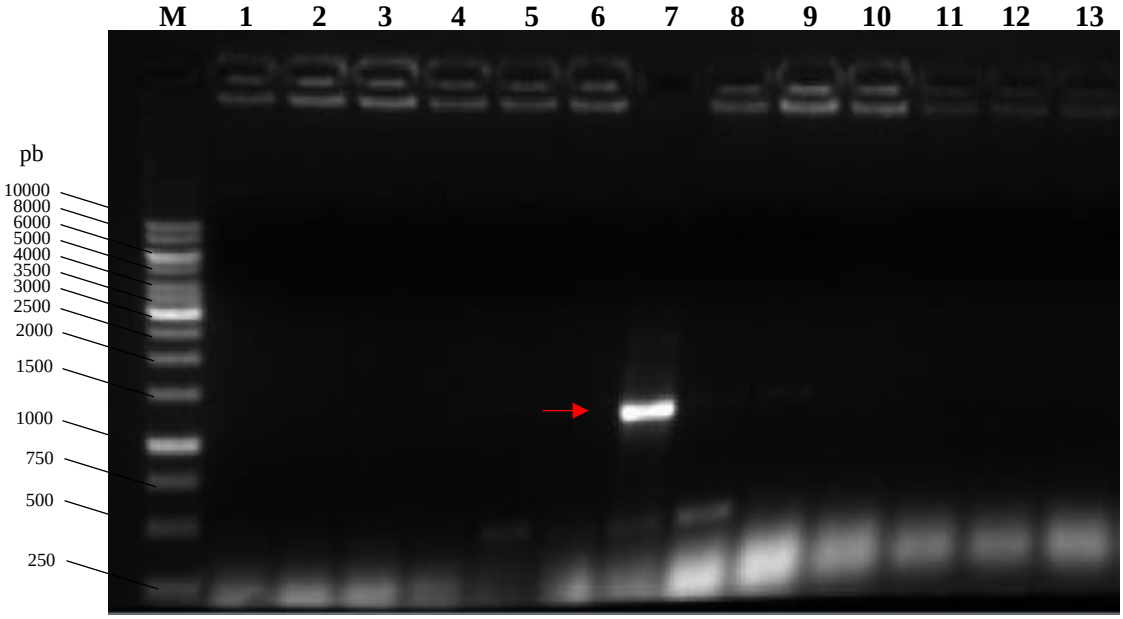

Figura 11. Fotografia da eletroforese em gel de agarose 1% da PCR de colônia para checagem do gene AFUA_4G07850 integrado nas colônias de *P. pastoris* X33 selecionadas. Legenda: M-marcador. Nas colunas (1-13) foi aplicada uma amostra de cada colônia.

Podemos observar que apenas um dos clones selecionados continha o gene integrado, pois foi possível visualizar a banda amplificada de aproximadamente 1000 pb, que corresponde ao tamanho de fragmento compreendido entre promotor e terminador da AOX1 e mais gene AFUA_4G07850 inserido nesse local. O clone foi selecionado e o fragmento amplificado enviado para sequenciamento no Laboratório Multiusuário de Sequenciamento de Ácidos Nucleicos da FCFRP (LMSeq), para confirmar se a sequência inserida estava livre de mutação.

Após análise do sequenciamento, e confirmação da integração do gene AFUA_4G07850 no lócus da enzima álcool oxidase (*AOX1*), realizou-se a expressão da enzima *Af*AA9_B. A indução do promotor da *AOX1* foi realizada com 1% de metanol durante 6 dias a 30 °C e 220 rpm, de modo que ao final as enzimas presentes meio de expressão (BMMY) foram concentradas, ressuspendidas em tampão fosfato de sódio 20 mM + 0,5 M NaCl (pH=7,4). Para purificação, a solução foi submetida à cromatografia de bioafinidade em resina de Ni Sepharose® 6 Fast Flow (GE Heathcare) aplicando-se gradiente linear de 0 a 500 mM de imidazol em solução aquosa. Todas as frações da purificação foram coletadas e aplicadas em gel SDS-PAGE 10%, que podem ser visualizadas na Figura 12.

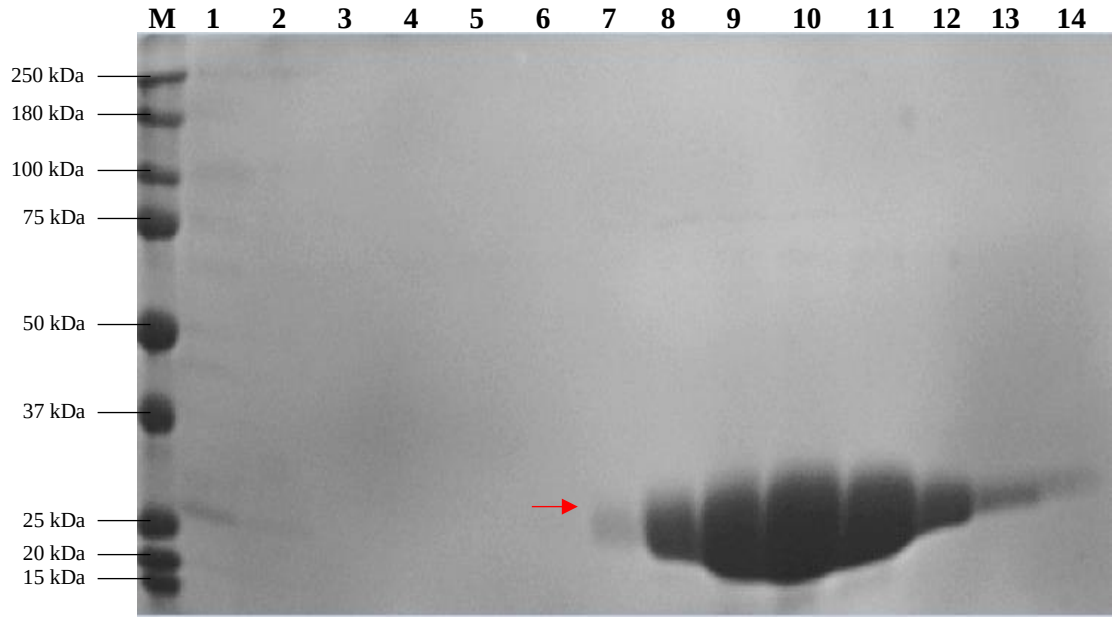

Figura 12. Purificação por bioafinidade da LPMO *Af*AA9_B fusionada com cauda de histidina. Legenda: (M) marcador; (1) Flow through; (2-4) 1ª,2ª e 3ª lavagem com tampão fosfato de sódio 20 mM + 0,5 M (pH=7,4), respectivamente. Frações eluídas com tampão contendo imidazol 5 mM (5); 10 mM (6); 20 mM (7); 40 mM (8); 80 mM (9); 160 mM (10); 250 mM - 1ª vez (11); 250 mM - 2ª vez (12); 500 mM - 1ª vez (13); 500 mM - 2ª vez (14).

Nas colunas referentes às frações eluídas a partir de 80 mM de Imidazol, é possível observar a presença de uma única banda intensa de aproximadamente 30 kDa, tamanho condizente com a enzima *Af*AA9_B que apresenta peso molecular de 26,1 kDa. Uma vez obtida a proteína *Af*AA9_B pura, todas as frações contendo a enzima foram concentradas e ressuspendidas em tampão sem imidazol. Após purificação, apresentou rendimento de 21,2 mg enzima/L meio de cultivo.

4.2) Alinhamento da *Af*AA9_B e análises estruturais por CD e ITFE

Para comparar a sequência da *Af*AA9_B com a de outras AA9s descritas na literatura, foi realizado um alinhamento múltiplo com outras 7 enzimas, conforme pode ser conferido na Figura 13 com mais detalhes.

Como pode-se observar, todas as AA9s do tipo 3 alinhadas apresentam diversos resíduos altamente conservados, com destaque para aqueles pertencentes à esfera de coordenação primária da estrutura catalítica denominada de braçadeira de histidina, a qual é constituída por 2 histidinas (sendo uma N-terminal e outra localizada no loop L2) e uma tirosina (BRANDER et al., 2020; HEMSWORTH et al., 2014; VAAJE-KOLSTAD et al., 2017; ZHOU; ZHU, 2020). No caso da *Af*AA9_B, a estrutura catalítica é constituída pelos resíduos His1, His86 e Tyr175, como pode ser visualizado no alinhamento.

Além desses resíduos diretamente coordenados ao cofator Cu(II), também estão presentes aqueles pertencentes à esfera de coordenação secundária que atuam (principalmente através de uma rede de ligações de hidrogênio) diretamente no mecanismo catalítico das LPMOs (BERTINI et al., 2018; SPAN et al., 2017). Dentre esses, podem ser citados os seguintes resíduos conservados apresentados na Figura 13: G42, V44, W82, E84, S85, E159, I160, I161, H164 e Q173 (sequência da *Af*AA9_B).

O alinhamento demonstrou a presença de duas ligações dissulfeto envolvendo os resíduos C97-C101 e C56-C178, as quais contribuem para a manutenção da forma nativa das enzimas e para o consequente aumento da termoestabilidade das mesmas (CALDERARO et al., 2020; DANNEELS et al., 2017; LAURENT et al., 2019).

De acordo com os servidores NetNGlyc 1.0 e NetOGlyc 4.0 foi possível determinar as possíveis posições de N-glicosilações e O-glicosilações de todas as AA9s alinhadas. A ocorrência de N-glicosilações ocorre por meio da adição de glicanas no

átomo de nitrogênio dos resíduos de asparagina (N) comumente localizados nos sítios N-X-S/T, onde que X obrigatoriamente não pode ser uma prolina (LOWENTHAL et al., 2016; TAHERZADEH et al., 2019). As O-glicosilações são decorrentes da adição de diferentes tipos de açúcares ao oxigênio de resíduos de serina (S) ou treonina (T) em sítios reconhecidos pelas enzimas que desempenham essa função (TAHERZADEH et al., 2019). De acordo com os dados fornecidos na Figura 13, a *Af*AA9_B apresenta apenas uma única N-glicosilação em N138 e duas O-glicosilações em S35 e T36.

Dentre as 8 LPMOs alinhadas, apenas as enzimas NCU07760 e *Pa*LPMO9A demonstraram possuir um módulo de ligação para substratos celulósicos (CBM1) localizados na região C-terminal. A *Af*AA9_B, apesar de não apresentar CBMs, possui afinidade pelo mesmo tipo de substrato (VELASCO et al., 2021), reforçando o fato de que a atividade das LPMOs não é obrigatoriamente determinada pela presença de tais módulos (HEMSWORTH et al., 2014). Vale destacar que na sequência de todas as LPMOs alinhadas foram evidenciados dois motivos conservados característicos: o Hx_nGP, onde se encontra o segundo resíduo de histina, e o QxYxxC, onde localiza-se a tirosina da braçadeira de histidina (VU et al., 2014a).

A Figura 14, ilustra a árvore filogenética obtida a partir do alinhamento da *Af*AA9_B com outras 25 AA9s de regiosseletividades diferentes como pode ser visto em Figura Suplementar 3 (valores de identidade apresentados em Tabela Suplementar 1). Foi possível separar as AA9s em três grandes grupos sendo aquelas dos ramos em amarelo do tipo 1 (ativas em C1), dos ramos em verde do tipo 2 (ativas em C4) e dos ramos em azul do tipo 3 (ativas em C1-C4).

Diferentes das AA9s do tipo 1, aquelas pertencentes ao tipo 3 apresentam na região do loop L2 cerca de 12 resíduos a mais, dentre os quais encontra-se uma tirosina altamente conservada. Essa inserção leva a formação de uma pequena hélice adicional localizada no plano do sítio ativo. Tanto as AA9s do tipo 2 como 3 apresentam no loop L3 um resíduo de serina antecedendo a segunda histidina da braçadeira, o qual possivelmente está associado a atividade em C4. No caso específico daquelas do tipo 2, anteriormente à segunda histidina encontra-se uma inserção adicional de 9 a 14 resíduos (em relação as do tipo 1), e logo em seguida da mesma um resíduo de lisina (K) também fortemente conservado (VU et al., 2014a).

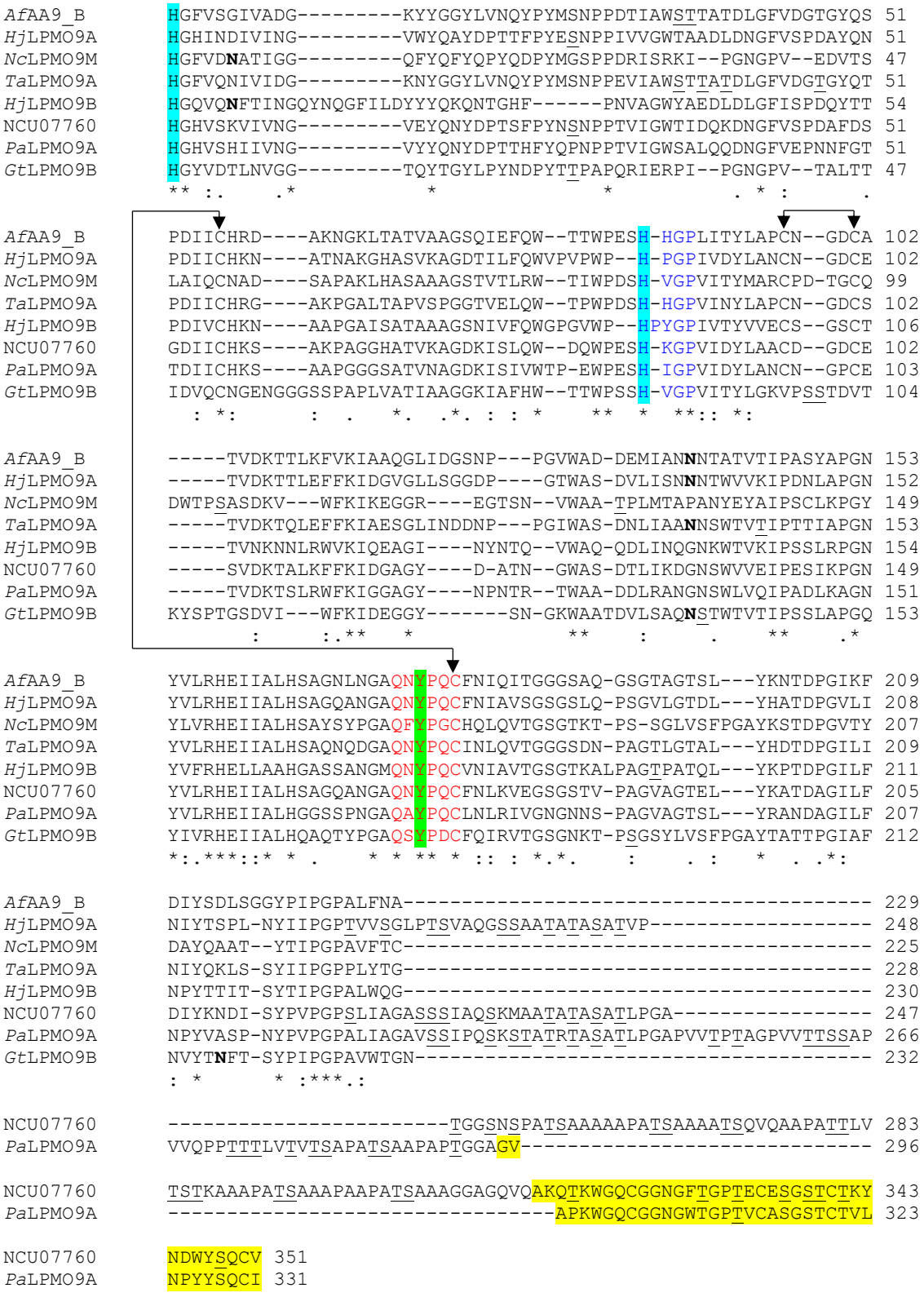

Figura 13. Alinhamento múltiplo da *Af*AA9_B com AA9s descritas na literatura. Histidinas e tirosina pertencentes à braçadeira destacadas em azul e verde, respectivamente; módulos CBM1 destacados em amarelo; ligações dissulfeto indicadas por setas; motivos conservados Hx_nGP e YxQxxC indicados em letras na cor azul e vermelho, respectivamente; N-glicosilações em negrito e O-glicosilações em sublinhado. Legenda: (*****) – resíduos fortemente conservados; (**:**) – resíduos pertencentes a um mesmo grupo; (**.**) – resíduos com poucas características estruturais semelhantes.

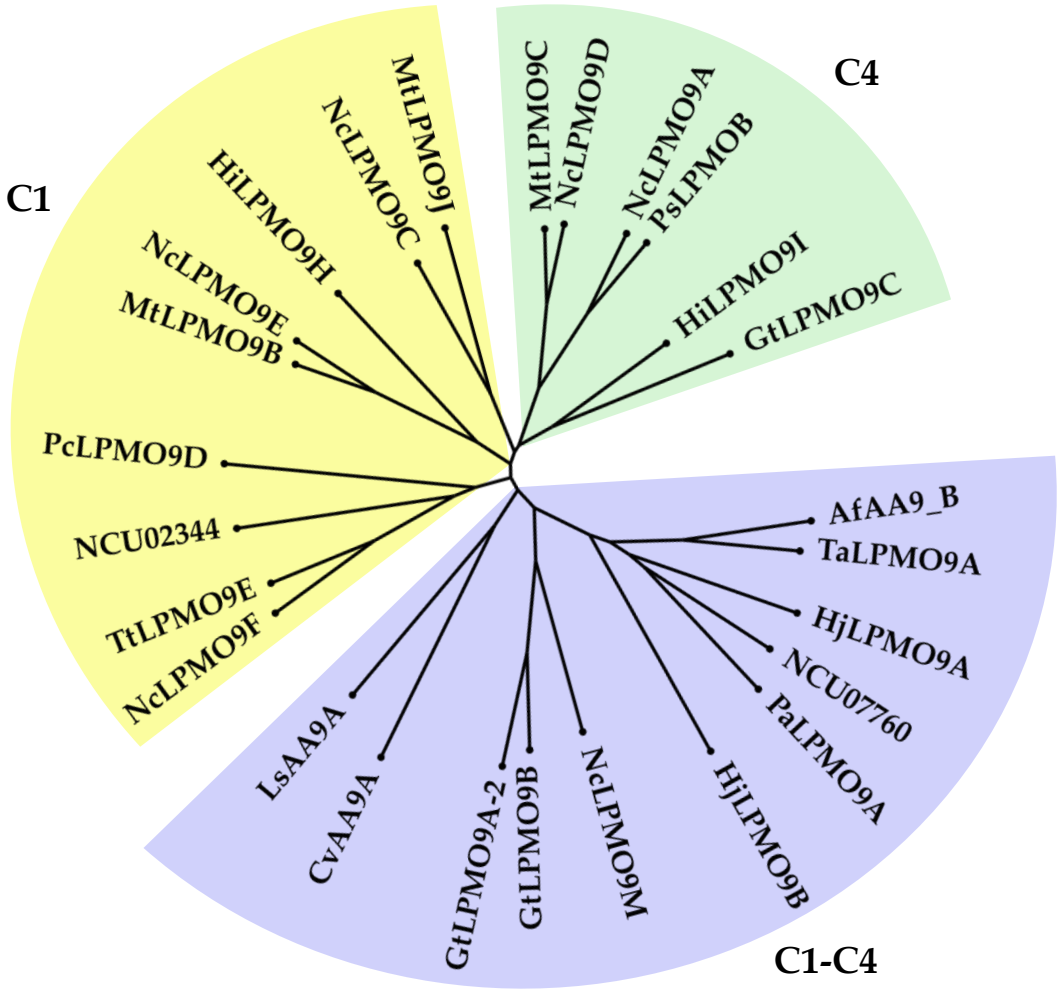

Figura 14. Árvore filogenética radial de 25 AA9s descritas na literatura e de diferentes regiosseletividades alinhadas com a *Af*AA9_B. Em amarelo estão agrupadas aquelas classificadas como sendo ativas em C1, em verde as ativas em C4 e em azul as ativas em C1-C4.

Com relação ao modelo tridimensional gerado através do servidor online Phyre2, como exibido na Figura 15a, foi possível visualizar a estrutura terciária da enzima. O modelo foi obtido com base na estrutura PDB: 2YET (QUINLAN et al., 2011) da enzima *Ta*LPMO9A do organismo *Thermoascus aurantiacus*, com a qual apresentou 98% de cobertura e 71% de identidade. Em comparação com o a estrutura cristalizada já existente para a *Af*AA9_B (PDB: 5X6A) (LO LEGGIO et al., 2018), conforme pode ser visto em Tabela Suplementar 2, apesar da estimativa fornecida pelo Phyre2 ser mais distante do esperado, ambas apresentam proporções muito próximas de estruturas secundárias quando o modelo é analisado usando-se o algoritmo Kabsch & Sander (KABSCH; SANDER, 1983), ou as estruturas são determinadas a partir de dicroísmo circular (CD).

Na figura 15a, é dado destaque aos principais loops expostos localizados na região do sítio ativo da AA9 (superfície), que compreendem os loops L2, L3, L8, LS e LC (LIU, 2019). Loops são regiões de alta variabilidade e em geral apresentam resíduos aromáticos cuja função está relacionada ao ancoramento do substrato (BERTINI et al., 2018; ZHOU; ZHU, 2020).

O loop L2 constituído pela alça interligando as folhas-β 1 e 2 possui um resíduo conservado Y20 em uma região helicoidal capaz de interagir com o anel piranose dos carboidratos; o loop L3 localizado entre as folhas-β 3 e 4 é onde está inserido a segunda histidina da braçadeira e o resíduo de serina que o precede; o loop L8 presente entre as folhas-β 8 e 9 apresenta os resíduos catalíticos H164 e Gln173 da segunda esfera de coordenação; o loop LS que é o de menor extensão (entre folhas-β 5 e 6) localiza-se na extremidade oposta ao L2 por se tratar de uma AA9; e por fim o loop LC, onde está presente outro importante resíduo conservado associado à ligação com o substrato (Y212), é o de maior extensão e localiza-se na região C-terminal (BERTINI et al., 2018; SPAN et al., 2017; VU et al., 2014a; ZHOU; ZHU, 2020).

As mudanças ocorridas na estrutura secundária da *Af*AA9_B foram analisadas através de dicroísmo circular (CD). Na Figura 15b é possível visualizar o impacto da adição do cofator Cu(II) ao sítio ativo da LPMO. Apesar de não serem observadas grandes alterações comparando-se os espectros da apo ou holoenzima, de acordo com a Tabela Suplementar 3, é possível afirmar que a holoenzima apresentou uma ligeira diminuição porcentual no conteúdo de folhas-β antiparalelas acompanhada por um leve aumento de folhas-β paralelas e estruturas desordenadas.

De maneira análoga, Kracher *et al*., (2018) também observou que o espectro da *holo-Nc*LPMO9C demonstrou baixa variação em seu perfil mediante a apo-forma, de tal modo que após a adição de Cu(II) passou a apresentar 30% de folhas-β e 44% de estruturas desordenadas, assemelhando-se à *Af*AA9_B. De uma forma geral, considerando-se que as LPMOs são enzimas contendo um núcleo rico em folhas-β (FRANDSEN et al., 2019, 2021; VAAJE-KOLSTAD et al., 2017), os dados obtidos são condizentes, uma vez que a *Af*AA9_B (PDB 5X6A) (Figura 15a) contém 31,4% de folhas-β, 12,6% de α-hélices e 55,9% de alças e estruturas desordenadas (LO LEGGIO et al., 2018).

Com relação à análise de termoestabilidade via CD baseada na ocorrência de alterações nos perfis de absorção durante 24 (Figura 15c), 48 e 72 horas (Figuras Suplementares 5a e 5b), as alterações registradas na proporção de estruturas secundárias (Tabelas Suplementares 4-6) possibilitaram avaliar a integridade da LPMO sob diferentes temperaturas. É possível notar que a *Af*AA9_B mantida a 25 °C durante 24 horas apresentou 2 diferentes picos negativos em regiões próximas de 208 e 222 nm, os quais são característicos da presença de α-hélice (10,9%), assim como um aspecto dominante de banda única com baixos valores de elipticidade em 190 nm, denotando assim a presença de folhas-β (36,7%) (WALLACE; JANES, 2009).

Com o aumento da temperatura para 50 °C, após 24, 48 e 72 horas de incubação, houve queda do pico negativo em torno de 222 nm, o que indica a perda de α-hélice, além do surgimento de um pico fraco em 200 nm característico de início de desnaturação (WALLACE; JANES, 2009). Baseando-se nos dados contidos na Tabela Suplementar 4 (para 24 horas), não apenas o percentual de α-hélice diminuiu (10,9 para 10,2%), mas também o conteúdo de folhas-β paralelas (14,2 para 13,2%). Apenas o percentual de alças registrou leve aumento de 44,6 para 47,5%; e o de estruturas desordenadas (43,0 para 44,3%). Nos tempos de 48 e 72 horas (Tabelas Suplementares 5 e 6), foram observadas as mesmas tendências.

No curto intervalo de 52 a 58°C, foram registradas consideráveis diferenças entre os espectros de absorção obtidos (Figuras 15c e Suplementares 5a e 5b). Na Tabelas Suplementares 4-6 é possível observar as gradativas alterações. No caso de 24 horas, o conteúdo de alfa hélices e folhas beta paralelas caíram de 9,1 para 7,9% e de 10,6 para 2,7%, respectivamente; e o de folhas beta antiparalelas, alças e estruturas desordenadas subiram de 26,7 para 30%, de 9,8 para 12,1% e de 43,8 para 47,3%, respectivamente. A mesma tendência foi observada para as demais temperaturas.

Já em 60 °C, conforme mencionado anteriormente, há um grande pico negativo em torno de 200 nm para ambos os tempos de incubação, o que evidencia um grande aumento de estruturas desordenadas, tendência essa observada de forma mais pronunciada a 70 °C após 24 horas. Como pode ser visto na Tabela Suplementar 4, de 60 a 70 °C o conteúdo folhas β-paralelas quase desaparece (2,8 para 0,1%); as α-hélices caem de 4,5 para 2,9%; as alças aumentam de 11,7 para 14,1%; e as estruturas desordenadas atingem a marca de 55,3% - como esperado devido à elevada temperatura (a 25°C representavam apenas 43,0%). Novamente, nos demais tempos observou-se similar

tendência e valores, corroborando que a enzima se manteve estável durante os 3 dias e que as temperaturas em si foram o principal fator de mudanças conformacionais.

Frommhagen *et al*., (2018) demonstrou que as LPMOs *Mt*LPMO9B e *Mt*LPMO9D quando aquecidas de 20 a 90 °C apresentaram espectros de CD semelhantes ao da *Af*AA9_B quando em altas temperaturas. Enquanto ambas as enzimas foram desnaturadas a 90 °C, a *Af*AA9_B atingiu similar estágio a partir de 70 °C. Além disso, com o aumento da temperatura, em ambas houve aumento de alças e estruturas desordenadas além de diminuição do conteúdo de α-hélice. A única diferença foi a diminuição das folhas-β antiparalelas registrada para a *Mt*LPMO9B e *Mt*LPMO9D. A análise via CD da *Ta*LPMO9A (PDB: 2YET) de Singh *et al*., 2019 resultou em um espectro muito semelhante ao perfil da *Af*AA9_B. Essa similaridade é esperada uma vez que ambas as enzimas compartilham 71% de identidade.

A temperatura de transição ou fusão aparente (T_{mapp}) é definida como aquela localizada no ponto médio entre a forma nativa e a desnaturada de uma proteína em que ambas coexistem em igual proporção (SANFELICE; TEMUSSI, 2016; SENISTERRA; CHAU; VEDADI, 2012). Na Figura 15d é possível observar que os valores de elipticidade em 222 nm apresentam alterações significativas dentro do intervalo de 50 a 60 °C, assim como os valores registrado em 215 nm para a *Mt*LPMO9D (FROMMHAGEN et al., 2018). Em temperaturas acima ou abaixo desse intervalo, os valores variaram pouco. Por meio da derivada primeira do gráfico da Figura 15d (após incubações de 24h), o valor de temperatura de transição encontrado para a *Af*AA9_B foi de 55,22 °C, valor similar àqueles determinados através das Figuras Suplementares 5c (após 48h) e 5d (após 72h) que foram de 55,05 °C e 55,02 °C, respectivamente. Considerando-se que o valor de T_{mapp} em pH neutro para *Ta*LPMO9A é 69,0 °C (SINGH et al., 2019) e para *Mt*LPMO9D é 68,0 °C (FROMMHAGEN et al., 2018), ambas as enzimas se mostraram mais termoestáveis que a *Af*AA9_B.

A *Af*AA9_B apresenta em sua estrutura primária quatro resíduos de triptofano (Trp ou W) (como pode ser visto na Figura 15a), com um único localizado nos loops LS (W129) e L2 (W34), e dois deles no loop L3 (W79 e W82), que são estruturas características de AA9s (LIU et al., 2017; VAAJE-KOLSTAD et al., 2017). A presença de aminoácidos aromáticos nesses loops podem estar associadas a ancoragem dos carboidratos às LPMOs (BERTINI et al., 2018; FRANDSEN et al., 2021). A recorrente presença de triptofano na estrutura de proteínas torna a análise de ITFE uma ferramenta

capaz de detectar mudanças no ambiente químico onde esses resíduos estão inseridos, o que por consequência possibilita a obtenção de informações a respeito da estrutura terciária de enzimas (LAKOWICZ, 2013).

Os espectros de emissão obtidos para *Af*AA9_B em diferentes temperaturas e tempos de incubação, exibidos na Figura 15e, demonstram que em comparação com a enzima incubada a 25 °C por 24 horas (que apresentou pico máximo de emissão em 328,4 nm), o aumento da temperatura para 50 °C provocou um desvio para o vermelho, uma vez que os máximos obtidos para os tempos de incubação de 24, 48 e 72 horas foram registrados em 333,8; 339,4 e 340,4 nm, respectivamente. Quando resíduos aromáticos excitados interagem com solventes polares como a água, ocorre relaxamento energético seguido pela maior emissão de fluorescência em comprimentos de onda mais elevados e de menor energia (LAKOWICZ, 2013). Apesar de os resíduos de triptofano ficarem mais expostos, a estrutura terciária não passou por alterações consideráveis, o que pode ser inferido pelo aumento da intensidade do sinal no ponto máximo.

A 60 °C foram observadas mudanças mais impactantes no espectro de emissão. Para os tempos de incubação de 24, 48 e 72 horas, foram obtidos valores máximos em 346,2; 347,0 e 347,8 nm, respectivamente. A 70 °C após 24 horas de incubação, o máximo foi registrado em 348,2 nm. Esse deslocamento para o vermelho indicou novamente uma maior exposição dos resíduos de triptofano, porém considerando que as intensidade dessa vez foram aproximadamente duas vezes maior que os valores registrados a 25 °C, estima-se que a estrutura terciária tenha passado por consideráveis mudanças conformacionais, de modo a estar altamente desordenada a 70 °C. De modo geral, com o aumento de temperatura, os resíduos de Trp presentes antes em um ambiente hidrofóbico tornaram-se altamente expostos ao solvente polar (tampão tris-HCl 20 mM, pH=7,4) acima de 60 °C. Interessantemente, apesar do deslocamento para o vermelho, ao invés das intensidades diminuírem, elas aumentaram. Esse fenômeno possivelmente se deve ao efeito de supressão proporcionado por resíduos próximos como histidinas localizadas no ambiente hidrofóbico (LAKOWICZ, 2013).

Com base no gráfico da Figura 15f, foi possível calcular novamente a derivada primeira e determinar a T_{mapp}. O valor encontrado de 53,60 °C, foi bem próximo do anterior (55,22 °C). Na literatura, o valor de T_{mapp} calculado a partir de ITFE para a enzima *Mt*LPMO9J foi reportado como 58,0 °C a pH = 6,0 utilizando o mesmo tampão (KADOWAKI et al., 2018), o qual é próximo ao obtido nesse trabalho. Devido a presença

de uma N-glicosilação em N-138 (Figura 13) e de duas ligações dissulfeto entre os resíduos Cys56-Cys178 e Cys97-Cys101 (Figura 15a), esses fatores possivelmente contribuem para os altos valores de T_{mapp} registrados. Estudos de Vaaje-Kolstad *et al*., (2012) demonstraram que a LPMO CBP21 registrou uma diminuição de 6 °C na T_{mapp} após o tratamento com DTT (para remoção de ligações dissulfeto), enquanto que de acordo com Tanghe *et al*., (2017) a LPMO *Sc*LPMO10C aumentou sua T_{mapp} em 12 °C devido às ligações dissulfeto adicionadas através de mutações à estrutura, evidenciando assim a contribuição dessas ligações covalentes para a manutenção das demais múltiplas interações fracas da enzima, e como consequência, para o aumento da termoestabilidade.

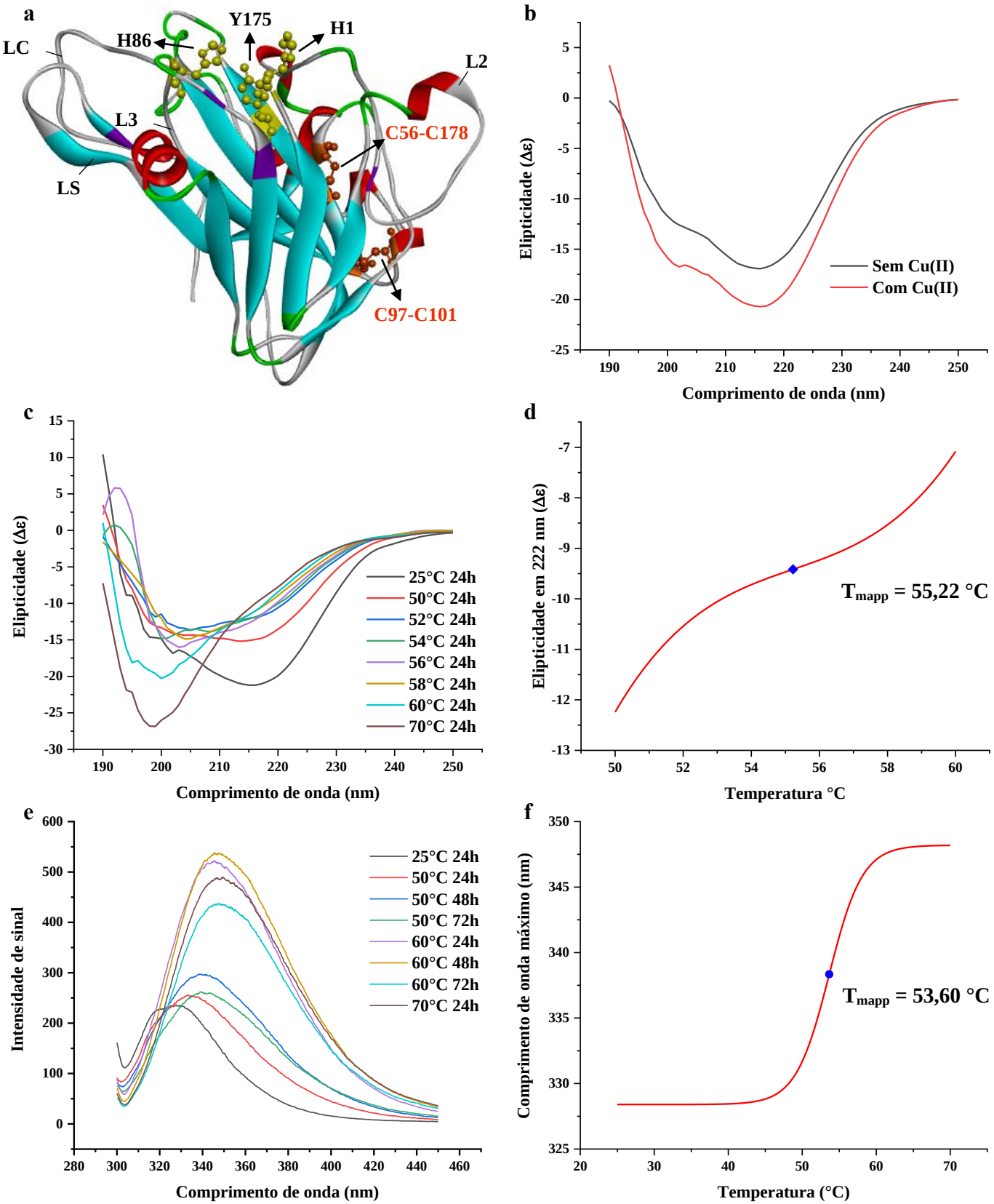

Figura 15: Análises estruturais da *Af*AA9_B. Modelo 3D (Ribbon) da LPMO (a), com os resíduos da braçadeira de histidina, de triptofano e as ligações dissulfeto destacados em amarelo, magenta e laranja, respectivamente. Espectros de absorção obtidos via CD da *Af*AA9_B na faixa de 190 – 250 nm na presença (*holo*) e ausência (*apo*) de Cu(II) a 25 °C (b); e da *holo*-*Af*AA9_B quando incubada por 24, 48 e 72 horas a 25 °C; 50 °C; 60 °C; e 70 °C (c). Espectros de emissão coletados via ITFE das amostras analisadas em "c" (e). Valores de temperatura aparente de transição (T_{mapp}) determinados pela derivada primeira dos gráficos de elipticidades registradas a 222 nm X temperatura (°C) (d) e de comprimentos de onda máximos (nm) X temperatura (°C) (f).

A fim de confirmar a presença de N-glicosilações na estrutura da *Af*AA9_B e analisar o impacto delas sobre o peso molecular, a LPMO foi tratada com Endoglucanase H e os resultados podem ser conferidos na Figura 16.

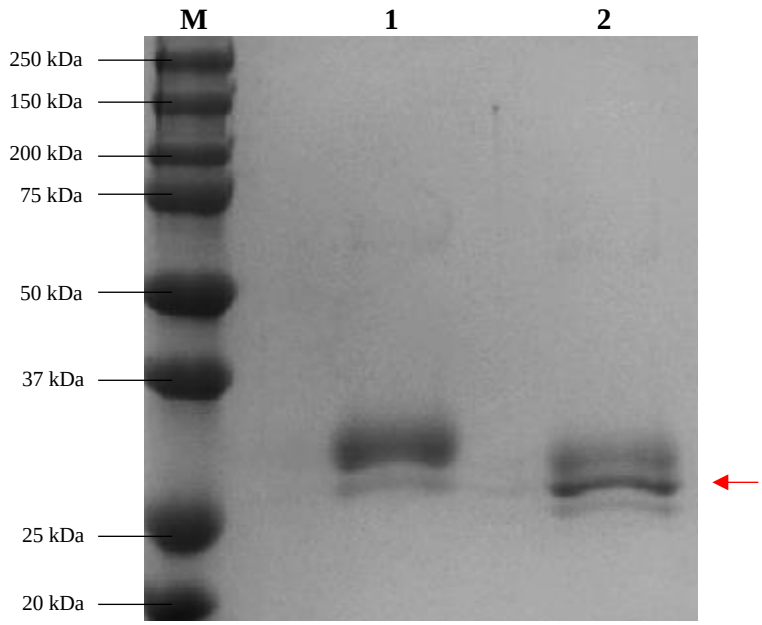

Figura 16. Análise da forma glicosilada e deglicosilada da enzima *Af*AA9_B. Legenda: M- Marcador; 1- *Af*AA9_B glicosilada; 2- *Af*AA9_B deglicosilada (incubada overnight com Endo H à 37°C).

Como pode ser visto, a *Af*AA9_B secretada pela *Pichia pastoris* X33 sem tratamento (coluna 1) apresenta cerca de 30 kDa, porém após a deglicosilação com a Endo H (coluna 2) nota-se uma pequena diminuição do peso molecular da fração reagida, culminando com o aparecimento de uma banda mais intensa próximas de 26 kDa.

Tal resultado é condizente com a predição da ocorrência de uma N-glicosilação em N138, como apresentado na Figura 13. Além disso a *Pichia pastoris* é um organismo conhecido por realizar hiper glicosilações devido a presença da enzima α-1,6-manosiltransferase a qual atua adicionando de 8 até 14 unidades de 1,6-manose nos sítios de N-glicosilação, justificando assim o peso molecular acima do esperado (CHOI et al., 2010; MEIRA et al., 2020). A presença de N-glicosilação nas enzimas em geral relaciona-se a fatores como por exemplo nível de secreção, estabilidade e até enovelamento correto (RUBIO et al., 2016). No caso das LPMOs do tipo 3 (C1/C4) como a *Af*AA9_B, a presença de N-glicosilação em regiões próximas a região da superfície plana do sítio ativo (como é o caso de N138) trata-se de uma característica recorrente e relacionada à regioseletividade das mesmas (DANNEELS; TANGHE; DESMET, 2019).

4.3) Análise de atividade, propriedades e constantes enzimáticas da *Af*AA9_B

Usando-se o substrato cromogênico 2,6-DMP, foram realizadas análises de algumas propriedades características da LPMO *Af*AA9_B, conforme demonstrado na Figura 17.

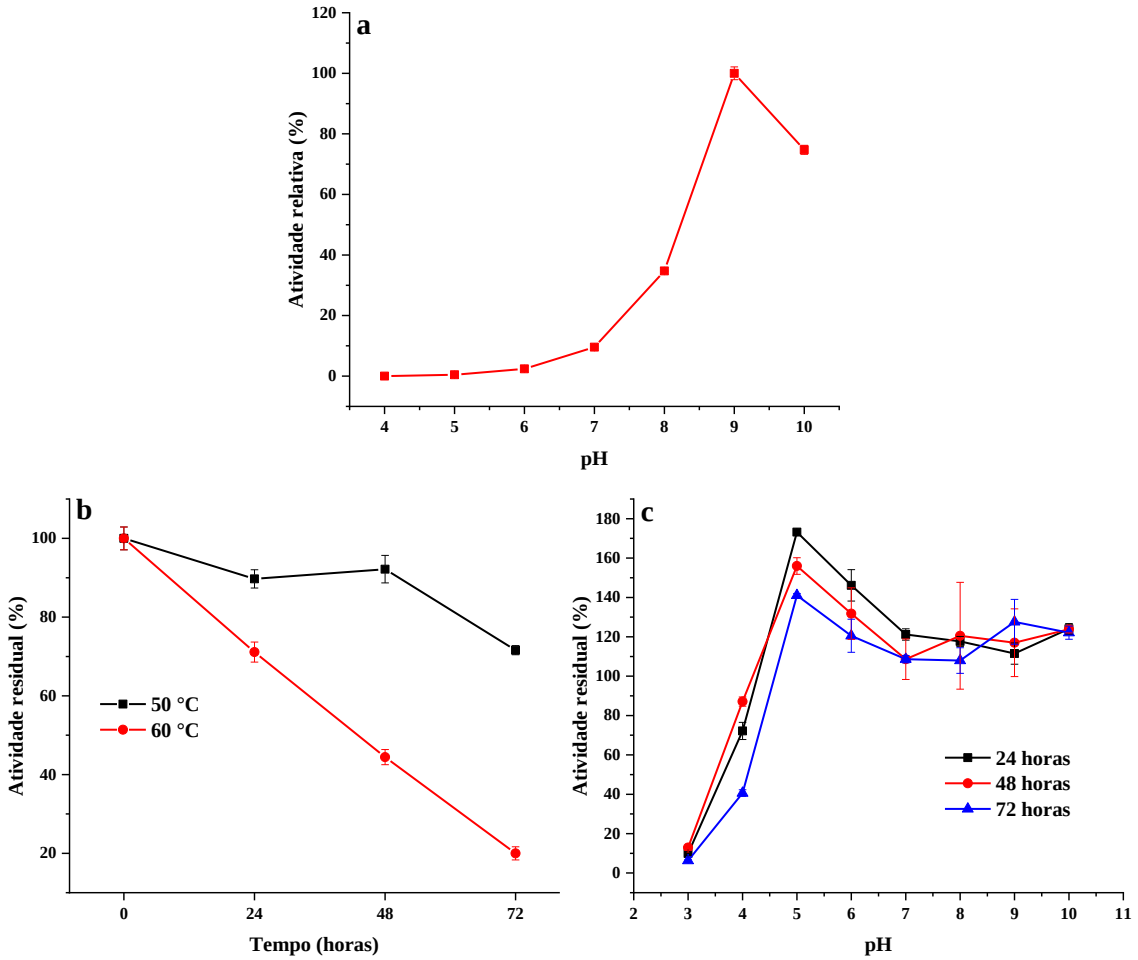

Figura 17. Propriedades da *Af*AA9_B determinadas usando-se 2,6-DMP e H_2O_2 como substrato e co-substrato, repectivamente. Foram realizadas as análises de atividade sob diferentes valores de pH a 30 °C (a); de termoestabilidade a 50 e 60 °C sob pH 9,0 (b); e de estabilidade a pH sob temperatura de 4 °C (c).

Como pode ser observado na Figura 17a, o pH ótimo da enzima sob as condições experimentais (30 °C por 5 minutos) é 9.0, contudo a *Af*AA9_B se apresenta estável numa faixa ampla de pH variando de 5,0 a 10,0 (Figura 17c). Dentro desse intervalo, a atividade enzimática manteve-se acima de 100% quando comparada ao valor registrado antes de iniciar a incubação, tendência essa que se estendeu até 72 horas e demonstrou a elevada estabilidade da LPMO mediante variações de pH.

Apesar de seu pH ótimo, moderadamente alcalino, ser equiparável ao de enzimas como PMO9D_MALCI (pH = 9,0), *Mt*LPMO9B e *Mt*LPMO9C (ambas pH = 8,0)

(AGRAWAL et al., 2019; FROMMHAGEN et al., 2018), diferentemente das outras LPMOs, a *Af*AA9_B foi a única capaz de se manter 100% estável diante de uma ampla faixa de pH chegando até 10,0 durante 72 horas (Tabela 2). Vale destacar que a maioria das LPMOs não toleram valores de pH muito elevados em decorrência do Cu(II) presente no sítio ativo das mesmas estar suscetível a precipitar em condições mais alcalinas (EIJSINK et al., 2019; JAGADEESWARAN et al., 2016).

Além disso, (Figura 17b), observou-se que a *Af*AA9_B sob temperatura de 50 °C foi capaz de reter mais de 90% de sua atividade até 48 horas e mais de 70% após 72 horas. A 60 °C no entanto, a LPMO apresentou cerca de 70% de atividade em apenas 24 horas, de modo a decrescer de forma mais acentuada até 72 horas, retendo apenas 20% de seu valor original. Essa faixa de termoestabilidade é semelhante à das enzimas *Mt*LPMO9D (FROMMHAGEN et al., 2018), *Mt*LPMO9J (KADOWAKI et al., 2018), PMO9D_SCYTH e PMO9D_MALCI (AGRAWAL et al., 2019), também exibidas na Tabela 2.

Tais resultados também estão de acordo com os dados de CD (Figura 15c) e ITFE (Figura 15e), através dos quais é possível observar que de fato até 50 °C tanto a estrutura secundária como a terciária da *Af*AA9_B mantêm-se praticamente inalteradas. Vale relembrar que o fato da enzima apresentar duas ligações dissulfeto também influem diretamente na alta termoestabilidade, a qual por sua vez é esperada para fungos mesofílicos como o *Aspergillus fumigatus* (GABRIEL et al., 2020; LI et al., 2020). O valor de temperatura ótima, apesar de não ser apresentado devido à alta oscilação, foi estimado como sendo próximo de 60 °C.

A determinação das constantes cinéticas como K_m, V_{max}, K_{cat} e K_{cat}/K_m (eficiência enzimática) foi realizada de acordo com Breslmayr *et al*., 2018, em pH 6,0 e 9,0 para as análises com o substrato 2,6-DMP e o co-substrato H_2O_2. Os gráficos obtidos são exibidos na Figura 18.

Tabela 2. Propriedades e constantes enzimáticas para LPMOs descritas na literatura.

Organismo	LPMO	Organismo para expressão	Substrato	Co-substrato	V_{max}	K_m	K_{cat}	K_{cat}/K_m	T ótima	pH ótimo	Termoestabilidade	Estabilidade a pH	Referência
***Aspergillus fumigatus* Af293**	*Af*AA9_B	*Pichia pastoris* X33	2,6-DMP	a § H_2O_2	78,52 ± 3,33 U g^{-1}	2,04 ± 0,24 µM	0,034 s^{-1}	0,017 μM^{-1} s^{-1}	-	***	-	-	Essa dissertação
				b § H_2O_2	1481 ± 72,19 U g^{-1}	0,79 ± 0,12 µM	0,64 s^{-1}	0,81 μM^{-1} s^{-1}	-	9,0	60 ºC: 50% após 48 h; 50 ºC: quase 100% após 48 h	Estável na faixa de pH 5,0-10,0	
			§ 2,6-DMP	a H_2O_2	49,26 ± 4,48 U g^{-1}	106,3 ± 27,9 µM	0,021 s^{-1}	1,98 x10^{-4} μM^{-1} s^{-1}	-	-	-	-	
				b H_2O_2	972,5 ± 28,31 U g^{-1}	12,15 ± 1,76 µM	0,42 s^{-1}	0,035 μM^{-1} s^{-1}	-	-	-	-	
Scytalidium thermophilum	PMO9D_SCYTH	*Pichia pastoris* X33	Avicel	§ H_2O_2	0,36 U mg^{-1}	4,54 mg mL^{-1}	2,99 X 10^{-2} min^{-1}	6,58 X 10^{-3} mg^{-1} mL min^{-1}	-	-	-	-	(AGRAWAL et al., 2019)
			CMC		14,96 U mg^{-1}	10,6 mg mL^{-1}	1,61 min^{-1}	1,52 X 10^{-1} mg^{-1} mL min^{-1}	60 °C	7,0	60 °C ($t_{1/2}$ = 60,58 h; pH 7,0)	Acima de 90% após 48 h; pH 7,0	
			2,6-DMP		0,13 U mg^{-1}	0,51 mM	1,84 X 10^{-1} min^{-1}	3,57 X 10^{-1} mM^{-1} min^{-1}		-	-	-	
Malbranchea cinnamomea	PMO9D_MALCI		Avicel		0,17 U mg^{-1}	5.87 mg mL^{-1}	1.05 X 10^{-2} min^{-1}	1.79 X 10^{-3} mg^{-1} mL min^{-1}		-	-	-	
			CMC		9,59 U mg^{-1}	29,27 mg mL^{-1}	0,76 min^{-1}	2,62 X 10^{-2} mg^{-1} mL min^{-1}	50 °C	9,0	50 °C ($t_{1/2}$ = 144 h; pH 7,0)	Acima de 80% após 72 h; pH 9.0	
			2,6-DMP		0,12 U mg^{-1}	1,17 mM	1,21 min^{-1}	1,03 X 10^{-1} mM^{-1} min^{-1}		-	-	-	
Thielavia terrestris	*Tt*LPMO9E	-	PWS	§ O_2	-	49,80 g L^{-1}	3,8 min^{-1}	*1,85 X 10^3 M^{-1} min^{-1}	-	-	-	-	(KELLER et al., 2019)
Myceliophthora thermophila	*Mt*PMO9E	*Neurospora crassa*	cellohexaose	§ O_2	-	32 µM	10,1 min^{-1}	0,30 μM^{-1} min^{-1}	-	-	-	-	(FORSBERG et al., 2019; HANGASKY; IAVARONE; MARLETTA, 2018)
			§ cellohexaose	O_2	-	230 µM	17 min^{-1}	7,4 X 10^{-2} μM^{-1} min^{-1}	-	-	-	-	
				H_2O_2	-	53 µM	#15,9 s^{-1}	3,0 X 10^5 M^{-1} s^{-1}	-	-	-	-	
Serratia marcescens	CBP21	*Escherichia coli* BL21(DE3) Star	CNW	§ H_2O_2	1,11 µM s^{-1}	0,58 mg mL^{-1}	6,7 s^{-1}	≅10^6 M^{-1} s^{-1}	-	-	-	-	(KUUSK et al., 2018)
			§ CNW	H_2O_2	-	2,8 µM	-	-	-	-	-	-	
Lentinus similis	*Ls*(AA9)A	*Aspergillus oryzae* MT3568	cellotetraose	§ O_2	-	43 µM	0,11 s^{-1}	2,6 X 10^3 M^{-1} s^{-1}	-	-	-	-	(FRANDSEN et al., 2016)
***Aspergillus fumigatus* NITDGPKA3**	** CAF32158.1	*Pichia pastoris* X33	2,6-DMP	§ H_2O_2	1,11 µM min^{-1}	11,23 µM	0,642 min^{-1}	5,7 X 10^{-2} µM min^{-1}	-	-	-	-	(MUSADDIQUE et al., 2020)
Myceliophthora thermophila	*Mt*LPMO9B	*Myceliophthora thermophila* C1	RAC	§ O_2	-	-	-	-	+ 40 °C	8,0	**** Tm_{app} (pH 7,0) > 70 °C	-	(FROMMHAGEN et al., 2018)
	*Mt*LPMO9D								+ 50 °C		**** Tm_{app} (pH 7,0) = 68 °C		
Myceliophthora thermophila	*Mt*LPMO9J	*Aspergillus nidulans*	-	-	-	-	-	-	-	-	**** Tm_{app} (pH 6,0) = 58 °C	-	(KADOWAKI et al., 2018)
Thermoascus aurantiacus	*Ta*LPMO9A	*Aspergillus oryzae*	-	-	-	-	-	-	-	-	**** Tm_{app} (pH 7,0) = 69 °C	-	(SINGH et al., 2019)
Thermoascus aurantiacus	*Ta*LPMO9A	*Trichoderma reesei* T1	2,6-DMP	§ H_2O_2	-	-	-	-	40 °C	-	-	Acima de 50% após 48 h, pH = 4,8	(ZHANG et al., 2019)
Talaromyces cellulolyticus	*Tc*LPMO9A				-	-	-	-	45 °C	-	-	Acima de 70% após 48 h, pH = 4,8	

OBS: (§) concentração fixa; (+) valores determinados na presença de ácido ascórbico; (*) K_{cat}/K_m calculado considerando-se massa de 24,2 kDa para a *Tt*LPMO9E; (**) enzima identificada pelo gene codificante; (***) pH ótimo não associado a estabilidade a pH; (****) Tm_{app} calculado com base nos dados de CD (*Mt*LPMO9B, *Mt*LPMO9D e *Ta*LPMO9A) e de ITFE (*Mt*LPMO9J); (#) K_{cat} estimado com base nos valores prévios de K_{cat}/K_m and K_m para a *Mt*PMO9E. Análises de cinética conduzidas em (a) pH = 6,0 e (b) pH = 9,0. Abreviações: PWS – palha de trigo pré-tratada; CNW – nanofibra de quitina; RAC – celulose regenerada amorfa.

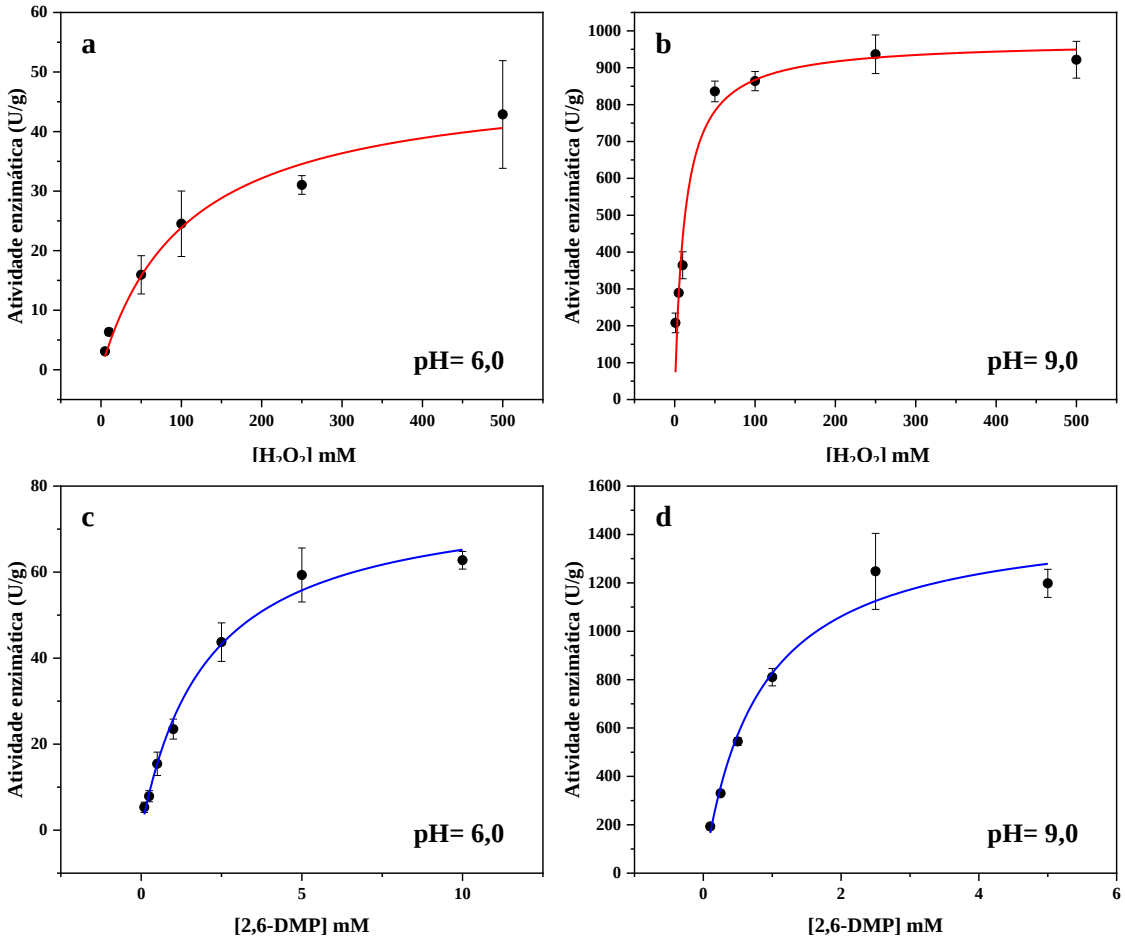

Figura 18. Cinética de Michaelis-Menten para a enzima *Af*AA9_B. Ensaios realizados a 50 °C em pH 6,0 (lateral esquerda) e pH 9,0 (lateral direita) usando-se concentração fixa de 1 mM para o substrato 2,6-DMP e variável (1 – 500 mM) para o co-substrato H_2O_2 ("a" e "b" em vermelho); e concentração fixa de 100 µM para H_2O_2 e variável (0,1 – 10 mM) para 2,6-DMP ("c" e "d" em azul).

Observa-se que através das curvas hiperbólicas que a *Af*AA9_B apresenta comportamento Michaeliano tradicional, tanto para o substrato quanto para o co-substrato, uma vez que com o aumento da concentração dos mesmos, em ambos os casos, a velocidade aumenta até a saturação total do sítio ativo das enzimas (LEONE et al., 2005).

Conforme é exibido na Tabela 2, foi determinado que em comparação com o pH 6,0, a *Af*AA9_B em pH 9,0 apresentou os maiores valores de V_{max} e menores valores de K_m tanto para a cinética com 2,6-DMP (V_{max} e K_m de 1481 U/g e 0,79 µM, respectivamente), quanto para com H_2O_2 (V_{max} e K_m de 972,5 U/g e 12,15 µM, respectivamente). Tais resultados são condizentes com o fato do pH ótimo da *Af*AA9_B ser 9,0 (Figura 17a) e indicam uma maior afinidade da mesma pelos dois substratos nesse valor de pH.

Em comparação com as enzimas PMO9_SCYTH, PMO9_MALCI (AGRAWAL et al., 2019) e CAF32158.1 (MUSADDIQUE et al., 2020), a *Af*AA9_B em pH 9,0 foi a que apresentou o menor valor de K_m pelo substrato 2,6-DMP (maior afinidade), assim como os maiores valores de V_{max}, constante de renovação (K_{cat}) e eficiência catalítica (K_{cat}/K_m) dentre as três.

4.4) Efeitos de aditivos e da concentração de produtos sobre a atividade da *Af*AA9_B

Buscando-se avaliar o impacto de aditivos sobre a atividade da *Af*AA9_B, diferentes íons, detergentes e agentes químicos foram adicionados ao meio reacional contendo a LPMO. Os resultados podem ser conferidos na Tabela 3.

Tabela 3. Efeitos de aditivos sob a atividade da *Af*AA9_B.

Aditivo	**Atividade relativa *Af*AA9_B (%)**
Sem aditivos	100.0 ± 1.0
SDS	107.8 ± 4.8
Tween 20	103.7 ± 9.6
EDTA	0
DMSO	108.3 ± 1.5
β-mercaptoetanol	36.7 ± 0,6
$ZnSO_4$	36.8 ± 6.1
$MnCl_2$	82.2 ± 0.7
$CoCl_2$	0
$CaCl_2$	93.6 ± 3.3
$FeSO_4$	0
$MgSO_4$	113.9 ± 1.9
$CuSO_4$	35.2 ± 4.6
$AgNO_3$	0
KCl	107.5 ± 2.1
$(NH_4)_2SO_4$	88.9 ± 3.2
DTT	0
Triton X-100	84.8 ± 2.3
SLS	115.3 ± 0.7

Observa-se que a adição de aditivos como o EDTA, DTT, β-mercaptoetanol e os sais dos metais de transição Co^{2+}, Fe^{2+}, Cu^{2+}, Zn^{2+} e Ag^{+} resultam na completa ou quase total inibição da atividade enzimática da enzima. O EDTA, molécula quelante, atua sequestrando o cofator Cu^{2+} coordenado à braçadeira de histidina (estrutura catalítica) das LPMOs e portanto elimina sua atividade (GUSAKOV et al., 2017; OBENG; BUDIMAN; ONGKUDON, 2017). De acordo com Semenova *et al*., 2020, foi verificado na enzima

*Pv*LPMO9A uma redução na T_{mapp} de aproximadamente 10 °C, após adição de EDTA e remoção do Cu^{2+}. O estudo de Kracher *et al*., 2018 também demonstrou que a incubação da *Nc*LPMO9C com apenas 300 µM do quelante resultou em uma redução de 8,8 °C na T_{mapp}.

Na presença dos íon dos metais de transição Fe^{2+}, Co^{2+}, Cu^{2+}, Zn^{2+} e Ag^{+}, devido a interação dos mesmos com resíduos de carga negativa e complexação com resíduos contendo grupos amino, o rompimento de pontes salinas e alterações estruturais levaram à desnaturação da enzima e consequente depleção de atividade (DEMIRDAL et al., 2014; PEREIRA et al., 2017). Os íons Cu^{2+}, Zn^{2+} e Ag^{+} também são propensos a atuarem desfazendo ligações dissulfeto, devido a afinidade por resíduos contendo enxofre (BLANCO; BLANCO, 2017; PEREIRA et al., 2017).

A adição dos agentes químicos DTT e β-mercaptoetanol também resultaram em uma acentuada diminuição da atividade enzimática, devido ao fato de ambos apresentarem a capacidade de reduzir ligações dissulfeto, ressaltando mais uma vez a importância dessas ligações covalentes para a estabilidade e manutenção da estrutura nativa da *Af*AA9_B (CALDERARO et al., 2020; PEREIRA et al., 2017; SINGH et al., 2019).

Para todos os demais aditivos, a *Af*AA9_B apresentou uma ótima estabilidade, perdendo pouco ou nada de sua atividade relativa, havendo até mesmo aqueles que promoveram aumento de sua atividade original. Esses resultados demonstram a alta tolerância da *Af*AA9_B frente surfactantes como SDS, SLS, Triton X-100 e Tween 20 e frente ao solvente apolar DMSO, indicando de que a interação desses agentes com regiões hidrofóbicas mais expostas pode contribuir para a o aumento da estabilidade da enzima (Pereira *et al*., 2017).

Considerando-se a relevância e potencial das LPMOs para design de novos coquetéis enzimáticos comerciais, é desejável que as mesmas também apresentem uma boa tolerância e manutenção de suas atividades frente aos produtos gerados durante a degradação de biomassas lignocelulósicas, quando associadas com outras enzimas clássicas (ATREYA; STROBEL; CLARK, 2016; CABANEROS LOPEZ et al., 2021; IPSEN et al., 2021). A Figura 19 ilustra o efeito de concentrações crescentes de glicose e celobiose, produtos comuns dos processos de hidrólise, sob a atividade da *Af*AA9_B.

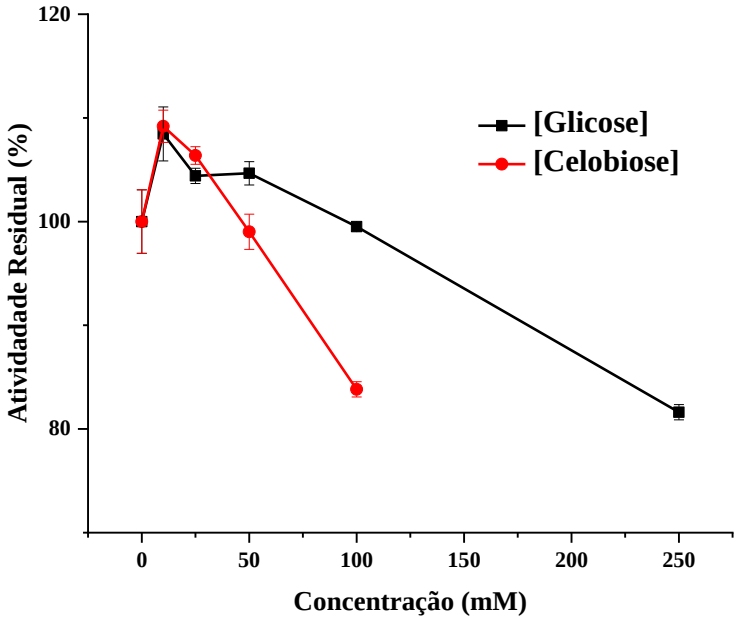

Figura 19. Efeito da concentração crescente de glicose (quadrados pretos) e celobiose (círculos vermelhos) sob a atividade da *Af*AA9_B.

Foi observado que *Af*AA9_B apresenta alta tolerância para ambos os açúcares analisados. A enzima foi capaz de reter praticamente 100% de sua atividade residual até concentrações de 100 mM para glicose e de 50 mM para celobiose, e mesmo em concentrações superiores de 250 mM e 100 mM dos respectivos açúcares, a atividade manteve-se acima de 80%.

Apesar de não haverem trabalhos na literatura comparando o efeito da maioria dos inibidores listados sobre LPMOs, incluindo os dois açúcares acima, é desejável que as mesmas sejam altamente toleráveis aos produtos oriundos da degradação de biomassa lignocelulósica, tendo em vista a crescente adição das enzimas AA9 em coquetéis celulolíticos (ADSUL et al., 2020; KADIĆ et al., 2021; RODRÍGUEZ-ZÚÑIGA et al., 2015).

Sreeja-Raju *et al*., 2020 demonstrou que na hidrólise de palha de arroz com uso do extrato enzimático de *Trichoderma reesei* RUT-C30 (contendo a LPMO CEL61A) houve inibição alta na atividade de enzimas celulolíticas – 28% menor comparado ao extrato do organismo *P.janthinellum* – por acúmulo de celobiose após 10 dias de incubação, reforçando a tese da necessidade da adição de enzimas como β-glicosidases, e da utilização de coquetéis ou extratos com tolerância satisfatória aos açúcares gerados durante o processo de sacarificação.

4.5) Ensaios de atividade e avaliação do efeito sinérgico

A avaliação da atividade sinérgica da *Af*AA9_B foi avaliada sob CMC 1% (m/v). Os resultados individuais da *Af*AA9_B e em conjunto com as enzimas *Af*Cel6A (celobiohidrolase tipo II), *Af*-EGL7 (endoglucanase) e coquetel enzimático Celluclast® 1,5L podem ser conferidos na Figura 20.

Como é possível observar na Figura 20a, individualmente a *Af*AA9_B não foi significativamente capaz de aumentar a liberação de açúcar redutor, mesmo aumentando a concentração em 10X após diferentes tempos (4, 8 ou 24 horas). Esses resultados estão de acordo com o fato de LPMOs não apresentarem atividade hidrolíticas significativas isoladamente (IPSEN et al., 2021; KIM et al., 2015; KRACHER et al., 2018; TOKIN et al., 2020; ZERVA et al., 2020). Em contrapartida, na presença exclusiva da *Af*Cel6A (CBH), seu aumento em 10X na concentração resultou em uma taxa de conversão 2,7X maior após 4 horas e praticamente dobrou após 24 horas.

Ainda na Figura 20a, quando associadas a *Af*AA9_B e *Af*Cel6A nas proporções de 10:10 e 1:10, em todos os 3 tempos de incubação o resultado das hidrólises foi similar aos registrados na presença individual da *Af*Cel6A (0,5 µg). Tal constatação demonstra não somente a atuação prevalente da *Af*Cel6A, como também a ausência de sinergia da mesma com a *Af*AA9_B – mesmo quando aumentado sua concentração em cerca de10X.

No estudo de Tokin *et al*., 2020 é demonstrado que a *Tt*AA9E ativa em C1 não atua de forma sinérgica com a celobiohidrolase do tipo I Cel7A, e isso pode ser em decorrência da oxidação mediada pela LPMO em C1 (na ponta redutora) não permitir a ligação da CBH na mesma. Em nosso estudo, a *Af*Cel6A (CBH II) atua na extremidade não redutora (C4) e a LPMO oxida em C1 e C4, contudo como o estudo de Ipsen *et al*., 2021 aponta, é possível que a *Af*AA9_B tenha preferência em oxidar a posição C4 quando o substrato for CMC, gerando assim extremidades não redutoras oxidadas que não são reconhecidas pela *Af*Cel6A.

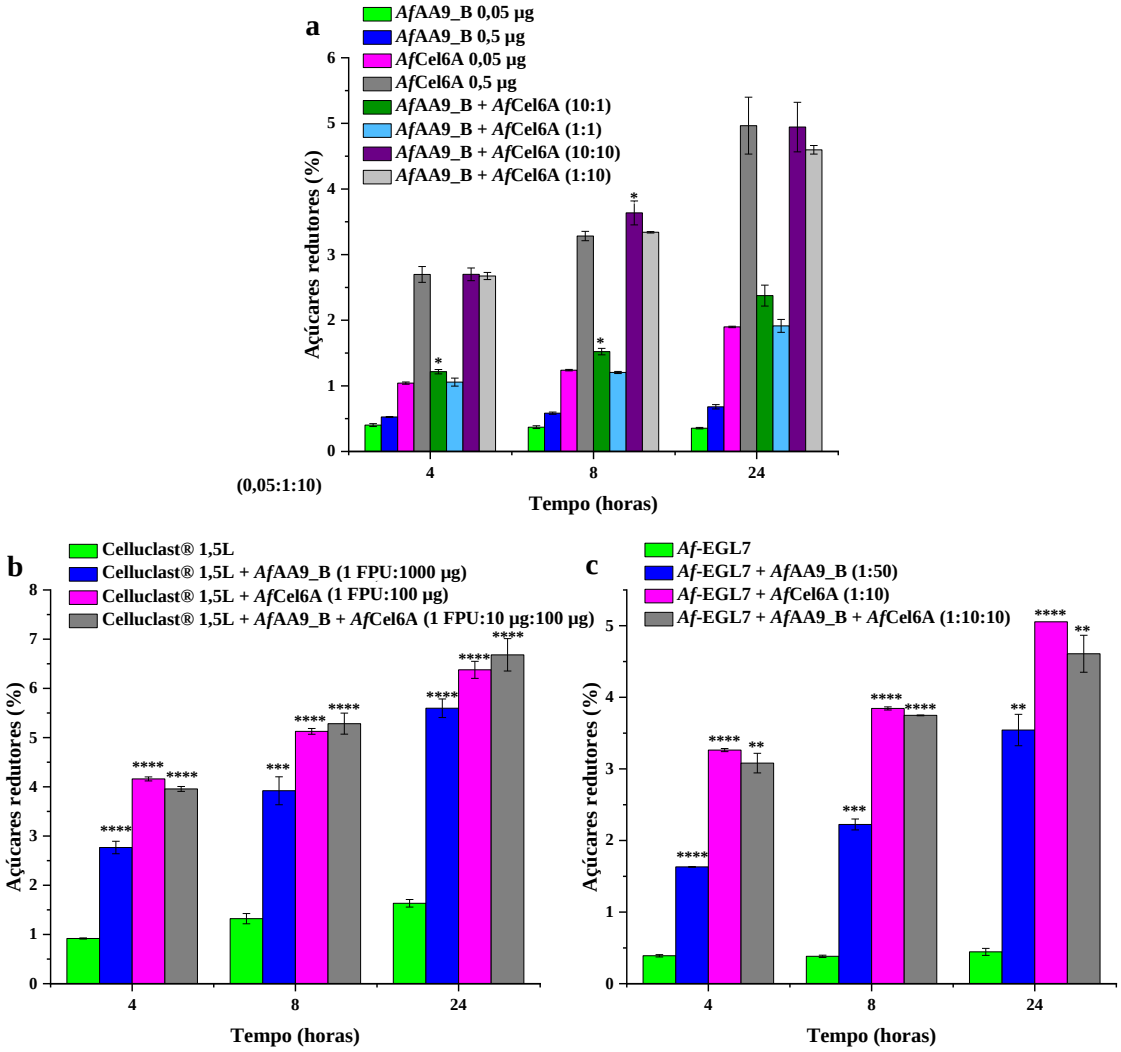

Figura 20. Ensaios de atividade sob CMC (1% m/v) das enzimas *Af*AA9_B e *Af*Cel6A. Foram analisados os efeitos da ação sinérgica e individual das enzimas em diferentes proporções (a); na presença do coquetel Celluclast® 1,5L (b); e da endoglucanase *Af*-EGL7 (c). Os asteriscos indicam diferença significativa ($p < 0,05$) em relação às reações controle com *Af*CEL6A (a), coquetel Celluclast® 1,5L (b) e *Af*-EGL7 (c).

Na Figura 20b, nota-se que após 4 horas, a hidrólise de CMC suplementada com coquetel e *Af*AA9_B na proporção 1 FPU:1000 ug liberou aproximadamente 3X mais açúcares redutores, quando comparada à hidrólise apenas com coquetel (controle), tendência essa mantida mesmo após 24 horas. A associação do coquetel com a *Af*Cel6A na proporção 1 FPU:100 ug aumentou a liberação em 4,5X e 3,9X em relação aos controles após 4 e 24 horas, respectivamente.

Novamente foi observado uma maior atividade da *Af*Cel6A, assim como a ausência de sinergia com a *Af*AA9_B, de tal forma que quando combinadas com o coquetel (1 FPU:10 ug:100 ug) não houve aumento significativo na liberação de açúcares comparado aos resultados da hidrólise com coquetel e *Af*Cel6A (1 FPU:100 ug), independentemente do tempo de incubação.

No caso das hidrólises suplementadas com *Af*-EGL7 (Figura 20c), após 24 horas, foi verificado que em relação ao controle (apenas com a *Af*-EGL7), houve aumento de 8,0 e 11,4X na liberação de açúcares quando associadas com *Af*AA9_B (1:50) e com *Af*Cel6A (1:10), respectivamente. Nos demais tempos a tendência foi mantida.

Observou-se que a adição individual da CBH promoveu os melhores resultados, enquanto a combinação da *Af*-EGL7 com ambas (1:10:10) resultou em valores sutilmente inferiores, indicativos de inibição e que reforçam a ausência de sinergia entre a *Af*AA9_B e a *Af*Cel6A.

Na literatura, vários exemplos de hidrólises com substratos celulósicos suplementados com LPMOs podem ser encontrados. Segundo Kim *et al*., 2015, enzima *Cg*AA9 (0,9 mg/g substrato) quando adicionada à hidrólise de Avicel 1% (m/v) contendo 0,9 FPU de Celluclast® 1,5L aumentou em 1,7X a conversão em glicose. Já Long *et al*., 2020 demonstrou que a suplementação do coquetel CTec2 (3 FPU/g substrato) com a LPMO *Pa*AA9B resultou num aumento de hidrólise de 1,4X (com 0,75 mg LPMO/g substrato) e de 2,3X (com 1,0 mg LPMO/g substrato) quando usados os substratos papel de filtro e Avicel, respectivamente.

Os efeitos sinérgicos promovidos pela adição da *Af*AA9_B ou da *Af*Cel6A às reações de sacarificação das biomassas (SEB, palha de arroz e sabugo de milho) na presença de coquetel Celluclast® 1,5L ou da endoglucanase *Af*-EGL7 podem ser conferidos na Figura 21.

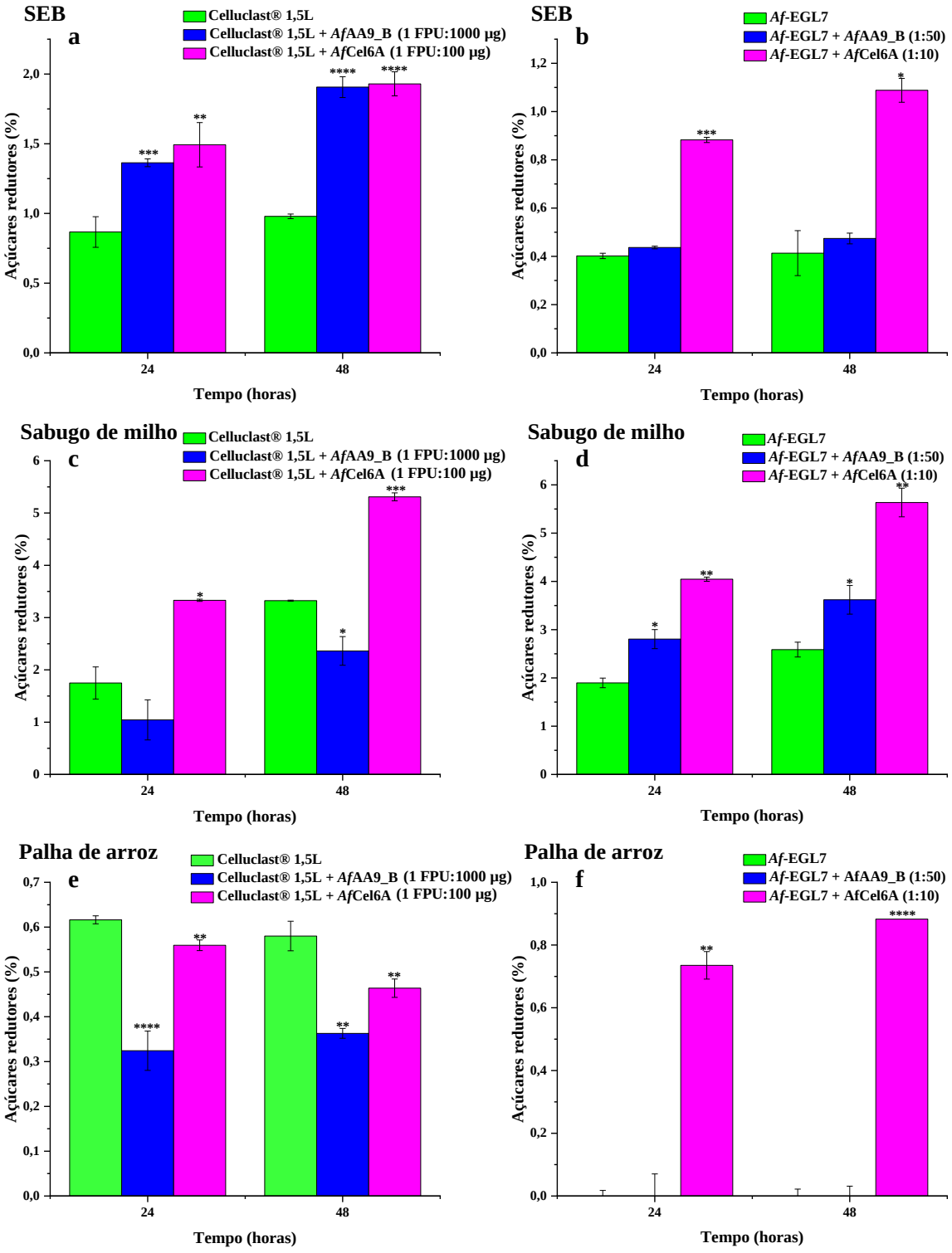

Figura 21. Efeito da suplementação das enzimas *Af*AA9_B e *Af*Cel6A à sacarificação de diferentes resíduos agroindustriais realizada na presença do coquetel Celluclast® 1,5L (lado esquerdo) e da endoglucanase *Af*-EGL7 (lado direito) à 50 °C e 1000 rpm. As biomassas utilizadas (1% m/v) foram SEB ("a" e "b"), sabugo de milho ("c" e "d") e palha de arroz ("e" e "f"). Os asteriscos indicam diferença significativa ($p < 0,05$) em relação às reações controle com coquetel Celluclast® 1,5L (lado esquerdo) e *Af*-EGL7 (lado direito).

Nas Figuras 21a e 21b é possível analisar os resultados da sacarificação do SEB (biomassa pré-tratada por explosão a vapor). Em comparação à reação apenas com coquetel (controle), a suplementação de *Af*AA9_B na proporção de 1FPU:1000 µg provocou aumento de 1,6X e 1,9X na liberação açúcares após 24 e 48 horas, respectivamente. A suplementação com *Af*Cel6A (1 FPU:100 µg) levou ao aumento de 1,7X e 1,9X na liberação após 24 e 48 horas, respectivamente. Apesar dos valores semelhantes, a *Af*Cel6A apresenta maior grau de sinergia com o coquetel devido a sua menor proporção.

Na Figura 21b, em relação ao controle contendo apenas a *Af*-EGL7, a suplementação com a *Af*AA9_B (1:50) resultou em aumentos insignificantes na liberação de açúcares independente do tempo analisado. A suplementação da *Af*Cel6A (1:10), por outro lado aumentou a liberação em 2,2X e 2,6X após 24 e 48 horas, respectivamente. Portanto, na sacarificação do SEB com *Af*-EGL7, a adição da LPMO não se mostrou efetivamente sinérgica, diferentemente da associação com a CBH.

Em estudo de Velasco *et al*., 2021 também com a *Af*AA9_B, foi constatado que a mesma quando suplementada a meio contendo 4% (m/v) de SEB na proporção de 1:4 LPMO/coquetel CBX [(1,0 mg enzima + 4,0 mg CBX)/g de SEB] aumentou em 20% a liberação de glicose, valor similar ao obtido pelo nosso grupo quando a LPMO expressa em *E.coli* na concentração de 10 mg/g substrato foi adicionada em meio com 1% SEB + 0,9 FPU Celluclast® 1,5L/g de substrato (GOUVÊA et al., 2019). Já no estudo de Long *et al*., 2020 as adições da enzima *Pa*AA9B (1,0 ou 0,5 mg/g de biomassa) em meios contendo bagaço de cana submetido a pré-tratamento organosolv com atmosfera de glicerol (AGO) alcalino ou AGO ácido, respectivamente, aumentaram em 20 e 30% a sacarificação na presença do coquetel CTec2 (3 FPU/g de substrato).

Com relação às sacarificações dos meios contendo sabugo de milho (Figuras 21c e 21d) na presença de coquetel (Figura 21c), independentemente do tempo, a suplementação com a *Af*AA9_B (1FPU:1000 µg) não resultou em aumento na sacarificação, mas sim em inibição. A suplementação com *Af*Cel6A (1 FPU:100 µg) levou a aumentos de 1,9X e 1,6X após 24 e 48 horas, respectivamente. É provável que devido à maior barreira de hemicelulose e lignina, as enzimas do coquetel e a LPMO não consigam atuar de forma sinérgica ou possam ficar adsorvidas de forma improdutiva, impossibilitando assim a catálise (DOS SANTOS et al., 2019; JØRGENSEN; PINELO, 2017; VELASCO et al., 2021).

Na sacarificação do meio contendo sabugo de milho com *Af*-EGL7 (Figura 21d), verificou-se aumento da liberação de açúcares com a adição de ambas as enzimas. A adição da *Af*AA9_B (1:50) em relação aos controles elevou a conversão em 1,5X e 1,4X após 24 e 48 horas respectivamente. A adição da *Af*Cel6A (1:10) promoveu aumentos de 2,1X e 2,2X após 24 e 48 horas, respectivamente. Os resultados demonstram que a *Af*Cel6A na presença do coquetel ou da *Af*-EGL7 apresentou portanto maior grau de sinergia.

O sabugo de milho é uma biomassa constituída de 39% celulose (baixo teor), 44% hemicelulose e 12% lignina (POINTNER et al., 2014). O desempenho inferior da *Af*AA9_B pode ser explicado por causa de sua maior afinidade por substratos celulósicos (VELASCO et al., 2021). Devido a presença de um módulo CBM1 na estrutura da *Af*Cel6A, apesar de estar suscetível à adsorção em lignina, é possível que prevaleça o seu ancoramento à celulose (JØRGENSEN; PINELO, 2017). De acordo com o trabalho de Zhang *et al*., 2019, as enzimas *Ta*AA9A e *Tc*AA9A (30 µg ambas) quando suplementadas em meio contendo sabugo de milho deslignificado 2% (m/v) + celulases (5 mg/g substrato) aumentaram a liberação de glicose em 8,55% e 24,20%, respectivamente.

Por fim, nas Figuras 21e e 21f, a sacarificação da palha de arroz foi a que apresentou menor sucesso considerando as taxas de conversão inferiores a 1%. Em 21e, na presença de coquetel, tanto a adição da *Af*AA9_B (1:1000 µg) como da *Af*Cel6A (1:100 µg) não resultaram em efeito sinérgico, mas sim inibitório.

Em 21f, diferentemente de todas as sacarificações analisadas anteriormente, na presença apenas da *Af*-EGL7 nenhuma atividade foi verificada, e o mesmo observou-se com a adição da *Af*AA9_B (1:50). O fato de apenas a suplementação com a *Af*Cel6A (1:10) ter resultado na liberação de açúcares sugere que o efeito se deva exclusivamente à ação da *Af*Cel6A sem haver sinergia com a *Af*-EGL7, a qual não se mostrou ativa na presença da palha de arroz.

A palha de arroz apresenta composição aproximada de 36% celulose, 22% hemicelulose e 24% lignina (IMMAN et al., 2015). Como pode ser percebido, em comparação ao sabugo de milho, apesar das porcentagens próximas de celulose, a biomassa apresenta metade do conteúdo de hemicelulose e o dobro de lignina. Com base nisso é possível que a camada 2X mais espessa de lignina promova a adsorção parcial da LPMO e da CBH fazendo com que as mesmas disputem os poucos sítios disponíveis com

as enzimas do coquetel, o que explicaria o efeito de inibição registrada para ambas (JØRGENSEN; PINELO, 2017). Com relação aos resultados observados na presença de *Af*-EGL7, em que apenas a *Af*Cel6A mostrou-se ativa (Figura 21f), existe a chance de que apesar de tanto a *Af*-EGL7 como a CBH apresentarem CBM1, a ocorrência de uma maior adsorção à fração exposta de celulose por parte da celobiohidrolase possibilite que apenas essa consiga atravessar a barreira de lignina.

O trabalho de Musaddique *et al*., 2020 demonstrou que a enzima *Af*LPMO16 após 72 horas de incubação quando adicionada em quantidades de 100 e 200 µg à sacarificação da palha de arroz (pré-tratada em condição alcalina) 1% (m/v) + coquetel celulósico (5 mg/mL), foi capaz de aumentar em 1,7X e 2,0X a liberação de glicose, respectivamente. Já de acordo com Zhou *et al*., 2020, a enzima *Vi*LPMO10 (0,15 mg/mL) quando utilizada nas proporções coquetel/LPMO de 9:1 e 1:1 em meios contendo 40 mg/mL de palha de arroz (com pré-tratamento alcalino) resultou em aumentos de 22 e 12% na liberação de açúcares redutores, respectivamente.

Esses resultados, ainda que careçam de análises em larga escala, reforçam o potencial da *Af*AA9_B como um possível aditivo para a formulação de novos coquetéis enzimáticos comerciais.

5. Conclusão

Neste trabalho a LPMO *Af*AA9_B de *Aspergillus fumigatus* Af293 teve seu gene codificante AFUA_4G07850 clonado no vetor pPICZB para a enzima ser expressa sob pelo organismo eucarioto *Pichia pastoris* X33.

Análises computacionais forneceram valiosas informações. Através do modelo tridimensional obtido com base na sua sequência e do alinhamento da *Af*AA9_B com outras LPMOs foi possível identificar importantes motivos e resíduos conservados, incluindo aqueles presente na braçadeira de histidina. Dados de dicroísmo circular (CD) e de fluorescência intrínseca de Trp (ITFE) no intervalo de temperatura de 25 a 70 °C permitiram observar mudanças gradativas tanto da estrutura secundária como da terciária, respectivamente.

Com o aumento de temperatura o conteúdo de α-hélices e folhas-β paralelas sofreram intensa queda, ao passo que folhas-β antiparalelas, alças e estruturas desordenadas apresentaram aumento. Paralelamente, com relação aos resíduos de triptofano foi constatado uma maior exposição dos mesmos para meio aquoso, demonstrando a exposição do interior hidrofóbico da LPMO. Por meio da determinação dos valores de temperatura de transição (T_M) do estado nativo para o desnaturado, foram obtidos os valores de 55,22 (via CD) e 53,60 °C (via ITFE), condizentes com o esperado para um organismo mesofílico.

A *Af*AA9_B apresentou pH ótimo de 9,0 e uma alta estabilidade a pH na faixa de 5,0 a 10,0 por até 72 horas. Além disso foi observado uma considerável estabilidade térmica considerando-se que a enzima foi capaz de reter mais de 70% de sua atividade residual após 72 horas a 50 °C e mais de 50% mesmo após 48 horas a 60°C. As constantes cinéticas registradas em pH ótimo foram: K_m = 0,79 µM e V_{max} = 1481 U/g para o substrato 2,6-DMP e K_m = 12,15 µM e V_{max} = 972,5 U/g para o co-substrato H_2O_2.

Outra importante característica foi a alta tolerância da *Af*AA9_B frente a diferentes agentes químicos. A enzima demonstrou ser capaz de manter mais de 80% de sua atividade na presença de surfactantes como o Tween 20, SDS, SLS, Triton X-100; dos íons Mn^{2+}, Ca^{2+}, K^+, NH_4^+; de DMSO; e na presença de 100 mM celobiose e 250 mM glicose, importantes produtos de hidrólise com ação inibitória.

Através de ensaios de atividade com CMC, concluiu-se que as enzimas *Af*AA9_B e *Af*Cel6A (celobiohidrolase) não são sinérgicas entre si. Na presença de Celluclast® 1,5L e *Af*-EGL7 (endoglucanase), foi verificado após 24 horas que com a adição da LPMO houve uma liberação de açúcares 3,5X e 8,0X maiores que os controles, respectivamente. Nos ensaios de sacarificação das biomassas, a suplementação com a *Af*AA9 foi efetivamente sinérgica para SEB na presença de Celluclast® 1,5L e para sabugo de milho na presença de *Af*-EGL7, onde os aumentos na liberação de açúcares foram 2,0X e em 1,5X maiores que seus controles após 48 e 24 horas, respectivamente. A LPMO demonstrou melhor performance na presença de biomassas ricas em celulose.

Todos os resultados obtidos nesse trabalho reforçam o fato de que a *Af*AA9_B é uma LPMO que apresenta enorme potencial à suplementação em coquetéis comerciais já existentes ou à aplicação em biorrefinarias com foco na produção de combustíveis 2G, os quais poderão ser de vital importância no futuro como alternativa ao uso de combustíveis fósseis e outras fontes de energia não renováveis.

6. Referências bibliográficas

ABRAHAM, Amith; MATHEW, Anil K.; PARK, Hyojung; CHOI, Okkyoung; SINDHU, Raveendran; PARAMESWARAN, Binod; PANDEY, Ashok; PARK, Jung Han; SANG, Byoung In. Pretreatment strategies for enhanced biogas production from lignocellulosic biomass. **Bioresource Technology**, *[S. l.]*, v. 301, n. October 2019, p. 122725, 2020. DOI: 10.1016/j.biortech.2019.122725.

ADAV, Sunil S.; RAVINDRAN, Anita; SZE, Siu Kwan. Quantitative proteomic study of Aspergillus Fumigatus secretome revealed deamidation of secretory enzymes. **Journal of Proteomics**, *[S. l.]*, v. 119, p. 154–168, 2015. DOI: 10.1016/j.jprot.2015.02.007.

ADSUL, Mukund; SANDHU, Simranjeet Kaur; SINGHANIA, Reeta Rani; GUPTA, Ravi; PURI, Suresh K. Enzyme and Microbial Technology Designing a cellulolytic enzyme cocktail for the e ffi cient and economical conversion of lignocellulosic biomass to biofuels. **Enzyme and Microbial Technology**, *[S. l.]*, v. 133, n. October 2019, p. 109442, 2020. DOI: 10.1016/j.enzmictec.2019.109442. Disponível em: https://doi.org/10.1016/j.enzmictec.2019.109442.

AGRAWAL, Dhruv; BASOTRA, Neha; BALAN, Venkatesh; TSANG, Adrian; CHADHA, Bhupinder Singh. Discovery and Expression of Thermostable LPMOs from Thermophilic Fungi for Producing Efficient Lignocellulolytic Enzyme Cocktails. **Applied Biochemistry and Biotechnology**, *[S. l.]*, 2019. DOI: 10.1007/s12010-019-03198-5.

ATREYA, Meera E.; STROBEL, Kathryn L.; CLARK, Douglas S. Alleviating product inhibition in cellulase enzyme Cel7A. **Biotechnology and Bioengineering**, *[S. l.]*, 2016. DOI: 10.1002/bit.25809.

AYDIN, Mucahit. The effect of biomass energy consumption on economic growth in BRICS countries: A country-specific panel data analysis. **Renewable Energy**, *[S. l.]*, v. 138, p. 620–627, 2019. DOI: 10.1016/j.renene.2019.02.001.

BENNATI-GRANIER, Chloé et al. Substrate specificity and regioselectivity of fungal AA9 lytic polysaccharide monooxygenases secreted by Podospora anserina. **Biotechnology for Biofuels**, *[S. l.]*, v. 8, n. 1, p. 90, 2015. DOI: 10.1186/s13068-015-0274-3. Disponível em: http://www.biotechnologyforbiofuels.com/content/8/1/90.

BERGMANN, Jessica C.; TRICHEZ, Débora; SALLET, Lunalva P.; DE PAULA E SILVA, Flávia Cristina; ALMEIDA, João R. M. Technological Advancements in 1G Ethanol Production and Recovery of By-Products Based on the Biorefinery Concept. **Advances in Sugarcane Biorefinery: Technologies, Commercialization, Policy Issues and Paradigm Shift for Bioethanol and By-Products**, *[S. l.]*, p. 73–95, 2018. DOI: 10.1016/B978-0-12-804534-3.00004-5.

BERNARDI, Aline Vianna et al. LPMO Af AA9 _ B and Cellobiohydrolase Af Cel6A from A . fumigatus Boost Enzymatic Saccharification Activity of Cellulase Cocktail. *[S. l.]*, 2021.

BERNARDI, Aline Vianna; GOUVÊA, Paula Fagundes De; GEROLAMO, Luis Eduardo; YONAMINE, Deborah Kimie; LOURDES, Laís De; BALICO, De Lima; UYEMURA, Sergio Akira. Functional characterization of GH7 endo-1,4-β-glucanase from Aspergillus fumigatus and its potential industrial application. **Protein Expression**

and Purification, *[S. l.]*, v. 150, n. April, p. 1–11, 2018. DOI: 10.1016/j.pep.2018.04.016.

BERNARDI, Aline Vianna; YONAMINE, Deborah Kimie; UYEMURA, Sergio Akira; DINAMARCO, Taisa Magnani. A Thermostable Aspergillus fumigatus GH7 Endoglucanase Over-Expressed in Pichia pastoris Stimulates Lignocellulosic Biomass Hydrolysis. *[S. l.]*, 2019.

BERTINI, Luca; BREGLIA, Raffaella; LAMBRUGHI, Matteo; FANTUCCI, Piercarlo; DE GIOIA, Luca; BORSARI, Marco; SOLA, Marco; BORTOLOTTI, Carlo Augusto; BRUSCHI, Maurizio. Catalytic Mechanism of Fungal Lytic Polysaccharide Monooxygenases Investigated by First-Principles Calculations. **Inorganic Chemistry**, *[S. l.]*, v. 57, n. 1, p. 86–97, 2018. DOI: 10.1021/acs.inorgchem.7b02005.

BISSARO, Bastien; KOMMEDAL, Eirik; RØHR, Åsmund K.; EIJSINK, Vincent G. H. Controlled depolymerization of cellulose by light-driven lytic polysaccharide oxygenases. **Nature Communications**, *[S. l.]*, v. 11, n. 1, 2020. DOI: 10.1038/s41467-020-14744-9. Disponível em: http://dx.doi.org/10.1038/s41467-020-14744-9.

BLANCO, Antonio; BLANCO, Gustavo. Enzymes. *In*: **Medical Biochemistry**. [s.l: s.n.]. p. 153–175. DOI: 10.1016/B978-0-12-803550-4/00008-2.

BORISOVA, Anna S. et al. Structural and Functional Characterization of a Lytic Polysaccharide Monooxygenase with Broad Substrate Specificity. **Journal of Biological Chemistry**, *[S. l.]*, v. 290, n. 38, p. 22955–22969, 2015. DOI: 10.1074/jbc.M115.660183.

BRANDER, Søren et al. Biochemical evidence of both copper chelation and oxygenase activity at the histidine brace. **Scientific Reports**, *[S. l.]*, v. 10, n. 1, p. 1–11, 2020. DOI: 10.1038/s41598-020-73266-y.

BRESLMAYR, Erik; HANŽEK, Marija; HANRAHAN, Aoife; LEITNER, Christian; KITTL, Roman; ŠANTEK, Božidar; OOSTENBRINK, Chris; LUDWIG, Roland. A fast and sensitive activity assay for lytic polysaccharide monooxygenase. **Biotechnology for Biofuels**, *[S. l.]*, 2018. DOI: 10.1186/s13068-018-1063-6.

BULL, Stanley R. Renewable energy today and tomorrow. **Proceedings of the IEEE**, *[S. l.]*, v. 89, n. 8, p. 1216–1226, 2001. DOI: 10.1109/5.940290.

CABANEROS LOPEZ, Pau; UDUGAMA, Isuru A.; THOMSEN, Sune T.; ROSLANDER, Christian; JUNICKE, Helena; IGLESIAS, Miguel M.; GERNAEY, Krist V. Transforming data to information: A parallel hybrid model for real-time state estimation in lignocellulosic ethanol fermentation. **Biotechnology and Bioengineering**, *[S. l.]*, v. 118, n. 2, p. 579–591, 2021. DOI: 10.1002/bit.27586.

CALDERARO, F.; KESER, M.; AKEROYD, M.; BEVERS, L. E.; EIJSINK, V. G. H.; VÁRNAI, A.; VAN DEN BERG, M. A. Characterization of an AA9 LPMO from Thielavia australiensis, TausLPMO9B, under industrially relevant lignocellulose saccharification conditions. **Biotechnology for Biofuels**, *[S. l.]*, v. 13, n. 1, p. 1–17, 2020. DOI: 10.1186/s13068-020-01836-3.

CANTAREL, B. L.; COUTINHO, P. M.; RANCUREL, C.; BERNARD, T.; LOMBARD, V.; HENRISSAT, B. The Carbohydrate-Active EnZymes database (CAZy): an expert resource for Glycogenomics. **Nucleic Acids Research**, *[S. l.]*, v. 37, n. Database, p. D233–D238, 2009. DOI: 10.1093/nar/gkn663.

CARVALHO, Walter; CANILHA, Larissa; FERRAZ, André; MILAGRES, Adriane Maria Ferreira. Uma visão sobre a estrutura, composição e biodegradação da madeira. **Química Nova**, *[S. l.]*, v. 32, n. 8, p. 2191–2195, 2009. DOI: 10.1590/s0100-40422009000800033.

CHANDEL, Anuj K.; ALBARELLI, Juliana Q.; SANTOS, Diego T.; CHUNDAWAT, Shishir Ps; PURI, Munish; MEIRELES, Maria Angela A. Comparative analysis of key technologies for cellulosic ethanol production from Brazilian sugarcane bagasse at a commercial scale. **Biofuels, Bioproducts and Biorefining**, *[S. l.]*, v. 13, n. 4, p. 994–1014, 2019. DOI: 10.1002/bbb.1990.

CHANDEL, Anuj K.; DA SILVA, Silvio S.; CARVALHO, Walter; SINGH, Om V. Sugarcane bagasse and leaves: Foreseeable biomass of biofuel and bio-products. **Journal of Chemical Technology and Biotechnology**, *[S. l.]*, v. 87, n. 1, p. 11–20, 2012. DOI: 10.1002/jctb.2742.

CHEN, Chen; CHEN, Jinyin; GENG, Zhigang; WANG, Meixia; LIU, Ning; LI, Duochuan. Regioselectivity of oxidation by a polysaccharide monooxygenase from Chaetomium thermophilum. **Biotechnology for Biofuels**, *[S. l.]*, v. 11, n. 1, p. 1–16, 2018. DOI: 10.1186/s13068-018-1156-2.

CHO, Sung Yeon et al. Characteristics of culture-positive invasive pulmonary aspergillosis in patients with hematologic diseases: Comparison between Aspergillus fumigatus and non-fumigatus Aspergillus species. **Medicine (United States)**, *[S. l.]*, v. 96, n. 49, 2017. DOI: 10.1097/MD.0000000000008841.

CHOI, Byung-kwon et al. Use of combinatorial genetic libraries to humanize N-linked glycosylation in the yeast Pichia pastoris. *[S. l.]*, v. 107, n. 15, 2010. DOI: 10.1073/pnas.1003237107.

CHYLENSKI, Piotr; BISSARO, Bastien; SØRLIE, Morten; RØHR, Åsmund K.; VÁRNAI, Anikó; HORN, Svein J.; EIJSINK, Vincent G. H. Lytic Polysaccharide Monooxygenases in Enzymatic Processing of Lignocellulosic Biomass. **ACS Catalysis**, *[S. l.]*, v. 9, n. 6, p. 4970–4991, 2019. DOI: 10.1021/acscatal.9b00246.

CIANO, Luisa; DAVIES, Gideon J.; TOLMAN, William B.; WALTON, Paul H. Bracing copper for the catalytic oxidation of C–H bonds. **Nature Catalysis**, *[S. l.]*, v. 1, n. 8, p. 571–577, 2018. DOI: 10.1038/s41929-018-0110-9.

CONAB. Acompanhamento da safra brasileira de cana-de-açúcar V.8 - Safra 2021/22 - N.3 - Terceiro levantamento | Novembro 2021. **Conab - Companhia Nacional de Abastecimento**, *[S. l.]*, v. 8, p. 1–63, 2021. Disponível em: https://www.conab.gov.br/info-agro/safras/cana/boletim-da-safra-de-cana-de-acucar.

COTA, Junio; CORRÊA, Thamy L. R.; DAMÁSIO, André R. L.; DIOGO, José A.; HOFFMAM, Zaira B.; GARCIA, Wanius; OLIVEIRA, Leandro C.; PRADE, Rolf A.; SQUINA, Fabio M. Comparative analysis of three hyperthermophilic GH1 and GH3 family members with industrial potential. **New Biotechnology**, *[S. l.]*, v. 32, n. 1, p. 13–20, 2015. DOI: 10.1016/j.nbt.2014.07.009.

COURTADE, Gaston; LE, Simone Balzer; SÆTROM, Gerd Inger; BRAUTASET, Trygve; AACHMANN, Finn L. A novel expression system for lytic polysaccharide monooxygenases. **Carbohydrate Research**, *[S. l.]*, v. 448, p. 212–219, 2017. DOI: 10.1016/j.carres.2017.02.003.

COUTURIER, Marie et al. Lytic xylan oxidases from wood-decay fungi unlock biomass degradation. **Nature Chemical Biology**, *[S. l.]*, v. 14, n. 3, p. 306–310, 2018. DOI: 10.1038/nchembio.2558.

DANNEELS, Barbara; TANGHE, Magali; DESMET, Tom. Structural Features on the Substrate-Binding Surface of Fungal Lytic Polysaccharide Monooxygenases Determine Their Oxidative Regioselectivity. **Biotechnology Journal**, *[S. l.]*, v. 14, n. 3, p. 1–10, 2019. DOI: 10.1002/biot.201800211.

DANNEELS, Barbara; TANGHE, Magali; JOOSTEN, Henk-Jan; GUNDINGER, Thomas; SPADIUT, Oliver; STALS, Ingeborg; DESMET, Tom. A quantitative indicator diagram for lytic polysaccharide monooxygenases reveals the role of aromatic surface residues in HjLPMO9A regioselectivity. **PLOS ONE**, *[S. l.]*, v. 12, n. 5, p. e0178446, 2017. DOI: 10.1371/journal.pone.0178446.

DE GOUVÊA, P. F.; GEROLAMO, L. E.; BERNARDI, A. V.; PEREIRA, L. M. S.; UYEMURA, S. A.; DINAMARCO, T. M. Lytic polysaccharide monooxygenase from aspergillus fumigatus can improve enzymatic cocktail activity during sugarcane bagasse hydrolysis. **Protein and Peptide Letters**, *[S. l.]*, v. 26, n. 5, 2019. DOI: 10.2174/0929866526666190228163629.

DE GOUVÊA, Paula Fagundes; BERNARDI, Aline Vianna; GEROLAMO, Luis Eduardo; DE SOUZA SANTOS, Emerson; RIAÑO-PACHÓN, Diego Mauricio; UYEMURA, Sergio Akira; DINAMARCO, Taisa Magnani. Transcriptome and secretome analysis of Aspergillus fumigatus in the presence of sugarcane bagasse. **BMC Genomics**, *[S. l.]*, v. 19, n. 1, p. 1–18, 2018. DOI: 10.1186/s12864-018-4627-8.

DE VRIES, Ronald P.; VISSER, Jaap. Aspergillus Enzymes Involved in Degradation of Plant Cell Wall Polysaccharides. **Microbiology and Molecular Biology Reviews**, *[S. l.]*, v. 65, n. 4, p. 497–522, 2001. DOI: 10.1128/mmbr.65.4.497-522.2001.

DEMIRDAŁ, Ramazan; YERLIKAYA, Emrah; ŞENTÜRK, Murat; KÜFREVIOŁLU, O. Irfan; SUPURAN, Claudiu T. Heavy metal ion inhibition studies of human, sheep and fish α-carbonic anhydrases. **Journal of Enzyme Inhibition and Medicinal Chemistry**, *[S. l.]*, v. 28, n. 2, p. 278–282, 2014. DOI: 10.3109/14756366.2011.640633.

DOS SANTOS, Antonio Carlos; XIMENES, Eduardo; KIM, Youngmi; LADISCH, Michael R. Lignin–Enzyme Interactions in the Hydrolysis of Lignocellulosic Biomass. **Trends in Biotechnology**, *[S. l.]*, v. 37, n. 5, p. 518–531, 2019. DOI: 10.1016/j.tibtech.2018.10.010. Disponível em: https://doi.org/10.1016/j.tibtech.2018.10.010.

EIJSINK, Vincent G. H.; PETROVIC, Dejan; FORSBERG, Zarah; MEKASHA, Sophanit; RØHR, Åsmund K.; VÁRNAI, Anikó; BISSARO, Bastien; VAAJE-KOLSTAD, Gustav. **On the functional characterization of lytic polysaccharide monooxygenases (LPMOs)Biotechnology for Biofuels**, 2019. DOI: 10.1186/s13068-019-1392-0.

FAO. Production quantities of Sugar cane by country. **Food and Agriculture Organization of the United States**, *[S. l.]*, 2019. Disponível em: http://www.fao.org/faostat/en/#data/QC/visualize.

FILIATRAULT-CHASTEL, Camille et al. AA16, a new lytic polysaccharide monooxygenase family identified in fungal secretomes. **Biotechnology for Biofuels**, *[S.*

l.], v. 12, n. 1, p. 1–15, 2019. DOI: 10.1186/s13068-019-1394-y.

FOGAÇA, Jennifer Rocha Vargas. Combustíveis Fósseis. **Brasil Escola**, *[S. l.]*, 2020. Disponível em: https://brasilescola.uol.com.br/quimica/combustiveis-fosseis.htm.

FORSBERG, Zarah; SØRLIE, Morten; PETROVIĆ, Dejan; COURTADE, Gaston; AACHMANN, Finn L.; VAAJE-KOLSTAD, Gustav; BISSARO, Bastien; RØHR, Åsmund K.; EIJSINK, Vincent GH. Polysaccharide degradation by lytic polysaccharide monooxygenases. **Current Opinion in Structural Biology**, *[S. l.]*, v. 59, p. 54–64, 2019. DOI: 10.1016/j.sbi.2019.02.015.

FRANDSEN, Kristian E. H. et al. The molecular basis of polysaccharide cleavage by lytic polysaccharide monooxygenases. **Nature Chemical Biology**, *[S. l.]*, v. 12, n. 4, p. 298–303, 2016. DOI: 10.1038/nchembio.2029.

FRANDSEN, Kristian E. H. et al. Insights into an unusual Auxiliary Activity 9 family member lacking the histidine brace motif of lytic polysaccharide monooxygenases. **Journal of Biological Chemistry**, *[S. l.]*, v. 294, n. 45, p. 17117–17130, 2019. DOI: 10.1074/jbc.RA119.009223.

FRANDSEN, Kristian E. H.; HAON, Mireille; GRISEL, Sacha; HENRISSAT, Bernard; LO LEGGIO, Leila; BERRIN, Jean-Guy. Identification of the molecular determinants driving the substrate specificity of fungal lytic polysaccharide monooxygenases (LPMOs). **Journal of Biological Chemistry**, *[S. l.]*, v. 296, p. 100086, 2021. DOI: 10.1074/jbc.ra120.015545.

FRANDSEN, Kristian E. H.; LO LEGGIO, Leila. Lytic polysaccharide monooxygenases: A crystallographer's view on a new class of biomass-degrading enzymes. **IUCrJ**, *[S. l.]*, v. 3, p. 448–467, 2016. DOI: 10.1107/S2052252516014147.

FROMMHAGEN, Matthias; KOETSIER, Martijn J.; WESTPHAL, Adrie H.; VISSER, Jaap; HINZ, Sandra W. A.; VINCKEN, Jean-Paul; VAN BERKEL, Willem J. H.; KABEL, Mirjam A.; GRUPPEN, Harry. Lytic polysaccharide monooxygenases from Myceliophthora thermophila C1 differ in substrate preference and reducing agent specificity. **Biotechnology for Biofuels**, *[S. l.]*, v. 9, n. 1, p. 186, 2016. DOI: 10.1186/s13068-016-0594-y.

FROMMHAGEN, Matthias; WESTPHAL, Adrie H.; HILGERS, Roelant; KOETSIER, Martijn J.; HINZ, Sandra W. A.; VISSER, Jaap; GRUPPEN, Harry; VAN BERKEL, Willem J. H.; KABEL, Mirjam A. Quantification of the catalytic performance of C1-cellulose-specific lytic polysaccharide monooxygenases. **Applied Microbiology and Biotechnology**, *[S. l.]*, v. 102, n. 3, p. 1281–1295, 2018. DOI: 10.1007/s00253-017-8541-9.

GABRIEL, Raphael et al. Development of genetic tools for the thermophilic filamentous fungus Thermoascus aurantiacus. **Biotechnology for Biofuels**, *[S. l.]*, v. 13, n. 1, p. 1–15, 2020. DOI: 10.1186/s13068-020-01804-x. Disponível em: https://doi.org/10.1186/s13068-020-01804-x.

GIBSON, Lorna J. The hierarchical structure and mechanics of plant materials. **Journal of the Royal Society Interface**, *[S. l.]*, v. 9, n. 76, p. 2749–2766, 2012. DOI: 10.1098/rsif.2012.0341.

GIL-CHÁVEZ, Joana; GURIKOV, Pavel; HU, Xihua; MEYER, Robert; REYNOLDS, Wienke; SMIRNOVA, Irina. Application of novel and technical lignins in food and

pharmaceutical industries: structure-function relationship and current challenges. **Biomass Conversion and Biorefinery**, *[S. l.]*, 2019. DOI: 10.1007/s13399-019-00458-6.

GOUVÊA, Paula Fagundes De; GEROLAMO, Luis Eduardo; BERNARDI, Aline Vianna; MATHEUS, Lucas; PEREIRA, Soares; UYEMURA, Sergio Akira; DINAMARCO, Taisa Magnani. Lytic Polysaccharide Monooxygenase from Aspergillus fumigatus can Improve Enzymatic Cocktail Activity During Sugarcane Bagasse Hydrolysis. *[S. l.]*, p. 1–9, 2019. DOI: 10.2174/0929866526666190228163629.

GREENBERG, C. S.; CRADDOCK, P. R. **Rapid single-step membrane protein assay.Clinical Chemistry**, 1982.

GUSAKOV, Alexander V.; BULAKHOV, Alexander G.; DEMIN, Ilya N.; SINITSYN, Arkady P. Monitoring of reactions catalyzed by lytic polysaccharide monooxygenases using highly-sensitive fluorimetric assay of the oxygen consumption rate. **Carbohydrate Research**, *[S. l.]*, v. 452, p. 156–161, 2017. DOI: 10.1016/j.carres.2017.10.015. Disponível em: https://doi.org/10.1016/j.carres.2017.10.015.

HANGASKY, John A.; IAVARONE, Anthony T.; MARLETTA, Michael A. Reactivity of O 2 versus H 2 O 2 with polysaccharide monooxygenases. *[S. l.]*, v. 115, n. 19, 2018. DOI: 10.1073/pnas.1801153115.

HANSSON, Henrik et al. High-resolution structure of a lytic polysaccharide monooxygenase from Hypocrea jecorina reveals a predicted linker as an integral part of the catalytic domain. **Journal of Biological Chemistry**, *[S. l.]*, v. 292, n. 46, p. 19099–19109, 2017. DOI: 10.1074/jbc.M117.799767.

HARRIS, Stephanie B.; TSCHIRNER, Ulrike W.; GILLESPIE, Adam; SEEGER, Madeleine J. Characteristic Properties of Novel Organosolv Lignin/Polylactide/Delta-Valerolactone Terpolymers. **Journal of Polymers and the Environment**, *[S. l.]*, v. 26, n. 8, p. 3262–3271, 2018. DOI: 10.1007/s10924-018-1212-9.

HEGNAR, Olav A.; PETROVIC, Dejan M.; BISSARO, Bastien; ALFREDSEN, Gry; VÁRNAI, Anikó; EIJSINK, Vincent G. H. pH-Dependent Relationship between Catalytic Activity and Hydrogen Peroxide Production Shown via Characterization of a Lytic Polysaccharide Monooxygenase from Gloeophyllum trabeum. **Applied and Environmental Microbiology**, *[S. l.]*, v. 85, n. 5, p. 1–15, 2018. DOI: 10.1128/AEM.02612-18.

HEMSWORTH, Glyn R.; HENRISSAT, Bernard; DAVIES, Gideon J.; WALTON, Paul H. Discovery and characterization of a new family of lytic polysaccharide monooxygenases. **Nature chemical biology**, *[S. l.]*, v. 10, n. 2, p. 122–126, 2014. DOI: 10.1038/nchembio.1417.

IEA. Total energy supply (TES) by source, Brazil 1990-2019. **IEA - International Energy Agency**, *[S. l.]*, 2020. Disponível em: https://www.iea.org/data-and-statistics.

IMMAN, Saksit; ARNTHONG, Jantima; BURAPATANA, Vorakan; CHAMPREDA, Verawat; LAOSIRIPOJANA, Navadol. Influence of alkaline catalyst addition on compressed liquid hot water pretreatment of rice straw. **Chemical Engineering Journal**, *[S. l.]*, v. 278, p. 85–91, 2015. DOI: 10.1016/j.cej.2014.12.032. Disponível em: http://dx.doi.org/10.1016/j.cej.2014.12.032.

IPSEN, Johan Ø.; HALLAS-MØLLER, Magnus; BRANDER, Søren; LO LEGGIO, Leila; JOHANSEN, Katja S. Lytic polysaccharide monooxygenases and other histidine-brace copper proteins: structure, oxygen activation and biotechnological applications. **Biochemical Society Transactions**, *[S. l.]*, v. 0, n. January, p. 531–540, 2021. DOI: 10.1042/bst20201031.

JAGADEESWARAN, Guru; GAINEY, Lawrie; PRADE, Rolf; MORT, Andrew J. A family of AA9 lytic polysaccharide monooxygenases in Aspergillus nidulans is differentially regulated by multiple substrates and at least one is active on cellulose and xyloglucan. **Applied Microbiology and Biotechnology**, *[S. l.]*, v. 100, n. 10, p. 4535–4547, 2016. DOI: 10.1007/s00253-016-7505-9.

JANUSZ, Grzegorz; PAWLIK, Anna; SULEJ, Justyna; ŚWIDERSKA-BUREK, Urszula; JAROSZ-WILKOLAZKA, Anna; PASZCZYŃSKI, Andrzej. Lignin degradation: Microorganisms, enzymes involved, genomes analysis and evolution. **FEMS Microbiology Reviews**, *[S. l.]*, v. 41, n. 6, p. 941–962, 2017. DOI: 10.1093/femsre/fux049.

JOHNSON, M.; ZARETSKAYA, I.; RAYTSELIS, Y.; MEREZHUK, Y.; MCGINNIS, S.; MADDEN, T. L. NCBI BLAST: a better web interface. **Nucleic Acids Research**, *[S. l.]*, v. 36, n. Web Server, p. W5–W9, 2008. DOI: 10.1093/nar/gkn201.

JØRGENSEN, Henning; PINELO, Manuel. Enzyme recycling in lignocellulosic biorefineries. **Biofuels, Bioproducts and Biorefining**, *[S. l.]*, v. 11, n. 1, p. 150–167, 2017. DOI: 10.1002/bbb.1724. Disponível em: https://onlinelibrary.wiley.com/doi/abs/10.1002/bbb.1724.

KABSCH, Wolfgang; SANDER, Christian. How good are predictions of protein secondary structure ? *[S. l.]*, v. 155, n. 2, p. 179–182, 1983.

KADIĆ, Adnan; VÁRNAI, Anikó; EIJSINK, Vincent G. H.; HORN, Svein Jarle; LIDÉN, Gunnar. In situ measurements of oxidation–reduction potential and hydrogen peroxide concentration as tools for revealing LPMO inactivation during enzymatic saccharification of cellulose. **Biotechnology for Biofuels**, *[S. l.]*, v. 14, n. 1, p. 1–10, 2021. DOI: 10.1186/s13068-021-01894-1. Disponível em: https://doi.org/10.1186/s13068-021-01894-1.

KADOWAKI, Marco A. S.; VÁRNAI, Anikó; JAMESON, John Kristian; LEITE, Ana E. T.; COSTA-FILHO, Antonio J.; KUMAGAI, Patricia S.; PRADE, Rolf A.; POLIKARPOV, Igor; EIJSINK, Vincent G. H. Functional characterization of a lytic polysaccharide monooxygenase from the thermophilic fungus Myceliophthora thermophila. **PLoS ONE**, *[S. l.]*, v. 13, n. 8, p. 1–16, 2018. DOI: 10.1371/journal.pone.0202148.

KARKEHABADI, Saeid; HANSSON, Henrik; KIM, Steve; PIENS, Kathleen; MITCHINSON, Colin; SANDGREN, Mats. The First Structure of a Glycoside Hydrolase Family 61 Member, Cel61B from Hypocrea jecorina, at 1.6 Å Resolution. **Journal of Molecular Biology**, *[S. l.]*, v. 383, n. 1, p. 144–154, 2008. DOI: 10.1016/j.jmb.2008.08.016.

KATOH, Kazutaka; ROZEWICKI, John; YAMADA, Kazunori D. MAFFT online service: Multiple sequence alignment, interactive sequence choice and visualization. **Briefings in Bioinformatics**, *[S. l.]*, v. 20, n. 4, p. 1160–1166, 2018. DOI: 10.1093/bib/bbx108.

KELLER, M. B.; FELBY, C.; LABATE, C. A.; PELLEGRINI, V. O. A.; HIGASI, P.; SINGH, R. K.; POLIKARPOV, I.; BLOSSOM, B. M. ORIGINAL RESEARCH PAPER A simple enzymatic assay for the quantification of C1-specific cellulose oxidation by lytic polysaccharide monooxygenases. **Biotechnology Letters**, *[S. l.]*, v. 9, n. Ii, 2019. DOI: 10.1007/s10529-019-02760-9.

KELLEY, Lawrence A.; MEZULIS, Stefans; YATES, Christopher M.; WASS, Mark N.; STERNBERG, Michael J. E. Europe PMC Funders Group The Phyre2 web portal for protein modelling , prediction and analysis. **Nature protocols**, *[S. l.]*, v. 10, n. 6, p. 845–858, 2015. DOI: 10.1038/nprot.2015.053.The.

KHATIWADA, Dilip; LEDUC, Sylvain; SILVEIRA, Semida; MCCALLUM, Ian. Optimizing ethanol and bioelectricity production in sugarcane biorefineries in Brazil. **Renewable Energy**, *[S. l.]*, v. 85, p. 371–386, 2016. DOI: 10.1016/j.renene.2015.06.009.

KIM, In Jung; NAM, Ki Hyun; YUN, Eun Ju; KIM, Sooah; YOUN, Hak Jin; LEE, Hee Jin; CHOI, In Geol; KIM, Kyoung Heon. Optimization of synergism of a recombinant auxiliary activity 9 from Chaetomium globosum with cellulase in cellulose hydrolysis. **Applied Microbiology and Biotechnology**, *[S. l.]*, v. 99, n. 20, p. 8537–8547, 2015. DOI: 10.1007/s00253-015-6592-3.

KOJIMA, Yuka et al. A Lytic Polysaccharide Monooxygenase with Broad Xyloglucan Specificity from the Brown-Rot Fungus Gloeophyllum trabeum and Its Action on Cellulose-Xyloglucan Complexes. **Applied and Environmental Microbiology**, *[S. l.]*, v. 82, n. 22, p. 6557–6572, 2016. DOI: 10.1128/AEM.01768-16.

KRACHER, Daniel; ANDLAR, Martina; FURTMÜLLER, Paul G.; LUDWIG, Roland. Active-site copper reduction promotes substrate binding of fungal lytic polysaccharide monooxygenase and reduces stability. **Journal of Biological Chemistry**, *[S. l.]*, v. 293, n. 5, p. 1676–1687, 2018. DOI: 10.1074/jbc.RA117.000109.

KUMARA, P. R.; MUNASINGHE, E. S.; RODRIGO, V. H. L.; KARUNARATNA, A. S. Carbon Footprint of Rubber/Sugarcane Intercropping System in Sri Lanka: A Case Study. **Procedia Food Science**, *[S. l.]*, v. 6, n. April, p. 298–302, 2016. DOI: 10.1016/j.profoo.2016.02.059.

KUUSK, Silja; BISSARO, Bastien; KUUSK, Piret; FORSBERG, Zarah; EIJSINK, Vincent G. H.; SØRLIE, Morten; VALJAMAE, Priit. Kinetics of H2O2-driven degradation of chitin by a bacterial lytic polysaccharide monooxygenase. **Journal of Biological Chemistry**, *[S. l.]*, v. 293, n. 2, p. 523–531, 2018. DOI: 10.1074/jbc.M117.817593.

LAEMMLI, U. K. Cleavage of structural proteins during the assembly of the head of bacteriophage T4. **Nature**, *[S. l.]*, v. 227, n. 5259, p. 680–685, 1970. DOI: 10.1038/227680a0.

LAKOWICZ, Joseph R. **Principles of Fluorescence Spectroscopy**. [s.l.] : Springer Science & Business Media, 2013.

LATGE, J. P. The pathobiology of Aspergillus fumigatus. **Trends in Microbiology**, *[S. l.]*, v. 9, n. 8, p. 382–389, 2001.

LAURENT, Christophe V. F. P. et al. Influence of lytic polysaccharide monooxygenase active site segments on activity and affinity. **International Journal of Molecular**

Sciences, *[S. l.]*, v. 20, n. 24, 2019. DOI: 10.3390/ijms20246219.

LEONE, Francisco Assis; BARANAUSKAS, José Augusto; FURRIEL, Rosa Prazeres Melo; BORIN, Ivana Aparecida. SigrafW: An easy-to-use program for fitting enzyme kinetic data. **Biochemistry and Molecular Biology Education**, *[S. l.]*, v. 33, n. 6, p. 399–403, 2005. DOI: 10.1002/bmb.2005.49403306399.

LESTRADE, Pieter P. et al. Voriconazole resistance and mortality in invasive aspergillosis: A multicenter retrospective cohort study. **Clinical Infectious Diseases**, *[S. l.]*, v. 68, n. 9, p. 1463–1471, 2019. DOI: 10.1093/cid/ciy859.

LI, Caiming; BAN, Xiaofeng; ZHANG, Yuzhu; GU, Zhengbiao; HONG, Yan; CHENG, Li; TANG, Xiaoshu; LI, Zhaofeng. Rational Design of Disulfide Bonds for Enhancing the Thermostability of the 1,4-α-Glucan Branching Enzyme from Geobacillus thermoglucosidans STB02. **Journal of Agricultural and Food Chemistry**, *[S. l.]*, v. 68, n. 47, p. 13791–13797, 2020. DOI: 10.1021/acs.jafc.0c04798.

LI, Xin; BEESON, William T.; PHILLIPS, Christopher M.; MARLETTA, Michael A.; CATE, Jamie H. D. Structural Basis for Substrate Targeting and Catalysis by Fungal Polysaccharide Monooxygenases. **Structure**, *[S. l.]*, v. 20, n. 6, p. 1051–1061, 2012. DOI: 10.1016/j.str.2012.04.002.

LIU, Bing. **Dissecting function and catalytic mechanism of fungal lytic polysaccharide monooxygenases**. [s.l: s.n.].

LIU, Bing; OLSON, Åke; WU, Miao; BROBERG, Anders; SANDGREN, Mats. Biochemical studies of two lytic polysaccharide monooxygenasesfrom the white-rot fungus Heterobasidion irregulare and their roles in lignocellulose degradation. **PLoS ONE**, *[S. l.]*, v. 12, n. 12, p. 1–21, 2017. DOI: 10.1371/journal.pone.0189479.

LIU, Xiaoqing; DUAN, Xiaoguang; WEI, Wei; WANG, Shaobin; NI, Bing Jie. Photocatalytic conversion of lignocellulosic biomass to valuable products. **Green Chemistry**, *[S. l.]*, v. 21, n. 16, p. 4266–4289, 2019. a. DOI: 10.1039/c9gc01728c.

LIU, Xueqiang; JIANG, Zhengqiang; LIU, Yu; YOU, Xin; YANG, Shaoqing; YAN, Qiaojuan. Biochemical characterization of a novel exo-oligoxylanase from Paenibacillus barengoltzii suitable for monosaccharification from corncobs. **Biotechnology for Biofuels**, *[S. l.]*, v. 12, n. 1, p. 1–14, 2019. b. DOI: 10.1186/s13068-019-1532-6.

LIU, Ya Jun; LI, Bin; FENG, Yingang; CUI, Qiu. Consolidated bio-saccharification: Leading lignocellulose bioconversion into the real world. **Biotechnology Advances**, *[S. l.]*, v. 40, n. February, p. 107535, 2020. DOI: 10.1016/j.biotechadv.2020.107535.

LO LEGGIO, Leila; WEIHE, Cecilia D.; POULSEN, Jens Christian N.; SWEENEY, Matt; RASMUSSEN, Frank; LIN, Janine; DE MARIA, Leonardo; WOGULIS, Mark. Structure of a lytic polysaccharide monooxygenase from Aspergillus fumigatus and an engineered thermostable variant. **Carbohydrate Research**, *[S. l.]*, v. 469, p. 55–59, 2018. DOI: 10.1016/j.carres.2018.08.009.

LONG, Lingfeng; YANG, Huimin; REN, Hongyan; LIU, Rukuan; SUN, Fubao Fuelbiol; XIAO, Zhihong; HU, Jinguang; XU, Zhenghong. Synergism of Recombinant Podospora anserina PaAA9B with Cellulases Containing AA9s Can Boost the Enzymatic Hydrolysis of Cellulosic Substrates. **ACS Sustainable Chemistry and Engineering**, *[S. l.]*, v. 8, n. 32, p. 11986–11993, 2020. DOI:

10.1021/acssuschemeng.0c02564.

LORENCI WOICIECHOWSKI, Adenise; DALMAS NETO, Carlos José; PORTO DE SOUZA VANDENBERGHE, Luciana; DE CARVALHO NETO, Dão Pedro; NOVAK SYDNEY, Alessandra Cristine; LETTI, Luiz Alberto Junior; KARP, Susan Grace; ZEVALLOS TORRES, Luis Alberto; SOCCOL, Carlos Ricardo. Lignocellulosic biomass: Acid and alkaline pretreatments and their effects on biomass recalcitrance – Conventional processing and recent advances. **Bioresource Technology**, *[S. l.]*, v. 304, n. October 2019, p. 122848, 2020. DOI: 10.1016/j.biortech.2020.122848.

LOWENTHAL, Mark S.; DAVIS, Kiersta S.; FORMOLO, Trina; KILPATRICK, Lisa E.; PHINNEY, Karen W. Identification of Novel N-Glycosylation Sites at Noncanonical Protein Consensus Motifs. **Journal of Proteome Research**, *[S. l.]*, v. 15, n. 7, p. 2087–2101, 2016. DOI: 10.1021/acs.jproteome.5b00733.

MABEY GILSENAN, J.; COOLEY, J.; BOWYER, P. CADRE: the Central Aspergillus Data REpository 2012. **Nucleic Acids Research**, *[S. l.]*, v. 40, n. D1, p. D660–D666, 2012. DOI: 10.1093/nar/gkr971.

MAGA, Daniel; THONEMANN, Nils; HIEBEL, Markus; SEBASTIÃO, Diogo; LOPES, Tiago F.; FONSECA, César; GÍRIO, Francisco. Comparative life cycle assessment of first- and second-generation ethanol from sugarcane in Brazil. **International Journal of Life Cycle Assessment**, *[S. l.]*, v. 24, n. 2, p. 266–280, 2019. DOI: 10.1007/s11367-018-1505-1.

MALACCO, Nathália Luísa Sousa de Oliveira et al. Eosinophil-associated innate IL-17 response promotes Aspergillus fumigatus lung pathology. **Frontiers in Cellular and Infection Microbiology**, *[S. l.]*, v. 9, n. JAN, p. 1–13, 2019. DOI: 10.3389/fcimb.2018.00453.

MALGAS, Samkelo; MAFA, Mpho S.; MKABAYI, Lithalethu; PLETSCHKE, Brett I. A mini review of xylanolytic enzymes with regards to their synergistic interactions during hetero-xylan degradation. **World Journal of Microbiology and Biotechnology**, *[S. l.]*, v. 35, n. 12, p. 1–13, 2019. DOI: 10.1007/s11274-019-2765-z.

MAMO, Gashaw. Alkaline Active Hemicellulases. *In*: [s.l: s.n.]. p. 245–291. DOI: 10.1007/10_2019_101.

MEIRA, Guilherme; BRIAN, E.; PELLIN, Henrique; FEIJOLI, Veronica; PESSOA, Adalberto; PALMISANO, Giuseppe; MONTEIRO, Gisele. Glycosylation of L-asparaginase from E . coli through yeast expression and site-directed mutagenesis. *[S. l.]*, v. 156, n. November 2019, 2020. DOI: 10.1016/j.bej.2020.107516.

MELLO, Bruno L.; ALESSI, Anna M.; RIAÑO-PACHÓN, Diego M.; DEAZEVEDO, Eduardo R.; GUIMARÃES, Francisco E. G.; ESPIRITO SANTO, Melissa C.; MCQUEEN-MASON, Simon; BRUCE, Neil C.; POLIKARPOV, Igor. Targeted metatranscriptomics of compost-derived consortia reveals a GH11 exerting an unusual exo-1,4-β-xylanase activity. **Biotechnology for Biofuels**, *[S. l.]*, v. 10, n. 1, p. 1–17, 2017. DOI: 10.1186/s13068-017-0944-4.

MEZEI, L. M.; STORTS, D. R. Purification of PCR products. **PCR Technology: Current Innovations**, *[S. l.]*, v. 21, 1994.

MICSONAI, András; WIEN, Frank; BULYÁKI, Éva; KUN, Judit; MOUSSONG, Éva; LEE, Young-Ho; GOTO, Yuji; RÉFRÉGIERS, Matthieu; KARDOS, József. BeStSel: a

web server for accurate protein secondary structure prediction and fold recognition from the circular dichroism spectra. **Nucleic Acids Research**, *[S. l.]*, v. 46, n. W1, p. W315–W322, 2018. DOI: 10.1093/nar/gky497. Disponível em: https://academic.oup.com/nar/article/46/W1/W315/5035652.

MILLER, Bruce. Introduction. *In*: **Fossil Fuel Emissions Control Technologies**. [s.l.] : Elsevier, 2015. p. 1–45. DOI: 10.1016/B978-0-12-801566-7.00001-4.

MILLER, Gail Lorenz. Use of Dinitrosalicylic Acid Reagent for Determination of Reducing Sugar. **Analytical Chemistry**, *[S. l.]*, v. 31, n. 3, p. 426–428, 1959. DOI: 10.1021/ac60147a030.

MOSES, Vuyani; HATHERLEY, Rowan; TASTAN BISHOP, Özlem. Bioinformatic characterization of type-specific sequence and structural features in auxiliary activity family 9 proteins. **Biotechnology for Biofuels**, *[S. l.]*, v. 9, n. 1, p. 239, 2016. DOI: 10.1186/s13068-016-0655-2.

MUSADDIQUE, Hossain; REDDY DODDA, Subba; KAPOOR, Bishwajit Singh; AIKAT, Kaustav; MUKHOPADHYAY, Sudit S. Investigation the biomass conversion efficiency , biochemical characterisation and structural insights of the newly isolated AA16 family of Lytic Polysaccharide Monooxygenase (LPMO)... *[S. l.]*, n. April, 2020. DOI: 10.1101/2020.04.24.059154.

NAKANO, Yuichiro et al. Characteristics of azole-resistant Aspergillus fumigatus attached to agricultural products imported to Japan. **Journal of Infection and Chemotherapy**, *[S. l.]*, v. 26, n. 10, p. 1021–1025, 2020. DOI: 10.1016/j.jiac.2020.05.008.

NGUYEN, Ngoc A.; BOWLAND, Christopher C.; BONNESEN, Peter V.; LITTRELL, Kenneth C.; KEUM, Jong K.; NASKAR, Amit K. Fractionation of lignin for selective shape memory effects at elevated temperatures. **Materials**, *[S. l.]*, v. 13, n. 8, 2020. DOI: 10.3390/MA13081940.

OBENG, Eugene M.; BUDIMAN, Cahyo; ONGKUDON, Clarence M. Identifying additives for cellulase enhancement—A systematic approach. **Biocatalysis and Agricultural Biotechnology**, *[S. l.]*, v. 11, n. June, p. 67–74, 2017. DOI: 10.1016/j.bcab.2017.06.006. Disponível em: http://dx.doi.org/10.1016/j.bcab.2017.06.006.

OUR WORLD IN DATA. Biofuel energy production, 2019. **Our World in Data**, *[S. l.]*, 2021. Disponível em: https://ourworldindata.org/grapher/biofuel-production?tab=table&time=1990..latest.

PACKAGING, Food. Hemicellulose-Based Film : Potential Green Films for. *[S. l.]*, p. 1–14, 2020.

PAO, Hsiao Tien; FU, Hsin Chia. Renewable energy, non-renewable energy and economic growth in Brazil. **Renewable and Sustainable Energy Reviews**, *[S. l.]*, v. 25, p. 381–392, 2013. DOI: 10.1016/j.rser.2013.05.004.

PATEL, Ilabahen; KRACHER, Daniel; MA, Su; GARAJOVA, Sona; HAON, Mireille; FAULDS, Craig B.; BERRIN, Jean-Guy; LUDWIG, Roland; RECORD, Eric. Salt-responsive lytic polysaccharide monooxygenases from the mangrove fungus Pestalotiopsis sp. NCi6. **Biotechnology for Biofuels**, *[S. l.]*, v. 9, n. 1, p. 108, 2016. DOI: 10.1186/s13068-016-0520-3.

PEREIRA, Josiani de Cassia; GIESE, Ellen Cristine; MORETTI, Marcia Maria de Souza; GOMES, Ana Carolina dos Santos; PERRONE, Olavo Micali; BOSCOLO, Maurício; DA SILVA, Roberto; GOMES, Eleni; MARTINS, Daniela Alonso Bocchini. Effect of Metal Ions, Chemical Agents and Organic Compounds on Lignocellulolytic Enzymes Activities. *In*: **Enzyme Inhibitors and Activators**. [s.l.] : InTech, 2017. DOI: 10.5772/65934. Disponível em: http://www.intechopen.com/books/enzyme-inhibitors-and-activators/effect-of-metal-ions-chemical-agents-and-organic-compounds-on-lignocellulolytic-enzymes-activities.

PETROVIĆ, Dejan M.; VÁRNAI, Anikó; DIMAROGONA, Maria; MATHIESEN, Geir; SANDGREN, Mats; WESTERENG, Bjørge; EIJSINK, Vincent G. H. Comparison of three C4-oxidizing lytic polysaccharide monooxygenases from Neurospora crassa suggests different roles in plant cell wall degradation. **Journal of Biological Chemistry accepted provided minor revisions**, *[S. l.]*, n. 6, p. 1–26, 2019. DOI: 10.1074/jbc.RA119.008196.

PHAKEENUYA, Vanarat; RATANAKHANOKCHAI, Khanok; KOSUGI, Akihiko; TACHAAPAIKOON, Chakrit. A novel multifunctional GH9 enzyme from Paenibacillus curdlanolyticus B-6 exhibiting endo/exo functions of cellulase, mannanase and xylanase activities. **Applied Microbiology and Biotechnology**, *[S. l.]*, v. 104, n. 5, p. 2079–2096, 2020. DOI: 10.1007/s00253-020-10388-3.

PHILLIPS, Christopher M.; BEESON, William T.; CATE, Jamie H.; MARLETTA, Michael A. Cellobiose Dehydrogenase and a Copper-Dependent Polysaccharide Monooxygenase Potentiate Cellulose Degradation by Neurospora crassa. **ACS Chemical Biology**, *[S. l.]*, v. 6, n. 12, p. 1399–1406, 2011. DOI: 10.1021/cb200351y.

POINTNER, M.; KUTTNER, P.; OBRLIK, T.; JÄGER, A.; KAHR, H. Composition of corncobs as a substrate for fermentation of biofuels. **Agronomy Research**, *[S. l.]*, v. 12, n. 2, p. 391–396, 2014.

QUAN, Jiayuan; TIAN, Jingdong. Circular polymerase extension cloning for high-throughput cloning of complex and combinatorial DNA libraries. **Nature Protocols**, *[S. l.]*, 2011. DOI: 10.1038/nprot.2010.181.

QUINLAN, R. J. et al. Insights into the oxidative degradation of cellulose by a copper metalloenzyme that exploits biomass components. **Proceedings of the National Academy of Sciences**, *[S. l.]*, v. 108, n. 37, p. 15079–15084, 2011. DOI: 10.1073/pnas.1105776108. Disponível em: http://www.pnas.org/cgi/doi/10.1073/pnas.1105776108.

REBELLO, Sharrel; ANOOPKUMAR, A. N.; ANEESH, Embalil Mathachan; SINDHU, Raveendran; BINOD, Parameswaran; PANDEY, Ashok. Sustainability and life cycle assessments of lignocellulosic and algal pretreatments. **Bioresource Technology**, *[S. l.]*, v. 301, n. October 2019, p. 122678, 2020. DOI: 10.1016/j.biortech.2019.122678.

RODRÍGUEZ-ZÚÑIGA, Ursula Fabiola; CANNELLA, David; GIORDANO, Roberto de Campos; GIORDANO, Raquel de Lima Camargo; JØRGENSEN, Henning; FELBY, Claus. Lignocellulose pretreatment technologies affect the level of enzymatic cellulose oxidation by LPMO. **Green Chemistry**, *[S. l.]*, v. 17, n. 5, p. 2896–2903, 2015. DOI: 10.1039/C4GC02179G. Disponível em: http://xlink.rsc.org/?DOI=C4GC02179G.

RUBIO, Marcelo Ventura; ZUBIETA, Mariane Paludetti; FRANCO CAIRO, João

Paulo Lourenço; CALZADO, Felipe; PAES LEME, Adriana Franco; SQUINA, Fabio Marcio; PRADE, Rolf Alexander; DE LIMA DAMÁSIO, André Ricardo. Mapping N-linked glycosylation of carbohydrate-active enzymes in the secretome of Aspergillus nidulans grown on lignocellulose. **Biotechnology for Biofuels**, *[S. l.]*, 2016. DOI: 10.1186/s13068-016-0580-4.

SABBADIN, Federico et al. An ancient family of lytic polysaccharide monooxygenases with roles in arthropod development and biomass digestion. **Nature Communications**, *[S. l.]*, v. 1723, p. 0–38, 2018. DOI: 10.1038/s41467-018-03142-x.

SABBADIN, Federico et al. Secreted pectin monooxygenases drive plant infection by pathogenic oomycetes. **Science**, *[S. l.]*, v. 373, n. 6556, p. 774–779, 2021. DOI: 10.1126/science.abj1342.

SAHOO, Kalpana; SAHOO, Rajesh Kumar; GAUR, Mahendra; SUBUDHI, Enketeswara. Cellulolytic thermophilic microorganisms in white biotechnology: a review. **Folia Microbiologica**, *[S. l.]*, v. 65, n. 1, p. 25–43, 2020. DOI: 10.1007/s12223-019-00710-6.

SAIKI, R.; SCHARF, S.; FALOONA, F.; MULLIS, Kary; HORN, G.; ERLICH, H.; ARNHEIM, N. **Enzymatic amplification of beta-globin genomic sequences and restriction site analysis for diagnosis of sickle cell anemiaScience**, 1985. DOI: 10.1126/science.2999980.

SANFELICE, Domenico; TEMUSSI, Piero Andrea. Cold denaturation as a tool to measure protein stability. **Biophysical Chemistry**, *[S. l.]*, v. 208, p. 4–8, 2016. DOI: 10.1016/j.bpc.2015.05.007.

SANGER, F.; NICKLEN, S.; COULSON, A. R. DNA sequencing with chain-terminating inhibitors. **Proceedings of the National Academy of Sciences**, *[S. l.]*, v. 74, n. 12, p. 5463–5467, 1977. DOI: 10.1073/pnas.74.12.5463.

SANTOS, Fernando; EICHLER, Paulo; DE QUEIROZ, José Humberto; GOMES, Fernando. **Production of second-generation ethanol from sugarcane**. [s.l.] : Elsevier Inc., 2020. DOI: 10.1016/b978-0-12-814236-3.00011-1.

SATO, Motoaki. Thermochemistry of the formation of fossil fuels. **Special Publication - The Geochemical Society**, *[S. l.]*, v. 2, n. Fluid-Miner. Interact., p. 271–283, 1991.

SAVITZKY, Abraham; GOLAY, Marcel J. E. Smoothing and Differentiation of Data by Simplified Least Squares Procedures. **Analytical Chemistry**, *[S. l.]*, v. 36, n. 8, p. 1627–1639, 1964. DOI: 10.1021/ac60214a047.

SAWANT, Shailesh S.; SALUNKE, Bipinchandra K.; KIM, Beom Soo. Degradation of corn stover by fungal cellulase cocktail for production of polyhydroxyalkanoates by moderate halophile Paracoccus sp. LL1. **Bioresource Technology**, *[S. l.]*, v. 194, p. 247–255, 2015. DOI: 10.1016/j.biortech.2015.07.019.

SEMENOVA, Margarita V.; GUSAKOV, Alexander V.; TELITSIN, Vadim D.; ROZHKOVA, Aleksandra M.; KONDRATYEVA, Elena G.; SINITSYN, Arkady P. Purification and characterization of two forms of the homologously expressed lytic polysaccharide monooxygenase (PvLPMO9A) from Penicillium verruculosum. **Biochimica et Biophysica Acta - Proteins and Proteomics**, *[S. l.]*, v. 1868, n. 1, p. 140297, 2020. DOI: 10.1016/j.bbapap.2019.140297. Disponível em: https://doi.org/10.1016/j.bbapap.2019.140297.

SENISTERRA, Guillermo; CHAU, Irene; VEDADI, Masoud. Thermal denaturation assays in chemical biology. **Assay and Drug Development Technologies**, *[S. l.]*, v. 10, n. 2, p. 128–136, 2012. DOI: 10.1089/adt.2011.0390.

SHARMA, Anuja; AGGARWAL, Neeraj K. Lignocellulolytic Enzymology. *In*: **Water Hyacinth: A Potential Lignocellulosic Biomass for Bioethanol**. Cham: Springer International Publishing, 2020. p. 21–35. DOI: 10.1007/978-3-030-35632-3_3.

SHARMA GHIMIRE, Prakriti; OUYANG, Haomiao; WANG, Qian; LUO, Yuanming; SHI, Bo; YANG, Jinghua; LÜ, Yang; JIN, Cheng. Insight into Enzymatic Degradation of Corn, Wheat, and Soybean Cell Wall Cellulose Using Quantitative Secretome Analysis of Aspergillus fumigatus. **Journal of Proteome Research**, *[S. l.]*, v. 15, n. 12, p. 4387–4402, 2016. DOI: 10.1021/acs.jproteome.6b00465.

SIEVERS, Fabian; HIGGINS, Desmond G. Clustal Omega. **Current Protocols in Bioinformatics**, *[S. l.]*, v. 48, n. 1, 2014. DOI: 10.1002/0471250953.bi0313s48.

SILVEIRA, Marcos H. L.; VANELLI, Bruno A.; CHANDEL, Anuj K. **Second Generation Ethanol Production : Potential Biomass Feedstock , Biomass Deconstruction , and Chemical Platforms for Process Valorization**. [s.l.] : Elsevier Inc., 2018. DOI: 10.1016/B978-0-12-804534-3.00006-9.

SIMMONS, T. J. et al. Structural and electronic determinants of lytic polysaccharide monooxygenase reactivity on polysaccharide substrates. **Nature Communications**, *[S. l.]*, v. 8, n. 1, p. 1064, 2017. DOI: 10.1038/s41467-017-01247-3.

SINGH, Raushan K.; BLOSSOM, Benedikt M.; RUSSO, D. A.; VAN OORT, B.; CROCE, R.; JENSEN, P. E.; FELBY, C.; BJERRUM, M. J. Thermal unfolding and refolding of a lytic polysaccharide monooxygenase from Thermoascus aurantiacus . **RSC Advances**, *[S. l.]*, v. 9, n. 51, p. 29734–29742, 2019. DOI: 10.1039/c9ra05920b.

SPAN, Elise A.; SUESS, Daniel L. M.; DELLER, Marc C.; BRITT, R. David; MARLETTA, Michael A. The Role of the Secondary Coordination Sphere in a Fungal Polysaccharide Monooxygenase. **ACS Chemical Biology**, *[S. l.]*, v. 12, n. 4, p. 1095–1103, 2017. DOI: 10.1021/acschembio.7b00016.

SREEJA-RAJU, Athira Raj; CHRISTOPHER, Meera; KOOLOTH-VALAPPIL, Prajeesh; KUNI-PARAMBIL, Rajasree; GOKHALE, Digambar Vittal; SANKAR, Meena; ABRAHAM, Amith; PANDEY, Ashok; SUKUMARAN, Rajeev K. Penicillium janthinellum NCIM1366 shows improved biomass hydrolysis and a larger number of CAZymes with higher induction levels over Trichoderma reesei RUT-C30. **Biotechnology for Biofuels**, *[S. l.]*, v. 13, n. 1, p. 1–15, 2020. DOI: 10.1186/s13068-020-01830-9. Disponível em: https://doi.org/10.1186/s13068-020-01830-9.

TAHERZADEH, Ghazaleh; DEHZANGI, Abdollah; GOLCHIN, Maryam; ZHOU, Yaoqi; CAMPBELL, Matthew P. SPRINT-Gly: Predicting N- and O-linked glycosylation sites of human and mouse proteins by using sequence and predicted structural properties. **Bioinformatics**, *[S. l.]*, v. 35, n. 20, p. 4140–4146, 2019. DOI: 10.1093/bioinformatics/btz215.

TAN, Tien-Chye; KRACHER, Daniel; GANDINI, Rosaria; SYGMUND, Christoph; KITTL, Roman; HALTRICH, Dietmar; HÄLLBERG, B. Martin; LUDWIG, Roland; DIVNE, Christina. Structural basis for cellobiose dehydrogenase action during oxidative cellulose degradation. **Nature Communications**, *[S. l.]*, v. 6, n. 1, p. 7542,

2015. DOI: 10.1038/ncomms8542.

TANGHE, Magali; DANNEELS, Barbara; LAST, Matthias; BEERENS, Koen; STALS, Ingeborg; DESMET, Tom. Disul fi de bridges as essential elements for the thermostability of lytic polysaccharide monooxygenase LPMO10C from Streptomyces coelicolor. *[S. l.]*, v. 30, n. 5, p. 401–408, 2017. DOI: 10.1093/protein/gzx014.

TETER, S. A.; SUTTON, K. Brandon; EMME, B. **Enzymatic processes and enzyme development in biorefining**. [s.l: s.n.]. DOI: 10.1533/9780857097385.1.199.

TOKIN, Radina; IPSEN, Johan Ørskov; WESTH, Peter; JOHANSEN, Katja Salomon. The synergy between LPMOs and cellulases in enzymatic saccharification of cellulose is both enzyme- and substrate-dependent. **Biotechnology Letters**, *[S. l.]*, 2020. DOI: 10.1007/s10529-020-02922-0.

ULAGANATHAN, Kandasamy; GOUD, Burragoni; REDDY, Mettu; KUMAR, Vanaparthi; BALSINGH, Jatoth; RADHAKRISHNA, Surabhi. **Proteins for Breaking Barriers in Lignocellulosic Bioethanol Production**. [s.l: s.n.]. v. 16 DOI: 10.2174/1389203716021502151657 18.

VAAJE-KOLSTAD, Gustav; BØHLE, Liv Anette; GÅSEIDNES, Sigrid; DALHUS, Bjørn; BJØRÅS, Magnar; MATHIESEN, Geir; EIJSINK, Vincent G. H. Characterization of the Chitinolytic Machinery of Enterococcus faecalis V583 and High-Resolution Structure of Its Oxidative CBM33 Enzyme. **Journal of Molecular Biology**, *[S. l.]*, v. 416, n. 2, p. 239–254, 2012. DOI: 10.1016/j.jmb.2011.12.033.

VAAJE-KOLSTAD, Gustav; FORSBERG, Zarah; LOOSE, Jennifer SM; BISSARO, Bastien; EIJSINK, Vincent GH. **Structural diversity of lytic polysaccharide monooxygenasesCurrent Opinion in Structural Biology**, 2017. DOI: 10.1016/j.sbi.2016.12.012.

VELASCO, Josman; DE OLIVEIRA ARNOLDI PELLEGRINI, Vanessa; SEPULCHRO, Ana Gabriela Veiga; KADOWAKI, Marco Antonio Seiki; SANTO, Melissa Cristina Espirito; POLIKARPOV, Igor; SEGATO, Fernando. Comparative analysis of two recombinant LPMOs from Aspergillus fumigatus and their effects on sugarcane bagasse saccharification. **Enzyme and Microbial Technology**, *[S. l.]*, v. 144, n. September 2020, p. 109746, 2021. DOI: 10.1016/j.enzmictec.2021.109746. Disponível em: https://doi.org/10.1016/j.enzmictec.2021.109746.

VU, Van V.; BEESON, William T.; PHILLIPS, Christopher M.; CATE, Jamie H. D.; MARLETTA, Michael A. Determinants of Regioselective Hydroxylation in the Fungal Polysaccharide Monooxygenases. **Journal of the American Chemical Society**, *[S. l.]*, v. 136, n. 2, p. 562–565, 2014. a. DOI: 10.1021/ja409384b. Disponível em: https://pubs.acs.org/doi/10.1021/ja409384b.

VU, Van V.; BEESON, William T.; SPAN, Elise A.; FARQUHAR, Erik R.; MARLETTA, Michael A. A family of starch-active polysaccharide monooxygenases. **Proceedings of the National Academy of Sciences of the United States of America**, *[S. l.]*, v. 111, n. 38, p. 13822–13827, 2014. b. DOI: 10.1073/pnas.1408090111.

WALLACE, Bonnie A.; JANES, R. W. **Modern techniques for circular dichroism and synchrotron radiation circular dichroism spectroscopy**. Vol. 1 ed. [s.l.] : IOS press, 2009.

WANG, Bao-Teng; HU, Shuang; YU, Xing-Ye; JIN, Long; ZHU, Yun-Jia; JIN, Feng-

Jie. Studies of Cellulose and Starch Utilization and the Regulatory Mechanisms of Related Enzymes in Fungi. **Polymers**, *[S. l.]*, v. 12, n. 3, p. 530, 2020. DOI: 10.3390/polym12030530.

WESTERENG, Bjørge; CANNELLA, David; WITTRUP AGGER, Jane; JØRGENSEN, Henning; LARSEN ANDERSEN, Mogens; EIJSINK, Vincent G. H.; FELBY, Claus. Enzymatic cellulose oxidation is linked to lignin by long-range electron transfer. **Scientific Reports**, *[S. l.]*, v. 5, n. 1, p. 18561, 2015. DOI: 10.1038/srep18561.

WU, Miao et al. Crystal Structure and Computational Characterization of the Lytic Polysaccharide Monooxygenase GH61D from the Basidiomycota Fungus Phanerochaete chrysosporium. **Journal of Biological Chemistry**, *[S. l.]*, v. 288, n. 18, p. 12828–12839, 2013. DOI: 10.1074/jbc.M113.459396.

YOO, Chang Geun; MENG, Xianzhi; PU, Yunqiao; RAGAUSKAS, Arthur J. The critical role of lignin in lignocellulosic biomass conversion and recent pretreatment strategies: A comprehensive review. **Bioresource Technology**, *[S. l.]*, v. 301, n. November 2019, p. 122784, 2020. DOI: 10.1016/j.biortech.2020.122784.

ZERVA, Anastasia; PENTARI, Christina; GRISEL, Sacha; BERRIN, Jean Guy; TOPAKAS, Evangelos. A new synergistic relationship between xylan-active LPMO and xylobiohydrolase to tackle recalcitrant xylan. **Biotechnology for Biofuels**, *[S. l.]*, v. 13, n. 1, p. 1–13, 2020. DOI: 10.1186/s13068-020-01777-x. Disponível em: https://doi.org/10.1186/s13068-020-01777-x.

ZHANG, Ruiqin et al. Identification of a thermostable fungal lytic polysaccharide monooxygenase and evaluation of its effect on lignocellulosic degradation. **Applied Microbiology and Biotechnology**, *[S. l.]*, v. 103, n. 14, p. 5739–5750, 2019. DOI: 10.1007/s00253-019-09928-3.

ZHANG, Ruiqin. Functional characterization of cellulose-degrading AA9 lytic polysaccharide monooxygenases and their potential exploitation. **Applied Microbiology and Biotechnology**, *[S. l.]*, p. 3229–3243, 2020. DOI: 10.1007/s00253-020-10467-5.

ZHANG, Sitong; XIAO, Jianlong; WANG, Gang; CHEN, Guang. Enzymatic hydrolysis of lignin by ligninolytic enzymes and analysis of the hydrolyzed lignin products. **Bioresource Technology**, *[S. l.]*, v. 304, n. February, p. 122975, 2020. DOI: 10.1016/j.biortech.2020.122975.

ZHOU, Xiaoli; QI, Xiaohua; HUANG, Hongxia; ZHU, Honghui. Sequence and structural analysis of AA9 and AA10 LPMOs: An insight into the basis of substrate specificity and regioselectivity. **International Journal of Molecular Sciences**, *[S. l.]*, v. 20, n. 18, 2019. DOI: 10.3390/ijms20184594.

ZHOU, Xiaoli; XU, Zhiqiang; HE, Jia; LI, Yueqiu; PAN, Chengxiang; WANG, Chunling; DENG, Ming Rong; ZHU, Honghui. A myxobacterial LPMO10 has oxidizing cellulose activity for promoting biomass enzymatic saccharification of agricultural crop straws. **Bioresource Technology**, *[S. l.]*, v. 318, n. September, p. 124217, 2020. DOI: 10.1016/j.biortech.2020.124217. Disponível em: https://doi.org/10.1016/j.biortech.2020.124217.

ZHOU, Xiaoli; ZHU, Honghui. Current understanding of substrate specificity and regioselectivity of LPMOs. **Bioresources and Bioprocessing**, *[S. l.]*, v. 7, n. 1, 2020.

DOI: 10.1186/s40643-020-0300-6.

ZHOU, Ziyuan; LEI, Fuhou; LI, Pengfei; JIANG, Jianxin. Lignocellulosic biomass to biofuels and biochemicals: A comprehensive review with a focus on ethanol organosolv pretreatment technology. **Biotechnology and Bioengineering**, *[S. l.]*, v. 115, n. 11, p. 2683–2702, 2018. DOI: 10.1002/bit.26788.

ZOGHLAMI, Aya; PAËS, Gabriel. Lignocellulosic Biomass: Understanding Recalcitrance and Predicting Hydrolysis. **Frontiers in Chemistry**, *[S. l.]*, v. 7, n. December, 2019. DOI: 10.3389/fchem.2019.00874.

7. Material Suplementar

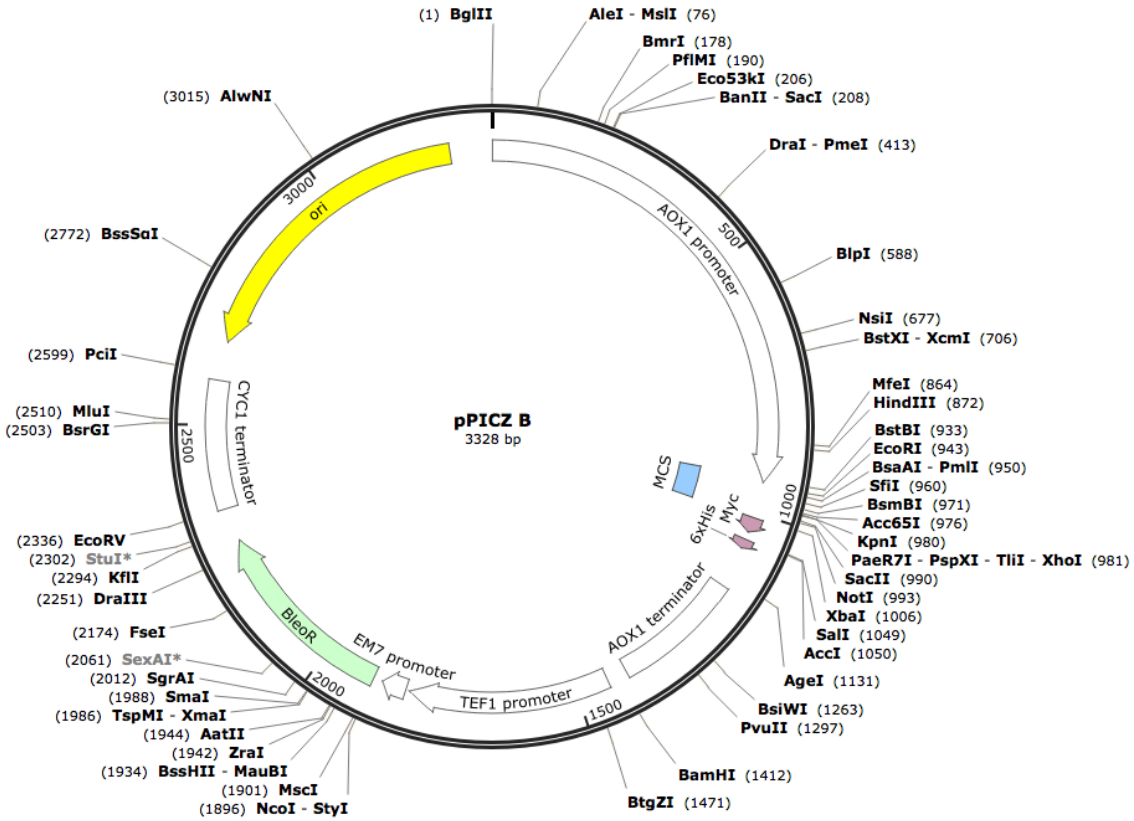

Figura Suplementar 1. Mapa geral do vetor pPICZB.

A

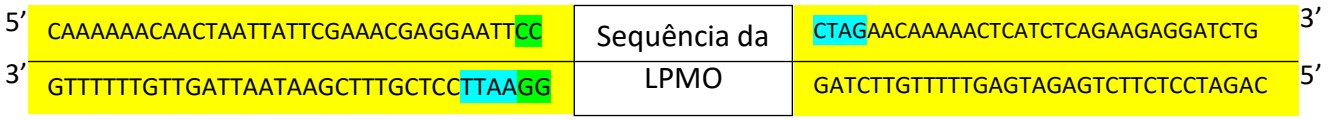

B

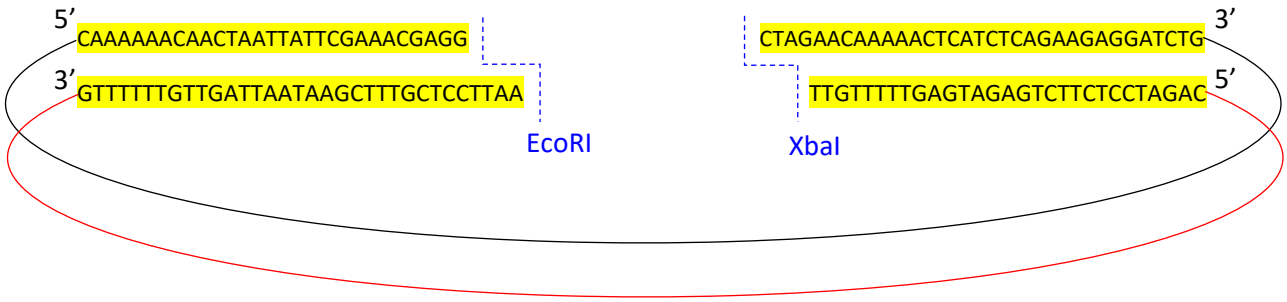

C

5’ CAAAAAACAACTAATTATTCGAAACGAGGAATTCCATGACTTTGTCCAAGATCAC 3’ FW

```
ATGACTTTGTCCAAGATCACTTCCATTGCTGGCCTTCTGGCCTCAGCGTCTCTCGTGGCT
GGCCACGGCTTTGTTTCTGGCATTGTTGCTGATGGGAAATATTACGGAGGGTACCTTGTT
AACCAATACCCCTACATGAGCAACCCTCCCGACACCATTGCCTGGTCCACCACCGCCACC
GACCTCGGCTTTGTGGACGGCACCGGCTACCAGTCTCCGGATATTATCTGCCACAGAGAC
GCAAAGAATGGCAAGTTGACCGCAACCGTTGCAGCCGGTTCACAGATCGAATTCCAGTGG
ACGACGTGGCCAGAGTCTCACCATGGACCGTTGATTACTTACCTCGCTCCATGCAACGGC
GACTGTGCCACCGTGGACAAGACCACCCTGAAGTTTGTCAAGATCGCCGCTCAAGGCTTG
ATCGACGGCTCCAACCCACCTGGTGTTTGGGCTGATGATGAAATGATCGCCAACAACAAC
ACGGCCACAGTGACCATTCCTGCCTCCTATGCCCCCGGAAACTACGTCCTTCGCCACGAG
ATCATCGCCCTTCACTCTGCGGGTAACCTGAACGGCGCGCAGAACTACCCCCAGTGTTTC
AACATCCAAATCACCGGTGGCGGCAGTGCTCAGGGATCTGGCACCGCTGGCACGTCCCTG
TACAAGAATACTGATCCTGGCATCAAGTTTGACATCTACTCGGATCTGAGCGGTGGATAC
      CCTATTCCTGGTCCTGCACTGTTCAACGCT    TAA - excluído
```

Sequência do gene sem stop códon

5’ CAGATCCTCTTCTGAGATGAGTTTTTGTTCTAGAGCGTTGAACAGTGCAGGAC 3’ RV

Figura Suplementar 2. Esquema para desenho dos *primers* para amplificação do gene AFUA_4G07850 e posterior clonagem via CPEC no vetor pPICZB digerido. Legenda: A- Construção desenhada para inserir o gene de interesse ao vetor usando a enzima Phusion High-Fidelity DNA Polymerase (Thermo Scientific). B- Vetor pPICZB digerido com as enzimas *Eco*RI e *Xba*I com destaque para as duas fitas. C- Sequência do gene sem o stop códon (em vermelho) e *primers* necessários para introduzir regiões de flanqueamento ao vetor. Regiões em azul: bases inseridas para reconstruir o sítio de restrição; regiões em verde: bases adicionadas para manter o frame inalterado; bases sublinhadas: região de sobreposição ao vetor. Fonte: autoria própria.

```
AfAA9_B       HGFVSGIV-ADGKYYGGYL------VNQYPYMS---NPPDTIAWSTTATDLGFVDGTGYQ    50
HjLPMO9A      HGHINDIV-INGVWYQAYD------PTTFPYES---NPPIVVGWTAADLDNGFVSPDAYQ    50
NcLPMO9M      HGFVDNAT-IGGQFYQFYQ------PYQDPYMG---SPPDRISRKIP--GNG--PVEDVT    46
TaLPMO9A      HGFVQNIV-IDGKNYGGYL------VNQYPYMS---NPPEVIAWSTTATDLGFVDGTGYQ    50
HjLPMO9B      HGQVQNFT-INGQYNQGFI------LDYYYQKQNTGHFPNVAGWYAEDLDLGFISPDQYT    53
NCU07760      HGHVSKVI-VNGVEYQNYD------PTSFPYNS---NPPTVIGWTIDQKDNGFVSPDAFD    50
PaLPMO9A      HGHVSHII-VNGVYYQNYD------PTTHFYQP---NPPTVIGWSALQQDNGFVEPNNFG    50
GtLPMO9B      HGYVDTLN-VGGTQYTGYL------PYNDPYTT---PAPQRIERPIP--GNG--PVTALT    46
CvAA9A        HTRMFSVW-VNGVDQGDGQNVYIRTP---P-------------------NTD--PIKDLA    35
LsAA9A        HTLVWGVW-VNGVDQGDGRNIYIRSP---P-------------------NNN--PVKNLT    35
GtLPMO9A-2    HGYVDQVT-IGGQVYTGYQ------PYQDPYES---PVPQRIERAIP--GNG--PVEDLT    46
NcLPMO9F      HYTFPKVW-ANSGTTADWQ--YVRRADNWQ-------------------NNG--FVDNVN    36
TtLPMO9E      HY----TW-PRVNDGADWQ--QVRKADNWQ-------------------DNG--YVGDVT    32
PcLPMO9D      HYTFPDFIEPSGTVTGDWV--YVRETQNHY-------------------SNG--PVTDVT    37
MtLPMO9B      HATFQALW-VDGVDYGA-Q--CARLP---A-------------------SNS--PVTDVT    32
NCU02344      HYTFPKGY-STGAVSGEYE--HIRMTENHY-------------------NRG--PVADVT    36
NcLPMO9E      HATFQALW-VDGADYGS-Q--CARVP---P-------------------SNS--PVTDVT    32
HiLPMO9H      HATFQEMW-VNGVDQGN-Y--CVRSP---A-------------------SNS--PVTSVT    32
MtLPMO9C      HTIFSSLE-VGGVNQGIGQ--GVRVP---S-------------------YNG--PIEDVT    33
NcLPMO9C      HTIFQKVS-VNGADQGQLK--GIRAP---A-------------------NNN--PVTDVM    33
NcLPMO9A      HTIFVQLE-ADGTTYPVSY--GIRTP---S-------------------YDG--PITDVT    33
HiLPMO9I      HTIFQEVY-VNGVDQGHIT--GIRVP---D-------------------YDG--PITDVT    33
NcLPMO9D      HTIFSSLE-VNGVNQGLGE--GVRVP---T-------------------YNG--PIEDVT    33
PsLPMOB       HTIFVQLE-SGGTTYDVSY--GIRDP---S-------------------YDG--PITDVT    33
MtLPMO9J      HAIFQKVS-VNGADQGSLT--GLRAP---N-------------------NNN--PVQNVN    33
GtLPMO9C      HTIFQRVY-VDGVGEGHLS--GIRIP---E-------------------SNW--PIMDLS    33
              *

AfAA9_B       SPDIICHRD----AK-NGKLTATVAAGSQIEFQWTT-W-------------PESHHGPLI    91
HjLPMO9A      NPDIICHKN----AT-NAKGHASVKAGDTILFQWVP-V-------------PWPHPGPIV    91
NcLPMO9M      SLAIQCNAD----SA-PAKLHASAAAGSTVTLRWTI-W-------------PDSHVGPVI    87
TaLPMO9A      TPDIICHRG----AK-PGALTAPVSPGGTVELQWTP-W-------------PDSHHGPVI    91
HjLPMO9B      TPDIVCHKN----AA-PGAISATAAAGSNIVFQWGPGV-------------WPHPYGPIV    95
NCU07760      SGDIICHKS----AK-PAGGHATVKAGDKISLQWDQ-W-------------PESHKGPVI    91
PaLPMO9A      TTDIICHKS----AA-PGGGSATVNAGDKISIVWTPEW-------------PESHIGPVI    92
GtLPMO9B      TIDVQCNGENGGGSS-PAPLVATIAAGGKIAFHWTT-W-------------PSSHVGPVI    91
CvAA9A        SPALACNVKGGE----PVPQFVSASAGDKLTFEWYRV-------KRGDDIIDPSHSGPIT    84
LsAA9A        SPDMTCNVDN-R----VVPKSVPVNAGDTLTFEWYHN-------TRDDDIIASSHHGPIA    83
GtLPMO9A-2    LLDIQCNGSGGSGTK-PAALIASAAAGDEIAFHWTT-W-------------PSSHVGPVI    91
NcLPMO9F      SQQIRCFQSTHS----PAQSTLSVAAGTTITYGAAPS---------------VYHPGPMQ    77
TtLPMO9E      SPQIRCFQATPS----PAPSVLNTTAGSTVTYWANPD---------------VYHPGPVQ    73
PcLPMO9D      SPEFRCYELDLQNTA-GQTQTATVSAGDTVGFKANSA---------------IYHPGYLD    81
MtLPMO9B      SNAIRCNANPSP-----ARGKCPVKAGSTVTVEMHQQPGDR---SCSSEAIGGAHYGPVM    84
NCU02344      SESMTCYELNPGK---GAPKTLSVAAGSNYTFVVGDN---------------IGHPGPLH    78
NcLPMO9E      SNAMRCNTGTSP-----VAKKCPVKAGSTVTVEMHQQANDR---SCSSEAIGGAHYGPVL    84
HiLPMO9H      TNDLACNAGASS-----SSGLCAVNPGDSVTVEMHQQPGDR---SCANEAIGGDHYGPIN    84
MtLPMO9C      SNSIACNGPPNPTTP--TNKVITVRAGETVTAVWRYMLSTT-G-SAPNDIMDSSHKGPTM    89
NcLPMO9C      SSDIICNAVTM-----KDSNVLTVPAGAKVGHFWGHEIGGAAGPNDADNPIAASHKGPIM    88
NcLPMO9A      SNDLACNGGPNPTTP--SDKIITVNAGSTVKAIWRHTLTS-----GADDVMDASHKGPTL    86
HiLPMO9I      SNDLICNGGINPYHQPMSTAIITVPAGAQVTTEWHHTLAGA-DPSDSADPIDPSHKGPII    92
NcLPMO9D      SASIACNGSPNTVAS--TSKVITVQAGTNVTAIWRYMLSTT-G-DSPADVMDSSHKGPTI    89
PsLPMOB       SDDLACNGGPNPTTP--SSDVIDVAAGSTVTAVWRHTLTS-----GADDVMDASHLGPTM    86
MtLPMO9J      SQDMICGQSGS-----TSNTIIEVKAGDRIGAWYQHVIGGAQFPNDPDNPIAKSHKGPVM    88
GtLPMO9C      SNAIICNGGVNPYHEPVSLAIIQVPAGSTITAEWHPTIDDV-N---TTESIRPDHKGPVI    89
                 . *                 *                          * *

AfAA9_B       TYLAPCNGDC--ATV--DKTTLKFVKIAAQGLI----DGSNPPGVWADDEMI-ANNNTAT   142
HjLPMO9A      DYLANCNGDC--ETV--DKTTLEFFKIDGVGLL----SGGD-PGTWASDVLI-SNNNTWV   141
NcLPMO9M      TYMARCPD-TGCQDWTPSASDKVWFKIKEGGRE----GT---SNVWAATPLMTAP-ANYE   138
TaLPMO9A      NYLAPCNGDC--STV--DKTQLEFFKIAESGLI----NDDNPPGIWASDNLI-AANNSWT   142
HjLPMO9B      TYVVECSGSC--TTV--NKNNLRWVKIQEAGIN----YN---TQVWAQQDLI-NQGNKWT   143
NCU07760      DYLAACDGDC--ESV--DKTALKFFKIDGAGYD----A----TNGWASDTLI-KDGNSWV   138
PaLPMO9A      DYLANCNGPC--ETV--DKTSLRWFKIGGAGYN----P--N-TRTWAADDLR-ANGNSWL   140
GtLPMO9B      TYLGKVPSSTDVTKYSPTGSDVIWFKIDEGGYS----N-----GKWAATDVLSAQNSTWT   142
CvAA9A        TWIAAFTSP----TM--DGTGPVWSKIHEEGYD-------ASTKSWAVDKLI-ANKGMWD   130
LsAA9A        VYIAPA-------AS--NGQGNVWVKLFEDAYN-------VTNSTWAVDRLI-TAHGQHS   126
GtLPMO9A-2    TYMGKVPSNTDITSYSPTGSDVIWFKIDEAGYE----N-----GKWAATDIMSAQNSTWT   142
NcLPMO9F      FYLARVPDGQDINSW--TGEGAVWFKIYHEQPT----F--GSQLTWS----S-NGKSSFP   124
TtLPMO9E      FYMARVPDGEDINSW--NGDGAVWFKVYEDHPT----F--GAQLTWP----S-TGKSSFA   120
PcLPMO9D      VMMSPASPAA-NSPE--AGTGQTWFKIYEEKPQ----FENG-QLVFD------TTQQEVT   127
MtLPMO9B      VYMSKVSDAA---SA--DGS-SGWFKVFEDGWAKNPSGGSGDDDYWGTKDLN-SCCGKMN   137
NCU02344      FYMAKVPEGKTAATF--DGKGAVWFKIYQDGPM----GLGTGQLTWP----S-AGATEVS   127
NcLPMO9E      VYMSKVSDAA---SA--DGS-SGWFKIFEDTWAKKPSSSSGDDDFWGVKDLN-SCCGKMQ   137
HiLPMO9H      IYLAKVTDAT---TA--VGSSASWFKIGEMGL------PSSDPDYWATEVLN-DNCGHFT   132
MtLPMO9C      AYLKKVDNAT---TD--SGVGGGWFKIQEDGLT---------NGVWGTERVI-NGQGRHN   134
NcLPMO9C      VYLAKVDNAA---TT--GTSGLKWFKVAEAGL---------SNGKWAVDDLI-ANNGWSY   133
NcLPMO9A      AYLKKVDDAL---TD--TGIGGGWFKIQEDGYN---------NGQWGTSTVI-TNGGFQY   131
```

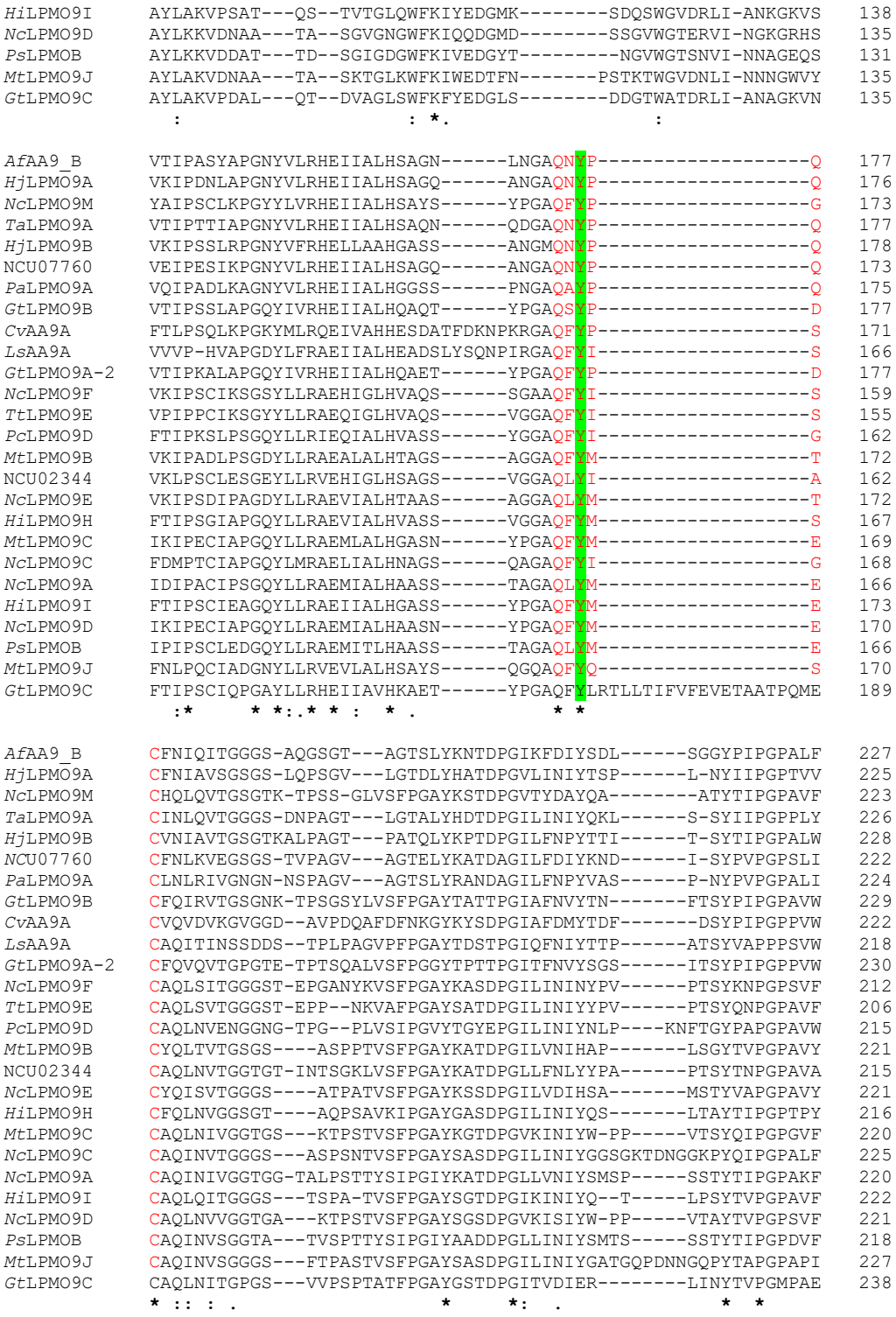

Figura Suplementar 3. Alinhamento múltiplo da *Af*AA9_B com importantes AA9s reportadas na literatura. Os resíduos conservados que formam a braçadeira de histidina foram destacados, sendo as 2 histidinas marcadas em azul, e a tirosina marcada em verde. Sequências coloridas de aminoácidos representam 2 motivos conservados encontrados nas LPMOs, sendo em azul o motivo [Hx_nGP], e em vermelho o motivo [QxYxxC]. Legenda: (*) – resíduos fortemente conservados; (:) – resíduos pertencentes a um mesmo grupo; (.) – resíduos com poucas características estruturais semelhantes.

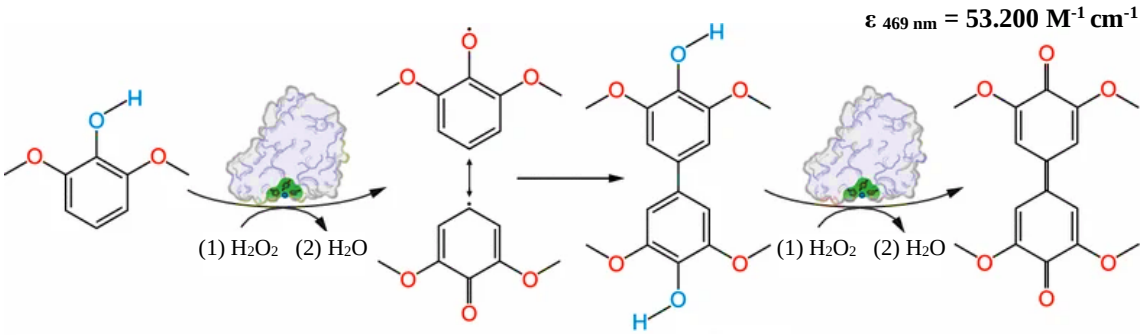

Figura Suplementar 4. Esquema simplificado da reação ocorrida entre a LPMO e o substrato 2,6 DMP na presença de H_2O_2. Fonte: Breslmayr *et al*., (2018) (figura adaptada). A Reação se inicia com a oxidação da molécula 2,6-DMP para reduzir o Cu(II) para Cu(I) a custo de uma molécula de H_2O_2. A partir de dois radicais 2,6-DMP gerados, ocorre uma rápida dimerização e formação de uma hidrocoerulignona que é oxidada novamente pela LPMO dando origem a coerulignona, que de fato é a espécie cromogênica que apresenta absortividade molar em 469 nm = 53200 M^{-1} cm^{-1}.

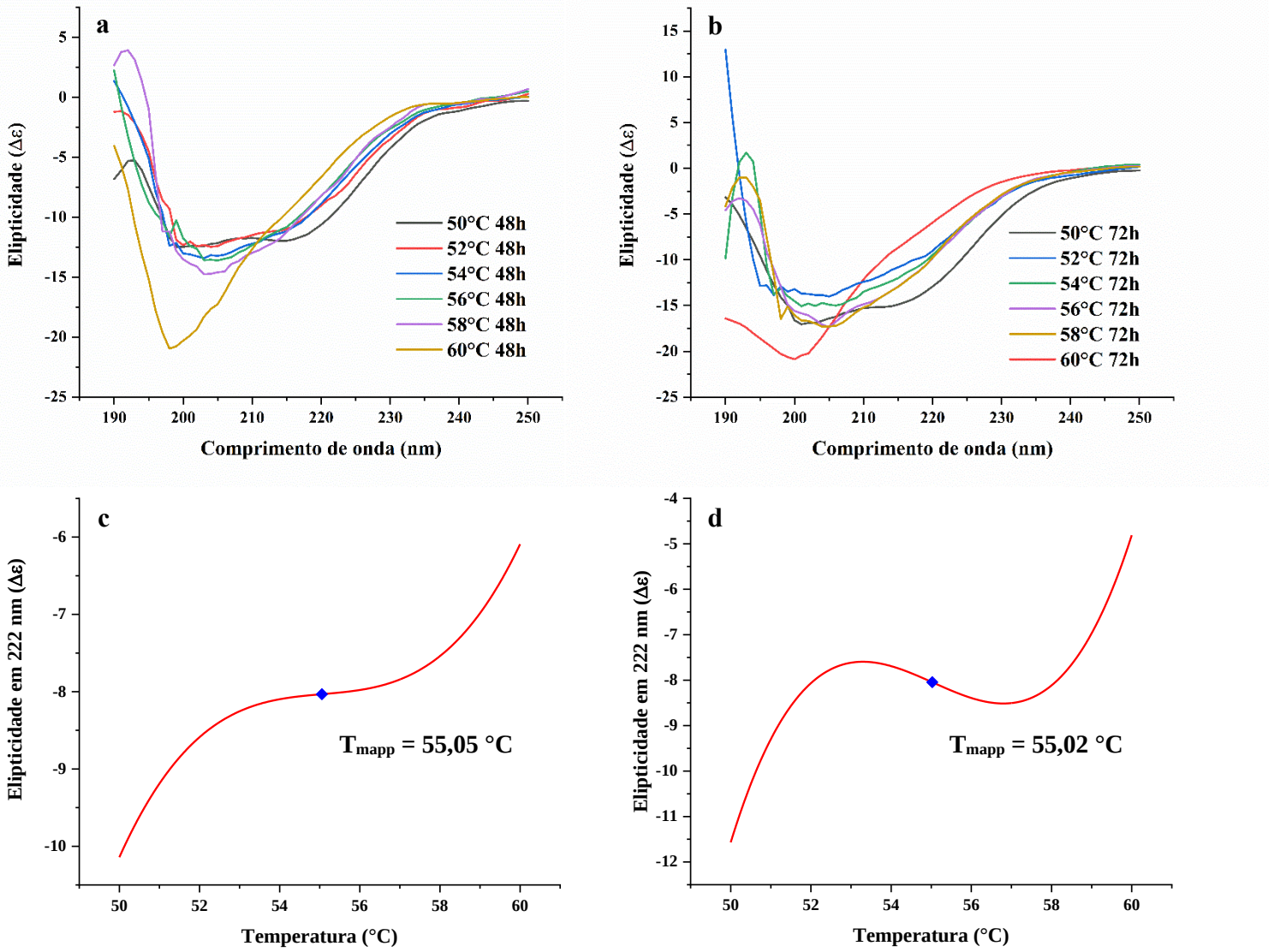

Figura Suplementar 5. Espectros obtidos via CD da *Af*AA9_B na faixa de 190 a 250 nm sob o intervalo de 50 °C a 60°C após 48h (a) e 72h (b) de incubação. Os respectivos valores de Tm foram determinados pela derivada primeira dos gráficos

Tabela Suplementar 1. Identidade das LPMOs alinhadas com a *Af*AA9_B.

LPMO	Referência	Identidade (%) com a *Af*AA9_B
***Hj*LPMO9A**	(HANSSON et al., 2017)	55,51
***Nc*LPMO9M**	(LI et al., 2012)	40,74
***Ta*LPMO9A**	(QUINLAN et al., 2011)	71,49
***Hj*LPMO9B**	(KARKEHABADI et al., 2008)	44,89
NCU07760	(VU et al., 2014a)	54,02
***Pa*LPMO9A**	(BENNATI-GRANIER et al., 2015)	50,67
***Gt*LPMO9B**	(HEGNAR et al., 2018)	42,20
***Cv*AA9A**	(SIMMONS et al., 2017)	32,99
***Ls*AA9A**	(SIMMONS et al., 2017)	31,44
***Gt*LPMO9A-2**	(KOJIMA et al., 2016)	40,64
***Nc*LPMO9F**	(TAN et al., 2015)	27,50
***Tt*LPMO9E**	(WESTERENG et al., 2015)	27,84
***Pc*LPMO9D**	(WU et al., 2013)	29,00
***Mt*LPMO9B**	(FROMMHAGEN et al., 2016)	30,30
NCU02344	(MOSES; HATHERLEY; TASTAN BISHOP, 2016)	30,69
***Nc*LPMO9E**	(PHILLIPS et al., 2011)	30,30
***Hi*LPMO9H**	(LIU et al., 2017)	30,46
***Mt*LPMO9C**	(FROMMHAGEN et al., 2016)	32,99
***Nc*LPMO9C**	(BORISOVA et al., 2015)	38,38
***Nc*LPMO9A**	(PETROVIĆ et al., 2019)	34,50
***Hi*LPMO9I**	(LIU et al., 2017)	37,69
***Nc*LPMO9D**	(LI et al., 2012)	31,82
***Ps*LPMOB**	(PATEL et al., 2016)	31,16
***Mt*LPMO9J**	(KADOWAKI et al., 2018)	32,00
***Gt*LPMO9C**	(KOJIMA et al., 2016)	34,85

Tabela Suplementar 2: Comparação do conteúdo percentual de estruturas secundárias da *Af*AA9_B estimado através de diferentes métodos.

*Af*AA9_B	BeStSel (CD)	PDB: 5X6A	Phyre2	Kabsch & Sander
α-hélices (%)	8,3	12,7	1,0	10,9
Folhas-β (%)	31,4	31,4	40,0	29,3
Alças (%)	11,9	-	-	-
Outras/desordenadas (%)	48,4	55,9	59,0	59,8

Tabela Suplementar 3: Conteúdo percentual de estruturas secundárias determinadas para *apo-Af*AA9_B e *holo-Af*AA9_B.

*Af*AA9_B	25°C				
		Folhas-β			
	α-hélices (%)	Antiparalelas (%)	Paralelas (%)	Alças (%)	Outras/ desordenadas (%)
Apo-forma	10,2	26,5	13,8	8,8	40,7
Holo-forma	10,4	29,3	12,4	8,7	39,1

Tabela Suplementar 4: Estruturas secundárias determinadas para o intervalo de 25-70 °C após 24 horas.

T (°C)	24h				
		Folhas-β			
	α-hélices (%)	Antiparalelas (%)	Paralelas (%)	Alças (%)	Outras/ desordenadas (%)
25	10,9	22,5	14,2	9,4	43,0
50	10,2	23,7	13,2	8,5	44,3
52	9,1	26,7	10,6	9,8	43,8
54	9,5	25,8	9,7	9,4	45,6
56	7,0	29,6	7,4	9,8	46,2
58	7,9	30,0	2,7	12,1	47,3
60	4,5	29,9	2,8	11,7	51,0
70	2,9	27,6	0,1	14,1	55,3

Tabela Suplementar 5: Estruturas secundárias determinadas para o intervalo de 50-60 °C após 48 horas.

T (°C)	48h				
		Folhas-β			
	α-hélices (%)	Antiparalelas (%)	Paralelas (%)	Alças (%)	Outras/ desordenadas (%)
50	8,6	27,6	9,3	10,6	43,9
52	8,2	23,0	9,6	12,6	46,6
54	8,3	24,4	6,2	11,8	49,3
56	7,8	22,5	4,2	14,2	49,8
58	6,9	24,4	4,4	14,1	50,1
60	3,7	30,0	0,4	13,6	52,3

Tabela Suplementar 6: Estruturas secundárias determinadas para o intervalo de 50-60 °C após 72 horas.

T (°C)	72h				
		Folhas-β			
	α-hélices (%)	Antiparalelas (%)	Paralelas (%)	Alças (%)	Outras/ desordenadas (%)
50	13,1	25,5	10,6	9,1	41,7
52	11,7	24,6	7,8	12,0	43,9
54	10,7	26,9	5,8	12,2	44,4
56	9,2	25,2	3,5	11,6	50,5
58	7,8	28,3	2,1	11,7	50,1
60	5,4	28,9	0,0	14,7	51,0

8. Apêndice

➔ **Eletroforese para amostras proteicas:**

Gel de empacotamento 5%

Acrilamida/bis-acrilamida 37,5/1 (Bio-Rad).....	325 µL
Tris-HCl 1,0 M pH 6,8	250 µL
SDS 10% (m/v).....	20 µL
Persulfato de amônio 10% (m/v).....	20 µL
TEMED (Bio-Rad)	2,5 µL
H_2O deionizada q.s.p.	**2000,0 µL**

Gel de corrida 10%

Acrilamida/bis-acrilamida 37,5/1 (Bio-Rad).....	1675 µL
Tris-HCl 1,5 M pH 8,8	1025 µL
SDS 10% (m/v).....	50 µL
Persulfato de amônio 10% (m/v).....	50 µL
TEMED (Bio-Rad)	2,5 µL
H_2O deionizada q.s.p.	**5000,0 µL**

- Primeiro, com auxílio de placas de vidro apropriadas e suporte, foi polimerizado o gel de corrida e em seguida a camada de gel de empilhamento logo acima

Tampão de amostra 5X

β-mercaptoetanol	2% (v/v)
Tris-HCl pH 6,8	62,5 mM
Glicerol	10% (v/v)
SDS	2% (m/v)
Azul de bromofenol	0,1% (m/v)

- Diluir em água

Tampão de corrida Tris-Glicina pH 8,3

Tris-HCl pH 8,3	25 mM
SDS	0,1% (m/v)
Glicina	250 mM

- Diluir em água

Solução corante de *Coomassie Brillant Blue G*

H_3PO_4	10% (m/v)
$(NH_4)_2SO_4$	10% (m/v)
Coomassie coloidal (G-250 – Sigma)	0,12% (m/v)
Metanol	20% (v/v)

- Diluir em água

- O preparo (em solução aquosa) seguiu a mesma ordem listada acima. Após a dissolução do ácido fosfórico e do sulfato de amônio, adicionou-se *coomassie* e utilizou-se aquecimento suave para a sua dissolução. Ao final adicionou-se o metanol.

➔ **Eletroforese para DNA:**

Tampão de corrida TAE 1X concentrado (eletroforese de DNA)

EDTA	10 mM
Tris-acetato pH 8,0	40 mM

- Diluir em água

Loading Buffer 6X:

Azul de bromofenol	0,25% (m/v)
Xileno cianol	0,25% (m/v)
Glicerol	30% (v/v)

- Diluir em água e distribuir volume total em tubos para armazenar a -20 °C.

➔ **Dosagem Proteínas:**

Reagente de Greenberg:

EtOH (96%)	8,0% (v/v)
Ácido acético	1,2% (v/v)
Triton X-100	2,0% (v/v)
Azul de bromofenol	0,03% (m/v)

- Diluir em água

Dosagem de proteínas com o reagente de Greenberg:

As dosagens foram realizadas em microplaca contendo alíquotas de 20 µL das amostras proteicas. Adicionou-se 180 µL do reagente de Greenberg às mesmas e após 5 minutos de incubação em temperatura ambiente as leituras de absorbância foram lidas em 610 nm. As determinações foram realizadas em triplicata e a curva padrão foi construída com BSA (0,1 mg/mL até 2,0 mg/mL).

➔ **Metodologia DNS:**

Preparo do reagente (em duas etapas) para 500 mL:

Solução A

DNS	5 g
NaOH.....	8 g
H_2O deionizada q.s.p.	**100 mL**

Solução B

$KNaC_4H_4O_6$. 4 H2O	150 g
H_2O deionizada q.s.p.	**250 mL**

- A Solução A deve ser lentamente misturada com a Solução B sob aquecimento de 100 °C e agitação intensa. Acertar volume para 500 mL e proteger o reagente da luz.

Dosagem de açúcares pelo método DNS:

Após o término da incubação das reações mantidas sob 50 °C, 1000 rpm por até 48 horas, os tubos de foram centrifugados a 10.0000 *g* por 5 minutos para baixar resíduos sólidos e coletar volume retido nas paredes e tampa. Na sequência, 100 µL das reações foram coletados e transferidos para microplaca de PCR, onde receberam adição de igual volume do reagente DNS.

As amostras foram aquecidas por 5 minutos a 98 °C, centrifugadas novamente (mesmas condições) e os volumes resultantes de 200 µL foram transferidos para microplaca de fundo chato para determinação dos açúcares redutores via leitura de absorbâncias utilizando-se $\lambda = 540$ nm. Todas as reações foram realizadas em triplicata e utilizou-se glicose (0,25 mg/mL até 5,0 mg/mL) para o preparo de curva padrão.

International Journal of
Molecular Sciences

MDPI

Article

LPMO *Af*AA9_B and Cellobiohydrolase *Af*Cel6A from *A. fumigatus* Boost Enzymatic Saccharification Activity of Cellulase Cocktail

Aline Vianna Bernardi [1], Luis Eduardo Gerolamo [1], Paula Fagundes de Gouvêa [1], Deborah Kimie Yonamine [1], Lucas Matheus Soares Pereira [1], Arthur Henrique Cavalcante de Oliveira [1], Sérgio Akira Uyemura [2] and Taisa Magnani Dinamarco [1,*]

[1] Faculdade de Filosofia Ciências e Letras de Ribeirão Preto, Universidade de São Paulo, Ribeirão Preto 14040-901, Brazil; alinevbernardi@gmail.com (A.V.B.); gerolamo00@hotmail.com (L.E.G.); paulafgouvea@yahoo.com.br (P.F.d.G.); deborah.yonamine@hotmail.com (D.K.Y.); lucas.matheus.pereira@usp.br (L.M.S.P.); arthurdeoliveira@ffclrp.usp.br (A.H.C.d.O.)

[2] Faculdade de Ciências Farmacêuticas de Ribeirão Preto, Universidade de São Paulo, Ribeirão Preto 14040-903, Brazil; suyemura@fcfrp.usp.br

* Correspondence: tdinamarco@ffclrp.usp.br; Tel.: +55-16-3315-9121; Fax: +55-16-3315-9101

Abstract: Cellulose is the most abundant polysaccharide in lignocellulosic biomass, where it is interlinked with lignin and hemicellulose. Bioethanol can be produced from biomass. Since breaking down biomass is difficult, cellulose-active enzymes secreted by filamentous fungi play an important role in degrading recalcitrant lignocellulosic biomass. We characterized a cellobiohydrolase (*Af*Cel6A) and lytic polysaccharide monooxygenase LPMO (*Af*AA9_B) from *Aspergillus fumigatus* after they were expressed in *Pichia pastoris* and purified. The biochemical parameters suggested that the enzymes were stable; the optimal temperature was ~60 °C. Further characterization revealed high turnover numbers (k_{cat} of 147.9 s^{-1} and 0.64 s^{-1}, respectively). Surprisingly, when combined, *Af*Cel6A and *Af*AA9_B did not act synergistically. *Af*Cel6A and *Af*AA9_B association inhibited *Af*Cel6A activity, an outcome that needs to be further investigated. However, *Af*Cel6A or *Af*AA9_B addition boosted the enzymatic saccharification activity of a cellulase cocktail and the activity of cellulase *Af*-EGL7. Enzymatic cocktail supplementation with *Af*Cel6A or *Af*AA9_B boosted the yield of fermentable sugars from complex substrates, especially sugarcane exploded bagasse, by up to 95%. The synergism between the cellulase cocktail and *Af*AA9_B was enzyme- and substrate-specific, which suggests a specific enzymatic cocktail for each biomass by up to 95%. The synergism between the cellulase cocktail and *Af*AA9_B was enzyme- and substrate-specific, which suggests a specific enzymatic cocktail for each biomass.

Keywords: GH6 cellobiohydrolase; AA9 LPMO; lignocellulose hydrolysis; bioethanol

Citation: Bernardi, A.V.; Gerolamo, L.E.; de Gouvêa, P.F.; Yonamine, D.K.; Pereira, L.M.S.; de Oliveira, A.H.C.; Uyemura, S.A.; Dinamarco, T.M. LPMO *Af*AA9_B and Cellobiohydrolase *Af*Cel6A from *A. fumigatus* Boost Enzymatic Saccharification Activity of Cellulase Cocktail. *Int. J. Mol. Sci.* **2021**, *22*, 276. https://doi.org/10.3390/ijms22010276

Received: 3 December 2020
Accepted: 24 December 2020
Published: 29 December 2020

1. Introduction

Fossil fuel depletion, increasing energy consumption, growing CO_2 emissions, and climate change have increased the demand for renewable energy sources. In this scenario, lignocellulosic residues stand out as a new generation of renewable energy sources, including second-generation (2G) ethanol [1–5]. Lignocellulosic biomass-derived biofuels can potentially substitute fossil fuels with the advantage that they can help to reduce the emission of greenhouse gases and global warming [6,7]. Every year, tons of agricultural residues, such as byproducts of sugarcane, corn, wheat, rice, and barley, are generated worldwide and have emerged as the most promising feedstock to produce biofuels by hydrolysis and subsequent fermentation [8].

The composition of the plant cell wall varies in terms of the percentage of cellulose (35–50%), hemicellulose (20–30%), and lignin (20–30%). The wall lignocellulosic structure is recalcitrant and resists chemical and biological treatments. Cellulose, a crystalline

homopolysaccharide, is made up of thousands of D-glucose subunits linked by β-1,4-glycosidic bonds, forming linear chains. The cellulose chains are bound through intra- and intermolecular hydrogen bonds, creating insoluble microfibrils [9]. The recalcitrant structure of the plant cell wall matrix makes the release of soluble sugars challenging [10].

Industrial processes that produce ethanol from cellulose require that mixtures of fungal cellulases be employed, so that soluble sugars are released for further fermentation into bioethanol [7,11]. These enzymes work synergistically to break down polysaccharides and crystalline cellulose [12,13]. First, endoglucanases (EGL, EC 3.2.1.4) hydrolyze β-1,4-glucosidic bonds in amorphous regions of the cellulose chains, to release cello-oligosaccharides; cellobiohydrolases (CBH; EC 3.2.1.91) act on short cellulose molecules and cello-oligosaccharides, releasing disaccharide units like cellobiose. Then, β-glucosidases (BG; EC 3.2.1.21) cleave cellobiose into glucose for further fermentation. Together, these enzymes are part of an enzymatic cocktail and are used to break down lignocellulose.

In contrast to cellulases, lytic polysaccharide monooxygenases (LPMO; EC: 1.14.99.53–56) degrade cellulose by an oxidative mechanism and enhance accessibility to cellulose, improving the hydrolytic performance of cellulases [14–16]. LPMOs are copper-dependent enzymes that act on crystalline cellulose and other polysaccharides in nature, to generate oxidized and non-oxidized chain ends. In addition, LPMO is a virulence factor in fungal meningitis [17].

The fact that LPMO boosts the activity of hydrolytic enzymes during chitin degradation was first described in 2005 [18]. The LPMO activity on cellulose and other biomasses has also been reported [19,20]. The copper ion in the LPMO catalytic structure is coordinated to three nitrogen atoms of the two conserved histidine residues in a histidine brace, which is essential for LPMO activity [21–27]. The LPMO oxidative mechanism is not fully understood, but analysis of reaction products has revealed that LPMO hydroxylates carbon C1 or C4, or both. To initiate oxidative cleavage, an enzyme, such as cellobiose dehydrogenase, or a small reductor molecule must reduce the LPMO copper center. Subsequently, the enzyme reacts with a co-substrate (O_2 or H_2O_2), to form oxygen species that can hydroxylate C1 or C4 in the glycosidic bond [28,29].

Some studies have described inhibitory results or no synergism between LPMOs and cellulases. For example, *Hj*LPMO9A addition to accellerase elicits no synergism until 100 h [30]. Moreover, *Nc*LPMO9F reduces CBHI efficiency in the degradation of mixed amorphous-crystalline cellulosic substrate (MACS) [31]. *Mt*LPMO9L affects CBHI and CBHII differently depending on the ratio between the enzymes, substrate characteristics, and incubation time. These data highlight that understanding the synergistic mechanism between LPMO and GHs is still necessary and will be helpful for the development of novel cellulase mixtures.

Enzymes from thermophilic microorganisms offer several advantages for industrial applications. For example, *Aspergillus fumigatus* produces thermophilic CAZymes, which have high cellulolytic activity and stability in a wide range of pH and at elevated temperatures, unlike commercial fungal cellulases [32–35].

To characterize the association of cellulases (*Af*Cel6A and *Af*-EGL7) and LPMO (*Af*AA9_B) from *A. fumigatus*, we evaluated their action on the degradation of different biomasses on a pilot scale. *Af*Cel6A is a cellobiohydrolase from the glycoside hydrolase (GH) class, family 6; it acts exclusively on nonreducing ends of cellulosic polymers. *Af*-EGL7 is a previously characterized endoglucanase that can potentially hydrolyze biomass [32,36].

Here, we present the biochemical characterization of *Af*Cel6A and *Af*AA9_B after they are expressed in *Pichia pastoris.* We will show that supplementation of enzymatic cocktails can enhance the production of fermentable sugars, and that LPMOs have a critical role in biomass hydrolysis. In addition, we evaluate the synergistic effect between *Af*AA9_B and cellulases (*Af*Cel6A and *Af*-EGL7) and show different effects for the two enzymes.

2. Results and Discussion

Enzymatic biomass hydrolysis underlies most of the cost involved in biofuel production [37,38]. Different commercially available cellulolytic cocktails such as Novozyme, Du-Pont-Genencor, and Dyadic are still expensive. These cocktails consist of several enzymes that promote complete lignocellulosic biomass conversion into fermentable sugars [39,40]. However, widely variable biomasses are available for biorefinery purposes; e.g., wheat straw, rice straw, corncob, cotton-stalk, and sugar cane bagasse, so these commercial cocktails may not have the same efficiency for all feedstocks [41].

Developing cheaper and more effective enzymatic cocktails for hydrolysis of different biomasses is one of the major interests of researchers devoted to biomass conversion. Such cocktails can only be achieved by reducing the amount of enzymes that is required for hydrolysis, by bioprospecting and characterizing new enzymes, and by developing new enzyme mixtures [42]. Moreover, the addition of an extra enzyme increases hydrolysis performance by increasing the release of fermentable sugars and reducing the time of hydrolysis.

LPMO (*Af*AA9_B) and Cellobiohydrolase GH6 (*Af*Cel6A) from *A. fumigatus* and expressed in *Escherichia coli* and *Aspergillus oryzae*, respectively, have been described [35,43]. However, to evaluate the action of the combined enzymes, we characterized and analyzed their biochemical properties after expressing them in *Pichia pastoris*, and we detected some differences.

2.1. Expression and Purification of Recombinant AfCel6A and AfAA9_B

We successfully expressed recombinant *Af*Cel6A and *Af*AA9_B in *P. pastoris* X-33. After induction for 144 h, we collected, concentrated, and purified the culture supernatants on Ni^{+} Sepharose 6 Fast Flow resin (Ge Healthcare, Little Chalfont, UK). SDS-PAGE revealed that the purified recombinant *Af*Cel6A and *Af*AA9_B had apparent molecular masses of approximately 65 and 30 kDa, respectively (Figure 1). After Endo H treatment, the molecular mass of *Af*Cel6A remained almost the same, while *Af*AA9_B migrated as a band of approximately 26 kDa. Analyses of potential N-glycosylation sites by the NetNGlyc 1.0 program (http://www.cbs.dtu.dk/services/NetNG lyc/) suggested that a potential site was present at position N413 in *Af*Cel6A and N159 in *Af*AA9_B, confirmed by deglycosylation of the recombinant proteins by the enzyme Endoglycosidase H. The presence of N-glycans at different sites in the structure of the enzyme can influence enzymatic properties, such as secretion, folding, and stability, among others [44].

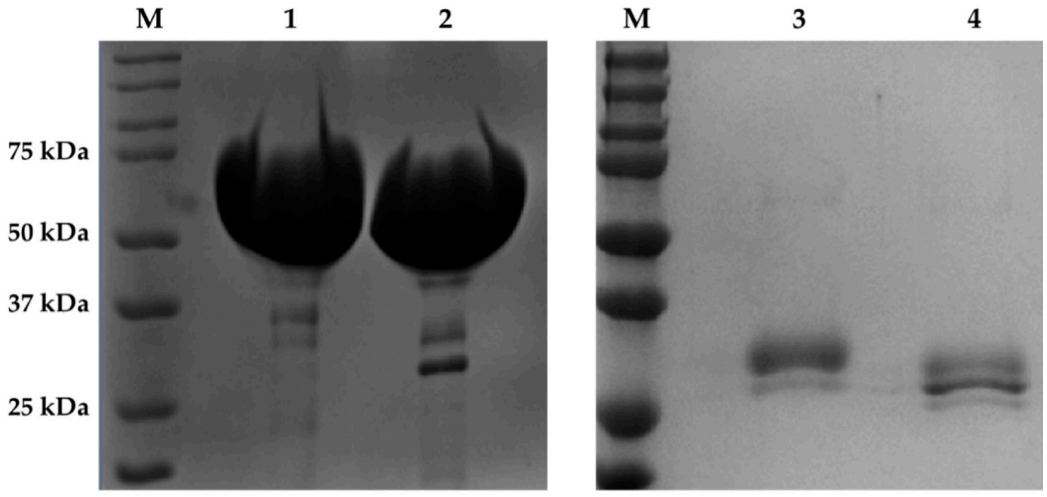

Figure 1. SDS-PAGE (10% polyacrylamide gel) analysis of the purified recombinant *Af*Cel6A and *Af*AA9_B. Lane M, molecular mass standards (Precision™ Protein Standards Dual Color—BioRad); lane 1, purified recombinant *Af*Cel6A; lane 2, deglycosylated *Af*Cel6A; lane 3, purified recombinant *Af*AA9_B; lane 4, deglycosylated *Af*AA9_B.

We excised the purified *Af*AA9_B from the gel and analyzed it on the LC-MS/MS Xevo TQS (Waters) system at the Multi-User Laboratory of Mass Spectrometry, which confirmed that the enzyme was LPMO (Table 1).

Table 1. Peptide sequences.

Protein Gene	Peptide Sequence	Precursor M_Z	Precursor Charge	Product M_Z	Product Charge
AFUA_4G07850	ITSIAGLLASASLVAGHGFVSGIVADGK	871.675226	3	1049.562586	1
AFUA_4G07850	ITSIAGLLASASLVAGHGFVSGIVADGK	871.675226	3	992.541122	1
AFUA_4G07850	ITSIAGLLASASLVAGHGFVSGIVADGK	871.675226	3	845.472708	1
AFUA_4G07850	ITSIAGLLASASLVAGHGFVSGIVADGK	871.675226	3	746.404294	1
AFUA_4G07850	ITSIAGLLASASLVAGHGFVSGIVADGK	871.675226	3	659.372266	1
AFUA_4G07850	ITSIAGLLASASLVAGHGFVSGIVADGK	871.675226	3	602.350802	1
AFUA_4G07850	NTDPGIK	372.912411	2	630.345717	1
AFUA_4G07850	NTDPGIK	372.912411	2	529.298038	1
AFUA_4G07850	NTDPGIK	372.912411	2	414.271095	1
AFUA_4G07850	NTDPGIK	372.912411	2	317.218332	1

2.2. Structural Analysis and Predictions by Circular Dichroism (CD)

LPMOs comprise a group of redox enzymes that belong to the auxiliary activity (AA) class (families 9–16, except 12) [45] and which bear a β-sandwich core (presence of 8–10 β-strands). The catalytic region of the enzyme is known as histidine brace [21,24,46], which contains many loops and accounts for the active site topology and substrate specificity. Specificity is due to the presence of aromatic residues and their weak interactions with polysaccharides [22,47]. Figure 2a shows the crystallized structure of LPMO *Af*AA9_B (PDB: 5 × 6A), where the active site residues H1, H86, and Y175 in the histidine brace are highlighted.

Due to its tunnel-shaped catalytic structure, *Af*Cel6A acts exclusively on nonreducing ends of cellulosic polymers. The cellulosic polymers enter this catalytic structure through one of their extremities, and *Af*Cel6A continuously cleaves the long chains into small cellobiose units via anomeric inversion (Figure 2c). The enzymatic core consists of a distorted α/β-barrel motif. Few parallel β-strands in sandwich conformation are connected by several loops, which are rich in α-helices [48–50]. As depicted in Figure 2c, *Af*Cel6A contains N-terminal CBM1 (carbohydrate-binding module) as well as the main residues involved in catalysis, namely Q229, P268, V217, N265, A269 [48], D165, D211, and D390 (determined by the Pfam database [51]).

Since the 1980s, thousands of three-dimensional protein structures have been resolved and deposited in the Protein Data Bank (PDB), allowing more detailed insights into the structure and function of proteins, including protein complexes [52]. However, performing structural studies under the conditions in which proteins actually operate (i.e., generally in solution), as well as under other conditions, is crucial, and providing measures of the rates of structural changes in proteins, which are often essential to their biological function [52], is vital. Circular dichroism (CD) has become increasingly recognized as a valuable structural technique for addressing these issues [52]. In this sense, the first important information to be obtained is whether the structure of the expressed proteins in solution corresponds to crystal or modeled structures. To this end, we obtained the secondary structure content on the basis of on circular dichroism spectra, from which we predicted the secondary structures of the enzymes by using BESTSEL [53]. This analysis showed substantial structural similarity between the enzymes and their templates from PDB:5X6A resolved by Q. Shen (unpublished) (for *Af*AA9_B) [54] and Phyre2 web server [55] (for *Af*Cel6A), as displayed in Figure 2 and Supplementary Table S1.

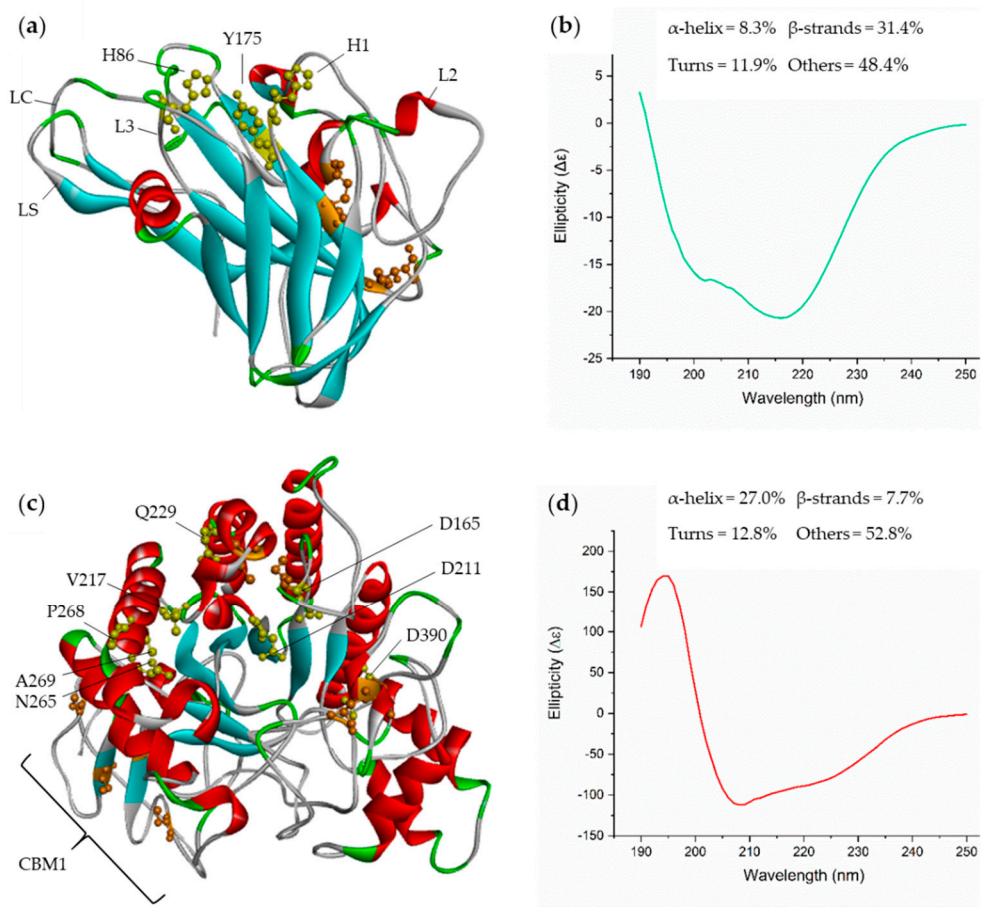

Figure 2. Ribbon representation of the enzymes *Af*AA9_B (**a**) and *Af*Cel6A (**c**) and their main conserved residues and structures. Active site residues are represented in yellow, and disulfide bonds are represented in orange. *Af*AA9_B loops are represented by LC (C-terminus), LS (short), L3, and L2. CBM1 residues are indicated by a brace in *Af*Cel6A. Circular dichroism spectra obtained from 190 to 250 nm (UV-distant) for *Af*AA9_B with Cu(II) (**b**) and *Af*Cel6A (**d**) at 25 °C. Both enzymes were in 20 mM sodium phosphate buffer (pH = 7.4), and the spectra were read by using a quartz cuvette with an optical path of 0.1 cm. The mean spectra for each sample were normalized by subtracting the buffer spectrum.

The CD spectrum of *Af*AA9_B and its predicted secondary structures (Figure 2b) demonstrated that the enzyme consisted of 8.3% α-helices and 31.4% β-strands. These values reinforced that LPMOs present a large number of β-strands in their cores, reflected by the well-defined negative peak at 218 nm, the small peak at 190 nm, and the approximated single band profile. Small negative peaks around 208 nm also evidenced the small number of helices [56]. Compared to the expected values based on the PDB: 5X6A structure, the percentage of β-strands was exactly the same, while the percentage of α-helices was −4.3%. *Ta*LPMO9A (PDB: 2YET) [26], an LPMO from *Thermoascus aurantiacus*, has been reported to share 71% identity with *Af*AA9_B and to present similar proportions of α-helices and β-strands: 30.8% and 15.0%, respectively.

*Af*Cel6A presented 27.0% α-helix and 7.7% β-strands, as estimated by BeStSel (Figure 2d). The accentuated peak at 190 nm and the two negative peaks near 208 nm and 222 nm indicated a large number of α-helices. The absence of a negative peak at approximately 218 nm and a single band profile are typical of proteins with low content of β-strands [56]. On the basis of the proportions of α-helices and β-strands estimated by Phyre2 [55] and the Kabsch and Sander method [57] for the modeled structure (Figure 2c), the differences were −4.3% and −1.0%, and −1.0% and −2.3%, respectively. The enzyme Cel6A from *Trichoderma reesei* (PDB:1QJW), which shares 69% identity, presents a similar proportion of 35.8% α-helices and 8.7% β-strands [58]. Furthermore, a cellobiohydrolase from a different *A. fumigatus* strain that shares 99% identity with *Af*Cel6A consists of 26.0%

α-helix and 15.4% β-strands, confirming that the prediction based on the CD spectrum is remarkably close.

Therefore, CD analysis of both enzymes obtained herein evidenced that their secondary structure profiles resembled the profiles described in the literature. This indicated that both enzymes were correctly folded during heterologous expression, and that their structures were maintained after they were purified.

Confirming that the structure of wild enzymes in solution corresponds to the structure obtained by crystallography or modeling allows enzymes to be efficiently improved by protein engineering. To increase the catalytic efficiency of cocktails, alterations modeled on the protein structure can be accompanied by spectroscopic studies in solution, allowing improved activity to be directly associated with conformational changes in the structure of the enzyme.

2.3. Enzymatic Properties of AfCel6A and AfAA9_B

We used CM-Cellulose and 2,6-DMP as substrates to determine the enzymatic properties of *Af*Cel6A and the activity of *Af*AA9_B, respectively.

The optimal temperature for *Af*Cel6A activity was 55–60 °C, and the enzyme retained over 54% of the maximum activity between 40 and 65 °C. At 70, 75, and 80 °C, *Af*Cel6A maintained 43.5%, 30%, and 26% of the maximum activity, respectively (Figure 3a). Most characterized cellobiohydrolases, shown in Table 2, were also active at these temperatures. We studied the *Af*Cel6A thermal stability after preincubating it at 50, 60, 70, 80, or 90 °C for different times (Figure 3b). The enzyme was stable after 30 min and retained 57.5%, 42.0%, 40.4%, and 26.9% of the initial activity at 60, 70, 80, and 90 °C, respectively. *Af*Cel6A maintained about 30% of the initial activity at 60–80 °C. However, the enzyme was completely inactivated after 5 h at 60–80 °C. *Af*Cel6A was stable at 50 °C. It lost only 30% of its original activity after 24 h and retained 64.2% and 47.7% of its initial activity after 48 and 72 h, respectively (Figure 3c). These results showed that *Af*Cel6A was stable at high temperatures, especially at 50 °C. In another study, after expression in *A. oryzae*, *Af*Cel6A was stable at 60 °C, but it completely lost its activity at 70 °C [35]. Therefore, *Af*Cel6A was more stable after expression in *P. pastoris* than in *A. oryzae.*

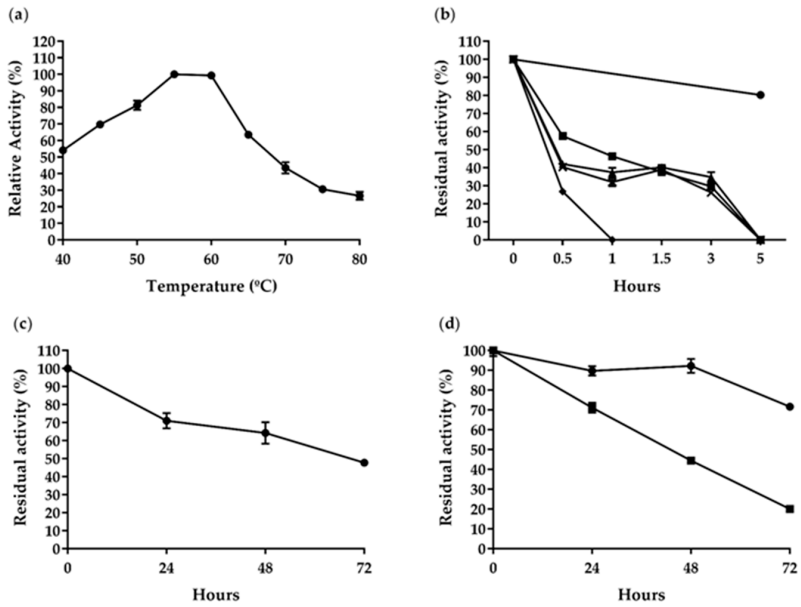

Figure 3. Temperature effects on *Af*Cel6A and *Af*AA9_B activity and stability. (**a**) *Af*Cel6A temperature-activity profiles at optimal pH for 45 min. (**b**) *Af*Cel6A thermostability at • 50, ■ 60, ▲ 70, × 80, and ♦ 90 °C for different times. (**c**) *Af*Cel6A thermostability at 50 °C for up to 72 h. (**d**) *Af*AA9_B thermostability at • 50 and ■ 60 °C for 72 h. Each value in the panel represents the mean of three experiments.

Table 2. Comparison among catalytic and biochemical properties of GH6 cellobiohydrolases.

Source Organism	Enzyme Name	Expression System	Substrate	V_{max}	K_M	k_{cat}	k_{cat}/K_M	Optimal T	Optimal pH	Thermal Stability	pH Stability	Ref.
Aspergillus fumigatus Af293	*Af*Cel6A	*Pichia pastoris*	CMC-Na	195.2 ± 4.65 U mg^{-1}	7.44 ± 0.51 g/L	147.9 s^{-1}	19.9 mL mg^{-1} s^{-1}	55–60 °C	pH 5.5–6.5	>70% after 24 h at 50 °C; about 40% after 90 min at 60–80 °C; more than 25% after 30 min at 90 °C	More than 70% at pH 3.0–10.0 after 72 h	This study
Aspergillus fumigatus	*Af*Cel6A	*Aspergillus oryzae*	Avicel PH101	-	48.6 ± 14.8 g L^{-1}	0.9 ± 0.1 s^{-1}	-	70 °C	-	No loss at 60 °C after 1 h	-	[35]
Aspergillus terreus	*At*Cel6A	*Aspergillus oryzae*	Avicel PH101	-	-	-	-	50 °C	-	>90% after 1 h at 50 °C	-	[35]
Talaromyces funiculosus	*Tf*Cel6A	*Aspergillus oryzae*	Avicel PH101	-	21.6 ± 3.2 g L^{-1}	0.5 ± 0.02 s^{-1}	-	60 °C	-	No loss at 50 °C after 1 h	-	[35]
Colletotrichum graminicola	*Cg*Cel6A	*Aspergillus oryzae*	Avicel PH101	-	-	-	-	40 ° C	-	>90% after 1 h at 40 °C	-	[35]
	*Cg*Cel6B				89.0 ± 13.2 g L^{-1}	1.8 ± 0.2 s^{-1}		50 °C		>90% after 1 h at 50 °C		
Trichoderma reesei	*Tr*Cel6A	*Aspergillus oryzae*	Avicel PH101	-	24.3 ± 4.0 g L^{-1}	0.6 ± 0.04 s^{-1}	-	70 °C	-	No loss at 50 °C after 1 h	-	[35]
	Cel6A[1]	*Pichia pastoris*	CMC-Na	10.7 mmol min^{-1} mg^{-1}	0.31 mg mL^{-1}	-	-	60 °C	pH 5.5	90% after 30 min at 60 °C	-	[59]
	Cel6A[2]	*Pichia pastoris*	PASC	-	-	-	-	55 °C	pH 5.5–6.0	100% at 40 °C and 50% at 60 °C, after 30 min	No loss at pH 5.0–6.0; rapid inactivation at more alkaline pH; and some instability at more acidic pH after 30 min	[60]
	CBHII	-	PASC	10 U mg^{-1}	3.8 mg mL^{-1}	-	-	60 °C	pH 5.0	80% after 30 min at 60 °C	Stable at pH 3.5–6.0 after 30 min	[61]
Magnaporthe oryzae Ina72	*Mo*Cel6A	*Magnaporthe oryzae*	Cellotetraose	454.5 μg min^{-1} mg^{-1}	24.3 mM	-	-	40 °C	pH 9.0	-	-	[62]
			Cellopentaose	63.3 μg min^{-1} mg^{-1}	3.3 mM							
Schizophyllum commune KMJ820	CBH II	*Escherichia coli*	pNPC	20.8 U mg^{-1}	1.4 mM	-	-	50 °C	pH 5.0	-	-	[63]
Penicillium occitanis Pol 6	CBH II	-	pNPC	-	5 mM	-	-	65 °C	pH 4.0–5.0	Almost 100% at 30–50 °C; 50% at 60 °C; and complete inactivation at 70 °C, after 30 min	Stable at pH 2.0–9.0 after 24 h	[64]
Talaromyces emersonii	CBH II	-	$CNPG_3$	9.1 U mg^{-1}	4.5 mM	8.9 s^{-1}	1.9 mM^{-1} s^{-1}	68 °C	pH 3.8	$t_{1/2}$ = 38 min at 80 °C (pH 5.0)	$t_{1/2}$ = 38 min at pH 5.0 (80 °C)	[65]
Trichoderma viride CICC13038	CBH II	*Saccharomyces cerevisiae*	CMC-Na	-	-	-	-	70 °C	pH 5.0	-	-	[66]
Neocallimastix patriciarum J11	J11 CelA	*Escherichia coli*	Barley β-glucan	-	-	-	-	50 °C	pH 6.0	More than 70% at up to 50 °C and approximately 50% at 70 °C, after 1 h	More than 80% at pH 5.2–11.3; and approximately 70% at pH 3.0, 4.2, and 12.3, after 1 h	[67]
Irpex lacteus MC-2	Ex-4	*Pichia pastoris*	PASC	-	-	-	-	50 °C	pH 5.0	More than 80% at 60 °C (pH 3.0–8.0) after 1 h	More than 80% at pH 3.0–8.0 (60 °C) after 1 h	[68]
Chaetomium thermophilum $HSAUP_{07}2651$	CBH II	*Pichia pastoris*	pNPC	-	-	-	-	50 °C	pH 4.0	No loss at 50 °C; approximately 20% at 60 °C; and complete inactivation at 80 °C, after 1 h	-	[69]

The optimal temperature for *Af*AA9_B activity was 60 °C (data not shown). *Af*AA9_B was stable at 50 and 60 °C and retained over 75% and 20% of its initial activity, respectively (Figure 3d). Like *Af*AA9_B, other LPMOs were stable at 50 and 60 °C; e.g., PMO9D_SCYTH, PMO9D_MALCI, *Mt*LPMO9D, *Mt*LPMO9J, and *Mt*LPMO9A (Table 3).

Figure 4 illustrates how pH influenced *Af*Cel6A and *Af*AA9_B. The highest *Af*Cel6A activity emerged at pH 5.5–6.0, but it was active in a narrow pH range (pH 4.0–7.5) and retained >50% of maximum activity therein (Figure 4a).

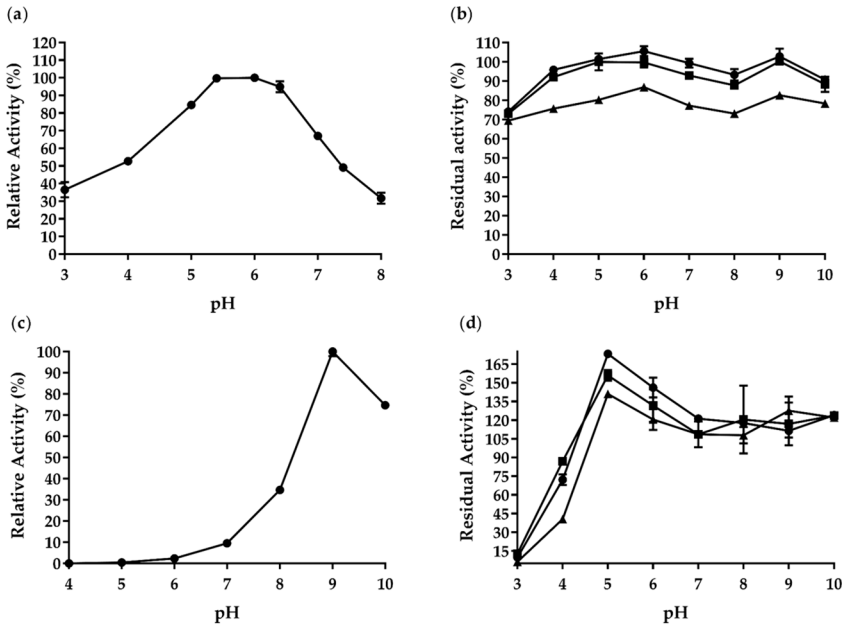

Figure 4. pH effects on the enzymatic activity and stability of purified recombinant *Af*Cel6A and *Af*AA9_B. (**a**) *Af*Cel6A pH-activity profile. (**b**) pH stability of *Af*Cel6A after • 24, ■ 48, and ▲ 72 h of preincubation at 4 °C. The enzyme activities were measured under standard conditions. (**c**) *Af*AA9_B pH-activity profile. (**d**) pH stability of *Af*AA9_B after • 24, ■ 48, and ▲ 72 h of preincubation at 4 °C. Each value in the panel represents the mean of three experiments.

Many cellobiohydrolases seem to belong to the class of acidic enzymes, with optimal pH ranging from 3.9 to 6.0; for example, CBH II from *Talaromyces emersonii* (pH 3.8), Cel6D (pH 3.9), CBH II from *Chaetomium thermophilum* (pH 4.0), CBH II from *Penicillium occitanis* (pH 3.0–5.0), CBH II from *Trichoderma viride* (pH 5.0), J11 CelA (pH 6.0), and EX4 (pH 5.0). Only one GH6 has been classified as active at pH 9.0: *Mo*Cel6A from *Magnaporthe oryzae* (Table 2).

We also investigated *Af*Cel6A pH stability (Figure 4b). Notably, *Af*Cel6A was stable at pH ranging between 3 and 10 and retained over 70% of its original activity after 72 h. Compared to other GH6 cellobiohydrolases, *Af*Cel6A was more stable over a wide pH range, whereas others had narrower range of pH stability—CBH II from *Talaromyces emersonii* (38 min at pH 5.0), Cel6D (over 60% activity at pH 4.0–6.0 and 47 °C and complete inactivation at pH 4.0 and 55 °C), CBH II from *Penicillium occitanis* (24 h at pH 2.0–9.0), J11 CelA (1 h), and EX4 (over 80% activity at pH 3.0–8.0 at 60 °C for 1 h).

*Af*AA9_B showed the highest activity at pH 9.0. At pH 10.0, it retained >74.0% of its activity (Figure 4c). The optimal *Af*AA9_B pH was pH 9.0, but this enzyme was stable at pH ranging between 5.0 and 10.0 and maintained 100% of the original activity after 72 h (Figure 4d). Compared to PMO9D_SCYTH (pH 7.0) and PMO9D_MALCI (pH 9.0), *Af*AA9_B was more stable, whereas the former LPMOs were stable at a specific pH (Table 3).

Table 3. Comparison among catalytic and biochemical properties of LPMOs.

Source Organism	Protein Name	Expression System	Substrate	Co-Substrate	V_{max}	K_M	k_{cat}	k_{cat}/K_M	Optimal T	Optimal pH	Thermostability	pH Stability	Ref.
Aspergillus fumigatus Af293	*Af* AA9_B	*Pichia pastoris* X33	2,6-DMP	§ [a] H_2O_2	78.52 ± 3.33 U g^{-1}	2.04 ± 0.24 μM	0.034 s^{-1}	0.017 μM^{-1} s^{-1}	-	*** 9	-	-	This study
				§ [b] H_2O_2	1481 ± 72.19 U g^{-1}	0.79 ± 0.12 μM	0.64 s^{-1}	0.81 μM^{-1} s^{-1}	-		60 °C: 50 % after 48 h 50 °C: almost 100% of activity after 48 h	No loss of activity at pH 5.0–10.0	
			§ 2,6-DMP	[a] H_2O_2	49.26 ± 4.48 U g^{-1}	106.3 ± 27.9 μM	0.021 s^{-1}	$1,98 \times 10^{-4}$ μM^{-1} s^{-1}	-	-	-	-	
				[b] H_2O_2	972.5 ± 28.31 U g^{-1}	12.15 ± 1.76 μM	0.42 s^{-1}	0.035 μM^{-1} s^{-1}	-	-	-	-	
Scytalidium thermophilum	PMO9D_SCYTH	*Pichia pastoris* X33	Avicel	§ H_2O_2	0.36 U mg^{-1}	4.54 mg mL^{-1}	2.99×10^{-2} min^{-1}	6.58×10^{-3} mg^{-1} mL min^{-1}	-	-	-	-	[70]
			CMC		14.96 U mg^{-1}	10.6 mg mL^{-1}	1.61 min^{-1}	1.52×10^{-1} mg^{-1} mL min^{-1}	60 °C	7	60 °C ($t_{1/2}$ = 60.58 h, pH 7.0)	Above 90% after 48 h at pH 7.0	
			2,6-DMP		0.13 U mg^{-1}	0.51 mM	1.84×10^{-1} min^{-1}	3.57×10^{-1} mM^{-1} min^{-1}		-	-	-	
Malbranchea cinnamomea	PMO9D_MALCI		Avicel		0.17 U mg^{-1}	5.87 mg mL^{-1}	1.05×10^{-2} min^{-1}	1.79×10^{-3} mg^{-1} mL min^{-1}		-	-	-	
			CMC		9.59 U mg^{-1}	29.27 mg mL^{-1}	0.76 min^{-1}	2.62×10^{-2} mg^{-1} mL min^{-1}	50 °C	9	50 °C ($t_{1/2}$ = 144 h, pH 7.0)	Above 80% after 72 h at pH 9.0	
			2,6-DMP		0.12 U mg^{-1}	1.17 mM	1.21 min^{-1}	1.03×10^{-1} mM^{-1} min^{-1}		-	-	-	
Thielavia terrestris	*Tt*LPMO9E	-	PWS	§ O_2	-	49.80 g L^{-1}	3.8 min^{-1}	* 1.85×10^3 M^{-1} min^{-1}	-	-	-	-	[71]
Myceliophthora thermophila	*Mt*PMO9E	*Neurospora crassa*	cellohexaose	§ O_2	-	32 μM	10.1 min^{-1}	0.30 μM^{-1} min^{-1}	-	-	-	-	[72,73]
			§ cellohexaose	O_2	-	230 μM	17 min^{-1}	7.4×10^{-2} μM^{-1} min^{-1}	-	-	-	-	
				H_2O_2	-	53 μM	# 15.9 s^{-1}	3.0×10^5 M^{-1} s^{-1}	-	-	-	-	
Serratia marcescens	CBP21	*Escherichia coli* BL21(DE3) Star	CNW	§ H_2O_2	1.11 μM s^{-1}	0.58 mg mL^{-1}	6.7 s^{-1}	$\cong 10^6$ M^{-1} s^{-1}	-	-	-	-	[74]
			§ CNW	H_2O_2	-	2.8 μM	-	-	-	-	-	-	
Lentinus similis	*Ls*(AA9)A	*Aspergillus oryzae* MT3568	cellotetraose	§ O_2	-	43 μM	0.11 s^{-1}	2.6×10^3 M^{-1} s^{-1}	-	-	-	-	[75]
Aspergillus fumigatus NITDGPKA3	** CAF32158.1	*Pichia pastoris* X33	2,6-DMP	§ H_2O_2	1.11 μM min^{-1}	11.23 μM	0.642 min^{-1}	5.7×10^{-2} μM min^{-1}	-	-	-	-	[76]
Myceliophthora thermophila	*Mt*LPMO9D	*Myceliophthora thermophila* C1	-	-	-	-	-	-	-	-	**** Tm_{app} at pH 7.0 = 68 °C	-	[77]
Myceliophthora thermophila	*Mt*LPMO9J	*Aspergillus nidulans*	-	-	-	-	-	-	-	-	**** Tm_{app} at pH 6.0 = 58 °C	-	[78]
Thermoascus aurantiacus	*Ta*LPMO9A	*Aspergillus oryzae*	-	-	-	-	-	-	-	-	**** Tm_{app} at pH 7.0 = 69 °C	-	[79]

Notations: (§) fixed concentration; (*) k_{cat}/K_M calculated for this paper considering the molecular weight of 24.2 kDa for *Tt*LPMO9E; (**) this enzyme has no name yet, the provided code is its codifying gene; (***) pH stability not correlated with analyzed pH values; (****) apparent midpoint transition temperatures (Tm_{app}) calculated on the basis of CD (*Mt*LPMO9D and *Ta*LPMO9A) and Intrinsic Trp fluorescence emission (ITFE) (*Mt*LPMO9J) analysis; (#) k_{cat} estimated based on previous k_{cat}/K_M and K_M values for *Mt*PMO9E. Kinetic studies were conducted at ([a]) pH = 6.0 and ([b]) pH = 9.0. Abbreviations: PWS—Pretreated wheat straw; CNW—Chitin nanowhisker. For more details, see the corresponding references.

2.4. Substrate Specificity and Kinetic Parameters

*Af*Cel6A exhibited broad substrate specificity, including CM-Cellulose, Avicel®, xyloglucan, and birchwood xylan. This enzyme displayed higher specific activities toward CM-Cellulose (36.6 ± 2.1 U mg^{-1}) and Avicel® (35.8 ± 2.6 U mg^{-1}) than birchwood xylan (21.1 ± 0.1 U mg^{-1}) and xyloglucan (19.9 ± 0.3 U mg^{-1}) (Figure 5). When CMC was the substrate, purified *Af*Cel6A had K_M, V_{max}, and k_{cat}/K_M of 7.44 ± 0.51 g L^{-1}, 195.2 ± 4.65 U mg^{-1}, and 19.9 mL mg^{-1} s^{-1}, respectively (Table 2).

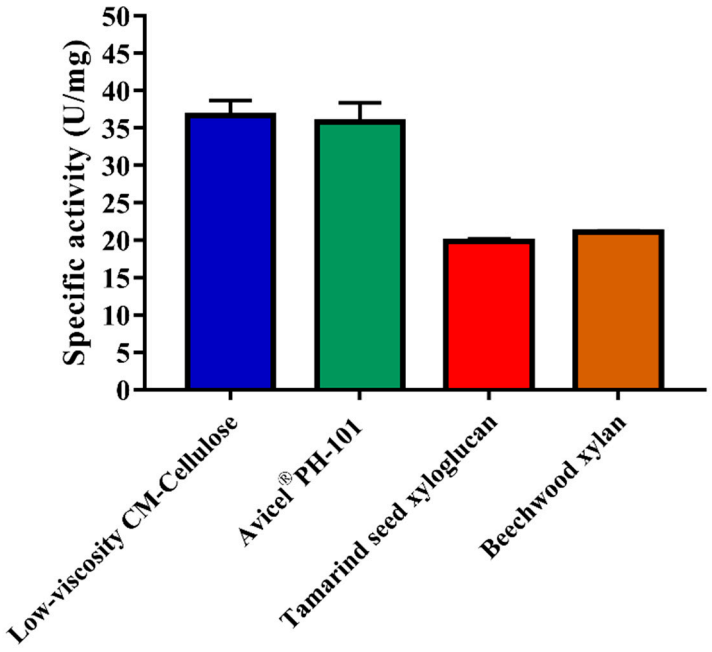

Figure 5. *Af*Cel6A specific activity (U mg^{-1}) toward CM-Cellulose, Avicel, xyloglucan, and xylan. Each reaction was performed in 50 mM phosphate bufer (pH 6.0) containing 0.5% (*w/v*) of each substrate at 55 °C for 30 min. Values are the mean ± SD of three replicates.

We evaluated recombinant *Af*AA9_B peroxidase activity toward the chromogenic substrate 2,6-DMP and the co-substrate H_2O_2, according to Breslmayr et al. (2018) [80], with some modifications. Table 3 summarizes the kinetic parameters determined when the reactions were carried out at pH 6.0 or 9.0 and 50 °C.

The V_{max} values were higher at pH 9.0 for both the substrate (1481 ± 72.19 U g^{-1}) and the co-substrate (972.5 ± 28.31 U g^{-1}). Since we performed the saccharification tests at pH 6.0, we also determined the kinetic parameters under these conditions. At this pH, V_{max} was 78.52 ± 3.33 U g^{-1} for the substrate and 49.26 ± 4.48 U g^{-1} for the co-substrate. These results were expected because pH 9.0 was optimal for *Af*AA9_B activity.

Compared to the kinetic parameters described for other LPMOs, *Af*AA9_B had lower K_{Mapp} (0.79 µM) than PMO9D_SCYTH (0.51 mM), PMO9D_SCYTH (0.51 mM), and PMO9D_MALCI (1.17 mM), which showed that *Af*AA9_B had higher binding affinity for 2,6-DMP (Table 3).

2.5. Effect of Different Metal Ions and Chemicals

Cellobiohydrolases are commonly used in many industrial processes. The effects of additives and products of cellulose hydrolysis on the activity of these enzymes must be considered during operation on an industrial scale.

Table 4 depicts how different ions and reagents influence CM-Cellulose hydrolysis by purified *Af*Cel6A. At 5 mM, $MnCl_2$ (189.25 ± 2.33%), DTT (150.68 ± 5.29%), $CoCl_2$ (116.75 ± 1.36%), $FeSO_4$ (125.83 ± 3.61%), β-mercaptoethanol (134.24 ± 1.02%), $AgNO_3$ (179.27 ± 20.04%), and ascorbic acid (121.40 ± 2.55%) stimulated *Af*Cel6A activity. EDTA, DMSO, SLS, Triton X-100, Tween 20, $CaCl_2$, $MgSO_4$, KCl, and $(NH_4)_2SO_4$ practically did

not affect *Af*Cel6A activity. On the other hand, SDS inhibited the enzyme by approximately 50%. The fact that β-mercaptoethanol and DTT boosted *Af*Cel6A activity by 134.64% and 150.68%, respectively, suggested that the presence of sulfhydryl groups such as the ones from cysteine residues in the active site is important for enzymatic catalysis [81].

Table 4. Effects of additives on *Af*Cel6A and *Af*AA9_B activity.

	***Af*AA9_B**	***AfCel6A***
Additive	**% Relative Activity**	
None	100.0 ± 1.0	100.0 ± 0.9
SDS	107.8 ± 4.8	53.72 ± 0.31
Tween 20	103.7 ± 9.6	93.24 ± 2.11
EDTA	0	91.88 ± 1.56
Ascorbic Acid	-	121.40 ± 2.55
DMSO	108.3 ± 1.5	101.03 ± 3.58
β-mercaptoethanol	36.7 ± 0.6	134.24 ± 1.02
$ZnSO_4$	36.8 ± 6.1	83.67 ± 0.65
$MnCl_2$	82.2 ± 0.7	189.25 ± 2.33
$CoCl_2$	0	116.75 ± 1.36
$CaCl_2$	93.6 ± 3.3	101.1 ± 2.4
$FeSO_4$	0	125.83 ± 3.61
$MgSO_4$	113.9 ± 1.9	95.92 ± 2.13
$CuSO_4$	35.2 ± 4.6	85.08 ± 0.65
$AgNO_3$	0	179.27 ± 20.04
KCl	107.5 ± 2.1	98.87 ± 2.44
$(NH_4)_2SO_4$	88.9 ± 3.2	99.9 ± 2.1
DTT	0	150.68 ± 5.29
Triton X-100	84.8 ± 2.3	91.55 ± 1.19
SLS	115.3 ± 0.7	93.80 ± 1.60

As for *Af*AA9_B, SLS (115.3 ± 0.7%), SDS (107.8 ± 4.8%), Tween 20 (103.7 ± 9.6%), DMSO (108.3 ± 1.5%), $MgSO_4$ (113.9 ± 1.9%), and KCl (107.5 ± 2.1%) did not inhibit this enzyme. DTT, EDTA, $CoCl_2$, $FeSO_4$, and $AgNO_3$ completely inhibited *Af*AA9_B. β-mercaptoethanol, $ZnSO_4$, and $CuSO_4$ decreased *Af*AA9_B activity by 70%. $MnCl_2$, $CaCl_2$, and $(NH_4)_2SO_4$ affected *Af*AA9_B little.

We described that cellobiohydrolases act on short cellulose molecules and cellooligosaccharides, releasing disaccharide units, such as cellobiose [35]. Cellobiose is the major product of cellulose hydrolysis by cellobiohydrolases, whereas glucose is the final product of cellulose hydrolysis.

Product inhibition can affect lignocellulosic hydrolysis to glucose and represents a barrier to achieving the high product yields that are necessary for an efficient process [82].

We examined how different glucose (10–250 mM) and cellobiose (10–100 mM) concentrations affected *Af*Cel6A activity (Figure 6a). Glucose at 100 and 250 mM inhibited the enzymatic activity by 12% and 13%, respectively. Cellobiose (100 mM) inhibited *Af*Cel6A activity by 50%. Cellobiohydrolase from *T. reesei* (*Cel6A*) has been described as the most efficient cellobiohydrolase, with IC_{50} of 240 mM for glucose and 20 mM for cellobiose [58]. Therefore, our results showed that *Af*Cel6A was more resistant to inhibition by both products because IC_{50} was higher than 250 mM for glucose and 100 mM for cellobiose.

Likewise, we investigated how both sugars affected *Af*AA9_B activity (Figure 6b). Surprisingly, the enzyme retained more than 80% of its initial activity when we added 250 mM glucose or 100 mM cellobiose to the reaction. Together, these findings indicated that *Af*Cel6A and *Af*AA9_B have potential application in enzymatic cellulose saccharification. However, to improve the efficiency of these enzymes and to increase glucose production, synergistic association with other enzymes is required.

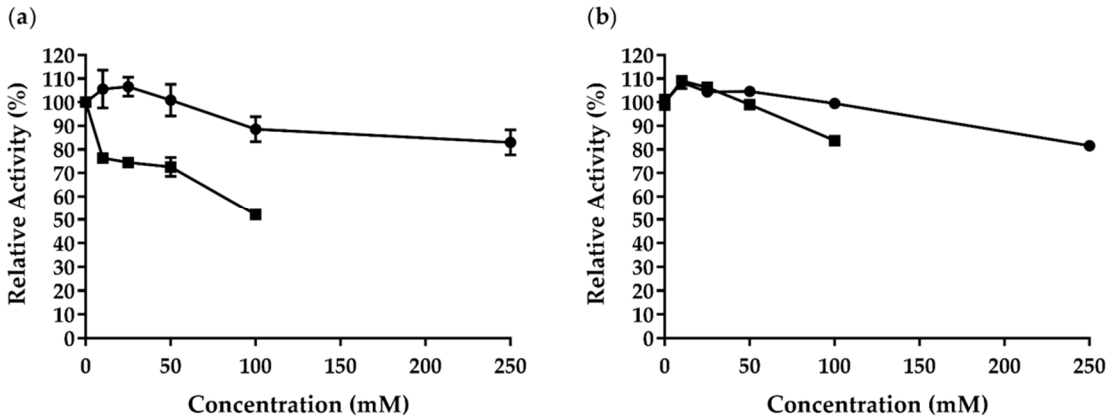

Figure 6. • Glucose and ■ cellobiose effects on (**a**) *Af*Cel6A and (**b**) *Af*AA9_B activity.

2.6. Synergistic Action on Cellulose Hydrolysis

To determine the synergistic effects of *Af*Cel6A and *Af*AA9_B, we performed cellulose degradation experiments by using CMC as substrate. We conducted the reactions at different relative proportions and for different incubation times. Surprisingly, we observed no synergistic effect between *Af*Cel6A and *Af*AA9_B (Figure 7a).

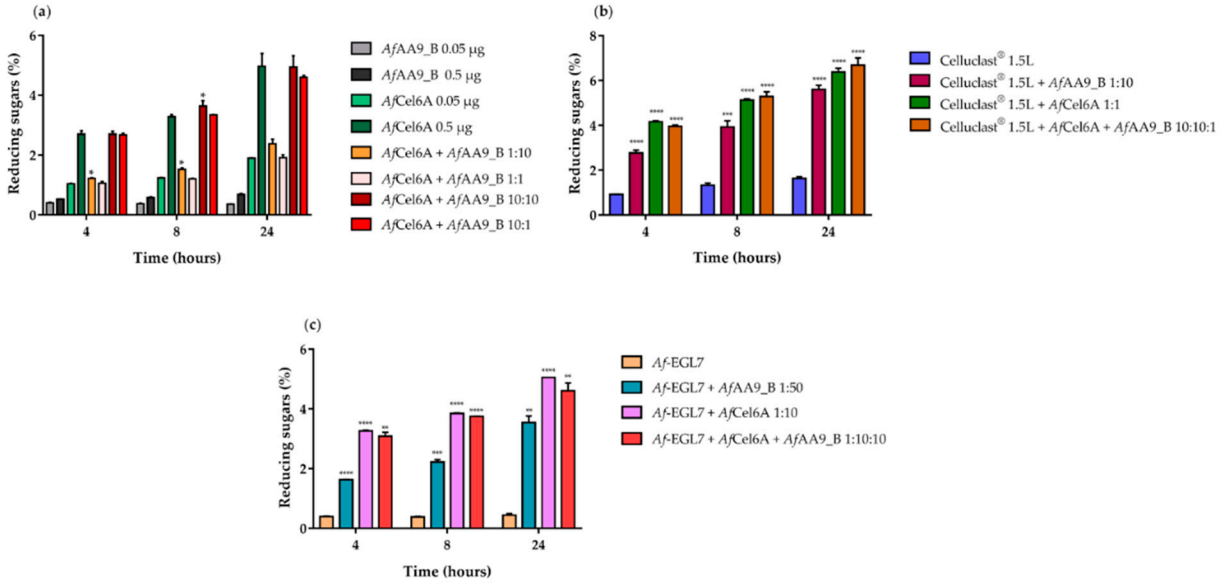

Figure 7. Synergistic action on 1% (*w*/*v*) CM-Cellulose of (**a**) *Af*Cel6A and *Af*AA9_B; (**b**) *Af*Cel6A, or *Af*AA9_B, or both with Celluclast® 1.5 L cocktail; and (**c**) *Af*Cel6A, or *Af*AA9_B, or both with *Af*-EGL7. All reactions were incubated in 50 mM sodium phosphate buffer (pH 6.0) at 1000 rpm and 50 °C for 4, 8, or 24 h. At the end of each reaction, the measured reducing sugars were plotted as a function of the relative proportions among the added enzymes. Asterisks indicate significant difference ($p < 0.05$) in relation to the control system (*Af*Cel6A, *Af*-EGL7, or cocktail alone).

We also investigated the synergistic effects between *Af*Cel6A and *Af*AA9_B and Celluclast® 1.5L at different incubation times. Hydrolysis increased over time, and the yield of reducing sugars peaked after 24 h. Compared to the cocktail alone, *Af*AA9_B or *Af*Cel6A addition to the reaction mixture containing Celluclast® 1.5L increased the release of reducing sugars by approximately 3.5 and 4.0 times, respectively. When Celluclast® 1.5L cocktail was simultaneously associated with *Af*Cel6A and *Af*AA9_B at a ratio of 1:1:10, the maximum release of reducing sugars was 4.5 times higher compared to the cocktail alone. We verified a slight synergistic degree for Celluclast® 1.5L cocktail, *Af*Cel6A, and *Af*AA9_B during CM-Cellulose hydrolysis. No inhibitory effect arose, probably

because *Af*AA9_B acted synergistically with other enzymes in Celluclast® 1.5L cocktail (Figure 7b).

LPMOs improve the efficiency of cellulase; i.e., endoglucanases and cellobiohydrolases, during cellulose hydrolysis, and they enhance cellulase adsorption and accessibility to cellulose [83,84]. We analyzed *Af*AA9_B and *Af*Cel6A synergism with endoglucanase *Af*-EGL7, which had been previously characterized [32]. Compared to *Af*-EGL7 alone, combination of *Af*-EGL7 and *Af*AA9_B released eight-fold more reducing sugars, whilst combination of *Af*-EGL7 and *Af*Cel6A increased hydrolyses by 11.5 times. When the three enzymes were associated at an *Af*-EGL7/*Af*AA9_B/*Af*Cel6A ratio of 1:10:10, 12.5 times more reducing sugars was released (Figure 7c). Thus, *Af*AA9_B acted synergistically with *Af*-EGL7, but not with *Af*Cel6A.

The efficiency of synergy among enzymes depends on the relative amount of crystalline to amorphous cellulose that is accessible within the substrate [85]. To evaluate how these enzymes acted on lignocellulosic biomass, we analyzed the associations of the enzymes in complex biomass, including SEB, rice straw, and corncob. SEB and corncob hydrolysis depended on time, but reducing sugars released from rice straw did not increase when we changed the reaction time from 24 to 48 h. Bernardi et al. (2019) [32] observed the same profile when they accomplished rice straw hydrolysis by a cocktail under similar conditions.

As shown in Figure 8a, compared to Celluclast® 1.5L cocktail alone, *Af*Cel6A or *Af*AA9_B addition increased SEB hydrolysis by ~70% and ~95% after 24 and 48 h, respectively. Similarly, association between commercial cellulases and *Af*Cel6A boosted corncob hydrolysis by ~90% and ~70% after 24 and 48 h, respectively. On the other hand, *Af*AA9_B addition seemed to affect hydrolysis negatively (Figure 8b). The same inhibitory effect of LPMOs has been observed on rice straw, while *Af*Cel6A addition almost did not impact the release of reducing sugars (Figure 8c). The divergent results among the three agricultural residues pointed to the substrate-dependence and substrate specificity of *Af*Cel6A and *Af*AA9_B synergism with cellulases [86].

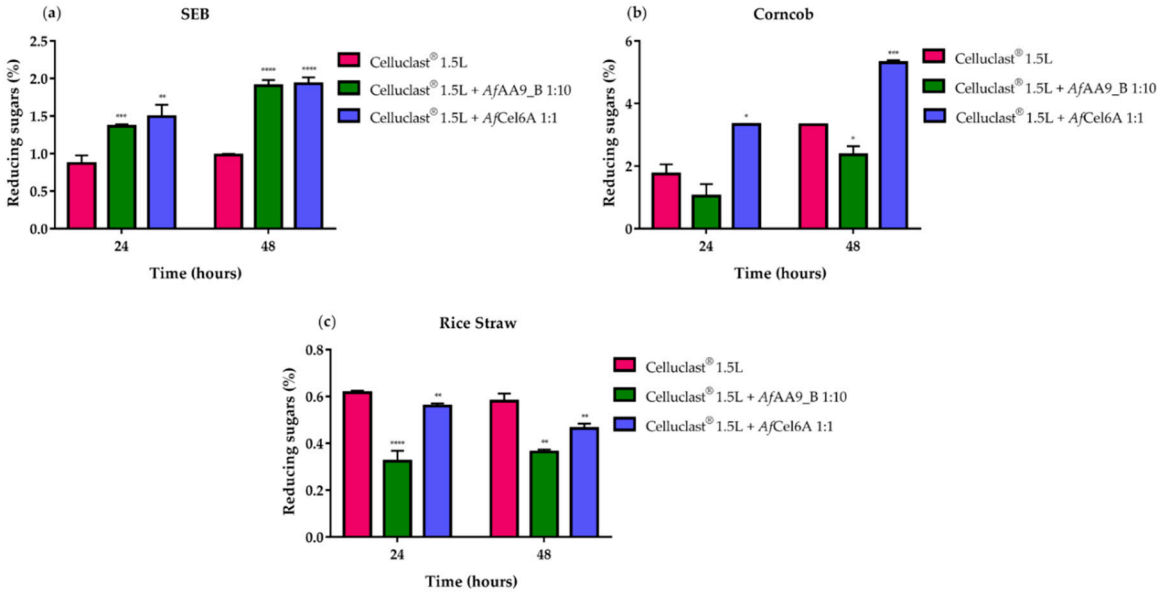

Figure 8. Effect of Celluclast® 1.5L cocktail supplementation with *Af*Cel6A or *Af*AA9_B on hydrolysis of (**a**) SEB, (**b**) corncob, and (**c**) rice straw. All reactions were incubated in 50 mM sodium phosphate buffer (pH 6.0) containing 1% (*w*/*v*) of each biomass at 1000 rpm and 50 °C for 24 and 48 h. At the end of each reaction, the measured reducing sugars was plotted as a function of the relative proportions between the recombinant enzymes and commercial cellulases. Asterisks indicate significant difference ($p < 0.05$) in relation to the cocktail alone.

Compared to *Af*-EGL7 alone, the association between *Af*-EGL7 and *Af*Cel6A increased the amount of reducing sugars released from the three biomasses: ~163%, ~118%, and ~88% for SEB (Figure 9a), corncob (Figure 9b), and rice straw (Figure 9c), respectively, after 48 h. The *Af*-EGL7 *Af*AA9_B combination also improved SEB and corncob hydrolysis, but it did not affect rice straw degradation.

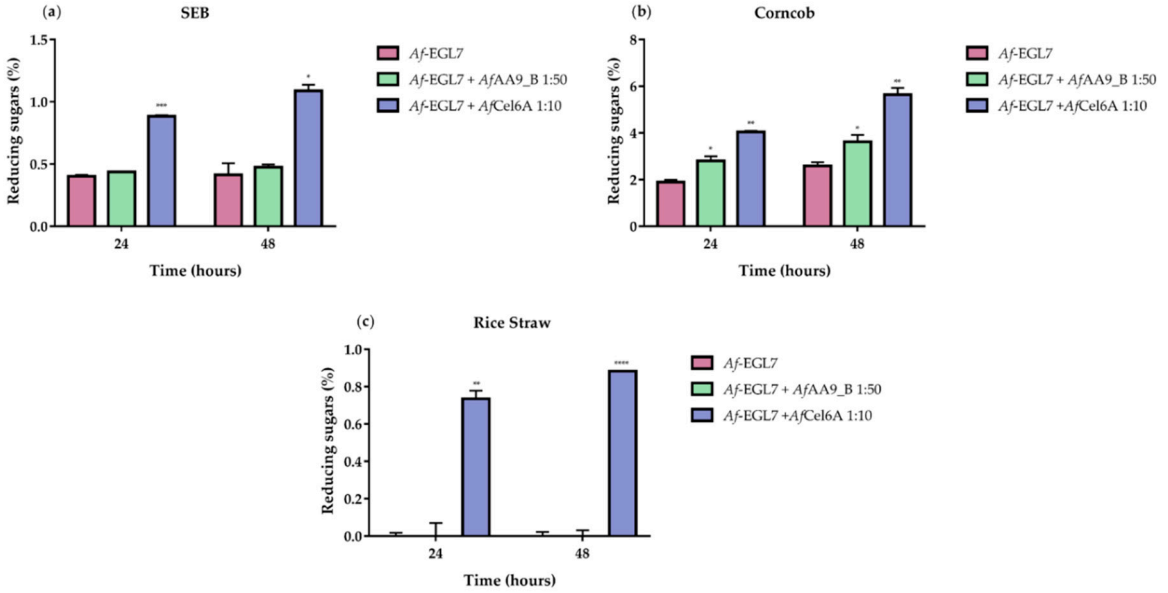

Figure 9. Combined activities of *Af*-EGL7 and *Af*Cel6A or *Af*AA9_B on the hydrolysis of (**a**) SEB; (**b**) corncob; and (**c**) rice straw. All reactions were incubated in 50 mM sodium phosphate buffer (pH 6.0) containing 1% (*w*/*v*) of each biomass for 24 and 48 h at 50 °C and 1000 rpm. At the end of each reaction, the measured reducing sugars were plotted in function of the relative proportions between the recombinant enzymes. Asterisks indicate significant difference ($p < 0.05$) in relation to the *Af*-EGL7 alone.

3. Materials and Methods

3.1. Strains, Culture Conditions, and Vectors

Mycelia of *Aspergillus fumigatus* Af293 (kindly donated by Professor Sérgio Akira Uyemura—University of São Paulo, Ribeirão Preto, Brazil) were obtained for RNA extraction. Fresh conidia (2×10^6 per mL) were inoculated in YNB minimal medium (1× salt solution, 0.1% (*v*/*v*) trace elements, and 0.05% (*w*/*v*) yeast extract) containing 1% (*w*/*v*) fructose and incubated under shaking at 200 rpm and 37 °C for 16 h. The mycelia were harvested, washed, and transferred to YNB medium containing 1% (*w*/*v*) sugarcane exploded bagasse (SEB) at 200 rpm and 37 °C for 24 h.

E. coli DH10β was used to clone and to propagate the recombinant vectors. The strain was kept in Luria–Bertani medium supplemented with the appropriate antibiotic.

Pichia pastoris strain X-33 (Invitrogen, Carlsbad, CA, USA) was used to produce the heterologous proteins. The employed growth conditions are described in the EasySelect™ Pichia Expression Kit manual (Invitrogen, Carlsbad, CA, USA).

The plasmids pPICZB and pPICZαA (Invitrogen, Carlsbad, CA, USA) were used to clone, to sequence, and to express *Af*AA9_B and *Af*Cel6A, respectively.

Xyloglucan from tamarind seed and xylan from beechwood were acquired from Megazyme (Megazyme International, Bray, Co., Wicklow, Ireland). Avicel® PH-101 and low-viscosity CM-Cellulose (CMC) were purchased from Sigma (Sigma–Aldrich, St. Louis, MO, USA).

Biomasses (rice straw and corncob) were provided by Professor Maria de Lourdes Teixeira de Moraes Polizeli (University of São Paulo, Ribeirão Preto, Brazil). Sugarcane

exploded bagasse (SEB) was provided by Professor João Atílio Jorge (University of São Paulo, Ribeirão Preto, Brazil).

3.2. RNA Extraction, cDNA Synthesis, and Gene Amplification

Total RNA from *A. fumigatus* mycelia was isolated by using the Direct-zol™ RNA MiniPrep kit (Zymo Research, Irvine, CA, USA); the manufacturer's instructions were followed. cDNA was synthesized by using SuperScript® II Reverse Transcriptase (Invitrogen, Carlsbad, CA, USA).

Table 5 describes the specific primer sequences obtained for *AfAA9_B* and *AfCel6A* amplification and cloning into the vectors pPICZB and pPICZαA, respectively:

Table 5. Primer sequences used to amplify and to clone genes.

Primer Name	Sequence (5′-3′)
*Af**AA9_B*** Fw	**CAAAAAACAACTAATTATTCGAAACGAGGAATTCC**ATGACTTTGTCCAAGATCAC
*Af**AA9_B*** Rv	**CAGATCCTCTTCTGAGATGAGTTTTTGTTCTAG**AGCGTTGAACAGTGCAGGAC
*Af**Cel6A*** Fw	**GAGAAAAGAGAGGCTGAAGCTGAATTC**CAGCAGACCGTATGG
*Af**Cel6A*** Rv	**ATCCTCTTCTGAGATGAGTTTTTGTTCTAG**AAAGGACGGGTTAGC

Notation: The overlapping regions between the vector and the insert are in bold.

The amplification reactions were performed with Phusion High-Fidelity DNA Polymerase (Thermo Fisher Scientific, Waltham, MS, USA), and the PCR product was analyzed by electrophoresis and purified from 1% (*w*/*v*) agarose gel by using the QIAquick Gel Extraction kit (Qiagen, Hilden, Germany).

3.3. Enzyme Production and Purification

AfAA9_B and *AfCel6A* ORFs (open reading frames) with and without predicted signal peptides, respectively, were cloned into the corresponding vectors pPICZB and pPICZαA (previously digested with the restriction enzymes *Eco*RI and *Xba*I) by the circular polymerase extension cloning (CPEC) method [87]. Both CPEC reactions were carried out with Phusion High-Fidelity DNA Polymerase (Thermo Scientific). The thermocycling conditions were as follows: 98 °C for 30 s; 35 cycles of 98 °C for 10 s, 55 °C for 30 s, and 72 °C for 2 min 30 s; and 72 °C for 10 min. The cloning products were transformed to *E. coli* DH10β, and the resistant transformants were selected with zeocin (50 μg mL^{-1}). Next, the recombinant vectors pPICZB/*AfAA9_B* and pPICZαA/*AfCel6A* were linearized with *Pme*I and transformed into competent *P. pastoris* X-33 cells by electroporation according to the EasySelect™ Pichia Expression Kit manual (Invitrogen).

Zeocin-resistant *P. pastoris* transformants were selected to produce the enzymes. The recombinant yeasts were cultivated in buffered glycerol-complex medium (BMGY) at 240 rpm and 30 °C. For heterologous *Af*AA9_B expression, *P. pastoris* cells were resuspended in buffered methanol-complex medium (BMMY). Methanol (1% (*v*/*v*)) was added to the medium at 24-h intervals for six days, and the supernatant was harvested from the grown culture. The supernatant containing secreted recombinant enzyme (*Af*AA9_B) was concentrated 10 times by using an Amicon Ultra-15 Centrifugal Filter—10-kDa cutoff (Millipore, Burlington, MS, USA). Protein expression was verified by SDS-PAGE.

*Af*Cel6A was expressed as described above, but 1.5% (*v*/*v*) methanol was added.

To purify the enzymes, the concentrates were resuspended in 20 mM sodium phosphate buffer containing 500 mM NaCl (pH 7.4) and loaded onto Ni^{+} Sepharose 6 Fast Flow resin (Ge Healthcare, Little Chalfont, UK). An imidazole gradient from 0 to 500 mM was applied to the columns to elute the recombinants His6-tagged *Af*AA9_B and His6-tagged *Af*Cel6A. The fractions were collected, and the enzymes were analyzed by 10% (*w*/*v*) SDS-PAGE, stained with Comassie Brilliant Blue R-250 (Sigma–Aldrich, St. Louis, MO, USA). Fractions containing the recombinant enzymes were mixed and buffer-exchanged by using an Amicon Ultra-15 Centrifugal Filter—10 kDa cutoff (Millipore) to remove excess imidazole.

To coordinate copper to the *Af* AA9_B active site, the purified recombinant enzyme was incubated with $CuSO_4$ at 1:3 molar ratio and 4 °C for 30 min. Then, the *Af* AA9_B solution was dialyzed against 20 mM sodium phosphate buffer containing 500 mM NaCl (pH 7.4) under shaking at 4 °C for 48 h, to remove traces of non-coordinated Cu^{2+}. The purified *Af* AA9_B concentration was determined by the Greenberg method [88].

The *Af* AA9_B band from the SDS-PAGE gel was manually excised, reduced, alkylated, digested with trypsin, purified (Promega, Madison, WI, EUA—V5111), and analyzed by mass spectrometry according to a previously described method [89].

3.4. Glycosylation

N-glycosylation sites were predicted by employing NetNGlyc 1.0 (http://www.cbs.dtu.dk/services/NetNGlyc/), and O-glycosylation was analyzed by using NetOGlyc 4.0 (http://www.cbs.dtu.dk/services/NetOGlyc/). Deglycosylation of recombinant *Af* AA9_B and *Af* Cel6A was accomplished by using Endoglycosidase H (Endo H, New England Biolabs, Ipswich, MA, USA) in non-denaturing conditions, as per the manufacturer's procedure. The resulting enzymes were further analyzed by SDS-PAGE.

3.5. Structural Analysis by Circular Dichroism (CD)

Circular dichroism (CD) spectra of the enzymes were obtained between 190 and 250 nm (far-UV) on a JASCO-810 spectropolarimeter; quartz cuvettes with optical path of 0.1 cm were employed. *Af* AA9_B (0.021 mg mL^{-1}) and *Af* Cel6A (0.0026 mg mL^{-1}) were diluted in 20 mM sodium phosphate (pH 7.4), and the readings were performed in quadruplicate at scanning speed, band width, and D.I.T. of 50 nm min^{-1}, 3 nm, and 1 s, respectively. All the spectra were corrected for the buffer contributions and converted from millidegrees (mdeg) to $\Delta\varepsilon$ in M^{-1} cm^{-1} according to the following equation: $\Delta\varepsilon = \theta\ [(0.1 \cdot MRW)/(d \cdot c \cdot 3298)]$, where θ is the ellipticity value originally given by equipment (millidegrees), MRW is the enzyme mean residual weight, d is the optical path (cm), and c is the enzyme concentration (mg mL^{-1}). All the secondary structures of the enzymes were predicted by using the BeStSel web server [53], and the results were compared with structures modeled on the Phyre2 [55] and Discovery Studio [90] web servers.

3.6. LPMO Activity Assay

Purified *Af* AA9_B activity was analyzed as reported by Breslmayr et al. (2018) [80]. The assay consisted of a reaction mixture containing 1 mM 2,6-dimethoxyphenol (2,6-DMP) (Sigma–Aldrich, St. Louis, MO, USA), 100 µM H_2O_2, and recombinant purified *Af* AA9_B in 50 mM sodium phosphate buffer (pH 8.0). For the blank, the enzyme was denatured by incubation at 99 °C for 30 min before the reaction mixture was added. After 5 min at 30 °C, absorbance was read at 469 nm to calculate the LPMO peroxidase activity.

3.7. AfCel6A Activity Assay

Af Cel6A activity was determined by measuring reducing sugars from the reaction by the 3,5-dinitrosalicylic acid (DNS) method [91]. Briefly, the reaction mixture consisting of 1% CM-Cellulose (*w/v*) in 50 mM sodium phosphate buffer (pH 6.0) was incubated at 55 °C for 30–45 min. The enzymatic action was stopped by adding an equal volume of the DNS reagent. The mixture was boiled for 5 min and cooled, and absorbance was measured at 540 nm. One unit of *Af* Cel6A was defined as the amount of enzyme that released 1 µmol of reducing sugar from the substrate per minute. Each assay was carried out in triplicate. Enzyme concentration was determined by the Greenberg method [88].

3.8. Enzymatic Properties of AfAA9_B and AfCel6A

The optimal pH for *Af* AA9_B activity was measured at pH ranging from 4.0 to 8.0 in McIlvaine buffer (citric acid-Na_2HPO_4) and at pH 9.0 and 10.0 in 100 mM Glycine-NaOH buffer at 30 °C. The relative activity was calculated with respect to the maximum activity of 100%; the aforementioned method was followed. The pH stability was estimated

by measuring the residual enzymatic activity after the enzyme was incubated without substrate in the aforementioned buffers at pH ranging from 3.0 to 10.0 and 4 °C for up to 72 h. To determine the *Af*AA9_B thermal stability, the enzyme was preincubated without substrate at 50 and 60 °C for up to 72 h. To measure the residual activity, the enzymatic activity without preincubation was considered 100%.

The optimal pH for *Af*Cel6A activity was measured from 3.0 to 8.0 in McIlvaine buffer (citric acid-Na_2HPO_4) at 55 °C. The optimal temperature was examined between 40 and 80 °C. The relative activity was calculated with respect to the maximum exhibited activity of 100%; the aforementioned method was followed.

The *Af*Cel6A pH stability was estimated by measuring the residual enzymatic activity under standard conditions after the enzyme was incubated without substrate in McIlvaine (citrate–phosphate) buffers pH 3.0–8.0 and in 100 mM Glycine-NaOH buffers pH 9.0 and 10.0 at 4 °C for up to 72 h. To determine the *Af*Cel6A thermal stability, the enzyme was preincubated without substrate at temperatures ranging from 50 to 90 °C for different times. To measure the residual activity, the enzymatic activity without preincubation was considered 100%.

3.9. Effect of Additives

How various metal ions affected *Af*AA9_B and *Af*Cel6A was determined by adding Mn^{2+}, Co^{2+}, Ca^{2+}, Fe^{2+}, Zn^{2+}, Mg^{2+}, Cu^{2+}, NH_4^+, K^+, or Ag^+ at a final concentration of 5 mM to the reaction mixture. The effects of EDTA, SDS, Tween 20, Triton X-100, SLS, β-mercaptoethanol, DTT, and DMSO were also tested. For *Af*Cel6A, the effect of ascorbic acid addition was also evaluated. Control reactions (100% activity) were performed without any additive. The relative activity was estimated as compared to the controls.

3.10. Glucose and Cellobiose Effects on AfCel6A and AfAA9_B Activity

The glucose (10–250 mM) and cellobiose (up to 100 mM) effects on the activity of *Af*AA9_B and *Af*Cel6A were determined in the presence of increasing concentrations of both sugars by using the chromogenic substrates 2,6-DMP and 4-nitrophenyl β-D-cellobioside (Sigma–Aldrich, St. Louis, MO, USA), respectively.

3.11. Kinetic Assays

The *Af*AA9_B kinetic parameters (K_M, V_{max}, and k_{cat}) were determined for the substrate 2,6-DMP (0.1 to 10 mM) and the co-substrate H_2O_2 (1 to 500 μM). The reactions were performed in 50 mM sodium phosphate buffer (pH 6.0) and 100 mM glycine-NaOH buffer (pH 9.0) at 50 °C. The parameters were calculated by Michaelis–Menten nonlinear regression.

The *Af*Cel6A kinetic parameters were determined when CM-Cellulose (0.5–30 mg mL^{-1}) was used as substrate. The reactions were performed in 50 mM sodium phosphate buffer (pH 6.0) as previously described. The parameters were calculated by the Michaelis-Menten nonlinear regression graphical method.

3.12. Combined Assays

*Af*AA9_B and *Af*Cel6A enzymatic assays were carried out concomitantly with the recombinant endoglucanase *Af*-EGL7 as previously described [32]. The assays were performed by adding 1 μg of *Af*-EGL7 to 50 μg of *Af*AA9_B (1:50) or 10 μg of *Af*Cel6A (1:10) per gram of substrate. The reaction mixtures consisted of CM-Cellulose (1% (*w*/*v*)) in 50 mM sodium phosphate buffer (pH 6.0) containing 1 mM ascorbic acid in a final volume of 1 mL. The reactions were performed in a thermomixer (Eppendorf) at 50 °C and 1000 rpm for 4, 8, or 24 h.

In the same way, *Af*AA9_B and *Af*Cel6A were combined at different concentration proportions (10:1, 1:1, 10:10, or 1:10), where the minimum and maximum enzyme loading corresponded to 5 and 50 μg of added enzyme per gram of CM-Cellulose, respectively.

Finally, the effect of the simultaneous association of the three recombinant enzymes on the degradation of CM-Cellulose was evaluated. While the *Af*-EGL7 concentration was

1 μg g^{-1}, the concentrations of both *Af*AA9_B and *Af*Cel6A were 10 μg per gram of CM-Cellulose, generating the ratio 1:10:10. The reactions were carried out as described above.

The degradation efficiencies were assessed by estimating the released reducing sugars by the DNS method. The reported results represent the mean ± SD calculated from at least three experimental replicates.

3.13. Synergistic Activity with Celluclast® 1.5L

*Af*AA9_B and *Af*Cel6A synergistic activity of during enzymatic hydrolysis was investigated in combination with Celluclast® 1.5L, a commercial cellulase cocktail from *Trichoderma reesei*.

To this end, 0.05 FPU of Celluclast® 1.5L cocktail was associated with 50 μg of *Af*AA9_B (ratio 1:10) or 5 μg of *Af*Cel6A (ratio 1:1) per gram of CM-Cellulose (1% (*w*/*v*) in 50 mM sodium phosphate buffer (pH 6.0) containing 1 mM ascorbic acid. The reactions were conducted at 1000 rpm and 50 °C for up to 24 h in a final volume of 1 mL.

The effect of the simultaneous association between commercial cellulases and the two recombinant enzymes from *A. fumigatus* on the degradation of CM-Cellulose was also evaluated. While the Celluclast® 1.5 L cocktail loading was fixed at 0.05 FPU g^{-1}, the *Af*Cel6A and *Af*AA9_B concentrations were 5 and 0.5 μg of enzyme added per gram of CM-Cellulose, respectively. The reactions were carried out as described above.

The percent hydrolysis yields were determined by estimating the released reducing sugars by the DNS method [91]. The reported results represent the mean ± SD calculated from at least three experimental replicates.

3.14. Lignocellulosic Biomass Saccharification

Enzymatic hydrolyses of some agro-industrial residues were carried out as described by Bernardi et al. (2019) with some modifications [32]. Saccharification was accomplished in 50 mM sodium phosphate buffer (pH 6.0) containing 1% (*w*/*v*) of one of the following biomasses: SEB (sugarcane exploded bagasse), rice straw, or corncob.

Different associations between the enzymes were used during biomass saccharifications. *Af*-EGL7 (18 μg g^{-1}) was combined with *Af*AA9_B (900 μg g^{-1}) or *Af*Cel6A (180 μg g^{-1}). Similarly, a fixed concentration of Celluclast 1.5L cocktail (0.9 FPU g^{-1}) was associated with *Af*AA9_B (900 μg g^{-1}) or *Af*Cel6A (90 μg g^{-1}). The reactions were conducted at 1000 rpm and 50 °C for up to 48 h in a final volume of 1 mL. DNS was added to stop the reactions and to measure the released reducing sugars. The reported results represent the mean ± SD calculated from at least three experimental replicates.

3.15. Reproducibility of the Results

All the data are the mean of at least three independent experiments and show consistent results.

4. Conclusions

Novel cellobiohydrolase and LPMO from *Aspergillus fumigatus* were characterized after they were expressed in *P. pastoris*. Supplementation of a cellulase cocktail with both enzymes improved the yield of saccharification of different biomasses, especially SEB. However, *Af*AA9_B did not have a positive effect on *Af*Cel6A activity. On the other hand, *Af*AA9_B acted synergistically with endoglucanase *Af*-EGL7. These different synergistic effects are important to understand the action of LPMOs with cellulases and would help to design new commercial enzymatic cocktails. Considering the reduction of costs in lignocellulose conversion, we can conclude that supplementation of Celluclast® 1.5L with *Af*Cel6A or *Af*AA9_B suffices to increase the hydrolytic activity, so the composition of cellulase cocktails may need to be reconsidered.

Supplementary Materials: Supplementary Materials can be found at https://www.mdpi.com/1422-0067/22/1/276/s1, Table S1: Secondary structure proportions of AfAA9_B and AfCel6A from

literature and different prediction methods in comparison with the one determined by BeStSel based on the CD spectra.

Author Contributions: Conceptualization: A.V.B., L.E.G. and T.M.D.; data curation: A.V.B., L.E.G., P.F.d.G., L.M.S.P. and D.K.Y.; formal analysis: A.V.B., L.E.G., P.F.d.G., L.M.S.P. and D.K.Y.; methodology: A.V.B., L.E.G., P.F.d.G., L.M.S.P. and D.K.Y.; supervision: A.H.C.d.O., S.A.U. and T.M.D.; writing (original draft): A.V.B. and T.M.D.; writing (review and editing): A.V.B., A.H.C.d.O., S.A.U. and T.M.D.; project administration: T.M.D.; funding acquisition: T.M.D. All authors have read and agreed to the published version of the manuscript.

Funding: This research was funded by Fundação de Amparo à Pesquisa do Estado de São Paulo (FAPESP, 2016/190950-0) and Conselho Nacional de Desenvolvimento Científico e Tecnológico (CNPq: 425465/2016-0). AVB was funded by a scholarship granted by Coordenação de Aperfeiçoamento de Pessoal de Nível Superior—Brasil (CAPES), Finance Code 001. DKY was funded by a scholarship granted by Fundação de Amparo à Pesquisa do Estado de São Paulo (FAPESP, 2018/11231-7).

Institutional Review Board Statement: Not applicable.

Informed Consent Statement: Not applicable.

Data Availability Statement: Data sharing is not applicable to this article.

Conflicts of Interest: The authors declare no conflict of interest. The funders had no role in the study design; data collection, analyses, or interpretation; writing of the manuscript; or the decision to publish the results.

Abbreviations

2G ethanol	Second-generation ethanol
LPMO	Lytic Polysaccharide Monooxygenase
AA	Auxiliary Activity
GH	Glycoside Hydrolase
CD	Circular Dichroism
CBM	Carbohydrate Binding Module
CMC-Na	Sodium Carboxymethyl Cellulose
2,6-DMP	2,6-Dimethoxyphenol
PASC	Phosphoric-acid Swollen Cellulose
pNPC	4(*p*)-nitrophenyl β-D-cellobioside
SEB	Sugarcane Exploded Bagasse
DNS	3,5-Dinitrosalicylic acid
FPU	Filter Paper Unit

References

1. El-Tayeb, T.S.; Abdelhafez, A.A.; Ali, S.H.; Ramadan, E.M. Effect of acid hydrolysis and fungal biotreatment on agro-industrial wastes for obtainment of free sugars for bioethanol production. *Braz. J. Microbiol.* **2012**, *43*, 1523–1535. [PubMed]
2. Anwar, M.; Lou, S.; Chen, L.; Li, H.; Hu, Z. Recent advancement and strategy on bio-hydrogen production from photosynthetic microalgae. *Bioresour. Technol.* **2019**, *292*, 121972. [PubMed]
3. Ren, H.Y.; Kong, F.; Zhao, L.; Ren, N.Q.; Ma, J.; Nan, J.; Liu, B.F. Enhanced co-production of biohydrogen and algal lipids from agricultural biomass residues in long-term operation. *Bioresour. Technol.* **2019**, *289*, 121774.
4. Boboescu, I.-Z.; Damay, J.; Chang, J.K.W.; Beigbeder, J.-B.; Duret, X.; Beauchemin, S.; Lalonde, O.; Lavoie, J.-M. Ethanol production from residual lignocellulosic fibers generated through the steam treatment of whole sorghum biomass. *Bioresour. Technol.* **2019**, *292*, 121975. [PubMed]
5. Dhakate, S.R.; Pathak, A.K.; Jain, P.; Singh, M.; Singh, B.P.; Subhedar, K.M.; Sharda, S.S.; Seth, R.K. Rice straw biomass to high energy yield biocoal by torrefaction: Indian perspective. *Curr. Sci.* **2019**, *116*, 831–838.
6. Hill, J.; Polasky, S.; Nelson, E.; Tilman, D.; Huo, H.; Ludwig, L.; Neumann, J.; Zheng, H.; Bonta, D. Climate change and health costs of air emissions from biofuels and gasoline. *Proc. Natl. Acad. Sci. USA* **2009**, *106*, 2077–2082. [PubMed]
7. Mudinoor, A.R.; Goodwin, P.M.; Rao, R.U.; Karuna, N.; Hitomi, A.; Nill, J.; Jeoh, T. Interfacial molecular interactions of cellobiohydrolase Cel7A and its variants on cellulose. *Biotechnol. Biofuels* **2020**, *13*, 1–16.
8. Kucharska, K.; Rybarczyk, P.; Hołowacz, I.; Łukajtis, R.; Glinka, M.; Kamiński, M. Pretreatment of lignocellulosic materials as substrates for fermentation processes. *Molecules* **2018**, *23*, 2937.
9. Ravindran, R.; Jaiswal, A.K. A comprehensive review on pre-treatment strategy for lignocellulosic food industry waste: Challenges and opportunities. *Bioresour. Technol.* **2016**, *199*, 92–102.

10. Nishiyama, Y. Structure and properties of the cellulose microfibril. *J. Wood Sci.* **2009**, *55*, 241–249.
11. Payne, C.M.; Knott, B.C.; Mayes, H.B.; Hansson, H.; Himmel, M.E.; Sandgren, M.; Ståhlberg, J.; Beckham, G.T. Fungal cellulases. *Chem. Rev.* **2015**, *115*, 1308–1448. [PubMed]
12. Medie, F.M.; Davies, G.J.; Drancourt, M.; Henrissat, B. Genome analyses highlight the different biological roles of cellulases. *Nat. Rev. Microbiol.* **2012**, *10*, 227–234.
13. Blumer-Schuette, S.E.; Kataeva, I.; Westpheling, J.; Adams, M.W.; Kelly, R.M. Extremely thermophilic microorganisms for biomass conversion: Status and prospects. *Curr. Opin. Biotechnol.* **2008**, *19*, 210–217. [PubMed]
14. Hu, J.; Chandra, R.; Arantes, V.; Gourlay, K.; van Dyk, J.S.; Saddler, J.N. The addition of accessory enzymes enhances the hydrolytic performance of cellulase enzymes at high solid loadings. *Bioresour. Technol.* **2015**, *186*, 149–153. [PubMed]
15. Hu, J.; Arantes, V.; Pribowo, A.; Saddler, J.N. The synergistic action of accessory enzymes enhances the hydrolytic potential of a "cellulase mixture" but is highly substrate specific. *Biotechnol. Biofuels* **2013**, *6*, 112. [PubMed]
16. Müller, G.; Várnai, A.; Johansen, K.S.; Eijsink, V.G.H.; Horn, S.J. Harnessing the potential of LPMO-containing cellulase cocktails poses new demands on processing conditions. *Biotechnol. Biofuels* **2015**, *8*, 1–9.
17. Garcia-Santamarina, S.; Probst, C.; Festa, R.A.; Ding, C.; Smith, A.D.; Conklin, S.E.; Brander, S.; Kinch, L.N.; Grishin, N.V.; Franz, K.J.; et al. A lytic polysaccharide monooxygenase-like protein functions in fungal copper import and meningitis. *Nat. Chem. Biol.* **2020**, *16*, 337–344.
18. Vaaje-Kolstad, G.; Horn, S.J.; Van Aalten, D.M.F.; Synstad, B.; Eijsink, V.G.H. The non-catalytic chitin-binding protein CBP21 from *Serratia marcescens* is essential for chitin degradation. *J. Biol. Chem.* **2005**, *280*, 28492–28497.
19. Merino, S.T.; Cherry, J. Progress and challenges in enzyme development for biomass utilization. *Adv. Biochem. Eng. Biotechnol.* **2007**, *108*, 95–120.
20. Vaaje-kolstad, G.; Westereng, B.; Horn, S.J.; Liu, Z.; Zhai, H.; Sørlie, M.; Eijsink, V.G.H. An oxidative enzyme boosting the enzymatic conversion of recalcitrant polysaccharides. *Science* **2010**, *330*, 219–222.
21. Frandsen, K.E.H.; Tovborg, M.; Jørgensen, C.I.; Spodsberg, N.; Rosso, M.N.; Hemsworth, G.R.; Garman, E.F.; Grime, G.W.; Poulsen, J.C.N.; Batth, T.S.; et al. Insights into an unusual Auxiliary Activity 9 family member lacking the histidine brace motif of lytic polysaccharide monooxygenases. *J. Biol. Chem.* **2019**, *294*, 17117–17130. [CrossRef] [PubMed]
22. Bertini, L.; Breglia, R.; Lambrughi, M.; Fantucci, P.; De Gioia, L.; Borsari, M.; Sola, M.; Bortolotti, C.A.; Bruschi, M. Catalytic Mechanism of Fungal Lytic Polysaccharide Monooxygenases Investigated by First-Principles Calculations. *Inorg. Chem.* **2018**, *57*, 86–97. [CrossRef]
23. Dimarogona, M.; Topakas, E.; Christakopoulos, P. Cellulose degradation by oxidative enzymes. *Comput. Struct. Biotechnol. J.* **2012**, *2*, e201209015. [CrossRef] [PubMed]
24. Vaaje-Kolstad, G.; Forsberg, Z.; Loose, J.S.; Bissaro, B.; Eijsink, V.G. Structural diversity of lytic polysaccharide monooxygenases. *Curr. Opin. Struct. Biol.* **2017**, *44*, 67–76. [CrossRef] [PubMed]
25. Hemsworth, G.R.; Henrissat, B.; Davies, G.J.; Walton, P.H. Discovery and characterization of a new family of lytic polysaccharide monooxygenases. *Nat. Chem. Biol.* **2014**, *10*, 122–126. [CrossRef] [PubMed]
26. Quinlan, R.J.; Sweeney, M.D.; Leggio, L.L.; Otten, H.; Poulsen, J.-C.N.; Johansen, K.S.; Krogh, K.B.R.M.; Jorgensen, C.I.; Tovborg, M.; Anthonsen, A.; et al. Insights into the oxidative degradation of cellulose by a copper metalloenzyme that exploits biomass components. *Proc. Natl. Acad. Sci. USA* **2011**, *108*, 15079–15084. [CrossRef]
27. Eijsink, V.G.H.; Petrovic, D.; Forsberg, Z.; Mekasha, S.; Røhr, Å.K.; Várnai, A.; Bissaro, B.; Vaaje-Kolstad, G. On the functional characterization of lytic polysaccharide monooxygenases (LPMOs). *Biotechnol. Biofuels* **2019**, *12*, 58. [CrossRef]
28. Bissaro, B.; Røhr, Å.K.; Müller, G.; Chylenski, P.; Skaugen, M.; Forsberg, Z.; Horn, S.J.; Vaaje-Kolstad, G.; Eijsink, V.G.H. Oxidative cleavage of polysaccharides by monocopper enzymes depends on H_2O_2. *Nat. Chem. Biol.* **2017**, *13*, 1123–1128. [CrossRef]
29. Walton, P.H.; Davies, G.J. On the catalytic mechanisms of lytic polysaccharide monooxygenases. *Curr. Opin. Chem. Biol.* **2016**, *31*, 195–207. [CrossRef]
30. Danneels, B.; Tanghe, M.; Desmet, T. Structural Features on the Substrate-Binding Surface of Fungal Lytic Polysaccharide Monooxygenases Determine Their Oxidative Regioselectivity. *Biotechnol. J.* **2019**, *14*, e1800211. [CrossRef]
31. Eibinger, M.; Ganner, T.; Bubner, P.; Rošker, S.; Kracher, D.; Haltrich, D.; Ludwig, R.; Plank, H.; Nidetzky, B. Cellulose surface degradation by a lytic polysaccharide monooxygenase and its effect on cellulase hydrolytic efficiency. *J. Biol. Chem.* **2014**, *289*, 35929–35938. [CrossRef] [PubMed]
32. Bernardi, A.V.; Yonamine, D.K.; Uyemura, S.A.; Dinamarco, T.M. A Thermostable *Aspergillus fumigatus* GH7 Endoglucanase Over-Expressed in *Pichia pastoris* Stimulates Lignocellulosic Biomass Hydrolysis. *Int. J. Mol. Sci.* **2019**, *20*, 2261. [CrossRef]
33. Paul, S.; Zhang, A.; Ludeña, Y.; Villena, G.K.; Yu, F.; Sherman, D.H.; Gutiérrez-Correa, M. Insights from the genome of a high alkaline cellulase producing *Aspergillus fumigatus* strain obtained from Peruvian Amazon rainforest. *J. Biotechnol.* **2017**, *251*, 53–58. [CrossRef] [PubMed]
34. Liu, D.; Zhang, R.; Yang, X.; Wu, H.; Xu, D.; Tang, Z.; Shen, Q. Thermostable cellulase production of *Aspergillus fumigatus* Z5 under solid-state fermentation and its application in degradation of agricultural wastes. *Int. Biodeterior. Biodegrad.* **2011**, *65*, 717–725. [CrossRef]
35. Christensen, S.J.; Bertel, K.; Mørkeberg, R.; Spodsberg, N.; Borch, K.; Westh, P. A biochemical comparison of fungal GH6 cellobiohydrolases. *Biochem. J.* **2019**, *6*, 2157–2172. [CrossRef] [PubMed]

36. Bernardi, A.V.; De Gouvêa, P.F.; Gerolamo, L.E.; Yonamine, D.K.; De Lourdes, L.; Balico, D.L.; Uyemura, S.A. Functional characterization of GH7 endo-1,4-β-glucanase from *Aspergillus fumigatus* and its potential industrial application. *Protein Expr. Purif.* **2018**, *150*, 1–11. [CrossRef] [PubMed]
37. Adsul, M.G.; Gokhale, D.V. The conundrum of making biomass-to-biofuels economic. *Biofuels* **2012**, *3*, 383–386. [CrossRef]
38. Jin, M.; Sousa, L.D.C.; Schwartz, C.; He, Y.; Sarks, C.; Gunawan, C.; Balan, V.; Dale, B.E. Toward lower cost cellulosic biofuel production using ammonia based pretreatment technologies. *Green Chem.* **2016**, *18*, 957–966. [CrossRef]
39. Chandel, A.K.; Chandrasekhar, G.; Silva, M.B.; Silva, S.D.S. The realm of cellulases in biorefinery development. *Crit. Rev. Biotechnol.* **2012**, *32*, 187–202. [CrossRef]
40. Puri, D.J.; Heaven, S.; Banks, C.J. Improving the performance of enzymes in hydrolysis of high solids paper pulp derived from MSW. *Biotechnol. Biofuels* **2013**, *6*, 107. [CrossRef]
41. Adsul, M.; Sandhu, S.K.; Singhania, R.R.; Gupta, R.; Puri, S.K. Enzyme and Microbial Technology Designing a cellulolytic enzyme cocktail for the e ffi cient and economical conversion of lignocellulosic biomass to biofuels. *Enzyme Microb. Technol.* **2020**, *133*, 109442. [CrossRef] [PubMed]
42. Brooks, D.; Tchelet, R. Next Generation Enzymes. *Biofuels Int.* **2014**, *12*, 49–50.
43. De Gouvêa, P.F.; Gerolamo, L.E.; Bernardi, A.V.; Matheus, L.; Pereira, S.; Uyemura, S.A.; Dinamarco, T.M. Lytic Polysaccharide Monooxygenase from *Aspergillus fumigatus* can Improve Enzymatic Cocktail Activity During Sugarcane Bagasse Hydrolysis. *Protein Pept. Lett.* **2019**, *126*, 377–385. [CrossRef] [PubMed]
44. Rubio, M.V.; Zubieta, M.P.; Cairo, J.P.L.F.; Calzado, F.; Leme, A.F.P.; Squina, F.M.; Prade, R.A.; Damásio, A.R.D.L. Mapping N-linked glycosylation of carbohydrate-active enzymes in the secretome of *Aspergillus nidulans* grown on lignocellulose. *Biotechnol. Biofuels* **2016**, *9*, 1–19. [CrossRef]
45. Bissaro, B.; Kommedal, E.; Røhr, Å.K.; Eijsink, V.G.H. Controlled depolymerization of cellulose by light-driven lytic polysaccharide oxygenases. *Nat. Commun.* **2020**, *11*, 1–12. [CrossRef]
46. Chylenski, P.; Petrović, D.M.; Müller, G.; Dahlström, M.; Bengtsson, O.; Lersch, M.; Siika-Aho, M.; Horn, S.J.; Eijsink, V.G.H. Enzymatic degradation of sulfite-pulped softwoods and the role of LPMOs. *Biotechnol. Biofuels* **2017**, *10*, 1–13. [CrossRef]
47. Courtade, G.; Wimmer, R.; Røhr, Å.K.; Preims, M.; Felice, A.K.G.; Dimarogona, M.; Vaaje-Kolstad, G.; Sørlie, M.; Sandgren, M.; Ludwig, R.; et al. Interactions of a fungal lytic polysaccharide monooxygenase with β-glucan substrates and cellobiose dehydrogenase. *Proc. Natl. Acad. Sci. USA* **2016**, *113*, 5922–5927. [CrossRef]
48. Dodda, S.R.; Sarkar, N.; Aikat, K.; Krishnaraj, N.R.; Bhattacharjee, S.; Bagchi, A.; Mukhopadhyay, S. Insights from the Molecular Dynamics Simulation of Cellobiohydrolase Cel6A Molecular Structural Model from *Aspergillus fumigatus* NITDGPKA3. *Comb. Chem. High Throughput Screen.* **2016**, *19*, 325–333. [CrossRef]
49. Thompson, A.J.; Heu, T.; Shaghasi, T.; Jones, A.; Friis, E.P.; Wilson, K.S.; Davies, G.J. research papers Structure of the catalytic core module of the *Chaetomium thermophilum* family GH6 cellobiohydrolase Cel6A. *Acta Crystallogr. Sect. D Biol. Crystallogr.* **2012**, *68*, 875–882. [CrossRef]
50. Mertz, B.; Kuczenski, R.S.; Larsen, R.T.; Hill, A.D.; Reilly, P.J. Phylogenetic Analysis of Family 6 Glycoside Hydrolases. *Biopolymers* **2005**, *79*, 197–206. [CrossRef]
51. Sonnhammer, E.L.L.; Eddy, S.R.; Durbin, R. Pfam: A comprehensive database of protein domain families based on seed alignments. *Proteins Struct. Funct. Genet.* **1997**, *28*, 405–420. [CrossRef]
52. Kelly, S.M.; Jess, T.J.; Price, N.C. How to study proteins by circular dichroism. *Biochim. Biophys. Acta (BBA) Proteins Proteom.* **2005**, *1751*, 119–139. [CrossRef] [PubMed]
53. Micsonai, A.; Wien, F.; Bulyáki, É.; Kun, J.; Moussong, É.; Lee, Y.-H.; Goto, Y.; Réfrégiers, M.; Kardos, J. BeStSel: A web server for accurate protein secondary structure prediction and fold recognition from the circular dichroism spectra. *Nucleic Acids Res.* **2018**, *46*, W315–W322. [CrossRef] [PubMed]
54. Lo Leggio, L.; Weihe, C.D.; Poulsen, J.C.N.; Sweeney, M.; Rasmussen, F.; Lin, J.; De Maria, L.; Wogulis, M. Structure of a lytic polysaccharide monooxygenase from *Aspergillus fumigatus* and an engineered thermostable variant. *Carbohydr. Res.* **2018**, *469*, 55–59. [CrossRef] [PubMed]
55. Kelley, L.A.; Mezulis, S.; Yates, C.M.; Wass, M.N.; Sternberg, M.J.E. The Phyre2 web portal for protein modeling, prediction and analysis. *Nat. Protoc.* **2015**, *10*, 845–858. [CrossRef] [PubMed]
56. Wallace, B.A.; Janes, R.W. *Modern Techniques for Circular Dichroism and Synchrotron Radiation Circular Dichroism Spectroscopy*; IOS Press: Amsterdam, NY, USA, 2009; Volume 1, ISBN 9781607500001.
57. Kabsch, W.; Sander, C. Dictionary of protein secondary structure: Pattern recognition of hydrogen-bonded and geometrical features. *Biopolymers* **1983**, *22*, 2577–2637. [CrossRef] [PubMed]
58. Teugjas, H.; Väljamäe, P. Product inhibition of cellulases studied with 14C-labeled cellulose substrates. *Biotechnol. Biofuels* **2013**, *6*, 1–14. [CrossRef]
59. Fuelbiol, F.; Bai, R.; Yang, H.; Wang, F.; He, J.; Wang, C.; Tu, M. Enzyme and Microbial Technology Heterologous expression of codon optimized *Trichoderma reesei* Cel6A in *Pichia pastoris*. *Enzyme Microb. Technol.* **2016**, *92*, 107–116.
60. Boonvitthya, N.; Bozonnet, S. Comparison of the Heterologous Expression of *Trichoderma reesei* Endoglucanase II and Cellobiohydrolase II in the Yeasts *Pichia pastoris* and *Yarrowia lipolytica*. *Mol. Biotechnol.* **2013**, *54*, 158–169. [CrossRef]

61. Okada, H.; Sekiya, T.; Yokoyama, K.; Tohda, H.; Kumagai, H.; Morikawa, Y. Efficient secretion of *Trichoderma reesei* cellobiohydrolase II in *Schizosaccharomyces pombe* and characterization of its products. *Appl. Microbiol. Biotechnol.* **1998**, *49*, 301–308. [CrossRef]
62. Takahashi, M.; Takahashi, H.; Nakano, Y.; Konishi, T.; Terauchi, R.; Takeda, T. Characterization of a Cellobiohydrolase (MoCel6A) Produced by *Magnaporthe oryzae*. *Appl. Environ. Microbiol.* **2010**, *76*, 6583–6590. [CrossRef] [PubMed]
63. Riyadh, S.K.; Vipin, I.A.I.K.; Kalia, C.; Lee, J. Characterization of Cellobiohydrolases from *Schizophyllum commune* KMJ820. *Indian J. Microbiol.* **2020**, *60*, 160–166.
64. Limam, F.; Chaabouni, S.E.; Ghrir, R.; Marzouki, N. Two cellobiohydrolases of *Penicillium occitanis* mutant Pol 6: Purification and properties. *Enzym. Microb. Technol.* **1995**, *0229*, 340–346. [CrossRef]
65. Tuohy, M.G.; Walsh, D.J.; Murray, P.G.; Claeyssens, M.; Cuffe, M.M.; Savage, A.V.; Coughlan, M.P. Kinetic parameters and mode of action of the cellobiohydrolases produced by *Talaromyces emersonii*. *Biochim. Biophys. Acta (BBA) Protein Struct. Mol. Enzym.* **2002**, *1596*, 366–380. [CrossRef]
66. Song, J.; Liu, B.; Liu, Z. Cloning of two cellobiohydrolase genes from *Trichoderma viride* and heterogenous expression in yeast *Saccharomyces cerevisiae*. *Mol. Biol. Rep.* **2010**, *37*, 2135–2140. [CrossRef]
67. Wang, H.; Chen, Y.; Huang, C.; Hseu, R. Cloning and characterization of a thermostable and pH-stable cellobiohydrolase from *Neocallimastix patriciarum* J11. *Protein Expr. Purif.* **2013**, *90*, 153–159. [CrossRef]
68. Toda, H.; Nagahata, N.; Amano, Y.; Nozaki, K.; Kanda, T.; Okazaki, M.; Shimosaka, M. Gene Cloning of Cellobiohydrolase II from the White Rot Fungus *Irpex lacteus* MC-2 and Its Expression in *Pichia pastoris*. *Biosci. Biotechnol. Biochem.* **2008**, *72*, 3142–3147. [CrossRef]
69. Wang, X.; Peng, Y.; Zhang, L. Directed evolution and structural prediction of cellobiohydrolase II from the thermophilic fungus *Chaetomium thermophilum*. *Appl. Microbiol. Biotechnol.* **2012**, *95*, 1469–1478. [CrossRef]
70. Agrawal, D.; Basotra, N.; Balan, V.; Tsang, A.; Chadha, B.S. Discovery and Expression of Thermostable LPMOs from Thermophilic Fungi for Producing Efficient Lignocellulolytic Enzyme Cocktails. *Appl. Biochem. Biotechnol.* **2019**, *191*, 463–481. [CrossRef]
71. Keller, M.B.; Felby, C.; Labate, C.A.; Pellegrini, V.O.A.; Higasi, P.; Singh, R.K.; Polikarpov, I.; Blossom, B.M. A simple enzymatic assay for the quantification of C1-specific cellulose oxidation by lytic polysaccharide monooxygenases. *Biotechnol. Lett.* **2020**, *42*, 93–102. [CrossRef]
72. Hangasky, J.A.; Iavarone, A.T.; Marletta, M.A. Reactivity of O 2 versus H 2 O 2 with polysaccharide monooxygenases. *Proc. Natl. Acad. Sci. USA* **2018**, *115*, 4915–4920. [CrossRef] [PubMed]
73. Forsberg, Z.; Sørlie, M.; Petrović, D.; Courtade, G.; Aachmann, F.L.; Vaaje-Kolstad, G.; Bissaro, B.; Røhr, Å.K.; Eijsink, V.G. Polysaccharide degradation by lytic polysaccharide monooxygenases. *Curr. Opin. Struct. Biol.* **2019**, *59*, 54–64. [CrossRef] [PubMed]
74. Kuusk, S.; Bissaro, B.; Kuusk, P.; Forsberg, Z.; Eijsink, V.G.H.; Sørlie, M.; Valjamae, P. Kinetics of H2O2-driven degradation of chitin by a bacterial lytic polysaccharide monooxygenase. *J. Biol. Chem.* **2018**, *293*, 523–531. [CrossRef] [PubMed]
75. Frandsen, K.E.H.; Simmons, T.J.; Dupree, P.; Poulsen, J.C.N.; Hemsworth, G.R.; Ciano, L.; Johnston, E.M.; Tovborg, M.; Johansen, K.S.; Von Freiesleben, P.; et al. The molecular basis of polysaccharide cleavage by lytic polysaccharide monooxygenases. *Nat. Chem. Biol.* **2016**, *12*, 298–303. [CrossRef]
76. Musaddique, H.; Reddy Dodda, S.; Kapoor, B.S.; Aikat, K.; Mukhopadhyay, S.S. Investigation the biomass conversion efficiency, biochemical characterisation and structural insights of the newly isolated AA16 family of Lytic Polysaccharide Monooxygenase (LPMO) from *Aspergillus fumigatus*. *bioRxiv* **2020**. [CrossRef]
77. Frommhagen, M.; Westphal, A.H.; Hilgers, R.; Koetsier, M.J.; Hinz, S.W.A.; Visser, J.; Gruppen, H.; van Berkel, W.J.H.; Kabel, M.A. Quantification of the catalytic performance of C1-cellulose-specific lytic polysaccharide monooxygenases. *Appl. Microbiol. Biotechnol.* **2018**, *102*, 1281–1295. [CrossRef]
78. Kadowaki, M.A.S.; Várnai, A.; Jameson, J.K.; Leite, A.E.T.; Costa-Filho, A.J.; Kumagai, P.S.; Prade, R.A.; Polikarpov, I.; Eijsink, V.G.H. Functional characterization of a lytic polysaccharide monooxygenase from the thermophilic fungus *Myceliophthora thermophila*. *PLoS ONE* **2018**, *13*, e0202148. [CrossRef]
79. Singh, R.K.; Blossom, B.M.; Russo, D.A.; Van Oort, B.; Croce, R.; Jensen, P.E.; Felby, C.; Bjerrum, M.J. Thermal unfolding and refolding of a lytic polysaccharide monooxygenase from: *Thermoascus aurantiacus*. *RSC Adv.* **2019**, *9*, 29734–29742. [CrossRef]
80. Breslmayr, E.; Hanžek, M.; Hanrahan, A.; Leitner, C.; Kittl, R.; Šantek, B.; Oostenbrink, C.; Ludwig, R. A fast and sensitive activity assay for lytic polysaccharide monooxygenase. *Biotechnol. Biofuels* **2018**, *11*, 79. [CrossRef]
81. Meleiro, L.P.; Carli, S.; Fonseca-Maldonado, R.; Torricillas, M.d.S.; Zimbardi, A.L.R.L.; Ward, R.J.; Jorge, J.A.; Furriel, R.P.M. Overexpression of a Cellobiose-Glucose-Halotolerant Endoglucanase from *Scytalidium thermophilum*. *Appl. Biochem. Biotechnol.* **2018**, *185*, 316–333. [CrossRef]
82. Atreya, M.E.; Strobel, K.L.; Clark, D.S. Alleviating product inhibition in cellulase enzyme Cel7A. *Biotechnol. Bioeng.* **2016**, *113*, 330–338. [CrossRef] [PubMed]
83. Kostylev, M.; Wilson, D. A distinct model of synergism between a processive endocellulase (TfCel9A) and an exocellulase (TfCel9A) from *Thermobifida fusca*. *Appl. Environ. Microbiol.* **2014**, *80*, 339–344. [CrossRef] [PubMed]
84. Song, B.; Li, B.; Wang, X.; Shen, W.; Park, S.; Collings, C.; Feng, A.; Smith, S.J.; Walton, J.D.; Ding, S.Y. Real-time imaging reveals that lytic polysaccharide monooxygenase promotes cellulase activity by increasing cellulose accessibility. *Biotechnol. Biofuels* **2018**, *11*, 1–11. [CrossRef] [PubMed]

85. Hu, J.; Arantes, V.; Pribowo, A.; Gourlay, K.; Saddler, J.N.; Stephen, J.D.; Mabee, W.E.; Saddler, J.N.; Hu, J.; Arantes, V.; et al. Substrate factors that influence the synergistic interaction of AA9 and cellulases during the enzymatic hydrolysis of biomass. *Energy Environ. Sci.* **2014**, *7*, 2308. [CrossRef]
86. Tokin, R.; Ipsen, J.Ø.; Westh, P.; Johansen, K.S. The synergy between LPMOs and cellulases in enzymatic saccharification of cellulose is both enzyme- and substrate-dependent. *Biotechnol. Lett.* **2020**, *42*, 1975–1984. [CrossRef]
87. Quan, J.; Tian, J. Circular polymerase extension cloning for high-throughput cloning of complex and combinatorial DNA libraries. *Nat. Protoc.* **2011**, *6*, 242–251. [CrossRef]
88. Greenberg, C.S.; Craddock, P.R. Rapid single-step membrane protein assay. *Clin. Chem.* **1982**, *28*, 1725–1726. [CrossRef]
89. Shevchenko, A.; Jensen, O.N.; Podtelejnikov, A.V.; Sagliocco, F.; Wilm, M.; Vorm, O.; Mortensen, P.; Shevchenko, A.; Boucherie, H.; Mann, M. Linking genome and proteome by mass spectrometry: Large-scale identification of yeast proteins from two dimensional gels. *Proc. Natl. Acad. Sci. USA* **1996**, *93*, 14440–14445. [CrossRef]
90. *BIOVIA Discovery Studio Visualisation*; Accelrys Software Inc.: San Diego, CA, USA, 2017.
91. Miller, G.L. Use of Dinitrosalicylic Acid Reagent for Determination of Reducing Sugar. *Anal. Chem.* **1959**, *31*, 426–428. [CrossRef]

Industrial Crops & Products 170 (2021) 113697

Contents lists available at ScienceDirect

Industrial Crops & Products

journal homepage: www.elsevier.com/locate/indcrop

A thermophilic, pH-tolerant, and highly active GH10 xylanase from *Aspergillus fumigatus* boosted pre-treated sugarcane bagasse saccharification by cellulases

Aline Vianna Bernardi [a], Luis Eduardo Gerolamo [a], Sergio Akira Uyemura [b], Taisa Magnani Dinamarco [a,*]

[a] Faculty of Philosophy, Sciences and Literature of Ribeirão Preto, Chemistry Department, University of São Paulo, Ribeirão Preto, São Paulo, Brazil
[b] Faculty of Pharmaceutical Science, Department of Clinical, Toxicological and Bromatological Analysis, University of São Paulo, Ribeirão Preto, São Paulo, Brazil

ARTICLE INFO

Keywords:
GH10 xylanase
Aspergillus fumigatus
Lignocellulose
Saccharification
Synergy
Central composite rotational design

ABSTRACT

We have heterogously expressed a recombinant GH10 xylanase from *Aspergillus fumigatus* Af293 (*Af*-XYLA) in *Pichia pastoris* X-33 and investigated its biochemical and kinetic properties and its synergy with cellulases during lignocellulose sacchararification. *Af*-XYLA showed optimal activity at 80 °C and pH 5–7, and it withstood a temperature of 50 °C and pH 4–8 for 72 h with about 50 % and 80 % of its maximal activity, respectively, in the absence of substrate. Kinetic assays revealed that it presented the highest V_{max} (35,756 U mg^{-1} at 50 °C and 88,082 U mg^{-1} at 80 °C) and k_{cat}/K_M (15,456 mL mg^{-1} s^{-1} at 50 °C and 15,081 mL mg^{-1} s^{-1} at 80 °C) constants among fungal GH10 xylanases. *Af*-XYLA was xylose- and glucose-tolerant and displayed >70 % activity at 10 % (v/v) ethanol. Few additives affected *Af*-XYLA negatively, and the surfactants Tween 20, Triton X-100, and SLS and the reducing agents DTT and β-mercaptoethanol improved enzyme performance by 28 %, 11 %, 8%, 44 %, and 32 %, respectively. We applied a 3-factor Central Composite Rotational Design (CCRD) to optimize important parameters for biomass saccharification and thus maximize the reducing sugars yields obtained from sugarcane exploded bagasse (SEB) and sugarcane delignified bagasse (SDB) hydrolyses. We carried out synergism assays under the previously determined optimal concentrations of Celluclast 1.5®L (1.8 FPU g^{-1}), *Af*-XYLA (3.75 μg g^{-1}), and Tween 20 (0.75 % *v/v*). *Af*-XYLA boosted SEB and SDB hydrolyses by cellulases by 155 % and 277 %, respectively, after 48 h. On the basis of the unique properties of *Af*-XYLA, it is a robust enzyme for application in biorefineries.

1. Introduction

Lignocellulose represents a promising inexhaustible source of raw material for bio-based chemicals (e.g., xylooligosaccharides and polymers) and biofuels (e.g., bioethanol and biodiesel), which are in high demand (Evangelista et al., 2018; Vanitjinda et al., 2019; Wu et al., 2019). It is chiefly composed by cellulose (40–50 %), hemicellulose (25–30 %), and lignin (15–20 %), which together configure the complex and recalcitrant cross-linked structure of plant cell wall biomass (Song et al., 2016; Wu et al., 2020; Zhang et al., 2020; Zhou et al., 2018).

Xylan is the major component of hemicellulose, so it is the second most abundant polysaccharide in nature (Chang et al., 2017; Li et al., 2019b). It consists of a linear backbone of 1,4-linked β-D-xylopyranose units, with D-glucuronic acid, L-arabinose, or other branches attached to the xylose residues at various levels (Mhiri et al., 2020; Monclaro et al., 2019; Uday et al., 2017).

Effective xylan depolymerization is a prerequisite for lignocellulosic biomass to be properly exploited (Uday et al., 2017). Due to the heterogeneous chemical structure of xylan, its breakdown requires a repertoire of carbohydrate-active enzymes (CAZymes) acting synergistically, including the backbone-hydrolyzing enzymes endo-β-1,4-xylanases (EC 3.2.1.8) and β-xylosidases (EC 3.2.1.37), and side-chain cleaving enzymes such as α-glucuronidases (EC 3.2.1.139), α-L-arabinofuranosidases (EC 3.2.1.55), acetyl xylan- (EC 3.1.1.72), and ferulic/coumaric acid esterases (EC 3.1.1.73) (Chen et al., 2019b; Liew et al., 2019; Monclaro et al., 2019; Saleh et al., 2021; Uday et al., 2017;

* Corresponding author.
E-mail addresses: alinevbernardi@gmail.com, aline.bernardi@usp.br (A.V. Bernardi), gerolamo00@hotmail.com, luis.gerolamo@usp.br (L.E. Gerolamo), suyemura@fcfrp.usp.br (S.A. Uyemura), tdinamarco@ffclrp.usp.br (T.M. Dinamarco).

https://doi.org/10.1016/j.indcrop.2021.113697
Received 19 February 2021; Received in revised form 6 May 2021; Accepted 31 May 2021
Available online 10 June 2021

Ullah et al., 2019).

Among these enzymes, xylanases are key biocatalysts that promote the initial attack on the internal β-1,4-glicosidic bonds of xylan, hydrolyzing it into xylooligosaccharides with different degrees of polymerization (DP) (Chen et al., 2019b; Evangelista et al., 2018; Han et al., 2019; Haq and Akram, 2019). These high-value products can be potentially exploited as prebiotics or still be converted into D-xylose for use in 2 G ethanol, xylitol, and lactic acid production (Evangelista et al., 2018; Turner et al., 2015; Wu et al., 2019). Also, xylanases play relevant roles in other manufacturing processes, such as juice clarification, beer finishing, bread making, industrial waste treatment, plant fiber degumming for the textile industry, and paper pulp bleaching, where they act as an ecofriendly substitute for chemicals, justifying the great interest in these enzymes (Chen et al., 2019b; de Amo et al., 2019; Evangelista et al., 2018). However, these reactions are usually carried out at higher temperatures and acid/alkaline environments, limiting the industrial applications of xylanases (Li et al., 2019a; Saleem et al., 2021; Takita et al., 2019; Xing et al., 2021; Yang et al., 2020).

Most native xylanases are mesophilic, do not withstand harsh conditions, and only work well within specific ranges of temperature, pH, and ionic strength (Han et al., 2019; Maitan-Alfenas et al., 2016; Saleem et al., 2021; Xu et al., 2016; Yang et al., 2020). They are little stable to operational conditions and may be inhibited by products, which negatively affect process yield and demand high enzymatic loadings (Chen et al., 2019a; Meleiro et al., 2018; Soozanipour et al., 2015; Vazquez-Ortega et al., 2018). Therefore, bioprospecting for xylanases with more appealing biotechnological characteristics and improving the properties of naturally occurring enzymes through immobilization or genetic engineering tools have been important and necessary focuses of research (Kumar et al., 2018, 2016; Pasin et al., 2020).

According to the CAZy database (www.cazy.org), several families of glycoside hydrolases (GH) are correlated with xylanases (e.g. 3, 5, 7, 8, 9, 10, 11, 12, 16, 26, 30, 43, 44, 51, 62, 98 and 141), but the overwhelming majority is represented by members of the GH10 and GH11 families (Joshi et al., 2020; Liew et al., 2019; Malgas and Pletschke, 2019). Both families catalyze hydrolysis through a retention mechanism involving two glutamate residues, but GH11 xylanases generally exhibit higher pIs, lower molecular weights (<30 kDa), and superior catalytic efficiencies as compared to GH10 xylanases. Nevertheless, GH10 xylanases usually present greater thermostability and can act on a wide variety of xylans. Besides that, GH10 xylanases display better performance than GH11 when associated with cellulases during biomass hydrolysis, which makes them more suitable targets for industrial purposes (He et al., 2019; Hu and Saddler, 2018; Joshi et al., 2020; Li et al., 2019a; Maitan-Alfenas et al., 2016; van Gool et al., 2013; Yang et al., 2020).

Filamentous fungi are the best at secreting xylanases and other enzymes required for biomass degradation (i.e., cellulases, hemicellulases, and lignases), but thermophilic fungi are of particular interest (Carli et al., 2016; Chen et al., 2019b; de Amo et al., 2019; Kumar et al., 2018; Liu et al., 2019; Miao et al., 2018; Uday et al., 2017). Numerous thermophilic fungi have been found to be efficient sources of thermo-alkali stable xylanases (Chadha et al., 2019). *Myceliophthora thermophila* contains 12 genes coding for xylanases (distributed into families 11 and 12), some of which have already been characterized as highly thermally stable and able to act under extreme alkaline conditions (Chadha et al., 2019; Karnaouri et al., 2014a). Also, *Thermomyces lanuginosus* is a well-known producer of high levels of thermostable, alkaline-active, and cellulase-free xylanases (48,000 U g^{-1} under solid substrate fermentation) (Chadha et al., 2019; Mathibe et al., 2020). Thermostable xylanases produced by *Malbranchea flava* boosted pulp bleaching and lignocellulose saccharification by cellulases (Chadha et al., 2019; Ghatora et al., 2006; Sharma et al., 2016). Likewise, the thermophilic species *Thermoascus aurantiacus* and *Humicola insolens* are potential producers of xylanases (Chadha et al., 2019). In addition to the aforementioned fungi, *Aspergillus fumigatus* has proven an excellent candidate to produce thermostable CAZymes, including xylanases, with great enzymatic activities (Bernardi et al., 2021, 2019, 2018; Chen et al., 2019b; Gouvêa et al., 2019). However, even though fungi can produce enzymes in higher amounts than other microbes, their expression levels do not always satisfy industrial requirements (de Amo et al., 2019; Han et al., 2019). In this context, expressing enzymes in heterologous systems has become an advantageous alternative. In this scenario, the yeast *Pichia pastoris* stands out as a well-described and broadly applied expression host that can produce pronounced amounts of soluble, correctly folded, and almost pure proteins (de Amo et al., 2019; Maitan-Alfenas et al., 2016).

Bearing in mind the essential contribution of xylanases for efficient and cost-effective use of biomass and its wide industrial application, we have cloned and expressed a GH10 xylanase (*Af*-XYLA), identified during the transcriptome and secretome analysis of *A. fumigatus* grown in sugarcane exploded bagasse (SEB) (de Gouvêa et al., 2018), in *P. pastoris* for further characterization. The recombinant enzyme presented optimum temperature of 80 °C, great stability to almost all the evaluated reaction conditions, and substantial catalytic efficiency. Moreover, it considerably boosted the saccharification yields by Celluclast®1.5 L. These unique properties of *Af*-XYLA indicated that it is a robust biocatalyzer for application in biorefinery processes.

2. Materials and methods

2.1. Strains, culture media, vectors, and materials

Aspergillus fumigatus Af293 was grown in Yeast-Agar-Glucose (YAG) medium [2.0 % *(w/v)* dextrose, 2.0 % *(w/v)* agar, 0.5 % *(w/v)* yeast extract, and 0.1 % *(v/v)* trace elements] at 37 °C for two days, to obtain a fresh conidium suspension. The conidia were inoculated to a final concentration of 1×10^8 per 50 mL of YNB medium [1X salts solution, 0.1 % (*v/v*) trace elements, and 0.05 % (*w/v*) yeast extract] containing 1% (*w/v*) fructose and incubated at 37 °C and 200 rpm for 16 h. Next, the mycelia were harvested, washed, and transferred to YNB medium containing 1% (*w/v*) SEB at 37 °C and 200 rpm for 24 h. Then, the mycelia were harvested for RNA extraction.

The plasmid pPICZαA (Invitrogen, Carlsbad, CA, USA) was used for gene cloning, sequencing, and expression. *Escherichia coli* DH10β grown at 37 °C and 200 rpm in low salt Luria-Bertani medium supplemented with zeocin (50 μg mL^{-1}) was used to propagate the recombinant vector *Af-xylA*/pPICZαA. *Pichia pastoris* X-33 cells harboring the recombinant expression vector *Af-xylA*/pPICZαA were used for heterologous protein production. The growth conditions are described in the EasySelect™ *Pichia* Expression Kit manual (Invitrogen, Carlsbad, CA, USA).

Beechwood xylan and tamarind seed xyloglucan were acquired from Megazyme (Megazyme International, Bray, Co., Wicklow, Ireland). Avicel® PH-101 and low-viscosity CM-Cellulose (CMC) were purchased from Sigma (Sigma–Aldrich, St. Louis, MO, USA).

SEB was provided by Professor João Atílio Jorge (University of São Paulo, Ribeirão Preto, Brazil). Sugarcane delignified bagasse (SDB) was obtained by chemical treatment and provided by Professor Richard John Ward (University of São Paulo, Ribeirão Preto, Brazil).

2.2. RNA extraction, cDNA synthesis, and gene amplification

After growth for 24 h in SEB-containing medium, the mycelia were harvested by centrifugation for RNA isolation with the Direct-zol™ RNA MiniPrep kit (Zymo Research, Irvine, CA, USA), according to the manufacturer's instructions. cDNA was synthesized from 1 μg of total RNA by using SuperScript® II Reverse Transcriptase (Invitrogen, Carlsbad, CA, USA). Then, cDNA was employed as template for PCR amplification of the ORF corresponding to the *Af*-XYLA-encoding gene (Afu6g13610), without the signal peptide-encoding region. Specific primer sequences

containing overlapping regions between the pPICZαA vector and the insert were applied (F: 5′– **GAGAAAAGAGAGGCTGAAGCTGAATT**GCT GGCCTGAACACA –3′ and R: 5′– **ATCCTCTTCTGAGATGAGTTTTTGT TCTAG**CAGGCACTGTGAGTA –3′; overlapping sites in bold). The amplification reaction was performed with Phusion High-Fidelity DNA Polymerase (Thermo Fisher Scientific, Waltham, MS, USA); the following thermo cycling conditions were used: 98 °C for 30 s; 30 cycles of 98 °C for 10 s, 55 °C for 30 s, and 72 °C for 1 min; and 72 °C for 10 min. The PCR product was analyzed by electrophoresis and purified from 1% (w/v) agarose gel by employing the QIAquick Gel Extraction kit (Qiagen, Hilden, Germany).

2.3. Cloning, transformation of P. pastoris, and screening for recombinant transformants

The amplified *Af-xylA* fragment was cloned into pPICZαA, previously digested with the restriction enzymes *Eco*RI and *Xba*I, by the Circular Polymerase Extension Cloning (CPEC) method (Quan and Tian, 2011). The CPEC reaction was performed with Phusion High-Fidelity DNA Polymerase (Thermo Scientific); the thermo cycling conditions were as follows: 98 °C for 30 s; 35 cycles of 98 °C for 10 s, 55 °C for 30 s, and 72 °C for 2 min 30 s; and 72 °C for 10 min. The cloning product was transformed into chemically competent *E. coli* DH10β cells, and the resistant transformants were selected with zeocin (50 μg mL^{-1}). Next, the *Af-xylA*/pPICZαA recombinant plasmid was linearized with *Pme*I and transformed into competent *P. pastoris* X-33 cells by electroporation, according to the EasySelect™ *Pichia* Expression Kit manual (Invitrogen). *P. pastoris* recombinant clones were screened by Zeocin resistance.

2.4. Heterologous expression of Af-XYLA in P. pastoris and protein purification

A Zeocin-resistant *P. pastoris* transformant was selected to produce the protein. The recombinant yeast was cultivated in buffered glycerol-complex medium (BMGY) [2% (*w/v*) peptone, 1.34 % (*w/v*) yeast nitrogen base, 1% (*w/v*) yeast extract, 1% (*v/v*) glycerol, 4×10^{-5} % (*w/v*) biotin, 100 mM potassium phosphate buffer, pH 6.0] at 30 °C and 240 rpm until the culture reached log-phase growth ($O.D._{600nm}$ = 2–6). Then, for *Af*-XYLA heterologous expression, the cells were re-suspended in buffered methanol-complex medium (BMMY) [2% (*w/v*) peptone, 1% (*v/v*) methanol, 1.34 % (*w/v*) yeast nitrogen base, 1% (*w/v*) yeast extract, 4×10^{-5} % (*w/v*) biotin, 100 mM potassium phosphate buffer, pH 6.0] to an $O.D._{600nm}$ = 1. To maintain expression levels, methanol (1% (*v/v*)) was added to the medium at 24-h intervals for six days. After this time, the supernatant containing secreted recombinant *Af*-XYLA was harvested from grown culture and concentrated 10 times by using an Amicon Ultra-15 Centrifugal Filter—10 kDa cutoff (Millipore, Burlington, MS, USA).

For protein purification, the concentrate was re-suspended in 20 mM sodium phosphate buffer containing 500 mM NaCl (pH 7.4) and loaded onto Ni Sepharose 6 Fast Flow resin (Ge Healthcare, Little Chalfont, United Kingdom). To elute the *Af*-XYLA His_6-tagged recombinant, an imidazole gradient from 0 to 500 mM was applied to the column. Protein elution was analyzed by 10 % (w/v) SDS-PAGE. Fractions containing the recombinant enzyme were mixed and buffer-exchanged by using Amicon Ultra-15 Centrifugal Filter - 10 kDa cutoff (Millipore) to remove excess imidazole. The protein concentration was determined by the Greenberg method (Greenberg, 1929).

2.5. Sequence and structural analysis

The signal peptide in *Af*-XYLA was predicted with SignalP (http://www.cbs.dtu.dk/services/SignalP/). The potential N-glycosylation sites were predicted with the NetNGlyc 1.0 Server (http://www.cbs.dtu.dk/services/NetNGlyc/). Multiple sequence alignment was performed with the Clustal Omega tool (https://www.ebi.ac.uk/Tools/msa/clustalo/). Homology modeling was performed with the Phyre2 software (http://www.sbg.bio.ic.ac.uk/phyre2/html/page.cgi?id=index). The three-dimensional structure of the protein modeled from Phyre2 was analyzed with the Swiss PDB viewer. The secondary structures present in the modeled *Af*-XYLA were accounted by checking the Phyre2 results and by running the Kabsch & Sander prediction algorithm (Kabsch and Sander, 1983) in the Discovery Studio visualizer.

2.6. Analysis by circular dichroism (CD) and intrinsic tryptophan fluorescence emission (ITFE)

The Circular Dichroism (CD) spectra were obtained on a JASCO-810 spectropolarimeter. *Af*-XYLA (0.000625 μg mL^{-1}) diluted in 20 mM sodium phosphate buffer (pH = 7.4) was analyzed between 190 and 250 nm in 0.1-cm quartz cuvettes (loaded with 200 μL) after preheating at 25, 40, 50, 60, 70, 80, or 90 °C for 30 min. The readings were performed in quadruplicate measurements at scan rate, data interval, band width, and D.I.T. values of 50 nm min^{-1}, 1 nm, 3 nm, and 1 s, respectively. After the baseline was corrected and the blank was subtracted, millidegree (mdeg) units were converted to Δε in M^{-1} cm^{-1} according to the equation:

$$\Delta\varepsilon = \frac{\theta.MRW}{d.c.32980}$$

where MRW (106.4 Da for *Af*-XYLA) is the protein mean residual weight, calculated by dividing the molecular weight in Da by the number of residues-1; θ is the ellipticity value originally given by the equipment (mdeg); d is the path length (cm); and c is the concentration (mg mL^{-1}). All the collected treated spectra were analyzed with the BeStSel free server (Micsonai et al., 2018) to estimate the content of secondary structures.

Intrinsic Tryptophan Fluorescence Emission (ITFE) analysis was performed on the spectrofluorometer HITACHI-F4500. By using the same concentration and sample treatment employed for CD analysis, 295 nm was selected to excite the tryptophan residues in *Af*-XYLA, and the fluorescent emissions were detected between 300 and 450 nm. The samples (1 mL) were placed in 1.0-cm quartz cuvettes, and the readings were conducted at scan rate of 240 nm min^{-1} and data interval of 0.2 nm. The blank was subtracted to correct the collected spectra.

To determine the apparent T_m (melting temperature), the first derivatives of the plots of ellipticity registered at 205 nm (from CD) *vs* temperature and maxima wavelength (from ITFE) *vs* temperature were calculated with the OriginPro 9.0 software. Both plots were fitted by using the Boltzmann function. All the CD and ITFE analyzed graphs were previously smoothed with the Savitzky-Golay filter (Savitzky and Golay, 1964).

2.7. Zymogram analysis and Af-XYLA deglycosylation

The *Af*-XYLA activity was evaluated by Zymogram on 10 % (w/v) polyacrylamide gel containing 0.5 % (*w/v*) xylan (Megazyme International, Bray, Co. Wicklow, Ireland). Before being loaded onto the gel, 10 μg of enzyme was mixed with a non-reducing 5x sample buffer. After electrophoresis, the gel was soaked twice in 50 mM sodium acetate buffer (pH 5.0) containing 1% (*v/v*) Triton X-100 for 30 min, to remove SDS and to allow the enzyme to refold. The gel was soaked in 50 mM sodium acetate buffer (pH 5.0) for 15 min for washing and incubated in the same buffer at 50 °C for 30 min. Finally, the gel was stained with 0.1 % (*w/v*) Congo red solution for 30 min and de-stained with 1 M NaCl until pale-red hydrolysis zones appeared against a red background.

Recombinant *Af*-XYLA was deglycosylated by using Endoglycosidase H (Endo H, New England Biolabs, Ipswich, MA, USA) in non-denaturing conditions, as per the manufacturer's procedure. The resulting enzyme was further analyzed by SDS-PAGE and compared to the non-treated one.

2.8. Endo-β-1,4-xylanase activity assay

The *Af*-XYLA activity was determined by measuring the released reducing sugars by the 3,5-dinitrosalicylic acid (DNS) method (Miller,

1959). Briefly, the reaction mixture consisting of 1% (*w/v*) beechwood xylan in 50 mM sodium phosphate buffer (pH 6.0) was incubated at 80 °C for 10 min. The enzyme action was stopped by adding an equal volume of DNS reagent. Then, the mixture was boiled for 5 min and cooled down, and the absorbance was measured at 540 nm. One unit of endoxylanase activity was defined as the amount of enzyme that released 1 μmol of reducing sugar from the substrate per minute. Each assay was carried out in triplicate.

2.9. pH and temperature profiles

The optimum pH for *Af*-XYLA activity was measured from 3.0 to 8.0, in McIlvaine buffer (citric acid-Na_2HPO_4), at 50 °C. The optimum temperature for *Af*-XYLA activity was examined from 30 to 90 ℃.

pH stability was estimated by measuring the residual enzymatic activity under standard conditions (pH 6.0, 80 °C, and 10 min) after pre-incubation of the enzyme without substrate in McIlvaine buffers pH 3.0–8.0 at 4 °C for up to 72 h. To determine the thermal stability of *Af*-XYLA, it was pre-incubated from 30 to 90 °C for different times, without the presence of substrate. To measure the residual activity, the activity of the enzyme with no pre-incubation was considered 100 %.

2.10. Influence of additives on Af-XYLA activity

The effect of different metal ions on the *Af*-XYLA activity was determined by adding Mn^{2+}, Co^{+2}, Ca^{2+}, Fe^{+2}, Zn^{2+}, Mg^{2+}, Cu^{2+}, NH_4^+, K^+, or Ag^+ to a final concentration of 5 mM in the reaction mixture. In the same way, the effect of adding the chemicals EDTA, SDS, SLS, Tween 20, Triton X-100, β-mercaptoethanol, DTT, ascorbic acid, or DMSO was also tested. The reactions were performed under standard conditions and stopped by DNS addition. The control reaction (100 % activity) was carried out without any additive. The relative activity was estimated by comparison with the control.

2.11. Effects of monosaccharides and ethanol on Af-XYLA activity

The effects of D-xylose and D-glucose on the recombinant xylanase activity were determined in the presence of increasing concentrations (10–250 mM) of these sugars; the chromogenic substrate azo-xylan from beechwood (Megazyme International, Bray, Co. Wicklow, Ireland) was used. The enzymatic assays were performed in 50 mM sodium acetate buffer (pH 4.5) at 40 °C for 10 min, according to the manufacturer's instructions with slight modifications. The reactions were stopped by adding 2.5 volumes of absolute ethanol. The supernatants were harvested by centrifugation at 1700 × *g* for 10 min, and the absorbances were measured at 590 nm.

To determine the effect of ethanol, increasing concentrations (0.5–50 % (*v/v*)) of this reagent were added to the reactions. The enzymatic assays were performed in 50 mM sodium phosphate buffer (pH 6.0) containing 1% (w/v) beechwood xylan at 50 °C for 10 min. The endoxylanase relative activities were calculated by measuring the released reducing sugars by the DNS method.

The activity of the enzyme in the absence of xylose, glucose, or ethanol was considered 100 %.

2.12. Substrate specificity

The *Af*-XYLA specificity for different substrates was determined by measuring the xylanase activity toward 0.5 % (*w/v*) low-viscosity CM-cellulose, xyloglucan from tamarind seed, or Avicel® PH-101; the activity toward beechwood xylan was considered as 100 %. Enzymatic reactions were carried out as described in *2.8*.

2.13. Kinetic assays

The *Af*-XYLA kinetic parameters (K_M, V_{max}, and k_{cat}) were determined for beechwood xylan (0.5–30 mg mL^{-1}) as substrate. The reactions were performed in 50 mM sodium phosphate buffer (pH 6.0) at two temperatures, 50 and 80 °C, for 10 min. The released reducing sugars were measured by the DNS method. The parameters were calculated by Michaelis-Menten non-linear regression with the OriginPro 9.0 software.

Table 1
Coded and actual values of independent variable levels.

	Levels				
Variables	**−1.68**	**−1**	**0**	**+1**	**+1.68**
A - Tween 20 (% (v/v))	0	0.2	0.5	0.8	1
B – Celluclast®1.5 L (FPU g^{-1})	0.2	0.5	1	1.5	1.8
C – *Af*-XYLA (μg g^{-1})	0	1	2.5	4	5

2.14. CCRD approach for optimization of sugarcane bagasse hydrolysis

A Central Composite Rotational Design (CCRD) of experiments was used to investigate the influence of the parameters A – Tween 20 (% (*v/v*)), B – Celluclast® 1.5 L (FPU/g of substrate), and C – *Af*-XYLA (μg/g of substrate) on SEB and SDB hydrolysis and to find the most suitable values of these three operational factors for optimum yield of reducing sugars.

The factors A, B, and C were considered independent variables, and the percentage of reducing sugars was the response (dependent variable). The operational parameters were examined at five different levels (−α, −1, 0, +1, +α), whose coded and actual values are presented in Table 1.

The hydrolysis reactions were performed in 50 mM sodium phosphate buffer (pH 6.0) containing 1% (*w/v*) of SEB or SDB at 50 °C and 1000 rpm for 48 h. The reducing sugars released in each assay were measured by the DNS method, and the percentage yields were calculated by using the following Eq. (1):

$$Yield\ (\%) = \frac{Reducing\ sugars\ obtained\ from\ biomass\ hydrolysis\ (mg)}{Amount\ of\ biomass\ used\ (mg)} \times 100 \quad (1)$$

The mathematical model to predict the response variable was fitted as a second-order polynomial Eq. (2):

$$y = \beta_o + \sum_{i=1}^{k} \beta_i x_i + \sum_{i=1}^{k} \beta_{ii} x_i^2 + \sum_{\substack{i=1 \\ i=1}}^{k} \beta_{ij} x_i x_j + \varepsilon \quad (2)$$

where **y** is the predicted mean response, βo is the constant term of the model, βi are the coefficients of the linear terms, βii are the coefficients of the quadratic terms, βij are the coefficients of the interaction terms, and ε is the random error component that is determined by fitting the model to the data.

An Analysis of Variance (ANOVA $p < 0.01$) was performed by using the STATISTICA 12 software to clarify the influence of independent variables and their interactions on the response and to find out whether the mathematical model was statically significant and presented an error (lack of fit). Thus, with a significant and predictive regression, the response surfaces could be obtained and then used to optimize the model.

2.15. Synergy of Af-XYLA with Celluclast®1.5 L cocktail

The effect of the synergistic activity between the recombinant *Af*-XYLA from *A. fumigatus* and the commercial cellulases from *Trichoderma reeesei* was evaluated during pre-treated sugarcane bagasse hydrolysis. The reactions were conducted in 50 mM sodium phosphate buffer (pH 6.0) containing 1% (*w/v*) SEB or SDB at 50 °C and 1000 rpm for 24 or 48 h. The optimum values for Tween 20 (0.75 % (*v/v*)), Celluclast® 1.5 L

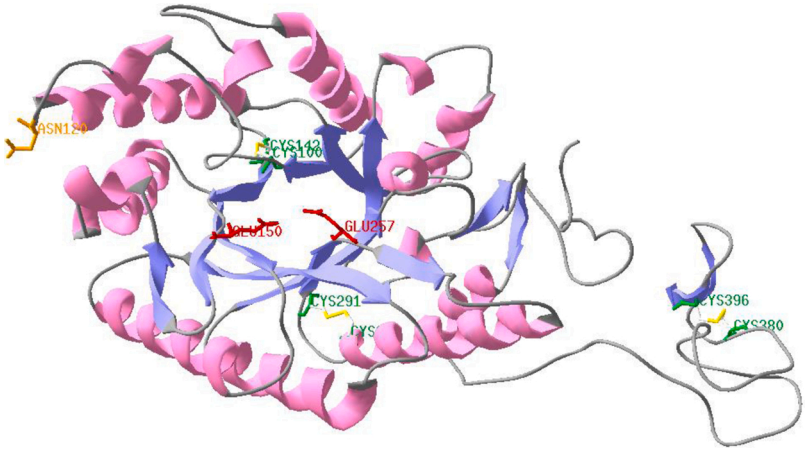

Fig. 1. *Af*-XYLA three-dimensional structure predicted by homology modeling (97 % of residues modelled at >90 % confidence) performed with the Phyre2 software and edited with the Swiss PDB Viewer tool. Helices, sheets, and coils are highlighted in pink, lilac, and grey, respectively. Putative catalytic glutamate residues and potential N-glycosylation site are highlighted in red and orange, respectively. Cysteine residues apt to form disulfide bonds (C100, C142, C285, C291, C380, and C396) are highlighted in green, and the S—S bonds are highlighted in yellow.

(1.8 FPU g^{-1}), and *Af*-XYLA (3.75 μg g^{-1}), previously stipulated by Response Surface Methodology (RSM) statistical analysis, were used in the mixtures. The percent hydrolysis yields were determined by estimating the released reducing sugars by the DNS method. The reported results represent the means ± SD calculated from at least three experimental replicates.

2.16. Reproducibility of the results

All the data are the mean of at least three independent experiments and show consistent results.

3. Results and discussion

3.1. Af-XYLA sequence and structural analysis

The *Af-xylA* gene from *A. fumigatus* (Afu6g13610, Gene ID 3508551, GenBank access number XM_746144.1) has a 1194 bp ORF encoding an endo-β-1,4-xylanase (*Af*-XYLA) with 397 amino acid residues and a theoretical molecular weight of 42.14 kDa (http://www.aspergillusgenome.org/; https://www.uniprot.org/uniprot/Q4WLG5). On the basis of sequence similarity and according to CAZy database, we classified recombinant *Af*-XYLA into glycoside hydrolase (GH) family 10. Xylanases belonging to this family are less selective and hydrolyze substituted forms of xylans as well as small xylooligosaccharides (Mhiri et al., 2020; Monclaro et al., 2019; Van Den Brink and De Vries, 2011).

The *A. fumigatus* Af293 genome contains six genes coding for endoxylanases, being three for GH10 (Afu6g13610, Afu4g09480, and Afu3g15210) and three for GH11 (Afu3g00320, Afu3g00470, and Afu6g12210). *Af*-XYLA is the only xylanase linked to a carbohydrate-binding module (CBM1) at C-terminal residues 361–397 (**GVAQKWGQCGGIGWTGPTTCVSGTTCQKLNDWYSQCL**) (Segato et al., 2014). CBMs are non-catalytic domains that assist enzymes in recognizing and binding to their respective substrates. CBMs increase the effective concentrations of enzymes around the target surface, increasing their catalytic efficiencies (Couturier et al., 2011; Guillén et al., 2010; Inoue et al., 2015).

In GH10 xylanases, these modular structures are typically linked to the hydrolase domain by a flexible linker region (Miao et al., 2018). Xylanase-related CBMs (e.g., CBM1, CBM2, CBM6, and CBM22) can play distinct polysaccharide-binding functions. In particular, the CBM1 family targets binding to crystalline cellulose surfaces (Miao et al., 2018). Cellulose-binding modules impact hemicellulase adsorption and action positively because cellulose and hemicellulose portions are very close in the plant cell wall matrix (Miao et al., 2018; Zhang et al., 2013).

Bioinformatics analysis of the *Af*-XYLA sequence revealed a signal peptide at N-terminal residues 1–19 (MVHLSSLAAALAALPLVYG). We removed this signal peptide before cloning *Af-xyl*A into the pPICZaA vector, in fusion with the α factor sequence (an essential step to obtain an extracellular recombinant enzyme). Also, the analysis indicated a potential N-glycosylation site at asparagine residue N120. The presence of N-glycans at different sites of the structure may influence the protein in different ways, including its secretion, folding, stability, and other enzymatic characteristics (Chang et al., 2017). Alignment of the *Af*-XYLA amino acid sequence with some GH10 xylanases from other fungi (Supplementary Fig. 1) revealed a percent identity of 62.28 %, 60.30 %, 48.43 %, 46.67 %, 45.48 %, and 43.49 % with the enzymes from *T. cellulolyticus* (Inoue et al., 2015), *G. trabeum* (Kim et al., 2014), *T. aurantiacus* (Natesh et al., 1999), *A. terreus* (Chantasingh et al., 2006), *T. leycettanus* (Wang et al., 2016), and *A. fumigatus* (Chang et al., 2017), respectively.

Furthermore, the alignment revealed some conserved regions, so we were able to predict the two putative catalytic residues–E150 and E257. Xylanases belonging to the GH10 and GH11 families usually act through an acid/base mechanism that generally involves two glutamate residues (Hoffmam et al., 2016; Segato et al., 2014).

We predicted the three-dimensional structure of *Af*-XYLA with the Phyre2 software and manipulated it by using Swiss-PDB viewer editing tools (Fig. 1). As expected for a GH10 xylanase, *Af*-XYLA exhibits an eight-fold TIM barrel structure [$(\beta/\alpha)_8$], consisting of eight α-helices and eight β-sheets around a deep groove active site. This structure is consistent with its endo mode of catalysis (Liew et al., 2019; Segato et al., 2014; Ullah et al., 2019). The three disulfide bonds highlighted in yellow evidence the presence of six cysteine residues. These covalent bonds are important post-translational modifications that interfere in proper protein function, folding, and stability (Lakbub et al., 2018). The two putative catalytic residues (in red) and the asparagine with potential to be glycosylated (in orange) are also highlighted.

Additionally, analysis of the spectrum obtained by Far-UV CD at 25 °C with the BeStSel server revealed that *Af*-XYLA is composed of α-helices (29.1 %), β-strands (22.8 %), turns (9.1 %), and disordered structures and other structures (39.0 %) (Table 2). Compared to other

Table 2
Percentage of secondary structures present in *Af*-XYLA determined with the BeStSel server on the basis of the CD spectra obtained at 25 °C and predictions with the Phyre2 server and Kabsch & Sander method on the basis of enzyme sequence.

	BeStSel (CD)	Phyre2	Kabsch & Sander
α-helix (%)	29.1	37.0	37.6
β-strand (%)	22.8	18.0	14.0
Turns (%)	9.1	–	–
Others/disordered (%)	39.0	45.0	48.4

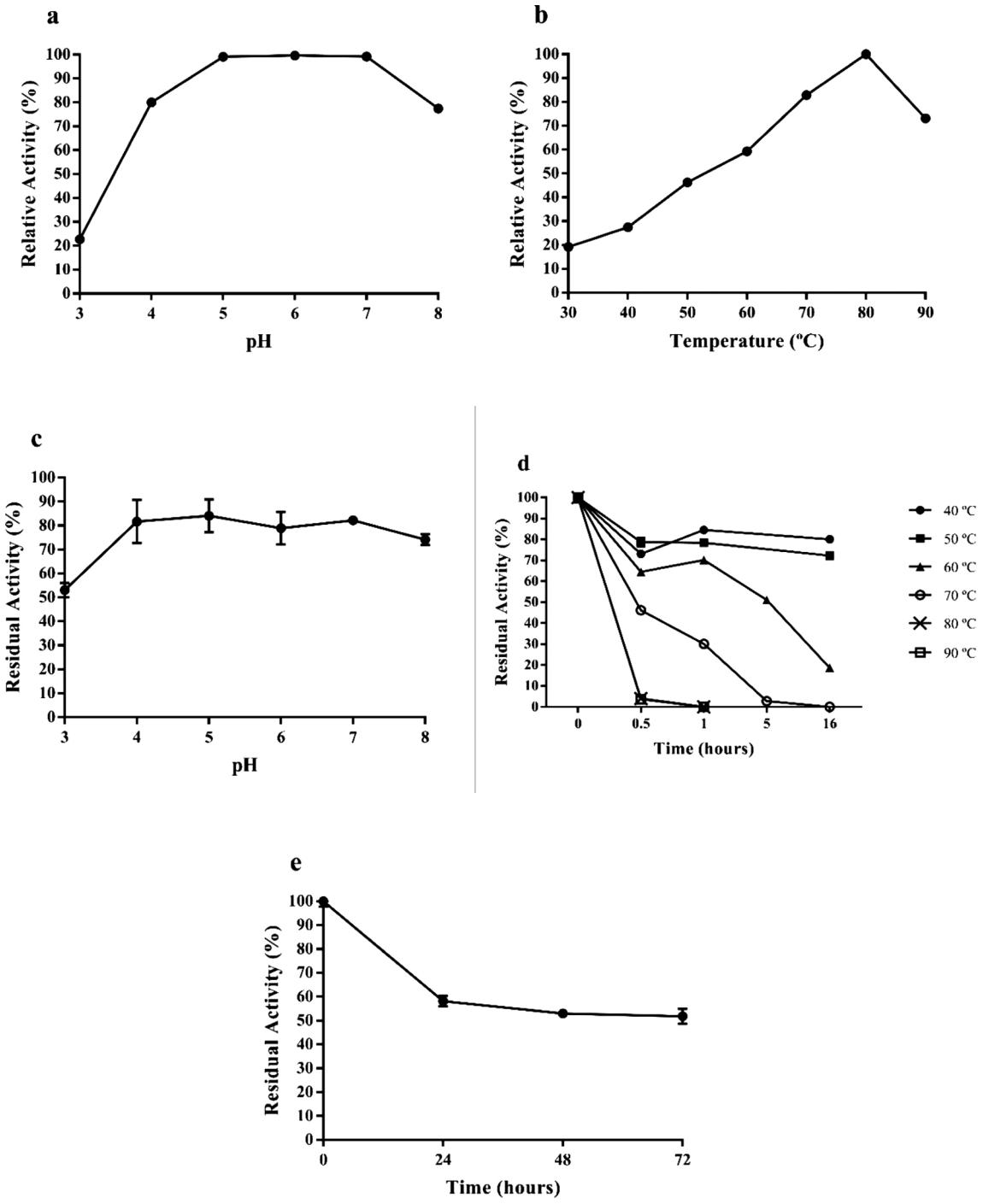

Fig. 2. *Af*-XYLA optimal conditions and stability. a) pH curve. b) Temperature curve. c) pH stability. d) Thermal stability. e) Stability at 50 °C.

predictions (Phyre2 model and Kabsch & Sander method (Kabsch and Sander, 1983)), the slightly super- or underestimated α-helix and β-strand structures, respectively, are noteworthy even though they are relatively close to the CD results. In fact, the similar proportions are related to the TIM barrel core, as observed in the crystallographic structure of *Cj*Xyn10C (PDB:1US2) (Pell et al., 2004), which presents 36.7 % α-helices and 22.9 % β-strands and was used as basis for *Af*-XYLA 3D modelling.

3.2. SDS-PAGE and Zymogram analysis of purified Af-XYLA

We cloned the *Af-xylA* gene into the pPICZαA vector and expressed it in *Pichia pastoris* X-33 under control of the AOX1 promoter. After induction for six days with 1% (*v/v*) methanol, we collected the culture supernatant by centrifugation and purified the recombinant *Af*-XYLA by one-step nickel affinity chromatography. We analyzed all the fractions collected during purification by SDS-PAGE (Supplementary Fig. 2 a). *Af*-XYLA elution started with 10 mM imidazole and finished with 250 mM imidazole, yielding 1.0 mg mL^{-1}. The electrophoretic band of pure *Af*-XYLA was slightly higher than expected for its estimated molecular weight (42 kDa), possibly due to the presence of N-linked glycans. To clarify this, we deglycosylated *Af*-XYLA by treating it with Endo H. In fact, we verified a subtle difference in the protein band migration (Supplementary Fig. 2b), which agreed with the previous prediction of only one site with potential for N-glycosylation in the *Af*-XYLA structure.

We started to characterize the *Af*-XYLA enzymatic activity with a

Table 3
Comparison of biochemical properties and kinetics of GH10 xylanases from different fungi.

Source Organism	Protein name	Expression System	Substrate	V_{max}	K_M	*kcat*	*kcat*/K_M	Optimal T	Optimal pH	Thermal stability	pH stability	Ref
Aspergillus fumigatus Af293	XYLA	*Pichia pastoris* X-33	Beechwood xylan[a]	35,756 ± 1279 U mg^{-1}	1.62 ± 0.19 mg mL^{-1}	25,039 s^{-1}	15,456 mL mg^{-1} s^{-1}	80 °C	pH 5.0–7.0	About 80 % of residual activity after 16 h at 40 and 50 °C; 50 % after 5 h and 30 min, respectively, at 60 °C and 70 °C	80 % of residual activity after 72 h at pH 4.0–8.0 (at 4 °C)	This study
			Beechwood xylan[b]	88,082 ± 2639 U mg^{-1}	4.09 ± 0.39 mg mL^{-1}	61,682 s^{-1}	15,081 mL mg^{-1} s^{-1}					
Aspergillus fumigatus Af293	Af-XYNA	*Pichia pastoris* GS115	Birchwood xylan	268 ± 7 U mg^{-1}	1.3 ± 0.1 mg mL^{-1}	–	–	75 °C	pH 5.0	> 80 % of relative activity after 1 h at 60 °C; rapid loss of activity at 70 °C	> 69 % of relative activity at pH 3.0–8.0 and more than 46% at pH 9.0–11.0	(Chang et al., 2017)
Talaromyces cellulolyticus CF-2612	Xyl10A	*Talaromyces cellulolyticus* YP-4	Birchwood xylan	–	2.51 ± 0.42 mg mL^{-1}	232 ± 12.4 s^{-1}	92.2 ± 16.2 s^{-1} mg^{-1} mL^{-1}	80 °C	pH 5.0	T_m equal to 81 °C	33 % of relative activity at pH 3.4	(Inoue et al., 2015)
Gloeophyllum trabeum KACC 43,361	Xyl10g	*Pichia pastoris* GS115	Beechwood xylan	1.82 mM min^{-1} mg^{-1}	101.91 mM	1941.43 s^{-1}	–	70 °C	pH 4.0–7.0	Stable below 50 °C, with 62.5 % of residual activity after 24 h; 85% of loss after 30 min at 70 °C	–	(Kim et al., 2014)
Myceliophthora thermophila C1	Xyl1 (Xyn10A)	*Myceliophthora thermophila* C1	Birch glucuronoxylan	–	–	43 s^{-1}	–	65–70 °C	pH 5.5–6.0	No loss after 1 h at 50 °C (pH 5.0 or 7.0) and more than 80 % of activity at 60 °C	> 60 % activity at pH 8.5	(Ustinov et al., 2008; van Gool et al., 2013)
			Beech glucuronoxylan			44 s^{-1}						
			Oat arabinoxylan			63 s^{-1}						
			Wheat arabinoxylan			55 s^{-1}						
	Xyl3 (Xyn10B)		Birch glucuronoxylan	–	–	28 s^{-1}	–	80–85 °C	pH 6.0–6.5	No loss after 1 h at 50 °C (pH 5.0 or 7.0) and more than 90% of activity at 60 °C		
			Beech glucuronoxylan			34 s^{-1}						
			Oat arabinoxylan			45 s^{-1}						
			Wheat arabinoxylan			37 s^{-1}						
Aspergillus terete BCC129	BCC129 xylanase	*Pichia pastoris* KM71	Birchwood xylan	757 ± 14.54 U mg^{-1}	4.8 ± 0.07 mg mL^{-1}	–	–	60 °C	pH 5.0	90 and 50 % of activity after 20 and 30 min, respectively, at 60 °C; complete inactivation after 10 min at 70 and 80 °C	> 80 % of residual activity after 4 h at pH 4.0–10.0 (at 40 °C)	(Chantasingh et al., 2006)
Talaromyces leycettanus JCM12802	TlXyn10A	*Pichia pastoris* GS115	Birchwood xylan	2542 ± 22 U mg^{-1}	1.01 ± 0.05 mg mL^{-1}	–	1626 ± 81 mL s^{-1} mg^{-1}	80 °C	pH 4.5	81.7%, 74.8 % and 58.2 % of activity after 1 h at 85, 90 and 95 °C, respectively	> 80 % of residual activity after 1 h at pH 2.0–8.0 (at 37 °C)	(Wang et al., 2016)
Malbranchea pulchella	MpXyn10A	*Aspergillus nidulans* A773	Birchwood xylan	82 U mg^{-1}	4.6 mg mL^{-1}	748 s^{-1}	162.6 mL mg^{-1} s^{-1}	80 °C	pH 5.5	About 85 % activity after 24 h at 65 °C; 80 % after 1 h at 70 °C	–	(Ribeiro et al., 2014)
Penicillium funiculosum	XynD	*Pichia pastoris* X-33	Wheat LVAX[c]	–	3.7 ± 0.2 mg mL^{-1}	399 s^{-1}	108 s^{-1} mg^{-1} mL	80 °C	pH 4.0–5.5	No loss after 1 h at 70 °C; lost of about 80 % activity after 10 min at 80 °C	–	(Lafond et al., 2011)
Humicola insolens Y1	XynW	–	Birchwood xylan	311.8 U mg^{-1}	2.8 mM	213.1 min^{-1}	–	70 °C	pH 6.0	Stable after 1 h at 50 °C	> 90 % of residual activity after 1 h at pH 5.0–10.0 (at 37 °C)	(Du et al., 2013)
	XynA	*Pichia pastoris* GS115		974.4 U mg^{-1}	1.6 mM	654.5 min^{-1}		80 °C	pH 6.0	Stable after 1 h at 60 °C		
	XynB				1.1 mM			70 °C	pH 7.0			

(*continued on next page*)

Table 3 (*continued*)

Source Organism	Protein name	Expression System	Substrate	V_{max}	K_M	*kcat*	*kcat*/K_M	Optimal T	Optimal pH	Thermal stability	pH stability	Ref
Bispora sp. MEY-1	XynC	*Pichia pastoris* GS115	Oat spelt xylan	306.8 U mg^{-1}	2.1 mM	198.4 min^{-1}	–	85 °C	pH 4.5–5.0	No loss after 1 h at 80 °C ($t_{1/2}$ = 45 h); more than 87% of residual activity after 10 min at 90 °C	> 80 % of residual activity after 1 h at pH 1.5–6.0 (at 37 °C)	(Luo et al., 2009)
			Birchwood xylan	287.7 U mg^{-1}		196.1 min^{-1}						
	XYL10C		Oat spelt xylan	23,728 U mg^{-1}	0.98 mg mL^{-1}							
			Birchwood xylan	18,744 U mg^{-1}	1.27 mg mL^{-1}							
Phanerochaete chrysosporium RP78	XynA	*Aspergillus niger* N593	Birchwood xylan	–	3.42 ± 0.69 mg mL^{-1}	–	–	70 °C	pH 4.5	No significant loss after 30 min at 60 °C; complete inactivation at 70 °C	No significant loss after 2 h at pH 3.0–8.0 (at 30 °C)	(Decelle et al., 2004)
	XynC				3.71 ± 0.69 mg mL^{-1}							
Thermoascus Aurantiacus CBMAI 756	Xylanase	–	Birchwood arabinoxylan	–	–	–	–	75 °C	pH 5.0	About 80 % activity after 1 h at 40–70 °C; 18% at 75 °C	About 90 % of residual activity after 24 h at pH 4.0–10.0; 62% at pH 3.5; 44% at pH 10.5 (at 25 °C)	(Oliveira et al., 2010)
Trichoderma sp. K9301	EX1	–	Oat spelt xylan	10.8 x 10^5 M min^{-1} mg^{-1}	20.0 mM	12.8 × 10^6 s^{-1}	6.41 × 10^5 L $mmol^{-1}s^{-1}$	70 °C	pH 5.5	> 50 % of residual activity after 48 h at 50 and 60 °C	> 80 % activity after 1 h at pH 4.0–9.0 (at room temperature)	(Chen et al., 2009)
			Beechwood xylan	7.14 x 10^5 M min^{-1} mg^{-1}	4.47 mM	8.47 × 10^6 s^{-1}	19 × 10^5 L $mmol^{-1}$ s^{-1}					
			Birchwood xylan	7.94 x 10^5 M min^{-1} mg^{-1}	8.87 mM	9.41 × 10^6 s^{-1}	10.6 × 10^5 L $mmol^{-1}s^{-1}$					
Aspergillus nidulans KK-99	Xylanase	–	Birchwood xylan	–	–	–	–	55 °C	pH 8.0	–	> 80 % activity after 1 h at pH 4.0–9.5 (at 55 °C)	(Taneja et al., 2002)

[a] Kinetic parameters determined at 50 °C.

[b] Kinetic parameters determined at 80 °C.

[c] Low-viscosity arabinoxylan.

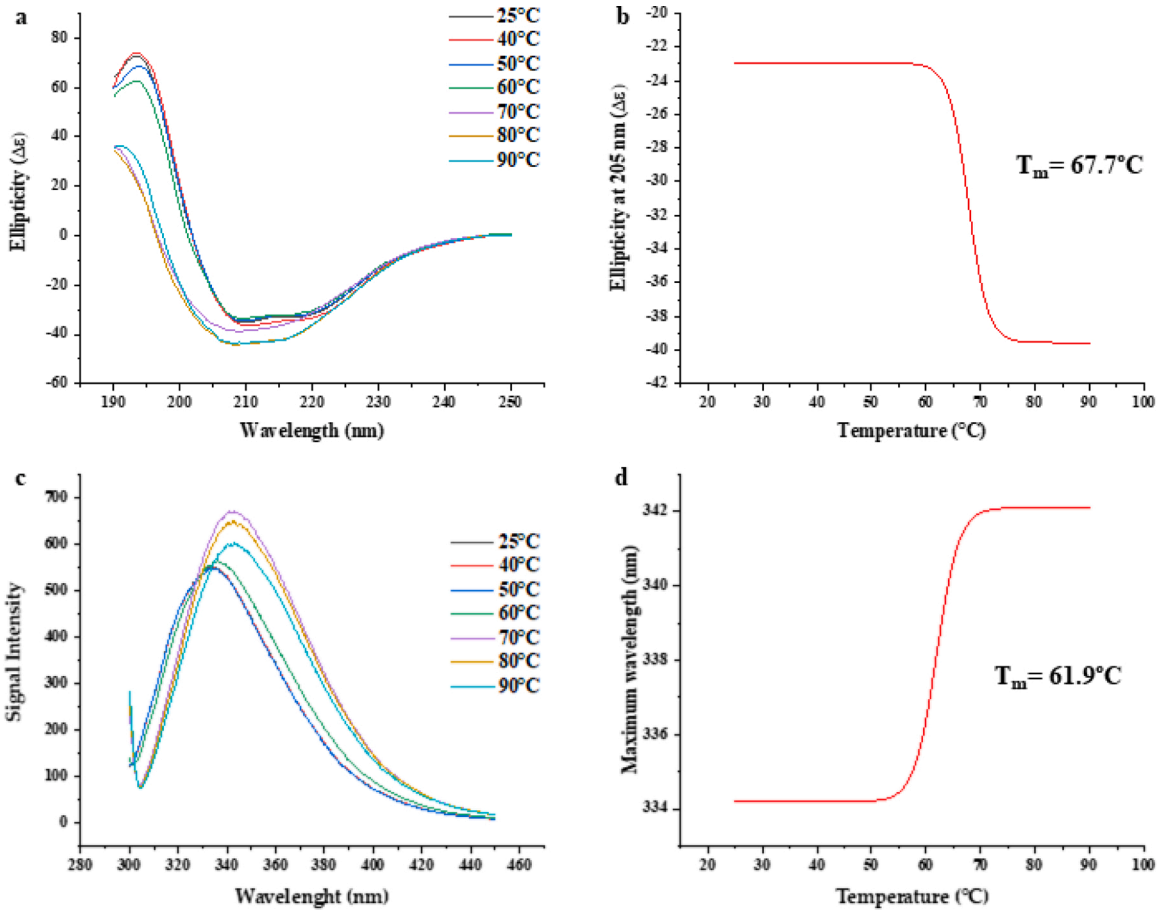

Fig. 3. Far-UV Circular Dichroism (CD) (top) and Intrinsic Tryptophan Fluorescence Emission (ITFE) (bottom) analysis of *Af*-XylA. Spectra obtained after incubation for 30 min at temperatures from 25 to 90 °C (a and c). The apparent melting temperature T_{mapp} was obtained by the first derivative of (b) ellipticity registered at 205 nm for CD X temperature; and (d) maximum wavelength values from ITFE X temperature plot. Ellipticity and signal intensity values were obtained with 0.0065 mg mL^{-1} *Af*-XylA samples in 20 mM sodium phosphate buffer (pH = 7.4) and 0.1-cm quartz cuvette for CD and 1.0-cm quartz cuvette for ITFE. The mean spectra for each condition were normalized by subtracting the buffer spectrum.

zymogram to investigate the ability of this enzyme to hydrolyze the xylan (0.5 % (w/v)) incorporated into a polyacrylamide gel. Indeed, after staining the gel with Congo Red and then de-staining with NaCl, a pale red band corresponding to the halo of substrate degradation emerged (Supplementary Fig. 3).

3.3. pH and Temperature profiles of Af-XYLA

We investigated the pH- and temperature-dependence of *Af*-XYLA activity. With beechwood xylan as substrate, the recombinant xylanase presented the highest activity at pH ranging from 5.0 to 7.0; the enzyme retained about 80 % of this activity at pH 4.0 and 8.0. In more acidic condition (pH 3.0), the enzyme lost almost all the activity—only about 20 % activity remained (Fig. 2a). We observed a similar profile when we assessed the recombinant enzyme stability by pre-incubating it at pH ranging from 3.0 to 8.0 in the absence of its substrate. After 72 h at pH 4.0–8.0 and pH 3.0, the residual activity was about 80 % and 53 %, respectively (Fig. 2c). Most fungal GH10 xylanases have optimal activity in acidic-neutral pH range (4.0–7.0). The exception is the enzyme from *Aspergillus nidulans* KK-99, which performs better in alkaline environment (pH 8.0) (Table 3).

The optimal temperature for xylan enzymatic catalysis was 80 °C (Fig. 2b). Even at 90 °C, a more extreme temperature, the enzyme maintained 73 % of its initial activity. In contrast, the *Af*-XYLA pre-incubated at these temperatures in the absence of its substrate became completely inactivated after 30 min (Fig. 2d). The main reason might have been the stabilizing effect caused by the substrate on the enzyme structure (Chang et al., 2017). Similar effects were observed for a GH10 xylanase from *T. flexuosa* (XYN10A) (Anbarasan et al., 2010) and for a GH11 xylanase from *T. lanuginosus* (Xiong et al., 2004), especially under more acidic conditions: both exhibited higher stability in the presence of substrate in a pH-dependent manner. The molecular mechanism behind this protective effect is still unclear, but a possible explanation is the conformational changes caused by substrate binding to the enzyme active site (Anbarasan et al., 2010; Lejeune et al., 2001; Xiong et al., 2004).

After pre-incubation at 50 °C for 24 h, the enzyme lost 40 % of its activity, but remained stable for the next 48 h (Fig. 2e).

The best conditions for *Af*-XYLA activity were consistent with the best conditions reported for many xylanases, but only a limited number of enzymes showed optimal activity at temperatures as high as 80 °C (Luo et al., 2009; Shibata et al., 2017; van Gool et al., 2013). Only two GH xylanases: Xyn10B from *Myceliophthora thermophila* C1 and XYL10C from *Bispora* sp. MEY-1 have higher optimal temperature (85 °C) than *Af*-XYLA, as shown in Table 3.

Different spectroscopy methods can be used to characterize the secondary structure of enzymes and their conformational changes under different conditions, providing valuable information about their properties (Ariaeenejad et al., 2019; Kishore et al., 2012). Analysis of the secondary structure by Far-UV CD (Fig. 3a) reinforced that *Af*-XYLA is a thermostable enzyme that can maintain its local conformations from 25 to 60 °C after heating for 30 min. At 70 °C, the spectrum of the enzyme

changed considerably, indicating that a structural transition occurred. The maximum peak at 190 nm and the minimum peaks at 208 and 222 nm decreased, pointing to α-helix content loss, and the spectrum shifted toward 200 nm, suggesting tendency to denaturation (Banerjee and Sheet, 2017; Crooks et al., 2011; Wallace and Janes, 2009). At 80 and 90 °C, these changes also took place, on a larger scale.

These results corroborated the previous ones: at 30 min, the residual activities were above 60 % from 40 to 60 °C; almost 50 % at 70 °C; and almost depleted at 80 and 90 °C. In fact, from 60 to 90 °C, the α-helix content decreased drastically to 11.9 %, whereas parallel β-strands, turns, and disordered/other structures increased slightly to 5.4 %, 12.8 %, and 43.7 %, respectively; antiparallel β-strands did not change significantly (Supplementary Table 1).

On the basis of the CD results, the melting temperature (T_m) value was 67.7 °C, and two well-defined stages were evident: native (25–60 °C) and denatured (80–90 °C) (Fig. 3b). For comparison, literature values based on CD are T_m of 58.1 °C (20 mM citrate buffer, pH = 5.0) for Xylanase II from *Trichoderma reesei* (López and Estrada, 2014), 45.2 °C (20 mM phosphate buffer, pH = 6.0 in the presence of 2.5 M urea) for BCX from *Bacillus circulans* (Shah et al., 2017), and 57.4 °C (20 mM phosphate buffer, pH = 6.5) for XynA from *Bacillus subtilis* (Alponti et al., 2016).

The elevated T_m value of *Af*-XYLA was expected because the three disulfide bonds in its structure should make it more resistant to conformational changes. The presence of disulfide bonds, especially at the N or C terminus or in the α-helix regions, is one of the major factors for increased thermal stability (Fan et al., 2020; Kumar et al., 2018; Li et al., 2019a; Takita et al., 2019).

The presence of 12 tryptophan residues made *Af*-XYLA more sensitive to Intrinsic Tryptophan Fluorescence Emission (ITFE) analysis (Fig. 3c). As in the case of CD, heating the enzyme from 25 to 60 °C did not elicit significant changes, showing that the polarity of the tryptophan residues did not change, either. On the other hand, from 60 to 70 °C, a red shift was evident, indicating transition and more exposure of the tryptophan residues to the polar solvent, which triggered a relaxation of the excitation, as evidenced by decreasing energy of the fluorescence emission–the maximum wavelength (λ_{max}) shifted from 336.4 to 342.2 nm (Supplementary Table 2) (Ghisaidoobe and Chung, 2014; Jayme et al., 2018; Lakowicz, 2013; Sindrewicz et al., 2019). At 80 and 90 °C, there were no marked shifts, but the intensities decreased due to higher exposure.

On the basis of the ITFE data, we determined T_m (Fig. 3d) as 61.9 °C, whilst Xylanase II has T_m of 56.3 °C (López and Estrada, 2014), *Au*Xyn11A from *Aspergillus usamii* has T_m of 57.6 °C (20 mM phosphate buffer, pH = 6.5) (Zhang et al., 2014), and *Ao*Xyn11A from *Aspergillus oryzae* has T_m of 52.3 °C (50 mM phosphate/citric acid buffer, pH = 5.5) (Li et al., 2017). These values reinforced that *Af*-XYLA has great thermostability due to its superior T_m, which is supposed to be above 60 °C as indicated by the CD and ITFE techniques.

Given that enzymes need to be exposed to extreme conditions during several industrial processes, one of the most desired properties is enzymatic stability to high temperatures and pH values (Liu et al., 2015; Pellegrini et al., 2015; Wang et al., 2019). Performing biomass saccharification at elevated temperatures is advantageous in many ways; e.g., it reduces polyssacharide viscosity and bacterial contamination risks (Moroz et al., 2015) and enables the enzyme to be directly used after steam pre-treatment, which saves time and energy and reduces the amount of enzyme required during the process (Karnaouri et al., 2014b; Shibata et al., 2017).

3.4. Effect of additives and reaction products on Af-XYLA activity

During industrial processes, GH10 xylanases can be affected by metal ions and other chemicals that may be present as additives in reaction mixtures and which can cause equipment corrosion (Li et al., 2019a; Pereira et al., 2017). Therefore, elucidating which ions or chemicals are inert or influence *Af*-XYLA activity positively/negatively is important (Table 4).

Table 4
Effect of different additives on *Af*-XYLA activity.

Additive	Relative Activity (%)	Additive	Relative Activity (%)
None	100.0 ± 0.8	$MgSO_4$	100.3 ± 0.3
SDS	44.4 ± 2.9	$AgNO_3$	0
Tween20	128.4 ± 4.2	$CoCl_2$	92.4 ± 2.0
EDTA	92.5 ± 1.3	$MnCl_2$	100.7 ± 3.0
β-mercaptoethanol	132.5 ± 1.3	$(NH_4)_2SO_4$	94.6 ± 0.2
DMSO	104.7 ± 3.8	$CaCl_2$	96.4 ± 0.4
Ascorbic acid	93.0 ± 0.7	KCl	106.1 ± 1.8
$CuSO_4$	50.7 ± 1.1	DTT	144.5 ± 3.5
$FeSO_4$	53.4 ± 1.7	Triton X-100	111.2 ± 0.2
$ZnSO_4$	64.8 ± 0.9	SLS	108.2 ± 1.2

EDTA, a chelating agent, does not affect *Af*-XYLA activity (92.5 %), so it has been suggested that this enzyme is not a metalloprotein (Benhmad et al., 2016). Both β-mercaptoethanol and DTT reducing agents stimulate *Af*-XYLA activity (132.5 % and 144.5 %, respectively), indicating that the sulfhydryl groups of free cysteine residues (i.e., not involved in disulfide bonds) are positive for enzymatic activity (Karnchanatat et al., 2008).

The surfactants tested herein had distinct effects on *Af*-XYLA activity. When we exposed the enzyme to SDS, an anionic surfactant, the enzymatic activity decreased to 44.4 %, as expected, because SDS is a well-known strong protein denaturant (Zhou et al., 2011). In contrast, *Af*-XYLA exposure to SLS and non-anionic surfactants (Triton X-100 and Tween 20), gave relative activities of 108.2 %, 111.2 %, and 128.4 %, respectively. Tolerance to these reagents is an industrially relevant feature because many surfactants are applied in biomass saccharification processes to avoid non-productive adsorption of enzymes onto lignin during hydrolysis (Li et al., 2016; Rocha-Martín et al., 2017).

The addition of K^+, NH_4^+, Co^{2+}, Ca^{2+}, Mn^{2+}, or Mg^{2+} did not affect *Af*-XYLA activity, but the addition of Cu^{2+}, Zn^{2+}, or Fe^{2+} reduced enzymatic activity to 50.7 %, 64.8 %, and 53.4 %, respectively. Cupric ions are known for strongly inhibiting xylanases because they catalyze the auto-oxidation of cysteines in disulfide bonds, to form sulfenic acid (Chen et al., 2019b; Maitan-Alfenas et al., 2016). Similarly, Fe^{2+} ions have been reported to affect other xylanases from *Aspergillus* sp. negatively because they oxidize the indole ring and interact with the amino acid residues present in the catalytic site of the enzymes (Chen et al., 2019b).

Bivalent cations such as Ca^{2+} and Mg^{2+} can act as activators by helping to stabilize the enzyme-substrate complex of some GH10 xylanases (Haq and Akram, 2019; Li et al., 2019a; Liew et al., 2019). For example, 2 mM Ca^{2+} or 5 mM Mg^{2+} enhances the activity of XynBCA from *Caldicoprobacter algeriensis* (relative activity > 120 %) (Mhiri et al., 2020). Likewise, Ca^{2+}improves both the stability and activity (~450 %) of Xyn10A from *Thermotoga thermarum* (Shi et al., 2013) and the activity of TnXynB from *Thermotoga naphthophila* RKU-10 (136 %) (Haq and Akram, 2019). However, these ions did not affect *Af*-XYLA.

Finally, $AgNO_3$ completely inhibited the enzyme. The theoretical reason for heavy metals, such as Ag and Hg, inhibiting the enzyme is their strong affinity for reduced sulfhydryl and other reactive groups like $CONH_2$, NH_2, COOH, and PO_4 (Liew et al., 2019; Meleiro et al., 2018; Narra et al., 2014).

As lignocellulose hydrolysis proceeds, it releases increasing amounts of compounds originating from lignocellulose degradation. These compounds accumulate in the reaction medium, which can affect the catalytic efficiency of xylanases and other CAZymes (Chen et al., 2019a). Particularly, products generated from the activities of xylanases and cellulases (e.g., xylose, xylitol, glucose, and cellobiose) and sugar fermentation (ethanol) can inhibit the action of hydrolases, preventing high final yields to be achieved at low cost (Chen et al., 2019a; Maulana Hidayatullah et al., 2020; Meleiro et al., 2018; Zou et al., 2021). Thus,

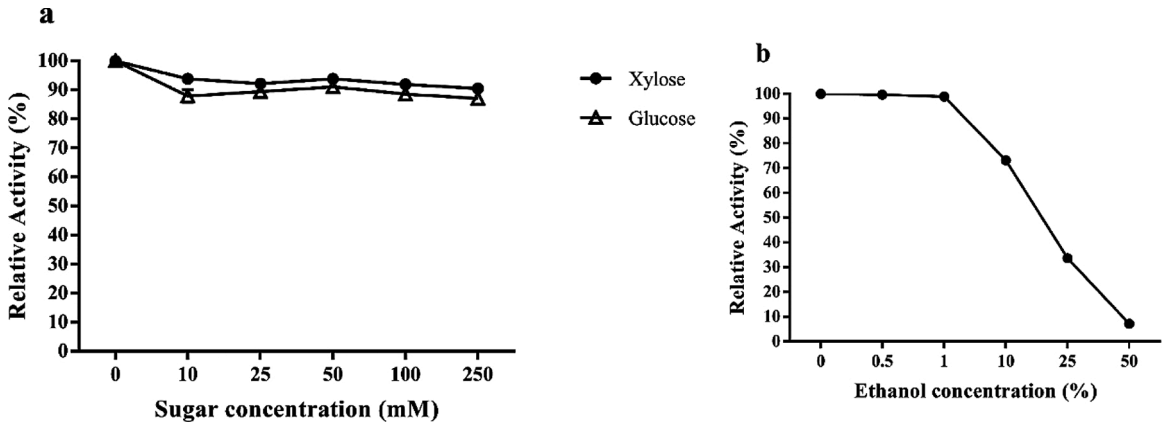

Fig. 4. (a) Monosaccharide and (b) ethanol effects on *Af*-XYLA activity.

Table 5
Af-XYLA relative activities on Beechwood xylan, Tamarind xyloglucan, Low viscosity CM-Cellulose, and Avicel® PH-101.

Substrate	Relative activity (%)
Beechwood xylan	100.0 ± 0.4
Tamarind xyloglucan	3.1 ± 0.06
Low viscosity CM-Cellulose	ND
Avicel® PH-101	ND

ND: Not detectable.

tolerance to inhibition by these hydrolysis-fermentation products is essential for efficient and economical application of enzymes in industrial biomass-converting processes (Meleiro et al., 2018). In this sense, investigating the effects of the end-products D-xylose, D-glucose, and ethanol on *Af*-XYLA activity during xylan degradation is crucial in our quest to elucidate the properties of this enzyme.

We added increasing concentrations of the aforementioned monosaccharides (10–250 mM) and ethanol (0.5–50 % (*v/v*)) individually to the reactions, and we measured the relative *Af*-XYLA activity as compared to the control system (Fig. 4).

Xylose and glucose at 10 mM inhibited xylanase activity by approximately 10 %. Regardless of this slight decline, higher sugar concentrations did not elicit any loss, and the enzyme remained surprisingly stable up to 250 mM.

Ethanol decreased *Af*-XYLA activity more markedly. At 1%, ethanol did not exert any effect; in the presence of 10 % ethanol, the enzyme retained 73 % of its maximum activity. However, the enzymatic activity dropped to 34 and 7% in the presence of 25 and 50 % ethanol, respectively. Hack & Akram (2019) reported a more ethanol-resistant GH10 xylanase from *Thermotoga naphthophila* RKU-10A (TnXynB), which displayed >45 % of activity at 50 % ethanol (*v/v*) (Haq and Akram, 2019). On the other hand, *Af*-XYLA was more tolerant to ethanol than Xyn11−1 (Wang et al., 2017) and XynAHJ3 (Zhou et al., 2012), which presented relative activities of 59.8 % and 44.2 %, respectively, in the presence of 10 % ethanol.

3.5. Substrate specificity and kinetic parameters

When we evaluated *Af*-XYLA specificity for other substrates besides xylan, we did not detect any activity (Table 5). In fact, most GH10 xylanases are enzymes without reported cellulase activity (Wang et al., 2019).

Nevertheless, the enzyme was substantially active toward beechwood xylan, as evidenced by the kinetic parameters (Table 3). At 50 °C, a temperature that is commonly used in biorefineries during biomass saccharification by enzyme cocktails (Mohd Azhar et al., 2017), the V_{max} and K_M values were 35,756 ± 1279 U mg^{-1} and 1.62 ± 0.19 mg mL^{-1}, respectively. When we conducted the reaction at the optimal temperature condition (80 °C), V_{max} was even better, 88,082 ± 2639 U mg^{-1}, and K_M was 4.09 ± 0.39 mg mL^{-1}. Only one fungal GH10 xylanase has kinetic constants of the same order of magnitude as *Af*-XYLA: XYL10C from *Bispora* sp. MEY-1. Even so, its V_{max} values (23,728 U mg^{-1} for oat spelt xylan and 18,744 U mg^{-1} for birchwood xylan) were far from those obtained for the recombinant enzyme from *A. fumigatus*.

The low K_M values of *Af*-XYLA meant that small amounts of substrate were required to saturate the enzyme. On the other hand, the high values for the k_{cat}/K_M ratio highlighted its remarkable catalytic efficiency in converting xylan (Uday et al., 2017).

Stability to operational conditions and catalytic performance are the most important characteristics to consider when selecting an enzyme for industrial purposes (Uday et al., 2017). Together, our results leave no doubt about the *Af*-XYLA potential for such applications. However, to overcome the barrier imposed by the recalcitrant structure of biomass and to achieve complete biomass degradation, enzymes need to be able to act synergistically with each other (Bernardi et al., 2021; Song et al., 2016).

3.6. Optimization of saccharification parameters for increased sugar yields

Enzymatic hydrolysis is a key step in lignocellulose processing to obtain bioproducts and bioenergy. Enzyme performance depends on several operational factors, including enzyme load, pH, temperature, reaction time, and substrate and surfactant concentrations. Many researchers aiming at improved reaction rates and yields have successfully applied statistical optimizations (Ben Taher et al., 2017; Das et al., 2015; Ferreira et al., 2009; Pandiyan et al., 2014; Sayed Jamaludin et al., 2013; Van Dyk and Pletschke, 2012).

Application of xylanases during saccharification of pre-treated biomass improves sugar yields: these enzymes solubilize xylan, thus increasing the accessibility of cellulases to cellulose and the overall efficiency of the process (Chen et al., 2019a; Ferreira et al., 2009; Uday et al., 2017). Furthermore, we have previously reported that Tween 20 positively affects *Af*-XYLA activity. In fact, the addition of surfactants benefits biomass saccharification and has thus been a target factor in DoE optimization studies (Ben Taher et al., 2017; Das et al., 2015; Ferreira et al., 2009; Noratiqah et al., 2013).

We used a CCRD 2^3 statistical approach to investigate how *Af*-XYLA behaves during hydrolysis of pre-treated SEB or SDB and to determine the optimal concentration of this enzyme (μg/g substrate) and the optimal values of the parameters Celluclast® 1.5 L load (FPU/g substrate) and Tween 20 (% (v/v)) for maximum release of reducing sugars.

The design matrixes consisted of 19 experiments, with eight factorial points, six axial points, and five repetitions at the central point (0) (Table 6).

Table 6
CCR Design matrix and experimental values for optimization of SEB and SDB hydrolyses.

Run	A- Tween 20 (% v/v)	B-Celluclast® 1.5 L (FPU/g)	C- *Af*-XYLA (μg/g)	Reducing sugars (%) SEB hydrolysis	Reducing sugars (%) SDB hydrolysis
1	−1	−1	−1	2.99	19.42
2	1	−1	−1	4.36	21.78
3	−1	1	−1	4.43	32.87
4	1	1	−1	5.79	28.61
5	−1	−1	1	3.21	23.34
6	1	−1	1	4.66	24.31
7	−1	1	1	5.11	35.36
8	1	1	1	6.49	39.43
9	−1.68	0	0	2.20	26.90
10	1.68	0	0	5.52	27.91
11	0	−1.68	0	3.02	16.67
12	0	1.68	0	5.69	36.29
13	0	0	−1.68	1.56	6.97
14	0	0	1.68	5.74	28.65
15	0	0	0	5.27	29.07
16	0	0	0	5.57	31.75
17	0	0	0	5.75	29.50
18	0	0	0	5.75	28.29
19	0	0	0	5.78	28.49

3.6.1. *Sugarcane exploded bagasse (SEB) hydrolysis optimization*

The quadratic polynomial that described the relationship between the three independent variables and the yield of reducing sugars (%) from SEB hydrolysis is shown in Eq. 2.

$$Y = 5.554868 + 0.816200\ A + 0.811017\ B + 0.652783\ C - 0.008725\ AB + 0.012602\ AC + 0.109543\ BC - 0.444636\ A^2 - 0.268779\ B^2 - 0.520199\ C^2 \quad (2)$$

A Pareto chart allows the effects of each individual parameter and their interactions to be visualized (Fig. 5). *P* values less than 0.01 suggest model terms are significant, so we can conclude that the linear effects of the three independent variables were positive and significant, indicating that all of them were critical to the success of the hydrolysis reaction.

We attested the statistical significance of the mathematical model by Fisher's *F*-test. ANOVA is given in Table 7. We checked the fit of the model by coefficient of determination ($R^2 > 0.75$ indicates the model is apt) (Ferreira et al., 2009).

The regression was significant, as evidenced by the F-test, which gave a calculated F value higher than 5.064 (*F*-critical value), while lack of fit was not significant ($F < 27.345$). These statistical results ensured that the model is adequate to predict the percentage of reducing sugars released under any sets of combination of the variables.

Fig. 6 represents the 3D response surface plots of two independent variables; the remaining variables are fixed at their respective zero levels. The maximal response (6.7 % or 67 mg g^{-1}) was predicted to be reached under the following conditions: 3.75 μg g^{-1} xylanase, 1.8 FPU g^{-1} Celluclast®1.5 L, and 0.75 % (*v/v*) Tween 20. We validated the predictions by conducting SEB hydrolysis under the aforementioned optimal values in a quadruplicate experiment. The actual response was 7.1 % (71 mg g^{-1}), which agreed well with the predicted response.

3.6.2. *Sugarcane delignified bagasse (SDB) hydrolysis optimization*

The quadratic polynomial that described the relationship between the three independent variables and the yield of reducing sugars (%) from SDB hydrolysis is shown in Eq. 3.

$$Y = 29.19930 + 0.35432\ A + 5.89137\ B + 4.11533\ C - 0.44108\ AB + 0.86762\ AC + 0.85793\ BC + 0.28154\ A^2 - 0.04819\ B^2 - 3.11881\ C^2 \quad (3)$$

Moreover, the Pareto chart in Fig. 7 provides a better view of the effects of the parameters. Both xylanase and cellulase loadings had positive and significant linear effects on the response. In contrast to our previous observation for SEB, addition of Tween 20 did not affect the

Table 7
Analysis of variance (ANOVA) for the fitted second-order model that describes release of reducing sugars from SEB as a function of independent variables.

Source of variation	Degree of Freedom	Sum of Squares	Mean Square	*F*-value	*F*-critical (α = 0.01)
Regression	5	28.01391	5.602782	9.9482929	5.064
Residual	12	6.75828	0.5631903		
Lack of fit	9	6.59535	0.732817	13.4931	27.345
Pure error	3	0.16293	0.054310		
Total	17	34.77219			

$R^2 = 0.81$.
Adj $R^2 = 0.72$.

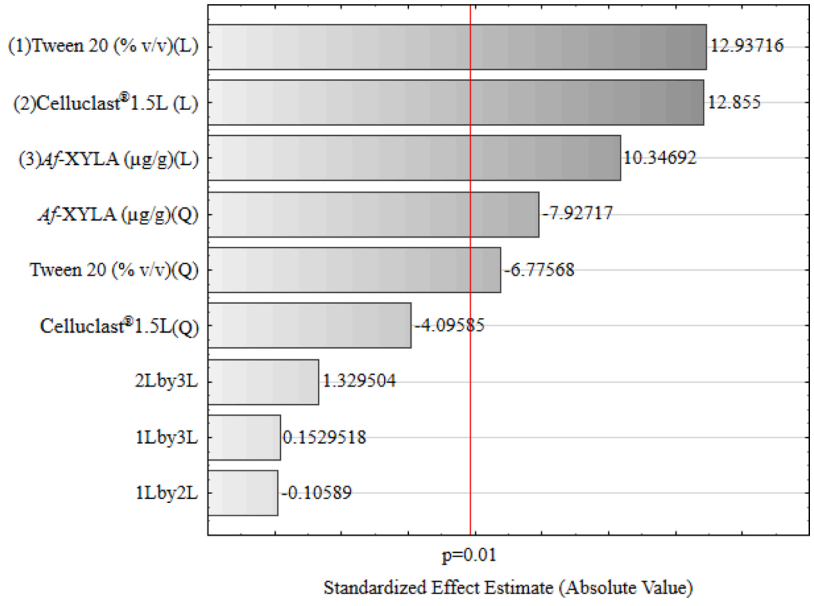

Fig. 5. Pareto chart of Standardized Effects for the yield of reducing sugars (%) from SEB hydrolysis.

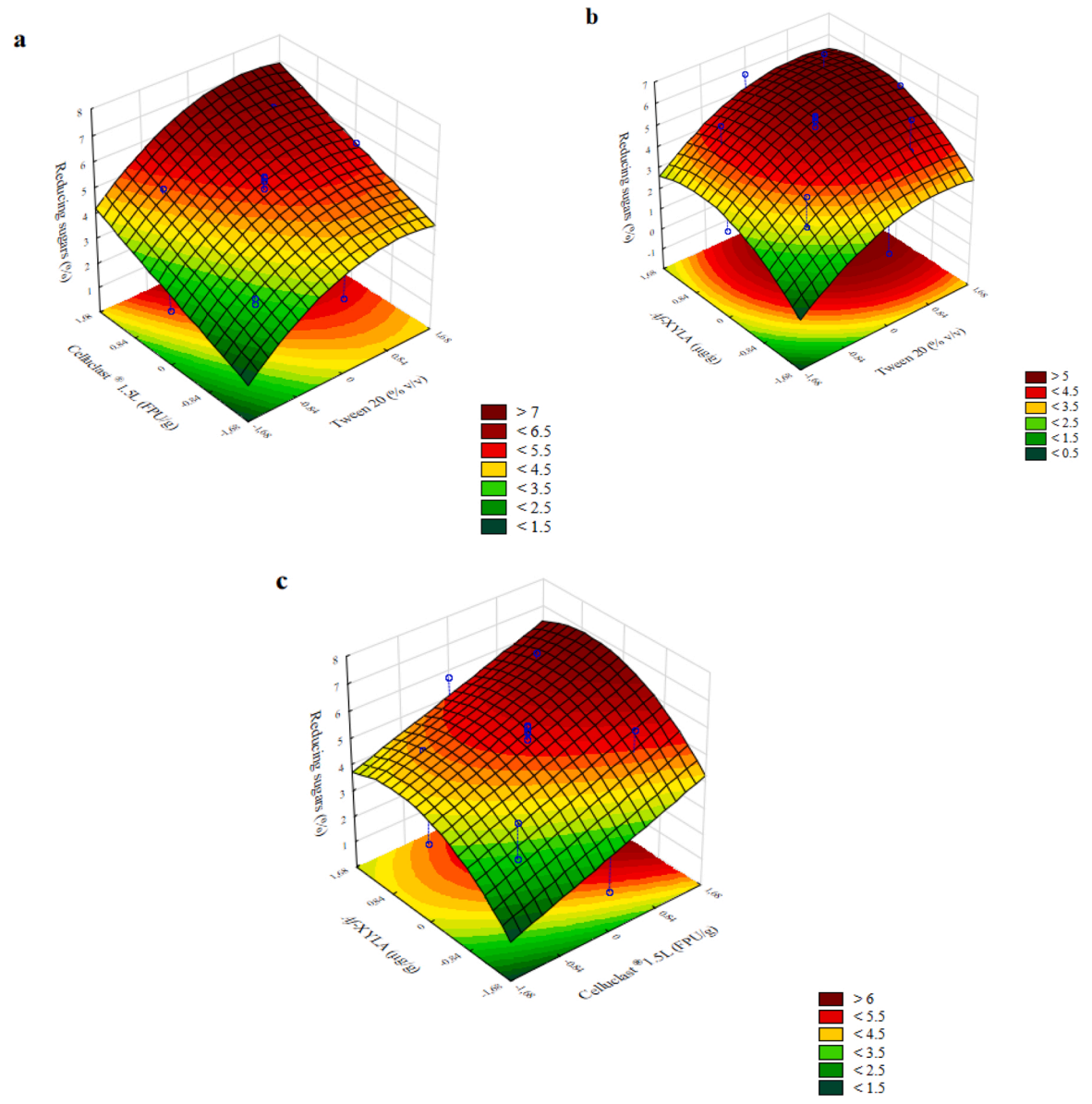

Fig. 6. 3D Response surface plots showing the effects of a) Celluclast®1.5 L and Tween 20, b) *Af*-XYLA and Tween 20, and c) *Af*-XYLA and Celluclast®1.5 L on the production of reducing sugars from SEB. The remaining variables were fixed at their zero levels.

SDB hydrolysis yields. Tween 20 assists in lignocellulose hydrolysis because it decreases non-productive adsorption of cellulases onto lignin by occupying the hydrophobic regions on the surface of these polymers (Ferreira et al., 2009). Because SDB results from a chemical pretreatment that removes the lignin fraction, Tween 20 was not even expected to have any effect on enzymatic degradation of this biomass. Supplementary Table 3 (de Gouvêa et al., 2018; Siqueira et al., 2013) compares the SEB and SDB compositions.

ANOVA is given in Table 8. The regression model proved to be significant and predictive, as indicated by the *F*-test results. Fig. 8 displays the response surface plot of the two significant factors (*Af*-XYLA and Celluclast®1.5 L loads). Maximal response (40.5 % or 405 mg g^{-1}) could be achieved with 3.75 µg g^{-1} xylanase and 1.8 FPU g^{-1} cellulases. Interestingly, we determined the same optimal values for SEB. Finally, we attested the validity of the method by performing the SDB hydrolysis with these optimal values of enzyme load, to find a reducing sugar percentage of 37.5 % (375 mg g^{-1}), which agreed well with the predicted response.

3.7. Effect of the synergistic action of enzymes on the saccharification of pre-treated sugarcane bagasses

The combined activities of cellulases and xylanases can improve the saccharification of various xylan-containing biomasses more effectively than increasing cellulase load (Chen et al., 2019a; Song et al., 2016). Therefore, we evaluated how the synergistic action between *Af*-XYLA and Celluclast® 1.5 L affected SEB and SDB depolymerization. We carried out the reactions at 50 °C and pH 6.0 for up to 48 h, and we used the optimal concentrations statistically estimated for the recombinant xylanase (3.75 µg g^{-1}) and Celluclast® 1.5 L (1.8 FPU g^{-1}). We also added 0.75 % Tween 20 (*v/v*) as additive in SEB hydrolysis.

Fig. 9 shows that the presence of *Af*-XYLA in the reactions enhanced the release of reducing sugars from both substrates in a time-dependent manner, demonstrating the high degree of synergy between the enzymes. For SEB, hydrolysis improved by about 155 % after 24 and 48 h (Fig. 9a). For SDB, saccharification was xylanase-boosted by 305 % and 277 % after 24 and 48 h, respectively (Fig. 9b). These data also

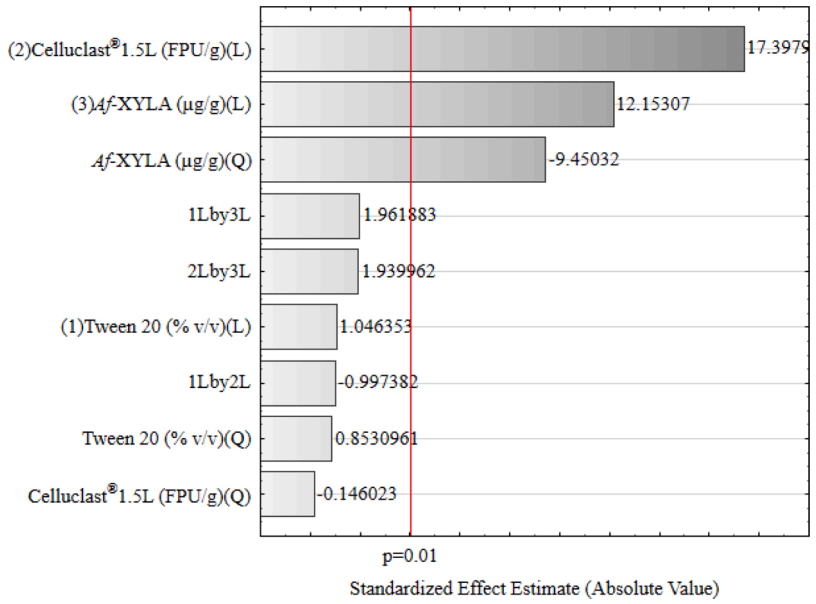

Fig. 7. Pareto chart of Standardized Effects for yields of reducing sugars yields (%) from SDB hydrolysis.

Table 8
Analysis of variance (ANOVA) for the fitted second-order model that describes the release of reducing sugars from SDB as a function of independent variables.

Source of variation	Degree of Freedom	Sum of Squares	Mean Square	*F*-value	*F*-critical (α = 0.01)
Regression	3	848.82265	282.94088	29.09564	5.292
Residual	16	155.59218	9.7245115		
Lack of fit	11	147.769	13.4336	8.5859	9.963
Pure error	5	7.823	1.5646		
Total	19	1004.415			

$R^2 = 0.85$.
Adj $R^2 = 0.82$.

reinforced the limits imposed by lignin on the recovery of sugars from biomass, evidenced by the magnitude of the difference between the scales of the graphs (Bernal-Lugo et al., 2019; Tian et al., 2017).

Numerous research works have focused on synergy studies involving xylanases and cellulases. Hu et al. (2011) reported that addition of Multifect xylanase increased the yield and extent of hydrolysis of steam-pretreated corn stover by Celluclast® 1.5 L from 45 % to 87 % (Hu et al., 2011). Similarly, hydrolysis of pre-treated corn stover performed by cooperative action of XynA (a xylanase from *Bacillus* sp.) and Celluclast® 1.5 L resulted in higher production of reducing sugars when compared to the cocktail alone: increases of 48.7 % and 77.6 % were respectively obtained with 2 and 4 U_{BirWX} of XynA (Wang et al., 2019). Both xylanases MYCTH_56237 and MYCTH_49824 from *Myceliophthora thermophila* also cooperated synergistically with Celluclast®1.5 L,

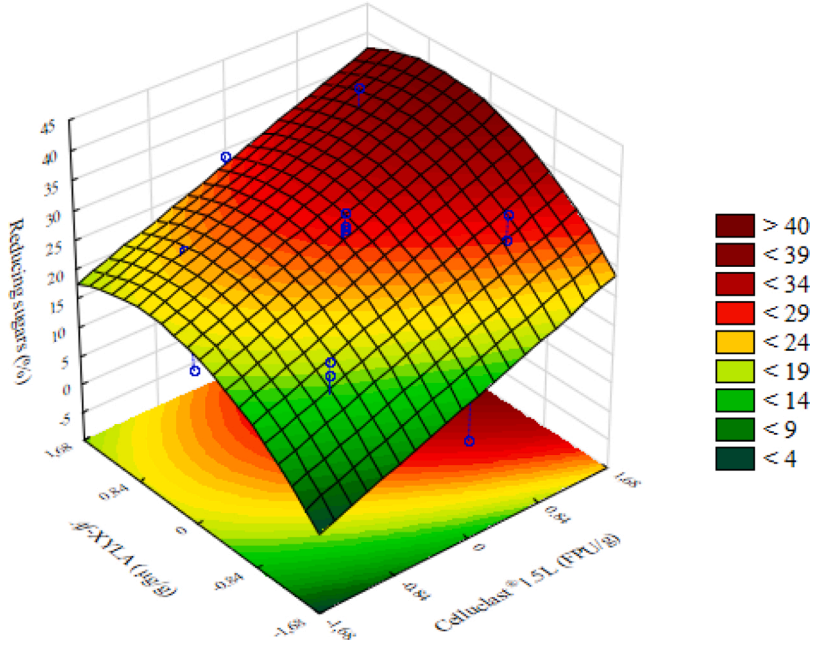

Fig. 8. 3D response surface plot showing the effects of Celluclast®1.5 L and *Af*-XYLA on the production of reducing sugars from SDB. Tween 20 was fixed at its zero level.

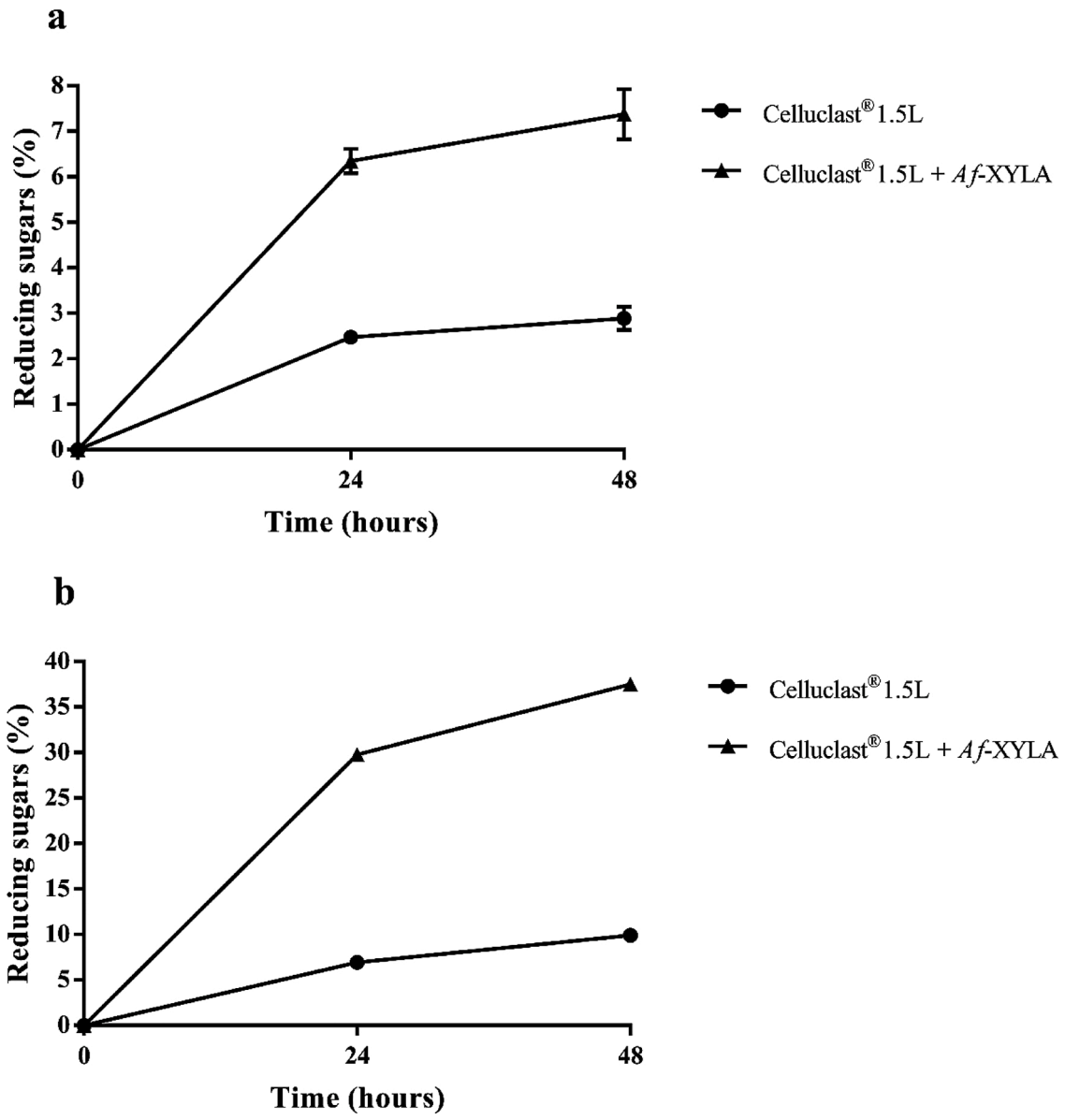

Fig. 9. Effect of synergistic action between *Af*-XYLA and Celluclast®1.5 L on the hydrolysis of a) SEB and b) SDB. All the reactions were incubated in 50 mM sodium phosphate buffer (pH 6.0) containing 1% (*w/v*) substrate at 1000 rpm and 50 °C for 24 or 48 h. The data represent the mean ± standard error obtained from at least three experimental replicates.

increasing hydrolysis of pretreated corn stover from 30 % to 50.3 and 55.6 %, respectively (Basit et al., 2018). Likewise, Song et al. (2016) observed that xylanase-cellulase co-treatment improved corncob powder, corn stover, and rice straw hydrolysis by 133 %, 164 %, and 545 %, respectively (Song et al., 2016). Together, these results evidenced the potential of applying synergistic strategies to improve the content of sugars released from biomass saccharification.

4. Conclusions

Stability to additives and operational conditions, high catalytic efficiency, and elevated degree of synergism with other CAZymes are major requirements that make a biocatalyst suitable for most industrial processes, and *Af*-XYLA met all of them. The recombinant xylanase from *A. fumigatus* displayed the best performance at 80 °C and withstood long pre-incubation at 50 °C well. Furthermore, it exhibited great activities over a wide pH range: its optimal activity was achieved at pH 5–7, but it worked with 80 % of its maximum potential at pH 4 and 8. Besides, to the best of our knowledge, *Af*-XYLA presented the best kinetic parameters among fungal GH10 xylanases. Finally, its cooperative action with Celluclast®1.5 L successfully boosted biomass saccharification rates. Together, the remarkable properties of *Af*-XYLA highlight it as a promising candidate for several biotechnological applications, from depolymerization of the plant cell wall, to obtain fermentation products, to pulp pre-bleaching in the paper industry.

Ethics approval and consent to participate

Not applicable

Consent for publication

Not applicable

Availability of data and materials

Data sharing is not applicable to this article.

Funding

This research was funded by Fundação de Amparo à Pesquisa do Estado de São Paulo (FAPESP, 2016/190950-0) and Conselho Nacional de Desenvolvimento Científico e Tecnológico (CNPq: 425465/2016-0). AVB and LEG were funded by a scholarship granted by Coordenação de Aperfeiçoamento de Pessoal de Nível Superior—Brasil (CAPES), Finance Code 001.

Authors' contributions

Conceptualization: A.V.B., L.E.G. and T.M.D.; data curation: A.V.B. and L.E.G., formal analysis: A.V.B. and L.E.G.; methodology: A.V.B.; supervision: S.A.U and T.M.D.; writing (original draft): A.V.B. and T.M.D.; writing (review and editing): A.V.B. and T.M.D.; project administration: S.A.U. and T.M.D.; funding acquisition: T.M.D. All authors have read and agreed to the published version of the manuscript.

CRediT authorship contribution statement

Aline Vianna Bernardi: Conceptualization, Data curation, Formal analysis, Methodology, Writing - original draft, Writing - review & editing. **Luis Eduardo Gerolamo:** Conceptualization, Data curation, Formal analysis. **Sergio Akira Uyemura:** Supervision, Project administration. **Taisa Magnani Dinamarco:** Conceptualization, Supervision, Writing - original draft, Writing - review & editing, Project administration, Funding acquisition.

Declaration of Competing Interest

The authors declare that they have no known competing financial interests or personal relationships that could have appeared to influence the work reported in this paper.

Acknowledgements

None.

Appendix A. Supplementary data

Supplementary material related to this article can be found, in the online version, at doi:https://doi.org/10.1016/j.indcrop.2021.113697.

References

Alponti, J.S., Fonseca Maldonado, R., Ward, R.J., 2016. Thermostabilization of *Bacillus subtilis* GH11 xylanase by surface charge engineering. Int. J. Biol. Macromol. 87, 522–528. https://doi.org/10.1016/j.ijbiomac.2016.03.003.

Anbarasan, S., Jänis, J., Paloheimo, M., Laitaoja, M., Vuolanto, M., Karimäki, J., Vainiotalo, P., Leisola, M., Turunen, O., 2010. Effect of glycosylation and additional domains on the thermostability of a family 10 xylanase produced by *thermopolyspora flexuosa*. Appl. Environ. Microbiol. 76, 356–360. https://doi.org/10.1128/AEM.00357-09.

Ariaeenejad, S., Hosseini, E., Maleki, M., Kavousi, K., Moosavi-Movahedi, A.A., Salekdeh, G.H., 2019. Identification and characterization of a novel thermostable xylanase from camel rumen metagenome. Int. J. Biol. Macromol. 126, 1295–1302. https://doi.org/10.1016/j.ijbiomac.2018.12.041.

Banerjee, R., Sheet, T., 2017. Ratio of ellipticities between 192 and 208 nm (R1): an effective electronic circular dichroism parameter for characterization of the helical components of proteins and peptides. Proteins Struct. Funct. Bioinforma. 85, 1975–1982. https://doi.org/10.1002/prot.25351.

Basit, A., Liu, J., Miao, T., Zheng, F., Rahim, K., Lou, H., Jiang, W., 2018. Characterization of two endo-β-1, 4-xylanases from *Myceliophthora thermophila* and their saccharification efficiencies, synergistic with commercial cellulase. Front. Microbiol. 9, 1–11. https://doi.org/10.3389/fmicb.2018.00233.

Ben Taher, I., Fickers, P., Chniti, S., Hassouna, M., 2017. Optimization of enzymatic hydrolysis and fermentation conditions for improved bioethanol production from potato peel residues. Biotechnol. Prog. 33, 397–406. https://doi.org/10.1002/btpr.2427.

Benhmad, I., Boudabbous, M., Yaîch, A., Rebai, M., Gargouri, A., 2016. A novel neutral, halophile *Stachybotrys microspora*-based endoglucanase active impact on β-glucan. Bioprocess Biosyst. Eng. https://doi.org/10.1007/s00449-016-1549-1.

Bernal-Lugo, I., Jacinto-Hernandez, C., Gimeno, M., Carmina Montiel, C., Rivero-Cruz, F., Velasco, O., 2019. Highly efficient single-step pretreatment to remove lignin and hemicellulose from softwood. BioResources 14, 3567–3577. https://doi.org/10.15376/biores.14.2.3567-3577.

Bernardi, A.V., Gouvêa, P.F..De, Gerolamo, L.E., Yonamine, D.K., Lourdes, L..De, Balico, D.L., Uyemura, S.A., 2018. Functional characterization of GH7 endo-1,4-β-glucanase from *Aspergillus fumigatus* and its potential industrial application. Protein Expr. Purif. 150, 1–11. https://doi.org/10.1016/j.pep.2018.04.016.

Bernardi, A.V., Yonamine, D.K., Uyemura, S.A., Dinamarco, T.M., 2019. A Thermostable *Aspergillus fumigatus* GH7 Endoglucanase Over-expressed in *Pichia pastoris* Stimulates Lignocellulosic Biomass Hydrolysis.

Bernardi, A.V., Gerolamo, L.E., Fagundes, P., Gouv, D., Yonamine, D.K., Matheus, L., Pereira, S., Henrique, A., Oliveira, C.De, Uyemura, A., Dinamarco, T.M., 2021. LPMO Af AA9 _ B and Cellobiohydrolase Af Cel6A From *A. Fumigatus* Boost Enzymatic Saccharification Activity of Cellulase Cocktail.

Carli, S., Meleiro, L.P., Rosa, J.C., Moraes, L.A.B., Jorge, J.A., Masui, D.C., Furriel, R.P. M., 2016. A novel thermostable and halotolerant xylanase from *Colletotrichum graminicola*. J. Mol. Catal., B Enzym. 133, S508–S517. https://doi.org/10.1016/j.molcatb.2017.05.002.

Chadha, B.S., Kaur, B., Basotra, N., Tsang, A., Pandey, A., 2019. Thermostable xylanases from thermophilic fungi and bacteria: current perspective. Bioresour. Technol. 277, 195–203. https://doi.org/10.1016/j.biortech.2019.01.044.

Chang, X., Xu, B., Bai, Y., Luo, H., Ma, R., Shi, P., Yao, B., 2017. Role of N-linked glycosylation in the enzymatic properties of a thermophilic GH 10 xylanase from *Aspergillus fumigatus* expressed in *Pichia pastoris*. PLoS One. https://doi.org/10.1371/journal.pone.0171111.

Chantasingh, D., Pootanakit, K., Champreda, V., Kanokratana, P., Eurwilaichitr, L., 2006. Cloning, expression, and characterization of a xylanase 10 from *Aspergillus terreus* (BCC129) in *Pichia pastoris*. Protein Expr. Purif. 46, 143–149. https://doi.org/10.1016/j.pep.2005.09.013.

Chen, L.L., Zhang, M., Zhang, D.H., Chen, X.L., Sun, C.Y., Zhou, B.C., Zhang, Y.Z., 2009. Purification and enzymatic characterization of two β-endoxylanases from *Trichoderma* sp. K9301 and their actions in xylooligosaccharide production. Bioresour. Technol. 100, 5230–5236. https://doi.org/10.1016/j.biortech.2009.05.038.

Chen, X., Xin, D., Wang, R., Qin, Y., Wen, P., Hou, X., Zhang, J., 2019a. Factors affecting hydrolytic action of xylanase during pennisetum saccharification: role of cellulose and its derivatives. Ind. Crops Prod. 130, 49–56. https://doi.org/10.1016/j.indcrop.2018.12.077.

Chen, Z., Zaky, A.A., Liu, Y., Chen, Y., Liu, L., Li, S., Jia, Y., 2019b. Purification and characterization of a new xylanase with excellent stability from *Aspergillus flavus* and its application in hydrolyzing pretreated corncobs. Protein Expr. Purif. 154, 91–97. https://doi.org/10.1016/j.pep.2018.10.006.

Couturier, M., Feliu, J., Haon, M., Navarro, D., Lesage-Meessen, L., Coutinho, P.M., Berrin, J.G., 2011. A thermostable GH45 endoglucanase from yeast: impact of its atypical multimodularity on activity. Microb. Cell Fact. 10 https://doi.org/10.1186/1475-2859-10-103.

Crooks, R.O., Rao, T., Mason, J.M., 2011. Truncation, randomization, and selection: generation of a reduced length c-jun antagonist that retains high interaction stability. J. Biol. Chem. 286, 29470–29479. https://doi.org/10.1074/jbc.M111.221267.

Das, S., Bhattacharya, A., Haldar, S., Ganguly, A., Gu, S., Ting, Y.P., Chatterjee, P.K., 2015. Optimization of enzymatic saccharification of water hyacinth biomass for bio-ethanol: comparison between artificial neural network and response surface methodology. Sustain. Mater. Technol. 3, 17–28. https://doi.org/10.1016/j.susmat.2015.01.001.

de Amo, G.S., Bezerra-Bussoli, C., da Silva, R.R., Kishi, L.T., Ferreira, H., Mariutti, R.B., Arni, R.K., Gomes, E., Bonilla-Rodriguez, G.O., 2019. Heterologous expression, purification and biochemical characterization of a new xylanase from *Myceliophthora heterothallica* F.2.1.4. Int. J. Biol. Macromol. 131, 798–805. https://doi.org/10.1016/j.ijbiomac.2019.03.108.

de Gouvêa, P.F., Bernardi, A.V., Gerolamo, L.E., de Souza Santos, E., Riaño-Pachón, D.M., Uyemura, S.A., Dinamarco, T.M., 2018. Transcriptome and secretome analysis of *Aspergillus fumigatus* in the presence of sugarcane bagasse. BMC Genomics 19. https://doi.org/10.1186/s12864-018-4627-8.

Decelle, B., Tsang, A., Storms, R.K., 2004. Cloning, functional expression and characterization of three *Phanerochaete chrysosporium* endo-1,4-β-xylanases. Curr. Genet. 46, 166–175. https://doi.org/10.1007/s00294-004-0520-x.

Du, Y., Shi, P., Huang, H., Zhang, X., Luo, H., Wang, Y., Yao, B., 2013. Characterization of three novel thermophilic xylanases from *Humicola insolens* Y1 with application potentials in the brewing industry. Bioresour. Technol. 130, 161–167. https://doi.org/10.1016/j.biortech.2012.12.067.

Evangelista, D.E., Kadowaki, M.A.S., Mello, B.L., Polikarpov, I., 2018. Biochemical and biophysical characterization of novel GH10 xylanase prospected from a sugar cane bagasse compost-derived microbial consortia. Int. J. Biol. Macromol. 109, 560–568. https://doi.org/10.1016/j.ijbiomac.2017.12.099.

Fan, G., Wu, Q., Li, Q., Sun, B., Ma, Y., Wu, K., Wang, C., Teng, C., Yang, R., Li, X., 2020. Impact of the disulfide bond on hydrolytic characteristics of a xylanase from *Talaromyces thermophiles* F1208. Int. J. Biol. Macromol. 164, 1748–1757. https://doi.org/10.1016/j.ijbiomac.2020.07.270.

Ferreira, S., Duarte, A.P., Ribeiro, M.H.L., Queiroz, J.A., Domingues, F.C., 2009. Response surface optimization of enzymatic hydrolysis of *Cistus ladanifer* and *Cytisus striatus* for bioethanol production. Biochem. Eng. J. 45, 192–200. https://doi.org/10.1016/j.bej.2009.03.012.

Ghatora, S.K., Chadha, B.S., Badhan, A.K., Saini, H.S., Bhat, M.K., 2006. Identification and characterization of diverse xylanases from thermophilic and thermotolerant fungi. BioResources 1, 18–33. https://doi.org/10.15376/biores.1.1.18-33.

Ghisaidoobe, A.B.T., Chung, S.J., 2014. Intrinsic tryptophan fluorescence in the detection and analysis of proteins: a focus on förster resonance energy transfer techniques. Int. J. Mol. Sci. 15, 22518–22538. https://doi.org/10.3390/ijms151222518.

Gouvêa, P.F.De, Gerolamo, L.E., Bernardi, A.V., Matheus, L., Pereira, S., Uyemura, S.A., Dinamarco, T.M., 2019. Lytic Polysaccharide Monooxygenase from *Aspergillus fumigatus* Can Improve Enzymatic Cocktail Activity during Sugarcane Bagasse Hydrolysis, pp. 1–9. https://doi.org/10.2174/0929866526666190228163629.

Greenberg, D.M., 1929. The colorimetric determination of the serum proteins. J. Biol. Chem. 82, 545–550. https://doi.org/10.1016/s0021-9258(20)78300-6.

Guillén, D., Sánchez, S., Rodríguez-Sanoja, R., 2010. Carbohydrate-binding domains: multiplicity of biological roles. Appl. Microbiol. Biotechnol. 85, 1241–1249. https://doi.org/10.1007/s00253-009-2331-y.

Han, N., Ma, Y., Mu, Y., Tang, X., Li, J., Huang, Z., 2019. Enhancing thermal tolerance of a fungal GH11 xylanase guided by B-factor analysis and multiple sequence alignment. Enzyme Microb. Technol. 131 https://doi.org/10.1016/j.enzmictec.2019.109422.

Haq, Iul, Akram, F., 2019. Insight into kinetics and thermodynamics of a novel hyperstable GH family 10 endo-1,4-β-xylanase (TnXynB) with broad substrates specificity cloned from *Thermotoga naphthophila*RKU-10T. Enzyme Microb. Technol. 127, 32–42. https://doi.org/10.1016/j.enzmictec.2019.04.009.

He, J., Tang, F., Chen, D., Yu, B., Luo, Y., Zheng, P., Mao, X., Yu, J., Yu, F., 2019. Design, expression and functional characterization of a thermostable xylanase from *Trichoderma reesei*. PLoS One 14, 1–13. https://doi.org/10.1371/journal.pone.0210548.

Hoffmam, Z.B., Zanphorlin, L.M., Cota, J., Diogo, J.A., Almeida, G.B., Damásio, A.R.L., Squina, F., Murakami, M.T., Ruller, R., 2016. Xylan-specific carbohydrate-binding module belonging to family 6 enhances the catalytic performance of a GH11 endo-xylanase. N. Biotechnol. 33, 467–472. https://doi.org/10.1016/j.nbt.2016.02.006.

Hu, J., Saddler, J.N., 2018. Why does GH10 xylanase have better performance than GH11 xylanase for the deconstruction of pretreated biomass? Biomass Bioenergy 110, 13–16. https://doi.org/10.1016/j.biombioe.2018.01.007.

Hu, J., Arantes, V., Saddler, J.N., 2011. The enhancement of enzymatic hydrolysis of lignocellulosic substrates by the addition of accessory enzymes such as xylanase: is it an additive or synergistic effect? Biotechnol. Biofuels 4. https://doi.org/10.1186/1754-6834-4-36.

Inoue, H., Kishishita, S., Kumagai, A., Kataoka, M., Fujii, T., Ishikawa, K., 2015. Contribution of a family 1 carbohydrate-binding module in thermostable glycoside hydrolase 10 xylanase from *Talaromyces cellulolyticus* toward synergistic enzymatic hydrolysis of lignocellulose. Biotechnol. Biofuels 8, 3–11. https://doi.org/10.1186/s13068-015-0259-2.

Jayme, C.C., Calori, I.R., Cunha, E.M.F., Tedesco, A.C., 2018. Evaluation of aluminum phthalocyanine chloride and DNA interactions for the design of an advanced drug delivery system in photodynamic therapy. Spectrochim. Acta - Part A Mol. Biomol. Spectrosc. 201, 242–248. https://doi.org/10.1016/j.saa.2018.05.009.

Joshi, N., Sharma, M., Singh, S.P., 2020. Characterization of a novel xylanase from an extreme temperature hot spring metagenome for xylooligosaccharide production. Appl. Microbiol. Biotechnol. 104, 4889–4901. https://doi.org/10.1007/s00253-020-10562-7.

Kabsch, W., Sander, C., 1983. How good are predictions of protein secondary structure? FEBS Lett. 155, 179–182.

Karnaouri, A., Topakas, E., Antonopoulou, I., Christakopoulos, P., 2014a. Genomic insights into the fungal lignocellulolytic system of *Myceliophthora thermophila*. Front. Microbiol. 5, 1–22. https://doi.org/10.3389/fmicb.2014.00281.

Karnaouri, A.C., Topakas, E., Christakopoulos, P., 2014b. Cloning, expression, and characterization of a thermostable GH7 endoglucanase from *Myceliophthora thermophila* capable of high-consistency enzymatic liquefaction. Appl. Microbiol. Biotechnol. 98, 231–242. https://doi.org/10.1007/s00253-013-4895-9.

Karnchanatat, A., Petsom, A., Sangvanich, P., Piapukiew, J., Whalley, A.J.S., Reynolds, C.D., Gadd, G.M., Sihanonth, P., 2008. A novel thermostable endoglucanase from the wood-decaying fungus *Daldinia eschscholzii* (Ehrenb.:Fr.) Rehm. Enzyme Microb. Technol. 42, 404–413. https://doi.org/10.1016/j.enzmictec.2007.11.009.

Kim, H.M., Lee, K.H., Kim, K.H., Lee, D.S., Nguyen, Q.A., Bae, H.J., 2014. Efficient function and characterization of GH10 xylanase (Xyl10g) from *Gloeophyllum trabeum* in lignocellulose degradation. J. Biotechnol. 172, 38–45. https://doi.org/10.1016/j.jbiotec.2013.12.013.

Kishore, D., Kundu, S., Kayastha, A.M., 2012. Thermal, chemical and pH induced denaturation of a multimeric β-Galactosidase reveals multiple unfolding pathways. PLoS One 7. https://doi.org/10.1371/journal.pone.0050380.

Kumar, V., Marín-Navarro, J., Shukla, P., 2016. Thermostable microbial xylanases for pulp and paper industries: trends, applications and further perspectives. World J. Microbiol. Biotechnol. 32, 1–10. https://doi.org/10.1007/s11274-015-2005-0.

Kumar, V., Dangi, A.K., Shukla, P., 2018. Engineering thermostable microbial xylanases toward its industrial applications. Mol. Biotechnol. 60, 226–235. https://doi.org/10.1007/s12033-018-0059-6.

Lafond, M., Tauzin, A., Desseaux, V., Bonnin, E., Ajandouz, E.H., Giardina, T., 2011. GH10 xylanase D from Penicillium funiculosum: biochemical studies and xylooligosaccharide production. Microb. Cell Fact. 10, 1–8. https://doi.org/10.1186/1475-2859-10-20.

Lakbub, J.C., Shipman, J.T., Desaire, H., 2018. Recent mass spectrometry-based techniques and considerations for disulfide bond characterization in proteins. Anal. Bioanal. Chem. 410, 2467–2484. https://doi.org/10.1007/s00216-017-0772-1.

Lakowicz, J.R., 2013. Principles of Fluorescence Spectroscopy. Springer Science & Business Media.

Lejeune, A., Vanhove, M., Lamotte-Brasseur, J., Pain, R.H., Frére, J.M., Matagne, A., 2001. Quantitative analysis of the stabilization by substrate of *Staphylococcus aureus* PC1 α-lactamase. Chem. Biol. 8, 831–842. https://doi.org/10.1016/S1074-5521(01)00053-9.

Li, Y., Sun, Z., Ge, X., Zhang, J., 2016. Effects of lignin and surfactant on adsorption and hydrolysis of cellulases on cellulose. Biotechnol. Biofuels 9, 0–9. https://doi.org/10.1186/s13068-016-0434-0.

Li, X.Q., Wu, Q., Hu, D., Wang, R., Liu, Y., Wu, M.C., Li, J.F., 2017. Improving the temperature characteristics and catalytic efficiency of a mesophilic xylanase from *Aspergillus oryzae*, AoXyn11A, by iterative mutagenesis based on in silico design. AMB Express 7. https://doi.org/10.1186/s13568-017-0399-9.

Li, G., Chen, X., Zhou, X., Huang, R., Li, L., Miao, Y., Liu, D., Zhang, R., 2019a. Improvement of GH10 family xylanase thermostability by introducing of an extra α-helix at the C-terminal. Biochem. Biophys. Res. Commun. 515, 417–422. https://doi.org/10.1016/j.bbrc.2019.05.163.

Li, Z., Li, X., Liu, T., Chen, S., Liu, H., Wang, H., Li, K., Song, Y., Luo, X., Zhao, J., Zhang, T., 2019b. The critical roles of exposed surface residues for the thermostability and halotolerance of a novel GH11 xylanase from the metagenomic library of a saline-alkaline soil. Int. J. Biol. Macromol. 133, 316–323. https://doi.org/10.1016/j.ijbiomac.2019.04.090.

Liew, K.J., Ngooi, C.Y., Shamsir, M.S., Sani, R.K., Chong, C.S., Goh, K.M., 2019. Heterologous expression, purification and biochemical characterization of a new endo-1,4-β-xylanase from *Rhodothermaceae bacterium* RA. Protein Expr. Purif. 164, 105464 https://doi.org/10.1016/j.pep.2019.105464.

Liu, Y., Dun, B., Shi, P., Ma, R., Luo, H., Bai, Y., Xie, X., Yao, B., 2015. A novel GH7 Endo-β-1,4-glucanase from *Neosartorya fischeri* P1 with good thermostability, broad substrate specificity and potential application in the brewing industry. PLoS One 10, 1–12. https://doi.org/10.1371/journal.pone.0137485.

Liu, Y., Sun, Y., Wang, H., Tang, L., 2019. Characterization of a novel multi-domain xylanase from *Clostridium clariflavum* with application in hydrolysis of corn cobs. Biotechnol. Lett. 41, 1177–1186. https://doi.org/10.1007/s10529-019-02721-2.

López, G., Estrada, P., 2014. Effect of Temperature on Xylanase II from *Trichoderma reesei* QM 9414: a calorimetric, catalytic, and conformational study. Enzyme Res. 2014 https://doi.org/10.1155/2014/708676.

Luo, H., Li, J., Yang, J., Wang, H., Yang, Y., Huang, H., Shi, P., Yuan, T., Fan, Y., Yao, B., 2009. A thermophilic and acid stable family-10 xylanase from the acidophilic fungus *Bispora* sp. MEY-1. Extremophiles 13, 849–857. https://doi.org/10.1007/s00792-009-0272-0.

Maitan-Alfenas, G.P., Oliveira, M.B., Nagem, R.A.P., de Vries, R.P., Guimarães, V.M., 2016. Characterization and biotechnological application of recombinant xylanases from *Aspergillus nidulans*. Int. J. Biol. Macromol. 91, 60–67. https://doi.org/10.1016/j.ijbiomac.2016.05.065.

Malgas, S., Pletschke, B.I., 2019. The effect of an oligosaccharide reducing-end xylanase, BhRex8A, on the synergistic degradation of xylan backbones by an optimised xylanolytic enzyme cocktail. Enzyme Microb. Technol. https://doi.org/10.1016/j.enzmictec.2018.12.010.

Mathibe, B.N., Malgas, S., Radosavljevic, L., Kumar, V., Shukla, P., Pletschke, B.I., 2020. Tryptic mapping based structural insights of endo-1, 4-β-Xylanase from *Thermomyces lanuginosus* VAPS-24. Indian J. Microbiol. 60, 392–395. https://doi.org/10.1007/s12088-020-00879-2.

Maulana Hidayatullah, I., Setiadi, T., Tri Ari Penia Kresnowati, M., Boopathy, R., 2020. Xylanase inhibition by the derivatives of lignocellulosic material. Bioresour. Technol. https://doi.org/10.1016/j.biortech.2020.122740.

Meleiro, L.P., Carli, S., Fonseca-Maldonado, R., da Silva Torricillas, M., Zimbardi, A.L.R.L., Ward, R.J., Jorge, J.A., Furriel, R.P.M., 2018. Overexpression of a cellobiose-glucose-Halotolerant endoglucanase from *Scytalidium thermophilum*. Appl. Biochem. Biotechnol. 185, 316–333. https://doi.org/10.1007/s12010-017-2660-8.

Mhiri, S., Bouanane-Darenfed, A., Jemli, S., Neifar, S., Ameri, R., Mezghani, M., Bouacem, K., Jaouadi, B., Bejar, S., 2020. A thermophilic and thermostable xylanase from *Caldicoprobacter algeriensis*: recombinant expression, characterization and application in paper biobleaching. Int. J. Biol. Macromol. https://doi.org/10.1016/j.ijbiomac.2020.07.162.

Miao, Y., Kong, Y., Li, P., Li, G., Liu, D., Shen, Q., Zhang, R., 2018. Effect of CBM1 and linker region on enzymatic properties of a novel thermostable dimeric GH10 xylanase (Xyn10A) from filamentous fungus *Aspergillus fumigatus* Z5. AMB Express 8, 1–10. https://doi.org/10.1186/s13568-018-0576-5.

Micsonai, A., Wien, F., Bulyáki, É., Kun, J., Moussong, É., Lee, Y.-H., Goto, Y., Réfrégiers, M., Kardos, J., 2018. BeStSel: a web server for accurate protein secondary structure prediction and fold recognition from the circular dichroism spectra. Nucleic Acids Res. 46, W315–W322. https://doi.org/10.1093/nar/gky497.

Miller, G.L., 1959. Use of dinitrosalicylic acid reagent for determination of reducing sugar. Anal. Chem. 31, 426–428. https://doi.org/10.1021/ac60147a030.

Mohd Azhar, S.H., Abdulla, R., Jambo, S.A., Marbawi, H., Gansau, J.A., Mohd Faik, A.A., Rodrigues, K.F., 2017. Yeasts in sustainable bioethanol production: a review. Biochem. Biophys. Reports. https://doi.org/10.1016/j.bbrep.2017.03.003.

Monclaro, A.V., Recalde, G.L., da Silva, F.G., de Freitas, S.M., Ferreira Filho, E.X., 2019. Xylanase from *Aspergillus tamarii* shows different kinetic parameters and substrate specificity in the presence of ferulic acid. Enzyme Microb. Technol. 120, 16–22. https://doi.org/10.1016/j.enzmictec.2018.09.009.

Moroz, O.V., Maranta, M., Shaghasi, T., Harris, P.V., Wilson, K.S., Davies, G.J., 2015. The three-dimensional structure of the cellobiohydrolase Cel7A from *Aspergillus fumigatus* at 1.5Å resolution. Acta Crystallogr. Sect. FStructural Biol. Commun. 71, 114–120. https://doi.org/10.1107/S2053230X14027307.

Narra, M., Dixit, G., Divecha, J., Kumar, K., Madamwar, D., Shah, A.R., 2014. Production, purification and characterization of a novel GH 12 family endoglucanase from *Aspergillus terreus* and its application in enzymatic degradation of delignified rice straw. Int. Biodeterior. Biodegrad. 88, 150–161. https://doi.org/10.1016/j.ibiod.2013.12.016.

Natesh, R., Bhanumoorthy, P., Vithayathil, P.J., Sekar, K., Ramakumar, S., Viswamitra, M.A., 1999. Crystal structure at 1.8 Å resolution and proposed amino acid sequence of a thermostable xylanase from *Thermoascus aurantiacus*. J. Mol. Biol. 288, 999–1012. https://doi.org/10.1006/jmbi.1999.2727.

Noratiqah, K., Madihah, M.S., Aisyah, B.S., Eva, M.S., Suraini, A.A., Kamarulzaman, K., 2013. Statistical optimization of enzymatic degradation process for oil palm empty fruit bunch (OPEFB) in rotary drum bioreactor using crude cellulase produced from *Aspergillus niger* EFB1. Biochem. Eng. J. 75, 8–20. https://doi.org/10.1016/j.bej.2013.03.007.

Oliveira, D.S., Meherb-Dini, C., Franco, C.M.L., Gomes, E., Da-Silva, R., 2010. Production of crude xylanase from *Thermoascus Aurantiacus* CBMAI 756 aiming the baking process. J. Food Sci. 75, 588–594. https://doi.org/10.1111/j.1750-3841.2010.01740.x.

Pandiyan, K., Tiwari, R., Singh, S., Nain, P.K.S., Rana, S., Arora, A., Singh, S.B., Nain, L., 2014. Optimization of enzymatic saccharification of alkali pretreated *Parthenium* sp. using response surface methodology. Enzyme Res. 2014 https://doi.org/10.1155/2014/764898.

Pasin, T.M., Salgado, J.C.S., Scarcella, A.Sde A., de Oliveira, T.B., de Lucas, R.C., Cereia, M., Rosa, J.C., Ward, R.J., Buckeridge, M.S., Polizeli, Mde L.Tde M., 2020. A halotolerant Endo-1,4-β-Xylanase from *Aspergillus clavatus* with potential application for agroindustrial residues saccharification. Appl. Biochem. Biotechnol. 191, 1111–1126. https://doi.org/10.1007/s12010-020-03232-x.

Pell, G., Szabo, L., Charnock, S.J., Xie, H., Gloster, T.M., Davies, G.J., Gilbert, H.J., 2004. Structural and biochemical analysis of *Cellvibrio japonicus* Xylanase 10C: how variation in substrate-binding cleft influences the catalytic profile of family GH-10 xylanases. J. Biol. Chem. 279, 11777–11788. https://doi.org/10.1074/jbc.M311947200.

Pellegrini, V.O.A., Serpa, V.I., Godoy, A.S., Camilo, C.M., Bernardes, A., Rezende, C.A., Junior, N.P., Franco Cairo, J.P.L., Squina, F.M., Polikarpov, I., 2015. Recombinant *Trichoderma harzianum* endoglucanase I (Cel7B) is a highly acidic and promiscuous carbohydrate-active enzyme. Appl. Microbiol. Biotechnol. 99, 9591–9604. https://doi.org/10.1007/s00253-015-6772-1.

Pereira, Jde C., Giese, E.C., Moretti, M.Mde S., Gomes, A.Cdos S., Perrone, O.M., Boscolo, M., da Silva, R., Gomes, E., Martins, D.A.B., 2017. Effect of metal ions, chemical agents and organic compounds on lignocellulolytic enzymes activities. Enzyme Inhibitors and Activators. InTech. https://doi.org/10.5772/65934.

Quan, J., Tian, J., 2011. Circular polymerase extension cloning for high-throughput cloning of complex and combinatorial DNA libraries. Nat. Protoc. https://doi.org/10.1038/nprot.2010.181.

Ribeiro, L.F.C., De Lucas, R.C., Vitcosque, G.L., Ribeiro, L.F., Ward, R.J., Rubio, M.V., Damásio, A.R.L., Squina, F.M., Gregory, R.C., Walton, P.H., Jorge, J.A., Prade, R.A., Buckeridge, M.S., Polizeli, M.D.L.T.M., 2014. A novel thermostable xylanase GH10 from *Malbranchea pulchella* expressed in *Aspergillus nidulans* with potential applications in biotechnology. Biotechnol. Biofuels 7, 1–11. https://doi.org/10.1186/1754-6834-7-115.

Rocha-Martín, J., Martinez-Bernal, C., Pérez-Cobas, Y., Reyes-Sosa, F.M., García, B.D., 2017. Additives enhancing enzymatic hydrolysis of lignocellulosic biomass. Bioresour. Technol. https://doi.org/10.1016/j.biortech.2017.06.132.

Saleem, A., Waris, S., Ahmed, T., Tabassum, R., 2021. Biochemical characterization and molecular docking of cloned xylanase gene from *Bacillus subtilis* RTS expressed in *E. coli*. Int. J. Biol. Macromol. 168, 310–321. https://doi.org/10.1016/j.ijbiomac.2020.12.001.

Saleh, S.A.A., Abdel Wahab, W.A., El-Dein, A.N., Abdelwahab, W.A., Ahmed, A.A.M., Helmy, W.A., Mostafa, F.A., 2021. Characterization of *Aspergillus niger* MK981235 xylanase with extraction of anti-hepatotoxic, antioxidant, hypocholesterolemic and prebiotic Corchorus olitorius stems xylooligosaccharides. Int. J. Biol. Macromol. 166, 677–686. https://doi.org/10.1016/j.ijbiomac.2020.10.225.

Savitzky, A., Golay, M.J.E., 1964. Smoothing and differentiation of data by simplified least squares procedures. Anal. Chem. 36, 1627–1639. https://doi.org/10.1021/ac60214a047.

Sayed Jamaludin, S.I., Syed Abd Kadir, S.A., Krishnan, J., Safri, N.H.M., 2013. Optimization of enzymatic hydrolysis of kitchen waste using response surface methodology (RSM) for reducing sugar production. BEIAC 2013 - 2013 IEEE Bus. Eng. Ind. Appl. Colloq. 322–326. https://doi.org/10.1109/BEIAC.2013.6560140.

Segato, F., Damásio, A.R.L., de Lucas, R.C., Squina, F.M., Prade, R.A., 2014. Genomics review of holocellulose deconstruction by aspergilli. Microbiol. Mol. Biol. Rev. 78, 588–613. https://doi.org/10.1128/MMBR.00019-14.

Shah, V., Pierre, B., Kirtadze, T., Shin, S., Kim, J.R., 2017. Stabilization of *Bacillus circulans* xylanase by combinatorial insertional fusion to a thermophilic host protein. Protein Eng. Des. Sel. 30, 281–290. https://doi.org/10.1093/protein/gzw081.

Sharma, M., Mahajan, C., Bhatti, M.S., Chadha, B.S., 2016. Profiling and production of hemicellulases by thermophilic fungus *Malbranchea flava* and the role of xylanases in improved bioconversion of pretreated lignocellulosics to ethanol. 3 Biotech 6, 1–12. https://doi.org/10.1007/s13205-015-0325-2.

Shi, H., Zhang, Y., Li, X., Huang, Y., Wang, L., Wang, Y., Ding, H., Wang, F., 2013. A novel highly thermostable xylanase stimulated by Ca2+ from *Thermotoga thermarum*: Cloning, expression and characterization. Biotechnol. Biofuels 6, 1–9. https://doi.org/10.1186/1754-6834-6-26.

Shibata, N., Suetsugu, M., Kakeshita, H., Igarashi, K., Hagihara, H., Takimura, Y., 2017. A novel GH10 xylanase from*Penicillium* sp. accelerates saccharification of alkaline-pretreated bagasse by an enzyme from recombinant *Trichoderma reesei* expressing Aspergillus β-glucosidase. Biotechnol. Biofuels 10, 1–17. https://doi.org/10.1186/s13068-017-0970-2.

Sindrewicz, P., Li, X., Yates, E.A., Turnbull, J.E., Lian, L.Y., Yu, L.G., 2019. Intrinsic tryptophan fluorescence spectroscopy reliably determines galectin-ligand interactions. Sci. Rep. 9, 1–12. https://doi.org/10.1038/s41598-019-47658-8.

Siqueira, G., Várnai, A., Ferraz, A., Milagres, A.M.F., 2013. Enhancement of cellulose hydrolysis in sugarcane bagasse by the selective removal of lignin with sodium chlorite. Appl. Energy 102, 399–402. https://doi.org/10.1016/j.apenergy.2012.07.029.

Song, H.T., Gao, Y., Yang, Y.M., Xiao, W.J., Liu, S.H., Xia, W.C., Liu, Z.L., Yi, L., Jiang, Z. B., 2016. Synergistic effect of cellulase and xylanase during hydrolysis of natural lignocellulosic substrates. Bioresour. Technol. 219, 710–715. https://doi.org/10.1016/j.biortech.2016.08.035.

Soozanipour, A., Taheri-Kafrani, A., Landarani Isfahani, A., 2015. Covalent attachment of xylanase on functionalized magnetic nanoparticles and determination of its activity and stability. Chem. Eng. J. 270, 235–243. https://doi.org/10.1016/j.cej.2015.02.032.

Takita, T., Nakatani, K., Katano, Y., Suzuki, M., Kojima, K., Saka, N., Mikami, B., Yatsunami, R., Nakamura, S., Yasukawa, K., 2019. Increase in the thermostability of GH11 xylanase XynJ from *Bacillus* sp. strain 41M-1 using site saturation mutagenesis. Enzyme Microb. Technol. 130, 109363 https://doi.org/10.1016/j.enzmictec.2019.109363.

Taneja, K., Gupta, S., Chander Kuhad, R., 2002. Properties and application of a partially purified alkaline xylanase from an alkalophilic fungus *Aspergillus nidulans* KK-99. Bioresour. Technol. 85, 39–42. https://doi.org/10.1016/S0960-8524(02)00064-0.

Tian, D., Chandra, R.P., Lee, J.S., Lu, C., Saddler, J.N., 2017. A comparison of various lignin-extraction methods to enhance the accessibility and ease of enzymatic hydrolysis of the cellulosic component of steam-pretreated poplar. Biotechnol. Biofuels 10, 1–10. https://doi.org/10.1186/s13068-017-0846-5.

Turner, T.L., Zhang, G.C., Kim, S.R., Subramaniam, V., Steffen, D., Skory, C.D., Jang, J. Y., Yu, B.J., Jin, Y.S., 2015. Lactic acid production from xylose by engineered *Saccharomyces cerevisiae* without PDC or ADH deletion. Appl. Microbiol. Biotechnol. 99, 8023–8033. https://doi.org/10.1007/s00253-015-6701-3.

Uday, U.S.P., Majumdar, R., Tiwari, O.N., Mishra, U., Mondal, A., Bandyopadhyay, T.K., Bhunia, B., 2017. Isolation, screening and characterization of a novel extracellular xylanase from *Aspergillus niger* (KP874102.1) and its application in orange peel hydrolysis. Int. J. Biol. Macromol. 105, 401–409. https://doi.org/10.1016/j.ijbiomac.2017.07.066.

Ullah, S.F., Souza, A.A., Hamann, P.R.V., Ticona, A.R.P., Oliveira, G.M., Barbosa, J.A.R. G., Freitas, S.M., Noronha, E.F., 2019. Structural and functional characterisation of xylanase purified from *Penicillium chrysogenum* produced in response to raw agricultural waste. Int. J. Biol. Macromol. 127, 385–395. https://doi.org/10.1016/j.ijbiomac.2019.01.057.

Ustinov, B.B., Gusakov, A.V., Antonov, A.I., Sinitsyn, A.P., 2008. Comparison of properties and mode of action of six secreted xylanases from *Chrysosporium lucknowense*. Enzyme Microb. Technol. 43, 56–65. https://doi.org/10.1016/j.enzmictec.2008.01.017.

Van Den Brink, J., De Vries, R.P., 2011. Fungal enzyme sets for plant polysaccharide degradation. Appl. Microbiol. Biotechnol. https://doi.org/10.1007/s00253-011-3473-2.

Van Dyk, J.S., Pletschke, B.I., 2012. A review of lignocellulose bioconversion using enzymatic hydrolysis and synergistic cooperation between enzymes-Factors affecting enzymes, conversion and synergy. Biotechnol. Adv. 30, 1458–1480. https://doi.org/10.1016/j.biotechadv.2012.03.002.

van Gool, M.P., van Muiswinkel, G.C.J., Hinz, S.W.A., Schols, H.A., Sinitsyn, A.P., Gruppen, H., 2013. Two novel GH11 endo-xylanases from *Myceliophthora thermophila* C1 act differently toward soluble and insoluble xylans. Enzyme Microb. Technol. 53, 25–32. https://doi.org/10.1016/j.enzmictec.2013.03.019.

Vanitjinda, G., Nimchua, T., Sukyai, P., 2019. Effect of xylanase-assisted pretreatment on the properties of cellulose and regenerated cellulose films from sugarcane bagasse. Int. J. Biol. Macromol. 122, 503–516. https://doi.org/10.1016/j.ijbiomac.2018.10.191.

Vazquez-Ortega, P.G., Alcaraz-Fructuoso, M.T., Rojas-Contreras, J.A., López-Miranda, J., Fernandez-Lafuente, R., 2018. Stabilization of dimeric β-glucosidase from *Aspergillus niger* via glutaraldehyde immobilization under different conditions. Enzyme Microb. Technol. 110, 38–45. https://doi.org/10.1016/j.enzmictec.2017.12.007.

Wallace, B.A., Janes, R.W., 2009. Modern Techniques for Circular Dichroism and Synchrotron Radiation Circular Dichroism Spectroscopy, Vol. 1. IOS press ed.

Wang, X., Huang, H., Xie, X., Ma, R., Bai, Y., Zheng, F., You, S., Zhang, B., Xie, H., Yao, B., Luo, H., 2016. Improvement of the catalytic performance of a hyperthermostable GH10 xylanase from *Talaromyces leycettanus* JCM12802. Bioresour. Technol. 222, 277–284. https://doi.org/10.1016/j.biortech.2016.10.003.

Wang, H., Li, Z., Liu, H., Li, S., Qiu, H., Li, K., Luo, X., Song, Y., Wang, N., He, H., Zhou, H., Ma, W., Zhang, T., 2017. Heterologous expression in *Pichia pastoris* and characterization of a novel GH11 xylanase from saline-alkali soil with excellent

tolerance to high pH, high salt concentrations and ethanol. Protein Expr. Purif. 139, 71–77. https://doi.org/10.1016/j.pep.2017.06.003.

Wang, K., Cao, R., Wang, M., Lin, Q., Zhan, R., Xu, H., Wang, S., 2019. A novel thermostable GH10 xylanase with activities on a wide variety of cellulosic substrates from a xylanolytic *Bacillus* strain exhibiting significant synergy with commercial Celluclast 1.5 L in pretreated corn stover hydrolysis. Biotechnol. Biofuels 12, 1–13. https://doi.org/10.1186/s13068-019-1389-8.

Wu, Q., Fan, G., Yu, T., Sun, B., Tang, H., Teng, C., Yang, R., Li, X., 2019. Biochemical characteristics of the mutant xylanase T-XynC(122)C(166) and production of xylooligosaccharides from corncobs. Ind. Crops Prod. 142, 111848 https://doi.org/10.1016/j.indcrop.2019.111848.

Wu, X., Zhang, S., Zhang, Q., Zhao, Y., Chen, G., Guo, W., Wang, L., 2020. The contribution of specific subsites to catalytic activities in active site architecture of a GH11 xylanase. Appl. Microbiol. Biotechnol. 104, 8735–8745. https://doi.org/10.1007/s00253-020-10865-9.

Xing, H., Zou, G., Liu, C., Chai, S., Yan, X., Li, X., Liu, R., Yang, Y., Zhou, Z., 2021. Improving the thermostability of a GH11 xylanase by directed evolution and rational design guided by B-factor analysis. Enzyme Microb. Technol. 143, 109720 https://doi.org/10.1016/j.enzmictec.2020.109720.

Xiong, H., Nyyssölä, A., Jänis, J., Pastinen, O., Von Weymarn, N., Leisola, M., Turunen, O., 2004. Characterization of the xylanase produced by submerged cultivation of *Thermomyces lanuginosus* DSM 10635. Enzyme Microb. Technol. 35, 93–99. https://doi.org/10.1016/j.enzmictec.2004.04.003.

Xu, X., Liu, M.Q., Huo, W.K., Dai, X.J., 2016. Obtaining a mutant of *Bacillus amyloliquefaciens* xylanase A with improved catalytic activity by directed evolution. Enzyme Microb. Technol. 86, 59–66. https://doi.org/10.1016/j.enzmictec.2016.02.001.

Yang, J., Ma, T., Shang-guan, F., Han, Z., 2020. Improving the catalytic activity of thermostable xylanase from *Thermotoga maritima* via mutagenesis of non-catalytic residues at glycone subsites. Enzyme Microb. Technol. 139, 109579 https://doi.org/10.1016/j.enzmictec.2020.109579.

Zhang, J., Moilanen, U., Tang, M., Viikari, L., 2013. The carbohydrate-binding module of xylanase from *Nonomuraea flexuosa* decreases its non-productive adsorption on lignin. Biotechnol. Biofuels 6, 1. https://doi.org/10.1186/1754-6834-6-18.

Zhang, H., Li, J., Wang, J., Yang, Y., Wu, M., 2014. Determinants for the improved thermostability of a mesophilic family 11 xylanase predicted by computational methods. Biotechnol. Biofuels 7, 1–10. https://doi.org/10.1186/1754-6834-7-3.

Zhang, W., Pan, K., Liu, C., Qu, M., OuYang, K., Song, X., Zhao, X., 2020. Recombinant Lentinula edodes xylanase improved the hydrolysis and in vitro ruminal fermentation of soybean straw by changing its fiber structure. Int. J. Biol. Macromol. 151, 286–292. https://doi.org/10.1016/j.ijbiomac.2020.02.187.

Zhou, J., Shi, P., Zhang, R., Huang, H., Meng, K., Yang, P., Yao, B., 2011. Symbiotic *Streptomyces* sp. TN119 GH 11 xylanase: a new pH-stable, protease- and SDS-resistant xylanase. J. Ind. Microbiol. Biotechnol. 38, 523–530. https://doi.org/10.1007/s10295-010-0795-5.

Zhou, J., Gao, Y., Dong, Y., Tang, X., Li, J., Xu, B., Mu, Y., Wu, Q., Huang, Z., 2012. A novel xylanase with tolerance to ethanol, salt, protease, SDS, heat, and alkali from actinomycete *Lechevalieria* sp. HJ3. J. Ind. Microbiol. Biotechnol. 39, 965–975. https://doi.org/10.1007/s10295-012-1113-1.

Zhou, Z., Lei, F., Li, P., Jiang, J., 2018. Lignocellulosic biomass to biofuels and biochemicals: a comprehensive review with a focus on ethanol organosolv pretreatment technology. Biotechnol. Bioeng. 115, 2683–2702. https://doi.org/10.1002/bit.26788.

Zou, G., Bao, D., Wang, Ying, Zhou, S., Xiao, M., Yang, Z., Wang, Yinmei, Zhou, Z., 2021. Alleviating product inhibition of *Trichoderma reesei* cellulase complex with a product-activated mushroom endoglucanase. Bioresour. Technol. 319, 124119 https://doi.org/10.1016/j.biortech.2020.124119.

Protein & Peptide Letters, 2019, *26*, 377-385

RESEARCH ARTICLE

Lytic Polysaccharide Monooxygenase from *Aspergillus fumigatus* can Improve Enzymatic Cocktail Activity During Sugarcane Bagasse Hydrolysis

Paula Fagundes de Gouvêa[1,#], Luis Eduardo Gerolamo[1,#], Aline Vianna Bernardi[1], Lucas Matheus Soares Pereira[1], Sergio Akira Uyemura[2] and Taisa Magnani Dinamarco[1,*]

[1]*Faculdade de Filosofia Ciências e Letras de Ribeirão Preto, Universidade de São Paulo, Ribeirão Preto, São Paulo, Brazil;* [2]*Faculdade de Ciências Farmacêuticas de Ribeirão Preto, Universidade de São Paulo, Ribeirão Preto, São Paulo, Brazil*

ARTICLE HISTORY

Received: December 11, 2018
Revised: February 13, 2019
Accepted: February 13, 2019

DOI:
10.2174/0929866526666190228163629

Abstract: ***Background*:** Lytic Polysaccharide Monooxygenases (LPMOs) are auxiliary accessory enzymes that act synergistically with cellulases and which are increasingly being used in second-generation bioethanol production from biomasses. Several LPMOs have been identified in various filamentous fungi, including *Aspergillus fumigatus*. However, many LPMOs have not been characterized yet.

***Objective*:** To report the role of uncharacterized *A. fumigatus Af*AA9_B LPMO.

***Methods*:** qRT-PCR analysis was employed to analyze the LPMO gene expression profile in different carbon sources. The gene encoding an *Af*AA9_B (Afu4g07850) was cloned into the vector pET-28a(+), expressed in the *E. coli* strain Rosetta™ (DE3) pLysS, and purified by a Ni^{2+}-nitrilotriacetic (Ni-NTA) agarose resin. To evaluate the specific LPMO activity, the purified protein peroxidase activity was assessed. The auxiliary LPMO activity was investigated by the synergistic activity in Celluclast 1.5L enzymatic cocktail.

***Results*:** LPMO was highly induced in complex biomass like sugarcane bagasse (SEB), Avicel® PH-101, and CM-cellulose. The LPMO gene encoded a protein comprising 250 amino acids, without a CBM domain. After protein purification, the *Af*AA9_B molecular mass estimated by SDS-PAGE was 35 kDa. The purified protein specific peroxidase activity was 8.33 ± 1.9 U g^{-1}. Upon addition to Celluclast 1.5L, Avicel® PH-101 and SEB hydrolysis increased by 18% and 22%, respectively.

***Conclusion*:** *A. fumigatus* LPMO is a promising candidate to enhance the currently available enzymatic cocktail and can therefore be used in second-generation ethanol production.

Keywords: Lytic polysaccharide monooxygenases, *Aspergillus fumigatus*, AA9 LPMO, sugarcane bagasse, biomass hydrolysis, bioethanol production.

1. INTRODUCTION

High emission of greenhouse gases causes global warming. This situation has called for replacement of fossil fuels with renewable and sustainable energy sources that lead to low CO_2 emissions and a more sustainable economy. In this context, renewable biomass (sugar cane bagasse, rice straw, corn straw and wheat straw) has become an attractive option to produce chemicals, biofuels, and biomaterials [1-4].

Lignocellulosic biomass consists of cellulose, hemicellulose and lignin. Cellulose, the main plant biomass polymeric component, usually contains highly crystalline regions. Cellulose is a linear polymeric chain of over 10,000 D-glucose residues linked by β-1,4-glycosidic bonds [5-7]. Due to its recalcitrant characteristic, lignocellulose degradation into fermentable sugars requires the synergistic action of cellulases and hemicellulases [8-11].

Pretreatment, such as a steam explosion, is usually a good strategy to open the lignocellulosic structure for hydrolysis by enzymatic cocktails. However, costs involved in pretreatment and enzymatic cocktails make lignocellulose breakdown expensive [1]. Although enzymes have become less expensive over the last decade, several attempts are still being made to reduce hydrolysis costs.

Lytic Polysaccharide Monooxygenases (LPMOs) have been recently described. LPMOs have revolutionized lignocellulose breakdown and greatly impacted lignocellulosic

*Address correspondence to this author at the Faculdade de Filosofia Ciências e Letras de Ribeirão Preto, Universidade de São Paulo, Ribeirão Preto, São Paulo, Brazil; E-mail: tdinamarco@ffclrp.usp.br

[#]*Both authors contributed equally to the work.*

1875-5305/19 $58.00+.00

biomass saccharification efficiency when they supplement commercial cellulase cocktails [3, 12-15].

LPMOs are described as metalloenzymes (EC 1.14.99). Their oxidation mechanism involves a divalent metal ion (usually copper), molecular oxygen, and an electron donor that acts on the polysaccharide matrix crystalline regions, favoring cellulase and hemicelullase action [14, 16, 17]. These enzymes are active mainly on cellulose and some hemicelluloses, and they are known to exert oxidative action on carbon C1, carbon C4, or both [18, 19].

Until now, only LPMOs from fungi that can act on different polysaccharides, like cellulose, xylan, chitin xyloglucan, and starch, have been characterized [15, 20-22].

According to the CAZy database (Carbohydrate Active Enzymes) [23], LPMOs are classified as an auxiliary activity class (AA) and are divided into AA families: AA9 LPMOs, which are active on cellulose; AA10 LPMOs, which are active on chitin or cellulose; AA11 LPMOs, which degrade chitin; and AA13 LPMOs, which act on starch [24]. Recently, two new LPMO families have been described: *Pycnoporus coccineus* AA14 LPMOs, which are active on xylan found in wood biomass [22]; and *Thermobia domestica* AA15 LPMOs, which act on chitin [25].

Filamentous fungi play an important role in the secretion of a large set of CAZymes, which can be further used to improve enzymatic cocktail activity [5, 26-29]. Recently, our group has shown that *Aspergillus fumigatus (A. fumigatus)* secretes many Carbohydrate-active enzymes (CAZymes), including AA9 LPMOs (*Af*AA9_B), when they are cultivated in the presence of sugarcane bagasse, but no *A. fumigatus* LPMOs have been characterized yet [29]. Although the *Af*AA9_B structure has been elucidated, no activity has been determined for this enzyme ([30] Q. Shen (unpublished)).

To gain more insight into the role played by *A. fumigatus* *Af*AA9_B LPMO, this work investigates the cloning, expression, and activity of this enzyme. This investigation will provide important information on the viability of using LPMOs to supplement enzymatic cocktails.

2. MATERIALS AND METHODS

2.1 Strains and Materials

A. fumigatus strain Af293, gently donated by Prof. Dr. Sérgio Akira Uyemura (University of São Paulo, BR), was cultivated in YAG medium [2.0% (w/v) dextrose, 2.0% (w/v) agar, 0.5% (w/v) yeast extract, and 0.1% (v/v) trace elements] at 37 ºC for two days to obtain a fresh conidia suspension.

Escherichia coli Rosetta (*E. coli*) (DE3) pLysS and DH5α were preserved at −80 °C in our laboratory.

Substrates were purchased from Sigma (Sigma-Aldrich, St. Louis, MO, USA). The natural substrate Sugarcane Exploded Bagasse (SEB), composed of 47.5% cellulose, 9.0% hemicelluloses, and 34.3% lignin, was kindly provided by Prof. Dr. João Atílio Jorge (University of São Paulo, BR).

2.2. qRT-PCR Analysis

2.2.1. Culture Conditions

Conidia were inoculated to a final concentration of 1 x 10^8 per 50 mL of Minimal Medium (MM) [1x salt solution (v/v) and 0.2% trace element solution] containing 1% (w/v) fructose and incubated at 37 °C, 200 rpm, for 16 h. Next, mycelia were harvested with sterile distilled water, washed, and transferred to MM containing 1% (w/v) fructose (control), 1% (w/v) SEB, 1% (w/v) low-viscosity carboxymethylcellulose (CM-Cellulose), 1% (w/v) β-glucan, 1% (w/v) xyloglucan, and 1% (w/v) microcrystalline cellulose (Avicel® PH-101, Sigma) at 37 ºC, 200 rpm for 3, 6, 12, and 24 h. Then, the mycelia were harvested by filtration through Whatman grade 1 filters (GE Healthcare, Grandview Blvd. Waukesha, WI, USA), washed once with sterile distilled water, and kept at −80 °C until RNA was extracted.

2.2.2. Total RNA Isolation and cDNA Synthesis

Mycelia (100 mg) from *A. fumigatus* were weighted to extract total RNA by using the Trizol® reagent (Invitrogen, Carlsbad, CA, USA) according to the manufacturer's instructions. cDNA was synthetized from 1 µg of total RNA by using SuperScript® II Reverse Transcriptase (Invitrogen, Carlsbad, CA, USA) according to the manufacturer's instructions.

2.2.3. Quantitative Real-Time PCR

Quantitative real-time PCR (qRT-PCR) analyses were accomplished according to Semighini *et al*., (2002) [31]. TaqMan® probe sequences are described in Supplementary Table **S1**. β-tubulin was used as a housekeeping gene control, and the qRT-PCR results were analyzed by using the $2^{-\Delta\Delta CT}$ method [32, 33]. Reactions were carried out as follows: 50 °C for 2 min, 95 °C for 10 min, 40 cycles of 95 ºC for 15 s, and 60 ºC for 1 min. Each experiment was carried out in triplicate, and three different biological experiments were conducted.

2.3. *Af*AA9_B Heterologous Expression in *E. coli*

2.3.1. AfAA9_B Expression Plasmid Construction

The *Af*AA9_B full complementary DNA (cDNA) "Open Reading Frame" (ORF) was amplified by PCR reactions with specific primer sequences containing restriction enzyme sites, as shown in Table **1**. PCR conditions were: 94 ºC/ 5 min (1 cycle), 94 °C/1 min, 55 °C/1 min, 68 °C/2 min (30 cycles), and 68 ºC/ 10 min (1 cycle); Platinum® Taq DNA polymerase High Fidelity (Invitrogen, Carlsbad, CA, USA) was employed.

Amplification products were purified with the aid of the kit QIAquick Gel Extraction (Qiagen, Hilden, Germany), cloned into the pGEM®-T easy vector (Promega, Madison, WI, USA), and transformed into *E. coli* strain DH5α. pGEM/*Af*AA9_B sequencing was performed to verify gene sequence in an automatic DNA sequencer (ABI Prism model 377; Perkin Elmer, Waltham, MA, USA).

Table 1. Sequence of primers used in this work.

Primer Name	Sequence	Enzyme
*Af*AA9_B fw	5' - GGATCCATGACTTTGTCCAAGATCAC - 3'	*Bam*HI
*Af*AA9_B rev	5' - AAGCTTTTAAGCGTTGAACAGTGCAG - 3'	*Hind*III

Enzyme restriction sites are underlined.

Plasmids pGEM/*Af*AA9_B and pET-28a(+) (Novagen; USA) were double digested with appropriate enzymes, and gene fragments were inserted into the expression vector pET-28a(+) by using T4 DNA Ligase (Invitrogen, Carlsbad, CA, USA). The resulting recombinant expression plasmid pET-28a/*Af*AA9_B encoded LPMO fused to the C-terminal 6-histidine tag in the coding sequence.

2.3.2. AfAA9_B Overexpression in E. coli

Competent *E. coli* Rosetta (DE3) pLysS transformed with plasmids pET-28a/*Af*AA9_B were grown in Luria-Bertani (LB) medium [1% (w/v) tryptone, 0.5% (w/v) yeast extract, and 1% (w/v) NaCl] added with 1% (w/v) glucose, 50 µg/mL kanamycin, and 25 µg/mL chloramphenicol and incubated overnight, at 37 ºC and 200 rpm. After this period, the bacterial culture was transferred to Terrific-Broth (TB) medium [2.4% (w/v) yeast extract, 1.2% (w/v) tryptone, 0.4% (v/v) glycerol, 17 mM KH_2PO_4, and 72 mM K_2HPO_4] added with 1% (w/v) glucose, 50 µg/mL kanamycin, and 25 µg/mL chloramphenicol. The expression conditions of temperature (17, 25, 30, and 37 °C), Isopropyl-D-Thiogalacto-pyranoside (IPTG) concentration (0.1, 0.25, 0.5, and 1.0 mM), and induction time (2, 4, 6, 12, and 24 h) were optimized. Cells were harvested by centrifugation at 18,514 x g and 4 °C for 10 min.

Inclusion bodies were purified and denatured according to the protocols described in the kit "iFOLD™ Protein Refolding System I" (Novagen, Darmstadt, HE, Germany). Protein refolding was performed concomitantly with dialysis in 20 mM Tris-HCl buffer pH 7 (Sigma-Aldrich, St. Louis, MO, USA) in dialysis membrane at 4 ºC for 24 h, under stirring.

2.4. Protein Purification

Recombinant *Af*AA9_B was purified by applying proteins onto a Ni^{2+}-nitrilotriacetic (Ni-NTA) agarose resin pre-equilibrated with 20 mM sodium phosphate and 0.5 M NaCl pH 7.4 (Ni Sepharose 6 Fast Flow resin, GE, Chicago, IL, USA). After LPMO inclusion bodies were purified, the buffer was exchanged with 20 mM sodium phosphate and 0.5 M NaCl pH 7.4, and the LPMO protein was bound to the resin at 4 °C for 2 h. Washes were carried out three times with sodium phosphate buffer without imidazole. Bound proteins were then eluted with the same buffer containing 250 mM imidazole. The purified LPMO protein was analyzed by 10% (w/v) SDS-polyacrylamide gel electrophoresis (SDS-PAGE), stained with Comassie Brilliant Blue R-250 (Sigma-Aldrich, St Louis, MI, EUA). Protein concentration was determined by Bradford's Assay (Bio-Rad Protein Assay Hercules, CA, EUA) [34].

2.5. SDS-PAGE and Western Blotting

Enzyme purity and molecular weight were analyzed by 10% (w/v) SDS-PAGE, according to the methodology described by Laemmli [35]. After the run, the gel was stained with Comassie Brilliant Blue R-250 (Sigma-Aldrich, St. Louis, MO, USA). SDS-PAGE was conducted with Mini-PROTEAN TGX Stain-Free precast gels (Biorad, Hercules, CA, USA) according to the manufacturer's instructions.

Protein Western blotting was performed according to Towbin *et al*., (1979) [36]. After electrophoresis, the protein was transferred to membranes and incubated in Tris-Buffered Saline, 0.1% Tween 20 (TBS-T) buffer 1x (v/v) (TBS 1x [20 mM Tris, 150 mM NaCl] and 0.1% (v/v) Tween 20) containing 5% (w/v) powdered milk at 4 °C for 1 h. Blots were sequentially treated with mouse Anti-polyHistidine (His-tag) (GE, Boston, MA, EUA) 1:5000 and anti-mouse IgG (alkaline phosphatase-conjugated goat) 1:5000 antibodies (Sigma-Aldrich, St. Louis, MO, USA). Phosphatase activity was detected with "ECL Western blotting detection reagents and analysis system" kit (Amersham Biosciences, UK).

2.6. *Af*AA9_B Activity Assay

The LPMO activity assay was performed according to Breslmayr *et al*., (2018) [37]. The reactions consisted of 100 mM sodium phosphate buffer (succinate phosphate buffer) (Sigma-Aldrich, St Louis, MI, EUA) pH 7.5, 1.0 mM 2,6-dimethoxyphenol (2,6-DMP) (Sigma-Aldrich, St Louis, MI, EUA), 100 µM H_2O_2 (Sigma-Aldrich, St Louis, MI, EUA), 0.5 µM purified *Af*AA9_B, and MilliQ® water to a final volume of 1.0 mL. The cuvette containing the reaction was pre-incubated at 30 ºC for 15 min before LPMO was added. Reactions were incubated at 30 ºC for 300 s, and absorbance was measured at 469 nm. Blank reactions were performed without LPMO. One unit of LPMO activity was defined as conversion of 2 µmol of 2,6-DMP or formation of 1 µmol of coerulignone (ε469 = 53,200 M^{-1} cm^{-1}) per min under reaction conditions. All the reactions were performed in triplicate.

2.7. *Af*AA9_B Auxiliary Enzymatic Activity with Cellulases

To evaluate synergistic activity in the enzymatic hydrolysis of different substrates, purified *Af*AA9_B was incubated with a commercial cellulase preparation Celluclast 1.5L (Novozymes), as follows: substrates, 1% (w/v) CM-cellulose, Avicel® PH-101 (Sigma-Aldrich, St. Louis, MO), xylan, xyloglucan, and SEB were incubated with Celluclast 1.5L (0.9 FPU/g of substrates) and enzyme *Af*AA9_B (10

mg/g of substrate) in reaction medium containing 50 mM sodium acetate buffer (pH 5.0). The reaction (1 mL) was conducted in Eppendorf tubes (2 mL) at 50 °C and 1000 rpm for 48 h, in a ThermoMixer (Eppendorf, Hamburg, Germany). Sodium azide (0.02%, w/v) was added as a reducing agent in all the synergistic reactions. Control experiments without enzymes or reducing agent were conducted under the same conditions.

After this time, the reaction was boiled at 95 °C for 5 min, to terminate the reaction, and centrifuged at 30,000 x g for 5 min. After reaction, reducing sugars were determined by the 3,5-dinitrosalicylic acid (DNS) assay at 540 nm; D-glucose was used as standard [38]. The increase in synergism is represented as described by Kim *et al*., (2017) [39]. All the enzyme assays were accomplished at least three times with appropriate controls.

2.8. Statistical Analysis

Data are expressed as the mean of replicates ± SD. Significant differences between the treatment groups were analyzed using Tukey's test (significance, $p < 0.05$).

2.9. Reproducibility of the Results

All data are the mean of at least three independent experiments and showed consistent results.

3. RESULTS AND DISCUSSION

LPMOs have been described as important industrial enzymes that can reduce the cost of biomass degradation when they are incorporated in commercial cocktails during hydrolysis. These enzymes impact the biofuel and biochemical industries [40, 41]. Several auxiliary activity enzymes have been characterized after heterologous enzyme expression in bacteria, yeast, and fungi [42-44], but to date no *A. fumigatus* auxiliary activity enzyme has been characterized.

The *A. fumigatus* genome contains different CAZymes (247 GHs, 105 GTs, 96 CEs, 59 AAs, 15 PLs, and 44 CBMs) related to plant cell hydrolysis. Among Auxiliary Activity enzymes, 11 correspond to LPMOs (six AA9s and five AA11s).

Our previous *A. fumigatus* transcriptome analysis identified three putative LPMO sequences in SEB culture, including Afu4g07850, an *Af*AA9_B [29]. The role of fungal LPMOs in breaking down different plant cell wall components has not been fully explained yet, and the substrate specificity of each AA9 remains unknown [45, 46].

To understand the *Af*AA9_B gene expression in different carbon sources, the qRT-PCR was used to measure the profile after the incubation of *A. fumigatus* in 1% (w/v) (Avicel® PH-101), CM-cellulose, xylan, xyloglucan, and SEB. The $2^{-\Delta\Delta CT}$ method was applied to analyze the relative changes in gene expression as compared to the culture in fructose.

The expression profile was monitored for 3, 6, 12, and 24 h. After incubation for 3 h, a distinct expression level pattern was observed in the presence of most carbon sources (Figure **1**). The highest expression occurred after six hours of induction in CM-cellulose, SEB, and Avicel® PH-101 - approximately 3,500-fold, 2,000-fold, and 1,000-fold, respectively. Miao *et al*., [47] described similar findings: AA9 genes are upregulated in *A. fumigatus* Z5 strain in different biomass. In the same way, six AA9 are upregulated in *A. tamarii* in the presence of sugarcane bagasse [48]. In addition, fungus *Malbranchea cinnamomea* cultivation in wheat bran revealed some up-regulated AA9 genes [49]. Together, these findings reinforce the direct role of these accessory proteins in the hydrolysis of different carbon sources, including complex biomass.

On the other hand, in xyloglucan, gene expression level increased by 50-fold after 24 h. In the same way, LPMOs from the brown-rot fungus *Gloeophyllum trabeum* and from *Neurospora crassa* and *Thermoascus auranticus* display activity in xyloglucan [50, 51]. Xylan and xyloglucan are present in the hemicellulose structure and initiate specific expression of different hemicellulases [52-54]. Although here the expression of this gene in xylan did not increase, Adav *et al*., (2015) [55] described that the *Af*AA9_B gene is highly expressed in this carbon source after incubation at 50 °C for four days. The fungus *Myceliophthora thermophila* has a LPMO that acts in xylan, as well, indicating that these enzymes also have a significant part in degrading hemicellulosic components [56].

Likewise, complex biomass like sorghum induces different LPMO expression in *Aspergillus nidulans* cultures. Furthermore, the LPMO induction profiles differ depending on the polysaccharide, as observed with the AN1602 gene, which is induced in cellulose and xylan, and the AN3860 and AN3046 genes, which are induced in cellulose and xyloglucan [57].

*Af*AA9_B may be involved in auxiliary cellulose hydrolysis even when it is present in complex biomass like sugarcane bagasse.

3.1. Recombinant *A. fumigatus* LPMO Heterologous Expression and Purification

To characterize and to investigate the biological function of the first *A. fumigatus* LPMO to be described, the ORF encoding *Af*AA9_B was amplified from the *A. fumigatus* strain Af293 SEB-induced cDNA and inserted into pET28a (+) to obtain the expression vector pET-28a/*Af*AA9_B. While the role of *Af*AA9_B was being studied, the X-ray crystal structure of the same sequence (Afu4g07850) was resolved [30; Q. Shen (unpubished)]. This LPMO does not contain a Carbohydrate-Binding Module 1 (CBM1) in addition to the catalytic domain, as reported for most fungal LPMOs [58-60].

The recombinant protein in *E. coli* was expressed under control of the T7 RNA polymerase promoter. Different conditions of temperature (17, 25, 30 and 37 °C), IPTG concentration (0.1, 0.25, 0.5 and 1.0 mM), and induction time (2, 4, 6, 12 and 24 h) to optimize protein expression (*data not shown*) were tested. However, the protein was exclusively detected in inclusion bodies under the evaluated conditions. The best expression conditions were achieved by adding 0.5 mM IPTG at 30 ºC and 200 rpm for 4 h. Then, the optimized expression for large-scale cultures was employed (Figure **2A**). The slightly higher molecular masses observed

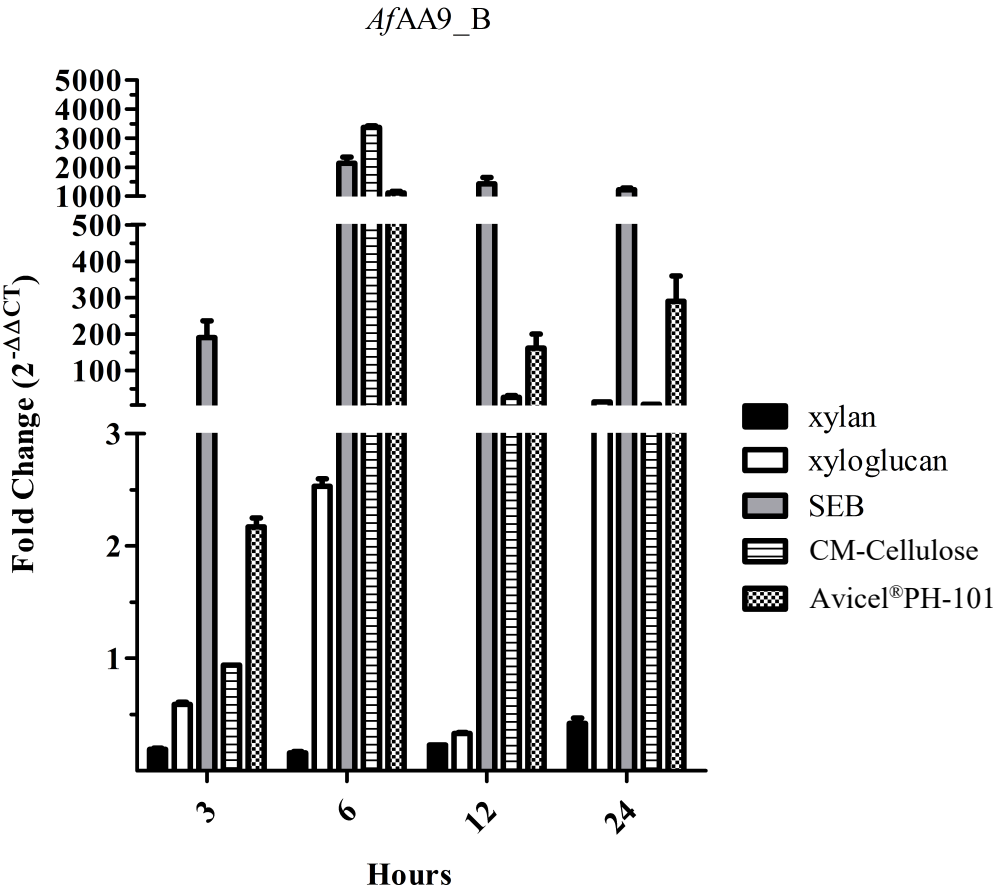

Figure 1. qRT-PCR. *Af*AA9_B gene expression levels after 3, 6, 12, and 24 h of *A. fumigatus* growth in the presence of 1% (w/v) xylan, xyloglucan, SEB, CM-Cellulose, or Avicel® PH-101. Genes were considered to be induced in the carbon sources when the fold change result higher than 1.0.

in SDS-PAGE after expression could result from addition of amino acids to the protein sequences by the pET-28a (+) vector. Western blot (Figure **2B**) confirmed that the purified protein was effectively expressed.

After protein expression and inclusion body purification, the recombinant protein, with 35 KDa, was purified by Ni^{2+} affinity chromatography, as shown in Figure **2C**.

3.2. LPMO Activities

The *Af*AA9_B peroxidase activity was measured in the presence of the substrate 2,6-dimethoxyphenol and hydrogen peroxide (H_2O_2) as co-substrate [37]. The specific activity of the purified peroxidase was 8.33 ± 1.9 U g^{-1} (Table **2**). Comparing NcLPMO9C and TrLPMOA activities, both enzymes exhibit higher activity, 32.3 and 14.4 U g^{-1}, respectively [4, 37], mainly due to glycosylation during expression in *P. pastoris*.

The *Af*AA9_B activities in complex substrates were also investigated. *Af*AA9_B auxiliary activities during cellulose hydrolysis were measured in the presence of Avicel® PH-101, as pure cellulose, and in CM-Cellulose. The commercial cellulase preparation, Celluclast 1.5L, without AA9, hydrolyzed both substrates.

However, when the enzyme *Af*AA9_B (10 mg/g of substrate) was added to the Celluclast 1.5L cocktail, the hydrolytic activity in Avicel® PH-101 increased 18% (1.2-fold), when compared with Celluclast hydrolyses, implying significant difference ($p < 0.05$) (Figure **3**). The enzyme *Af*AA9_B alone did not have any auxiliary activity (*data not shown*).

Also, the enzyme *Af*AA9_B didn´t presented enhanced hydrolysis activity in CM-Cellulose, xylan, or xyloglucan, even when it was added to supplement the Celluclast 1.5L cocktail.

When a complex biomass such as sugarcane bagasse (47.5% cellulose, 9.0% hemicelluloses, and 34.3% lignin) was used, there was low hydrolytic activity by the Celluclast 1.5L cocktail due to biomass cell wall rigidity. Comparing to Avicel® PH-101, the cocktail hydrolysed 8 times less SEB. However, when the cocktail was supplemented with the enzyme *Af*AA9_B, the hydrolytic activity of SEB increased 22%, statically significant ($p < 0.05$), suggesting that *A. fumigatus* LPMO aided lignocellulosic biomass hydrolysis.

Studies have shown that *Podospora anserina* LPMOs increase the Celluclast 1.5L hydrolytic activity by 88% in the case of exploded and delignified miscanthus biomass [62]. Likewise, efficient degradation has been detected in cocktail preparations supplemented with LPMOs in different complex biomasses such as sulfite-pulped softwoods [45].

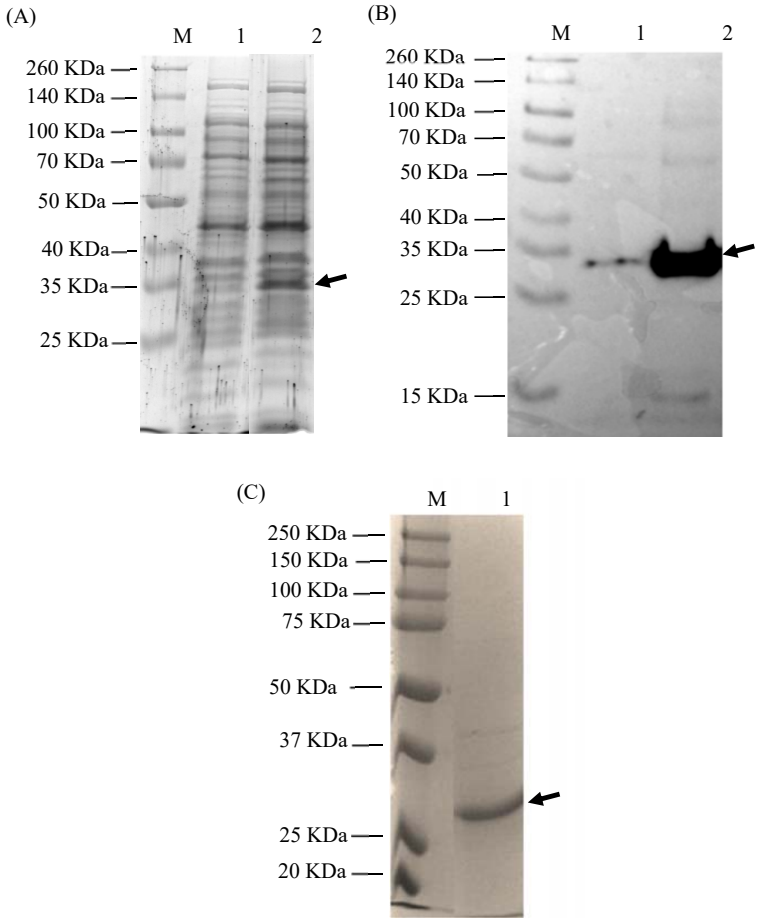

Figure 2. *Af*AA9_B protein expression and purification. (**A**) Protein expression after 4 h of induction with 0.5 mM IPTG, at 30 ºC; Lane M: Molecular weight marker (Precision standards dual color - BioRad), Lane 1: 0 h of *Af*AA9_B protein induction and Lane 2: 4 h of *Af*AA9_B induction; (**B**) *Af*AA9_B Anti-polyHistidine western blotting analyses, Lane 1: negative control and Lane 2: *Af*AA9_B (**C**) Lane M: molecular weight marker, Lane 1: purified *Af*AA9_B.

Table 2. List of some AA9 LPMO activities and their respective substrates as reported in the literature.

Enzyme	Organism	Activity	Substrates	Methodology	References
*Af*AA9_B	*Aspergillus fumigatus*	8.33 $U.g^{-1}$	2,6 - DMP / H_2O_2	Chromogenic substrate assay (2,6 - DMP)	*This study*
TrLPMOA	*Trichoderma reesei*	14.4 $U.g^{-1}$	O_2	[+]Amplex Red/ horseradish peroxidase assay	[4]
NcLPMO9C	*Neurospora crassa*	32.3 $U.g^{-1}$	2,6 - DMP / H_2O_2	Chromogenic substrate assay (2,6 - DMP)	[37]
*Af*AA9_B	*Aspergillus fumigatus*	1.8 fold higher	SEB	LPMO/cocktail coupled assay (DNS)	*This study*
TtAA9E	*Thielavia terrestris*	[a]1.8 - 1.9 fold higher	Rice Straw / O_2	LPMO/cocktail coupled assay (DNS)	[39]
TaAA9A	*Thermoascus aurantiacus*	[a]1.5 - 1.9 fold higher			
PcLPMO9D	*Phanerochaete chrysosporium*	[b]>0,0125 $\mu mol.g^{-1}$ BMCC.h^{-1}	BMCC / O_2	Fluorescence-labeling assay (ANDA/EDAC) [#]	[61]

[#] - Specific for C-degrading LPMOs

[+] - Measure of H_2O_2 generation by oxygen consumption in the absence of carbohydrate.

[a] - Result compared to rice straw hydrolyzed only by Celluclast® 1.5L at 2.8 FPU and 1.4 FPU, respectively.

[b] - Estimated value for the insoluble BMCC (Bacterial Microcrystalline Cellulose) oxidized fraction.

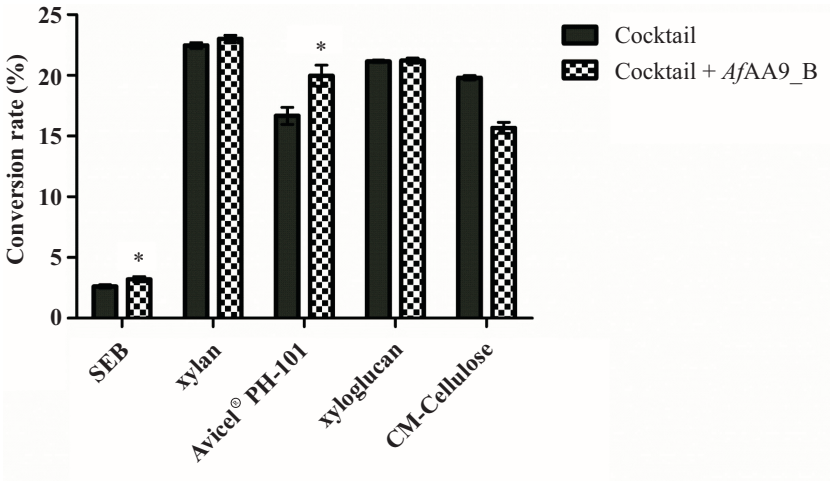

Figure 3. *Af*AA9_B auxiliary activities in (1% w/v) CM-cellulose, SEB, xylan, Avicel® PH-101, and xyloglucan hydrolyses. The substrates were hydrolyzed by using Celluclast 1.5 L (0.9 FPU/g of substrate) only or Celluclast and the enzyme *Af*AA9_B (10 mg/g of substrate) in 50 mM sodium acetate buffer (pH 5.0) containing sodium azide (NaN_3) at 50 ^oC for 48 h. The reducing sugar was determined as described by Kim *et al*., (2017) [39]. The data represent the means ± standard errors obtained from three experimental replicates. For each incubation time, the asterisks (*) indicates a significant difference between *Af*AA9_B and Celluclast, determined by one-way ANOVA followed by Student´s t-test ($p < 0.05$).

The *Af*AA9_B auxiliary activity provided a similar boost to the boost described by Kim *et al*., (2017) [39] for the enzymes TtAA9A and TtAA9E (1.2-fold and 1.9-fold higher activity, respectively). In contrast, TrCel61 and Aspte6 from *Thrichoderma reesei* and *Aspergillus terreus*, respectively, showed significant hydrolytic boosting: 36% glucose was released when the enzymes were combined with endoglucanase and beta-glucosidase [63]. Likewise, studies on other LPMOs have not reported much higher increases in enzymatic activity than the increase obtained with the enzyme *Af*AA9_B [64, 65]. To date, few studies have described LPMOs that act on xyloglucan *via* cleavage of unsubstituted glycosyl residues [17, 20, 57].

The synergism between Celluclast 1.5L and the enzyme *Af*AA9_B in sugarcane bagasse probably resulted from the complementary functions of the activities of the monooxygenase and the endoglucanases present in the commercial mixture. Endoglucanases in cellulolytic mixtures create a synergistic interaction with LPMOs: the former enzymes prefer to act on the cellulose amorphous regions, while they manifest very low activity in the crystalline zones. Our group has recently described that *A. fumigatus* endoglucanase (GH7) displays important hydrolytic activity in SEB, which has emphasized the biotechnological potential of supplementing enzyme cocktails [66]. The association of the endoglucanase (GH5 family) and the LPMO9 from the thermophilic fungus *Myceliophthora thermophila* increases enzymatic hydrolysis against regenerated amorphous cellulose (PASC) [67]. Studies associating GHs and LPMOs are being conducted and may aid more effective hydrolysis of different biomasses.

CONCLUSION

The enzyme *Af*AA9_B has auxiliary activity in commercial enzymatic cocktail: it increases the cocktail enzymatic activity by up to 22% in SEB. Besides low LPMO peroxidase activity, *Af*AA9_B has significant biotechnological potential: it boosts the activity of commercially available cocktails. *Af*AA9_B activity depends on biomass, biomass pretreatment, and substrates on which it acts. In the future, this enzyme could be used to supplement commercial enzymatic cocktails in 2G ethanol production.

ETHICS APPROVAL AND CONSENT TO PARTICIPATE

Not applicable.

HUMAN AND ANIMAL RIGHTS

No Animals/Humans were used for studies that are the basis of this research.

CONSENT FOR PUBLICATION

Not applicable.

CONFLICT OF INTEREST

The authors declare no conflict of interest, financial or otherwise.

ACKNOWLEDGEMENTS

This research was funded by Fundação de Amparo à Pesquisa do Estado de São Paulo (FAPESP, 2016/19095-0) and Conselho Nacional de Desenvolvimento Científico e Tecnológico (CNPq: 425465/2016-0). PFG was funded by a scholarship granted by FAPESP, 2018/10296-8. Also, this study was partly financed by the Coordenação de Aperfeiçoamento de Pessoal de Nível Superior - Brasil (CAPES) - Finance Code 001. AVB and LEG were funded by scholarships granted by Conselho Nacional de Desenvolvimento Científico e Tecnológico (CNPq).

SUPPLEMENTARY MATERIAL

Supplementary material is available on the publisher's website along with the published article.

REFERENCES

[1] Sheldon, R.A. Engineering a more sustainable world through catalysis and green chemistry. *J. R. Soc. Interface*., **2016**, *13*, 20160087.

[2] Santos, F.A.; De Queiróz, J.H.; Colodette, J.L.; Fernandes, S.A.; Guimaraes, V.M.; Rezende, S.T. Potencial da palha de cana-de-açúcar para produção de etanol. *Quim. Nova*, **2012**, *35*, 1004-1010.

[3] Farzad, S.; Mandegari, M.A.; Guo, M.; Haigh, K.F.; Shah, N.; Görgens, J.F. Multi-product biorefineries from lignocelluloses: A pathway to revitalisation of the sugar industry? *Biotechnol. Biofuels*., **2017**, *10*, 87.

[4] Guo, Z.P.; Duquesne, S.; Bozonnet, S.; Nicaud, J.M.; Marty, A.; O'Donohue, M.J. Expressing accessory proteins in cellulolytic *Yarrowia lipolytica* to improve the conversion yield of recalcitrant cellulose. *Biotechnol. Biofuels*, **2017**, *10*, 298.

[5] Glass, N.L.; Schmoll, M.; Cate, J.H.D.; Coradetti, S. Plant cell wall deconstruction by Ascomycete fungi. *Annu. Rev. Microbiol*., **2013**, *67*, 477-498.

[6] Wang, Y.; Fan, C.; Hu, H.; Li, Y.; Sun, D.; Wang, Y.; Peng, L. Genetic modification of plant cell walls to enhance biomass yield and biofuel production in bioenergy crops. *Biotechnol. Adv*., **2016**, *34*, 997-1017.

[7] Sun, Y.; Cheng, J. Hydrolysis of lignocellulosic materials for ethanol production: A review. *Bioresour. Technol*., **2002**, *83*(1), 1-11.

[8] Souza, G.M.; Victoria, R.L.; Joly, C.A.; Verdade, L.M. Bioenergy and Sustainability: Bridging the gaps. SCOPE:Paris, **2015**.

[9] Cota, J.; Corrêa, T.L.R.; Damásio, A.R.L.; Diogo, J.A.; Hoffmam, Z.B.; Garcia, W.; Oliveira, L.C.; Prade, R.A.; Squina, F.M. Comparative analysis of three hyperthermophilic GH1 and GH3 family members with industrial potential. *N. Biotechnol*., **2015**, *32*, 13-20.

[10] Carvalho, W.; Canilha, L.; Ferraz, A.; Ferreira, M. Uma visão sobre a estrutura, composição e biodegradação da madeira. *Quim. Nova*, **2009**, *32*, 2191-2195.

[11] Whitaker, J.R.; Stauffer, C.E. Principles of enzymology for the food sciences, 2nd ed.; CRC Press: New York, **1994**.

[12] Busk, P.K.; Lange, L. Classification of fungal and bacterial lytic polysaccharide monooxygenases. *BMC Genomics*, **2015**, *16*, 368.

[13] Müller, G.; Chylenski, P.; Bissaro, B.; Eijsink, V.G.H.; Horn, S.J. The impact of hydrogen peroxide supply on LPMO activity and overall saccharification efficiency of a commercial cellulase cocktail. *Biotechnol. Biofuels*, **2018**, *11*, 209.

[14] Vaaje-kolstad, G. An oxidative enzyme boosting the enzymatic conversion of recalcitrant polysaccharides. *Science*, **2010**, *330*, 219-222.

[15] Quinlan, R.J.; Sweeney, M.D.; Lo Leggio, L.; Otten, H.; Poulsen, J.-C.N.; Johansen, K.S.; Krogh, K.B.R.M.; Jorgensen, C.I.; Tovborg, M.; Anthonsen, A.; Tryfona, T.; Walter, C.P.; Dupree, P.; Xu, F.; Davies, G.J.; Walton, P.H. Insights into the oxidative degradation of cellulose by a copper metalloenzyme that exploits biomass components. *Proc. Natl. Acad. Sci*., **2011**, *108*, 15079-15084.

[16] Bomble, Y.J.; Lin, C.Y.; Amore, A.; Wei, H.; Holwerda, E.K.; Ciesielski, P.N.; Donohoe, B.S.; Decker, S.R.; Lynd, L.R.; Himmel, M.E. Lignocellulose deconstruction in the biosphere. *Curr. Opin. Chem. Biol*., **2017**, *41*, 61-70.

[17] Agger, J.W.; Isaksen, T.; Varnai, A.; Vidal-Melgosa, S.; Willats, W.G.T.; Ludwig, R.; Horn, S.J.; Eijsink, V.G.H.; Westereng, B. Discovery of LPMO activity on hemicelluloses shows the importance of oxidative processes in plant cell wall degradation. *Proc. Natl Acad. Sci*., **2014**, *111*, 6287-6292.

[18] Berrin, J.G.; Rosso, M.N.; Abou Hachem, M. Fungal secretomics to probe the biological functions of lytic polysaccharide monooxygenases. *Carbohydr. Res*., **2017**, *448*, 155-160.

[19] Monclaro, A.V.; Filho, E.X.F. Fungal lytic polysaccharide monooxygenases from family AA9: Recent developments and application in lignocelullose breakdown. *Int. J. Biol. Macromol*., **2017**, *102*, 771-778.

[20] Bennati-Granier, C.; Garajova, S.; Champion, C.; Grisel, S.; Haon, M.; Zhou, S.; Fanuel, M.; Ropartz, D.; Rogniaux, H.; Gimbert, I.; Record, E.; Berrin, J. G. Substrate specificity and regioselectivity of fungal AA9 lytic polysaccharide monooxygenases secreted by *Podospora anserina*. *Biotechnol. Biofuels*, **2015**, *8*, 90.

[21] Vu, V.V.; Beeson, W.T.; Span, E.A.; Farquhar, E.R.; Marletta, M.A. A family of starch-active polysaccharide monooxygenases. *Proc. Natl Acad. Sci*., **2014**, *111*, 13822-13827.

[22] Couturier, M.; Ladevèze, S.; Sulzenbacher, G.; Ciano, L.; Fanuel, M.; Moreau, C.; Villares, A.; Cathala, B.; Chaspoul, F.; Frandsen, K.E.; Labourel, A.; Herpoël-Gimbert, I.; Grisel, S.; Haon, M.; Lenfant, N.; Rogniaux, H.; Ropartz, D.; Davies, G.J.; Rosso, M.-N.N.; Walton, P.H.; Henrissat, B.; Berrin, J.-G.G. Lytic xylan oxidases from wood-decay fungi unlock biomass degradation. *Nat. Chem. Biol*., **2018**, *14*, 306-310.

[23] Cantarel, B.L.; Coutinho, P.M.; Rancurel, C.; Bernard, T.; Lombard, V.; Henrissat, B. The Carbohydrate-Active EnZymes database (CAZy): An expert resource for glycogenomics. *Nucleic Acids Res*., **2009**, *37*, D233-D238.

[24] Levasseur, A.; Drula, E.; Lombard, V.; Coutinho, P.M.; Henrissat, B. Expansion of the enzymatic repertoire of the CAZy database to integrate auxiliary redox enzymes. *Biotechnol. Biofuels*, **2013**, *6*, 41.

[25] Sabbadin, F.; Hemsworth, G.R.; Ciano, L.; Henrissat, B.; Dupree, P.; Tryfona, T.; Marques, R.D.S.S.; Sweeney, S.T.; Besser, K.; Elias, L.; Pesante, G.; Li, Y.; Dowle, A.A.; Bates, R.; Gomez, L.D.; Simister, R.; Davies, G.J.; Walton, P.H.; Bruce, N.C.; Mcqueen-Mason, S.J. An ancient family of lytic polysaccharide monooxygenases with roles in arthropod development and biomass digestion. *Nat. Commun*., **2018**, *9*, 756.

[26] Cragg, S.M.; Beckham, G.T.; Bruce, N.C.; Bugg, T.D.H.; Distel, D.L.; Dupree, P.; Etxabe, A.G.; Goodell, B.S.; Jellison, J.; McGeehan, J.E.; McQueen-Mason, S.J.; Schnorr, K.; Walton, P.H.; Watts, J.E.M.; Zimmer, M. Lignocellulose degradation mechanisms across the tree of life. *Curr. Opin. in Chem. Biol*., **2015**, *29*, 108-119.

[27] Sharma, R.K.; Arora, D.S. Fungal degradation of lignocellulosic residues: An aspect of improved nutritive quality. *Crit. Rev. Microbiol*., **2015**, *41*, 52-60.

[28] Borin, G.P.; Sanchez, C.C.; De Souza, A.P.; De Santana, E.S.; De Souza, A.T.; Leme, A.F.P.; Squina, F.M.; Buckeridge, M.; Goldman, G.H.; De Castro Oliveira, J.V. Comparative secretome analysis of *Trichoderma reesei* and *Aspergillus niger* during growth on sugarcane biomass. *PLoS One*, **2015**, *10*, e0129275.

[29] de Gouvêa, P.F.; Bernardi, A.V.; Gerolamo, L.E.; Santos, E.S.; Riano-Pachon, D.; Uyemura, S.A.; Dinamarco, T.M. Transcriptome and secretome analysis of *Aspergillus fumigatus* in the presence of sugarcane bagasse. *BMC Genomics*, **2018**, *19*, 232.

[30] Lo Leggio, L.; Weihe, C.D.; N Poulsen, J.-C.; Sweeney, M.; Rasmussen, F.; Lin, J.; De Maria, L.; Wogulis, M. Structure of a lytic polysaccharide monooxygenase from *Aspergillus fumigatus* and an engineered thermostable variant. *Carbohydr. Res*., **2018**, *469*, 55-59.

[31] Semighini, C.P.; Marins, M.; Goldman, M.H.S.; Goldman, G.H. Quantitative analysis of the relative transcript levels of ABC transporter Atr genes in *Aspergillus nidulans* by real-time reverse transcription-PCR assay. *Appl. Environ. Microbiol*., **2002**, *68*, 1351-1357.

[32] Livak, K.J.; Schmittgen, T.D. Analysis of relative gene expression data using real-time quantitative PCR and the 2-ΔΔCT method. *Methods*, **2001**, *25*, 402-408.

[33] Schmittgen, T.D.; Livak, K.J. Analyzing real-time PCR data by the comparative CT method. *Nat. Protoc*., **2008**, *3*, 1101-1108.

[34] Hammond, J.B.; Kruger, N.J. The bradford method for protein quantitation. *Methods Mol. Biol*., **1988**, *3*, 25-32.

[35] Laemmli, U.K. Cleavage of structural proteins during the assembly of the head of bacteriophage T4. *Nature*, **1970**, *227*, 680-685.

[36] Towbin, H.; Staehelin, T.; Gordon, J. Electrophoretic transfer of proteins from polyacrylamide gels to nitrocellulose sheets: procedure and some applications. *Proc. Natl. Acad. Sci*., **1979**, *76*, 4350-4354.

[37] Breslmayr, E.; Hanžek, M.; Hanrahan, A.; Leitner, C.; Kittl, R.; Šantek, B.; Oostenbrink, C.; Ludwig, R. A fast and sensitive activity assay for lytic polysaccharide monooxygenase. *Biotechnol. Biofuels*, **2018**, *11*, 79.

[38] Miller, G.L. Use of dinitrosalicylic acid reagent for determination of reducing sugar. *Anal. Chem*., **1959**, *31*, 426-428.

[39] Kim, I.J.; Seo, N.; An, H.J.; Kim, J.H.; Harris, P.V.; Kim, K.H. Type-dependent action modes of TtAA9E and TaAA9A acting on cellulose and differently pretreated lignocellulosic substrates. *Biotechnol. Biofuels*, **2017**, *10*, 46.

[40] Frommhagen, M.; Sforza, S.; Westphal, A.H.; Visser, J.; Hinz, S.W.A.; Koetsier, M.J.; Van Berkel, W.J.H.; Gruppen, H.; Kabel, M.A. Discovery of the combined oxidative cleavage of plant xylan and cellulose by a new fungal polysaccharide monooxygenase. *Biotechnol. Biofuels*, **2015**, *8*, 101.

[41] Hemsworth, G.R.; Johnston, E.M.; Davies, G.J.; Walton, P.H. Lytic polysaccharide monooxygenases in biomass conversion. *Trends Biotechnol*., **2015**, *33*, 747-761.

[42] Rodrigues, K.B.; Macêdo, J.K.A.; Teixeira, T.; Barros, J.S.; Araújo, A.C.B.; Santos, F.P.; Quirino, B.F.; Brasil, B.S.A. F.; Salum, T. F.C.; Abdelnur, P.V.; Fávaro, L.C.L. Recombinant expression of *Thermobifida fusca* E7 LPMO in *Pichia pastoris* and *Escherichia coli* and their functional characterization. *Carbohydr. Res*., **2017**, *448*, 175-181.

[43] Zhang, H.; Zhao, Y.; Cao, H.; Mou, G.; Yin, H. Expression and characterization of a lytic polysaccharide monooxygenase from *Bacillus thuringiensis*. *Int. J. Biol. Macromol*., **2015**, *79*, 72-75.

[44] Liu, B.; Olson, Å.; Wu, M.; Broberg, A.; Sandgren, M. Biochemical studies of two lytic polysaccharide monooxygenasesfrom the white-rot fungus *Heterobasidion irregulare* and their roles in lignocellulose degradation. *PLoS One*, **2017**, *12*, e0189479.

[45] Chylenski, P.; Petrović, D.M.; Müller, G.; Dahlström, M.; Bengtsson, O.; Lersch, M.; Siika-Aho, M.; Horn, S.J.; Eijsink, V.G.H. Enzymatic degradation of sulfite-pulped softwoods and the role of LPMOs. *Biotechnol. Biofuels*, **2017**, *10*, 177.

[46] Nekiunaite, L.; Arntzen, M.; Svensson, B.; Vaaje-Kolstad, G.; Hachem, M. A. Lytic polysaccharide monooxygenases and other oxidative enzymes are abundantly secreted by *Aspergillus nidulans* grown on different starches. *Biotechnol. Biofuels*, **2016**, *19*, 187.

[47] Miao, Y.; Li, J.; Xiao, Z.; Shen, Q.; Zhang, R. Characterization and identification of the xylanolytic enzymes from *Aspergillus fumigatus* Z5. *BMC Microbiol*., **2015**, *15*, 126.

[48] Emy, G.; Midorikawa, O.; Correa, C.L.; Noronha, E.F.; Ximenes, E.; Filho, F.; Togawa, R.C.; Mota, M.; Silva-junior, O.B.; Grynberg, P.; Neil, R.; Miller, G.; Silva, R. Analysis of the transcriptome in *Aspergillus tamarii* during enzymatic degradation of sugarcane bagasse. *Front. Bioeng. Biotechnol*., **2018**, *6*, 123.

[49] Hüttner, S.; Nguyen, T. T.; Granchi, Z.; Chin-A-Woeng, T.; Ahrén, D.; Larsbrink, J.; Thanh, V. N.; Olsson, L. Combined genome and transcriptome sequencing to investigate the plant cell wall degrading enzyme system in the thermophilic fungus *Malbranchea cinnamomea*. *Biotechnol. Biofuels*., **2017**, *10*, 265.

[50] Petrovi, D.M.; Bissaro, B.; Chylenski, P.; Skaugen, M.; Sørlie, M.; Jensen, M.S.; Aachmann, F.L.; Courtade, G.; Várnai, A.; Eijsink, V.G.H. Methylation of the N-terminal histidine protects a lytic polysaccharide monooxygenase from auto-oxidative inactivation. *Protein Sci*., **2018**, *27*, 16360-1650.

[51] Kojima, Y.; Várnai, A.; Ishida, T.; Sunagawa, N.; Petrovic, D.M.; Igarashi, K.; Jellison, J.; Goodell, B.; Alfredsen, G.; Westereng, B.; Eijsink, V.G.H.; Yoshida, M. A lytic polysaccharide monooxygenase with broad xyloglucan specificity from the brown-rot fungus *Gloeophyllum trabeum* and its action on cellulose-xyloglucan complexes. *Appl. Environ. Microbiol*., **2016**, *82*, 6557-6572.

[52] Miao, Y.; Liu, D.; Li, G.; Li, P.; Xu, Y.; Shen, Q.; Zhang, R. Genome-wide transcriptomic analysis of a superior biomass-degrading strain of *A. fumigatus* revealed active lignocellulose-degrading genes. *BMC Genomics*, **2015**, *16*, 459.

[53] Yang, B.; Wyman, C.E. Effect of xylan and lignin removal by batch and flowthrough pretreatment on the enzymatic digestibility of corn stover cellulose. *Biotechnol. Bioeng*., **2004**, *86*, 88-95.

[54] Wong, D.D.W.S.; Chan, V.J.; McCormack, A.A.; Batt, S.B. A novel xyloglucan-specific endo-β-1,4-glucanase: Biochemical properties and inhibition studies. *Appl. Microbiol. Biotechnol*., **2010**, *86*, 1463-1471.

[55] Adav, S.S.; Ravindran, A.; Sze, S.K. Quantitative proteomic study of *Aspergillus fumigatus* secretome revealed deamidation of secretory enzymes. *J. Proteomics*, **2015**, *119*, 154-168.

[56] Frommhagen, M.; Koetsier, M.J.; Westphal, A.H.; Visser, J.; Hinz, S.W.A.; Vincken, J.P.; Van Berkel, W.J.H.; Kabel, M.A.; Gruppen, H. Lytic polysaccharide monooxygenases from *Myceliophthora thermophila* C1 differ in substrate preference and reducing agent specificity. *Biotechnol. Biofuels*, **2016**, *9*, 186.

[57] Jagadeeswaran, G.; Gainey, L.; Prade, R.; Mort, A.J. A family of AA9 lytic polysaccharide monooxygenases in *Aspergillus nidulans* is differentially regulated by multiple substrates and at least one is active on cellulose and xyloglucan. *Appl. Microbiol. Biotechnol*., **2016**, *100*, 4535-4547.

[58] Crouch, L.I.; Labourel, A.; Walton, P.H.; Davies, G.J.; Gilbert, H.J. The contribution of non-catalytic carbohydrate binding modules to the activity of lytic polysaccharide monooxygenases. *J. Biol. Chem*., **2016**, *291*, 7439-7449.

[59] Harris, P.V.; Welner, D.; McFarland, K.C.; Re, E.; Navarro Poulsen, J.C.; Brown, K.; Salbo, R.; Ding, H.; Vlasenko, E.; Merino, S.; Xu, F.; Cherry, J.; Larsen, S.; Lo Leggio, L. Stimulation of lignocellulosic biomass hydrolysis by proteins of glycoside hydrolase family 61: Structure and function of a large, enigmatic family. *Biochemistry*, **2010**, *49*, 3305-3316.

[60] Jagadeeswaran, G.; Gainey, L.; Mort, A.J. An AA9-LPMO containing a CBM1 domain in *Aspergillus nidulans* is active on cellulose and cleaves cello-oligosaccharides. *AMB Express*, **2018**, *8*, 171.

[61] Vuong, T.V.; Liu, B.; Sandgren, M.; Master, E.R. Microplate-based detection of lytic polysaccharide monooxygenase activity by fluorescence-labeling of insoluble oxidized products. *Biomacromolecules*., **2017**, *18*, 610-616.

[62] Chabbert, B.; Habrant, A.; Herbaut, M.; Foulon, L.; Aguié-Béghin, V.; Garajova, S.; Grisel, S.; Bennati-Granier, C.; Gimbert-Herpoël, I.; Jamme, F.; Réfrégiers, M.; Sandt, C.; Berrin, J.G.; Paës, G. Action of lytic polysaccharide monooxygenase on plant tissue is governed by cellular type. *Sci. Rep*., **2017**, *7*, 17792.

[63] Pierce, B.C.; Agger, J.W.; Zhang, Z.; Wichmann, J.; Meyer, A.S. A comparative study on the activity of fungal lytic polysaccharide monooxygenases for the depolymerization of cellulose in soybean spent flakes. *Carbohydr. Res*., **2017**, *449*, 85-94.

[64] Jung, S.; Song, Y.; Kim, H.M.; Bae, H.J. Enhanced lignocellulosic biomass hydrolysis by oxidative Lytic Polysaccharide Monooxygenases (LPMOs) GH61 from *Gloeophyllum trabeum*. *Enz. Mic. Technol*., **2015**, *77*, 38-45.

[65] Kim, I.J.; Nam, K.H.; Yun, E.J.; Kim, S.; Youn, H.J.; Lee, H.J.; Choi, I.G.; Kim, K.H. Optimization of synergism of a recombinant auxiliary activity 9 from *Chaetomium globosum* with cellulase in cellulose hydrolysis. *App. Microbiol. Biotechnol*., **2015**, *99*, 8537-8547.

[66] Bernardi, A.V.; Gouvêa, P.F.De; Gerolamo, L.E.; Yonamine, D.K.; Lourdes, L.De; Balico, D.L.; Uyemura, S.A. Functional characterization of GH7 endo-1,4-β-glucanase from *Aspergillus fumigatus* and its potential industrial application. *Protein. Expr. Purif*., **2018**, *150*, 1-11.

[67] Karnaouri, A.; Muraleedharan, M.N.; Dimarogona, M.; Topakas, E.; Rova, U.; Sandgren, M.; Christakopoulos, P. Recombinant expression of thermostable processive MtEG5 endoglucanase and its synergism with MtLPMO from *Myceliophthora thermophila* during the hydrolysis of lignocellulosic substrates. *Biotechnol. Biofuels*, **2017**, *10*, 126.